ihp·hwrp germany

IHP/HWRP - BERICHTE

HEFT 4
KOBLENZ 2006

Runoff from Nepalese Headwater Catchments – Measurements and Modelling

AUS DER ARBEIT DES
DEUTSCHEN IHP/HWRP-NATIONALKOMITEES

IHP –INTERNATIONAL HYDROLOGICAL PROGRAMME OF UNESCO
HWRP – HYDROLOGY AND WATER RESOURCES PROGRAMME OF WMO

Runoff from Nepalese Headwater Catchments – Measurements and Modelling

Markus Konz, Ludwig Braun,
Wolfgang Grabs, Arun Shrestha and
Stefan Uhlenbrook

Koblenz 2006

IHP – International Hydrological Programme of UNESCO

HWRP – Hydrology and Water Resources Programme of WMO

BfG – Federal Institute of Hydrology, Koblenz, Germany

A German contribution to UNESCO IHP VI Theme 1 Global Changes and Water Resources, Focal Area 1.3 Integrated assessment of water resources in the context of global land-based activities and climate change, and to Hindu Kush-Himalayan FRIEND.

Authors:

Markus Konz
Institute of Hydrology, University of Freiburg, Germany
Commission for Glaciology, Bavarian Academy of Sciences, Munich, Germany

Ludwig Braun
Commission for Glaciology, Bavarian Academy of Sciences, Munich, Germany

Wolfgang Grabs
World Meteorological Organization (WMO), Geneva, Switzerland

Arun Shrestha
Department of Hydrology and Meteorology, Kathmandu, Nepal

Stefan Uhlenbrook
UNESCO-IHE Institute of Water Education, Delft, The Netherlands

Herausgeber: Deutsches Nationalkomitee für das
International Hydrological Programme (IHP) der UNESCO und das
Hydrology and Water Resources Programme (HWRP) der WMO
Koblenz 2005
ISSN 1614-1180

Bundesanstalt für Gewässerkunde
Postfach 200253
56002 Koblenz, Deutschland

Fax +49 (0)261 1306 5422

Foreword

The main themes of IHP Phase VI are: Global changes and water resources, integrated watershed and aquifer dynamics, Land habitat hydrology, Water and society, and Water education and training. In addition to these themes, FRIEND (**F**low **R**egimes from **I**nternational **E**xperimental and **N**etwork **D**ata) is a cross-cutting programme component in which regional scientific research on a number of interconnected topics is carried out. The objective of FRIEND is a better understanding of the spatial and temporal variability of hydrological regimes. FRIEND has grown to become a worldwide network of similarly structured projects. There are now eight regional FRIEND programmes: Western and Central Africa, Southern Africa, the Nile, Asian Pacific, Hindu Kush – Himalayan, Latin American and Caribbean, Alpine and Mediterranean (AMHY) and Northern Europe. The general aims of each international project within the regions are to:

- understand hydrological variability in space and time,
- exchange data, techniques and research results between countries,
- advance understanding of hydrological processes and flow regimes,
- improve techniques for analysing environmental change,
- develop techniques for water resource management, particularly under extreme events, and
- increase hydrological capacity throughout the world.

FRIEND aims to promote research at the regional level without the constraints of national boundaries and with free exchange of information. The German IHP/HWRP National Committee has consistently supported Hindu Kush – Himalayan FRIEND by contributing to workshops, training courses and publications.

Cooperation between the Nepalese Department of Hydrology and Meteorology (DHM) and the Deutsche Gesellschaft für Technische Zusammenarbeit (GTZ) in the project Establishment of a Measuring Service for Snow and Glacier Hydrology, and the projects and long years of experience of the Commission for Glaciology at the Bavarian Academy of Sciences, Munich, Germany, formed the basis for the promotion of further research in the field of snow and ice hydrology in the Hindu Kush – Himalayan FRIEND region. As the setting up and operation of observation networks in the mountainous regions of Nepal have their limits, use has to be made of the simulation of discharge from the high Himalayan headwater catchments for, primarily, the management of water resources. The German IHP/HWRP National Committee willingly took up this matter and requested the Commission for Glaciology at the Bavarian Academy of Sciences to put hydrological models for such a task to the test. This publication reports on the development of a glacier routine for a process-oriented catchment model and the modification of the model routines for application to remote, highly glacierized catchments in the Himalayas of Nepal.

The German IHP/HWRP National Committee would like to thank the authors for their excellent work and valuable contribution.

Professor Dr S. Demuth
Director of the German IHP/HWRP Secretariat

Contents

Abbreviations and symbols

*_box	Water content of storage (general)	(mm)
*_H	Limit of storage capacity (general)	(mm)
*_K	Storage coefficient (general)	(1/time step)
*_P	Percolation capacity (general)	(mm/time step)
α	Surface albedo	(-)
ΔH_l	Change in snowpack latent heat content (i.e. snowmelt or sublimation)	(W/m^2)
ΔH_s	Change in snowpack sensible heat content (i.e. snow temperature)	(W/m^2)
ΔS	Changes in storages, here primarily in the form of snow accumulation which feeds the glaciers	(mm/a)
Δz	Altitude difference	(m)
a	Year	
a(t)	Ablation rate over time t	(m/day)
A,B,C	Coefficients	(-)
a.s.l.	Above sea level	
a_a	Annual ablation	(m)
ActET	Actual evaporation	(mm/time step)
a_i	Ablation rate of bare ice	(mm/day)
AltDiff	Vertical distance between target cell and climatic station	(m)
a_m	Ablation rate under the debris layer	(mm/day)
b_a	Specific annual mass balance at a given point	(m)
B_a	Total annual mass balance of the glacier	(m^3)
Balance	Internal water balance of simulation period	(mm)
BETA	Empirical parameter	(-)
c(i)	Weight	(-)
c(t)	Accumulation rate over time t	(m/day)
c_a	Annual accumulation	(m)
Cfmax	Degree-day factor	(mm/°C day)
CFR	Coefficient of refreezing	(-)
CounterDay	Day (starting from 1 October = day 272)	
CPERC	Percolation capacity into lower zone	(mm/day)
CWH	Water-holding capacity of snow	(-)
DAV	German Alpine Club	
DEM	Digital elevation model	
DHM	Department of Hydrology and	

	Meteorology	
DistToClim	Horizontal distance between target cell and climatic station	(km)
dt	Time derivative	
du	Time derivative	
EML	Environmental modelling language	
ETGrad	Vertical evapotranspiration gradient	((%/100m)/100)
ETH	Eidgenössische Technische Hochschule	
ETmax	Maximum of potential evapotranspiration	(mm/day)
FC	Maximum soil moisture storage (field capacity)	(mm)
$F_{r,m}$	Mean ratio of amount of precipitation between station r and SGHU station of the month m	(-)
GIS	Geographic information system	
GlacierLS_box	Water content of glacier storage	(mm)
GlacierLS_H	Limit of glacier storage	(mm)
GlacierLS_K	Storage coefficient of glacier storage	(1/time step)
GlacierQ_LS	Outflow of glacier storage	(mm/time step)
GLOF	Glacier lake outburst flood	
G_{melt}	Glaciermelt	(mm/a)
grad	Vertical temperature gradient	(K/100m)
GTZ	German Agency for Technical Cooperation	
h	Moraine-cover thickness	(cm)
h	Gauge height	(m)
h	Hour	
HQ	Highest flow in observation period	(m^3/s)
HRU	Hydrological response unit	
i	Time step	
ICIMOD	International Center for Integrated Mountain Development	
$Input_{i,j}$	Input of water fluxes at actual time step	(mm)
InSoil	Output from snow and glacier routine	(mm/time step)
j	Raster cell	(-)
k	Number of grid cells	(-)
k	Storage coefficient	(1/time step)
K	Kelvin	
l	Day of maximum potential evapotranspiration	
ldd	Local drainage direction	
$\overline{\log(Q_{obs})}$	Mean logarithmic observed runoff for the whole observation period	(mm/time step)

LP	Reduction parameter of field capacity	(-)
LS_box	Water content of lower storage	(mm)
LS_K	Storage coefficient of lower storage	(1/time step)
Q_LS	Outflow of lower storage	(mm/time step)
m	Month	
MassBalance	Annual glacier mass balance	(mm)
MaxBas	Empirical parameter	(-)
MaxDay	Maximum days of the year (365 or 366)	
MaxShade	Maximum potential sunshine duration	(h/day)
MeltWaterGlacierClean	Meltwater of the debris-free glaciers	(mm/time step)
MeltWaterGlacierDebris	Meltwater of the debris-covered glaciers	(mm/time step)
MeltWaterGlacierforBalance	Annual meltwater of glaciers	(mm)
MeltWaterSnow	Amount of snow melt	(mm/time step)
MeltWaterSnowPack	Meltwater of the snowpack	(mm/time step)
MeltWaterSnowpackforBalance	Annual meltwater of snow	(mm)
MHQ	Mean high flow	(m^3/s)
MinShade	Minimum potential sunshine duration	(h/day)
MNQ	Mean low flow	(m^3/s)
MQ	Mean flow (arithmetic mean)	(m^3/s)
N	Number of reference stations	
n	Duration of simulation period	(-)
NQ	Lowest flow in observation period	(m^3/s)
nRGType	Runoff generation type units	
$Output_{i,j}$	Output of water fluxes at actual time step	(mm)
Overflow	Overflow of the storage	(mm/time step)
P	Precipitation	(mm)
P_b	Basin precipitation	(mm/a)
PCF	Precipitation correction factor for rain	(-)
PGrad	Vertical precipitation gradient	((%/100m)/100)
PHorizGrad	Horizontal precipitation gradient	((%/1000m)/100)
PotET	Potential evaporation	(mm/time step)
PotETAltitude	Altitude-corrected potential evapotranspiration	(mm/time step)
POTRAD 5	Potential Radiation Equator Model	
P_r	Measured precipitation at reference station r	(mm/day)
Prec	Corrected solid precipitation	(mm/time step)
PrecAltitude	Altitude-corrected precipitation	(mm/time step)
PrecCor	Corrected liquid precipitation	(mm/time step)
PrecHorizontal	Horizontally corrected precipitation	(mm/time step)
PrecStation	Measured precipitation	(mm/time step)

P_{SGHU}	Precipitation at SGHU station	(mm/day)
Q	Discharge	(m^3/s)
Q_*	Runoff of storage (general)	(mm/time step)
Q_{adv}	Heat flux advected by precipitation across the snowpack surface	(W/m^2)
$Q_{beforerouting}$	Simulated discharge before routing	(m^3/s)
Q_{gnd}	Ground heat flux across the snowpack base	(W/m^2)
$Q_{i,obs}$	Observed runoff at time step i	(mm/time step)
$Q_{i,sim}$	Simulated runoff at time step i	(mm/time step)
Q_{il}	Incoming long-wave radiation	(W/m^2)
Q_{is}	Incoming short-wave radiation	(W/m^2)
Q_{lat}	Latent heat flux across the snowpack surface	(W/m^2)
$\overline{Q_{obs}}$	Mean observed runoff for the whole observation period	(mm/time step)
Q_{ol}	Outgoing long-wave radiation	(W/m^2)
Q_{rad}	Net all-wave radiation flux across the snowpack surface	(W/m^2)
Q_{sen}	Sensible heat flux across the snowpack surface	(W/m^2)
$\overline{Q_{sim}}$	Mean simulated discharge for the whole observation period	(mm/time step)
$Q_{sim}(t)$	Simulated discharge	(m^3/s)
r	Reference station	
R^2	Coefficient of determination	(-)
R_{eff}	Model efficiency	(-)
Refreeze	Refreezing water in snowpack	(mm/time step)
Rexp	Correction factor for cells with maximum potential sunshine duration	(-)
RexpMap	Correction factor for degree-day method	(-)
R_{logeff}	Logarithmic model efficiency	
Rmult	Multiplicative factor to account for accelerated melt over ice as compared to snow	(-)
Rmultd	Reduction factor of glaciermelt over debris-covered parts of the glacier	(-)
s_{ab}	Ablation area of the glacier	(m^2)
s_{ac}	Accumulation area of the glacier	(m^2)
SFCF	Snowfall correction factor	(-)
s_g	Area of the glacier	(m^2)
SGHU	Snow and Glacier Hydrology Unit	(m)
Shade	Potential sunshine durations	(h/day)

SMHI	Swedish Meteorological and Hydrological Institute	
SnowPack	Snowpack storage	(mm snow water equivalent)
SnowpackforBalance	Annual snow accumulation	(mm)
SoilMoisture	Soil moisture storage	(mm)
$Storages_{1,j}$	Sum of storage levels at first time step of simulation period	(mm)
$Storages_{i,j}$	Sum of storage levels of all storages at actual time step	(mm)
t	Time step	(time step)
T	Temperature	(°C)
t_0	First day of the measurement year (usually 1 October)	
t_1	Last day of measurement year (usually 30 September the following year)	
TAC^d	Tracer-aided catchment model, distributed	
Temp	Altitude-corrected air temperature	(°C)
TempStation	Measured air temperature at climatic station	(°C)
TGrad	Vertical temperature gradient	(°C/100m)
TIN	Triangular irregular network	
ToRunoffGeneration	Infiltration into runoff generation routine as fraction of the actual soil moisture	(mm/time step)
T_{Ref}	Temperature at reference station	(°C)
T_{SGHU}	Temperature at SGHU station	(°C)
TT	Threshold value of temperature for snowfall, also general temperature correction	(°C)
u	Time step	(day)
UNEP	United Nations Environment Programme	
US_box	Water content of upper storage	(mm)
US_H	Limit of upper storage	(mm)
US_K	Storage coefficient of upper storage	(1/time step)
US_P	Percolation capacity	(mm/time step)
Q_US	Outflow of upper storage	(mm/time step)
V	Storage level	(mm)
V(t)	Storage level at time t	(mm)
V_0	Storage level at time t = 0	(mm)
ValleyLS_box	Water content of valley storage	(mm)
ValleyLS_H	Limit of valley storage	(mm)

ValleyLS_K	Storage coefficient of valley storage	(1/time step)
ValleyQ_LS	Outflow of valley storage	(mm/time step)
VE	Volume error	(mm/a)
WaterContent	Water content of snow cover	(mm)
$W_{i,m}$	Weighting of station i according to the joint occurrence probability of precipitation at target station and reference stations for the month m	(-)

Summary

The objective of this work was the simulation of discharge of high Himalayan headwater catchments. Therefore, the development of a glacier routine for the distributed process-oriented catchment model TAC^d (Tracer Added Catchment Model, distributed) and the modification of the model routines for application to the remote, highly glacierized Langtang Khola, Modi Khola and Imja Khola catchments in the Himalayas of Nepal are the object of this study. The HBV-ETH model has also been applied to these catchments and the simulation results of both models are compared. In addition, statistical methods to compute complete time series of climatic input data are presented.

The distributed process-oriented catchment model TAC^d was developed in the Brugga catchment (Black Forest, Germany) and has a modular structure. Experimental results were the basis for the development of the runoff generation routine which is the core piece of the model. Laterally and vertically connected simple linear storages simulate the runoff generation processes of the hydrological response units (HRUs). Sophisticated approaches are used in the model to calculate the sections of the land phase hydrological cycle, for instance, potential evapotranspiration based on the data-intensive method of Penman-Monteith. For the regionalisation of climatic input data the inverse distance weighting method, which requires a dense observation network, is implemented.

Fundamental modifications were necessary for the application of TAC^d to the Langtang Khola, Modi Khola and Imja Khola catchments. The modification and development work was carried out using the dynamic GIS PCRaster. With this environmental component a high-level linkage of the spatial data base with the dynamic modelling is achieved, which is a prerequisite for effective distributed hydrological modelling.

Vertical gradients for the regionalisation of air temperature and potential evapotranspiration are implemented in conjunction with an additional horizontal gradient for the regionalisation of precipitation. Evapotranspiration plays a minor role in the annual water balance of a high alpine catchment and potential evapotranspiration is calculated using a simple sinusoidal function with a fixed calibrated maximum on 1 August and the minimum of 0.0 mm/day on 1 February.

Ice- and snowmelt are calculated with the modified “classical” temperature-index method using the degree-day factor as proportionality coefficient that determines melt rates on the basis of air temperature. Incoming short-wave radiation expressed as potential sunshine duration per day and per raster cell is used to distribute the meltwater calculation. This regionalisation approach enables a temporal and spatial meltwater calculation based on topographic and astronomic information. Differences in melt conditions between ice and snow as well as between debris-free and debris-covered glaciers are considered, based on empirical factors.

The delineation of hydrological response units is achieved using topographic and physiographic information. Four units are determined for conceptualisation of the runoff generation processes. The glacier and non-glacier areas are the dominating units whose runoff generation processes are simulated on the basis of two vertically connected simple linear storages. Two other units are delineated and are considered to store water during the monsoon season for the maintenance of winter runoff. These units are the glacier tongues with an inclination of less than 3° and debris cover, and the valley bottom with an inclination of less

than 8°. They account for a small percentage of the catchments' area but are designed as large storages.

In the preprocessing section, extrapolation methods were applied to bridge gaps in the time series of air temperature and precipitation data. Further, cumulated precipitation sums were redistributed over the previous days if necessary.

The spatial resolution of the raster maps of 200 x 200 m² is necessary for the realistic calculation of meltwater, but it is in conflict with the temporal resolution of daily time steps. A reduction of the delay of the onset of the simulated discharge at the beginning of the monsoon season caused by the disadvantageous ratio between the temporal and spatial resolutions was achieved by extending the river network to include the glacier-covered parts. This accounts further for the subglacial drainage networks which were not included in the original river network.

The model was calibrated to the Langtang Khola catchment using glacier mass balance data as additional calibration criteria beside discharge data to adjust the parameters of the snow and glacier routine. The parameter set obtained was used as the starting point for the adaptation of the model to the other catchments. For the Modi Khola catchment the unchanged parameter set was taken, whereas few modifications were necessary for the Imja Khola catchment. The simulation results are generally satisfactory, especially in the Langtang Khola and Imja Khola catchments. The data quality of the Modi Khola catchment is questionable and the application of a hydrological model is necessary to provide a reliable assessment of the terms of the hydrological conditions of the catchment.

The comparison with the semi-distributed HBV-ETH model revealed that the main advantages of TAC^d are the distributed treatment of runoff components and storages of the catchment. As the output of the snow and glacier routine shows no significant differences between the two models, the runoff generation routine of TAC^d is able to store the water during the monsoon season for the maintenance of winter discharge.

Weak spots of the model application were revealed in the calculation of ablation at high altitudes and in the simulation of discharge at the beginning of the monsoon season. Ablation is calculated by the temperature-index method if air temperature is above a threshold value. This leads to an unrealistic snow cover at high altitudes where air temperature is below the threshold value and sublimation plays a significant role for ablation. Further, distribution of snow by avalanches is not considered as an ablation process in the model. This among other factors also affects the simulation of the onset of discharge at the beginning of the monsoon season, since snow at lower altitudes starts melting earlier and thus contributes to the runoff generation of the early monsoon season.

The presented version of TAC^d is seen as the framework for further investigations and developments. The subjectively conceptualised runoff generation routine and the dimensions of the assumed storages need to be checked by experimental investigations in the catchment. An energy balance approach could simulate sublimation processes of the high altitudes and further knowledge of the redistribution of snow is necessary for an exact description of the hydrological cycle with a numerical model.

The results of this study encourage continuing investigations of this climatically highly sensitive region. Interdisciplinary approaches are necessary to determine the impacts of

climate change in this region from both the hydrological and the socio-economic points of view.

1 Introduction and objectives

Mountainous regions occupy a special place in the world's water cycle. Although they cover only 20% of the land surface, 40-60% of surface fresh water originates in these regions (Bandyopadhyay et al., 1997). There are many different aspects to the hydrological significance of mountainous regions. The orographic effect causes increasing precipitation amounts with altitude which, in the end, contribute to runoff generation. Solid precipitation is stored as snow and at a larger time scale in glaciers, and contributes to the runoff generation with a seasonal delay. This water is available not only in the mountainous regions, but the surplus is transported via the river systems and contributes to the water supply of the lowlands. Summer runoff variability in the lowlands is reduced, particularly through temporally highly regular melting processes and the long-term compensatory effect of glacier storage in mountains. Mountains are therefore called "water towers" which store large amounts of water and distribute them spatially and temporally. The significance of these "water towers" strongly depends on the climatic conditions of the surrounding lowlands. The hydrological relevance of mountainous regions is more pronounced if the lowlands are arid or their water supply is controlled by special precipitation patterns like the monsoon circulation. In some regions of the world mountains are the only source of water supply. Viviroli and Weingartner (2004) stated that the most important "water towers" of the world are located in arid and semi-arid regions where mountains contribute from 50 to 90% of total discharge, with extremes of over 95%.

Melting snow and ice supply water to much of the Himalayan region in the dry months before the summer monsoon (Kattelmann, 1993). The seven most important rivers in southern and eastern Asia are fed by glaciers during the dry season: Indus, Ganges, Brahmaputra, Salween, Mekong, Yangtze and the Yellow River. Snow- and icemelt comprises about 70% of the annual discharge of the Indus and its tributaries (Tarar, 1982).

With regard to the increasing population of the world, the increasing water demand, global change and the conflict potential which accompanies the uneven distribution of fresh water, one can only speculate about the importance that water management plans and international treaties will have in the future. Water is the primary renewable resource of Nepal and is the primary source of energy for the country. An improved water resources management in Nepal aims at sustainable irrigation agriculture, drinking water supply, and the minimisation of damage to life and property due to floods. The efficient management of water resources in Nepal requires knowledge of the regional and seasonal distribution of river runoff which is influenced by snow- and glaciermelt from the high Himalayas.

Mountainous regions of the Himalaya are generally hard to access and the data source for sustainable water resources management is scarce. Although it is known that hydrological models have certain limitations, they nevertheless are able to contribute largely to water resources management in these regions. Hydrological models are tools for water resources management which can bridge the gap in a reliable way between the available data base and the demand for information about hydrological processes, such as snow accumulation and ablation, runoff production from rain and snowmelt and runoff from glaciers. In view of the effects of global change, it is, however, not sufficient to get a good fit between simulated and measured hydrographs by optimal calibration of model parameters, especially when calculating the impact of climate change scenarios.

Many models of different complexity have been developed to simulate the dynamics of snow accumulation and ablation phenomena (e.g. Cazorzi and Fontana, 1996; Verbunt et al., 2003;

Zappa et al., 2003). Model complexity strongly depends on the available data base. A main objective of this study is to incorporate the knowledge about high alpine hydrological processes and about the modelling of these processes, gained from highly sophisticated hydrological models and "laboratory-like" research catchments, into a conceptual hydrological model which is able to simulate the most important sequences of the land-phase hydrological cycle of high alpine catchments with limited data availability. Since data scarcity is the most common limitation factor in the application of hydrological models, the underlying modelling philosophy is that the model should require only input data that are readily available, even in remote regions of the Nepalese Himalayas. These data include daily mean air temperature and daily sums of precipitation, while topographic and physiographic information has to be implemented for the regionalisation of, for instance, snow- and icemelt. The objectives of this study are as follows:

- The development and application of statistical extrapolation methods for filling the gaps in the time series of air temperature and precipitation to provide a reliable data base for hydrological modelling.
- The implementation of snow- and glaciermelt into the process-oriented catchment model TAC^d. Potential sunshine duration is used for a distributed simulation of snow- and glaciermelt. Since data availability of the Himalayan catchments is limited to air temperature and precipitation, the routines of TAC^d have to be simplified or replaced.
- As the simulation of the year-to-year variation of runoff requires an adequate conceptualisation of the runoff generation routine, the hydrological response units are determined from available topographic and land use maps as well as from observations during field visits. Storage concepts and hydrological response units need to account for the hydrological situation of the catchment; however, they have to be adapted to the limited knowledge about the runoff generation processes of the catchment. Thus, the most obvious runoff generation processes which are related to physiographic and topographic characteristics of the catchment have to be discerned.

The target areas of this study are three highly glacierized headwater catchments in the Himalayas of Nepal, where continuous climatological and hydrological observations began in 1987, initiated by the German Agency for Technical Cooperation (GTZ). The kingdom of Nepal is situated in the central part of the Himalayan Arc separating the Gangetic plains of India from the Tibetan plateau of China. The Himalayan belt extends over 2,400 km from the Punjab Himalayas in the West to the Bhutan and Assam Himalayas in the East. The Nepal Himalayas, situated between 26° 15' to 30° 30' N latitude and 80° 00' to 88° 15' E longitude, extend over 800 km from northwest to southeast. Their total area of about 150,000 km² spans the mountainous region with varying widths of between 90 and 230 km. Within an average width of only about 150 km the altitude range varies from less than 100 m a.s.l. to 8,848 m a.s.l. About 83% of the country of Nepal is covered by the rugged terrain of the hills and mountains, and the land above 4,500 m a.s.l. accounts for approximately 14.7% of the total area. These physical features of Nepal are taken from ICIMOD's inventory of glaciers (ICIMOD/UNEP, 2002). The catchments were chosen to represent different climatological conditions of the Nepal Himalayas. Initial simulations with a conceptual precipitation-runoff model were conducted by Braun et al. (1993) in the Langtang Khola catchment. Their findings are the basis for the model development of this study.

2 Methodology and modelling theory

2.1 Modelling of snow- and icemelt

In this study only a brief overview of the different modelling approaches is given and literature is referred to for detailed discussion of the approaches.

2.1.1 Energy balance models

Physically based models calculate energy input into the snowpack by considering the components of the surface energy balance and they simulate the resultant changes in snowpack heat and mass balance (e.g. in Hock, 1998; Escher-Vetter, 2000). The principal and most influential terms of the energy balance are as follows:

$$\Delta H_s + \Delta H_l = Q_{rad} + Q_{sen} + Q_{lat} + Q_{adv} + Q_{gnd} \quad (2.1)$$

ΔH_s: Change in snowpack sensible heat content (i.e. snow temperature) (W/m²)
ΔH_l: Change in snowpack latent heat content (i.e. snowmelt or sublimation) (W/m²)
Q_{rad}: Net all-wave radiation flux across the snowpack surface (W/m²)
Q_{sen}: Sensible heat flux across the snowpack surface (W/m²)
Q_{lat}: Latent heat flux across the snowpack surface (W/m²)
Q_{adv}: Heat flux advected by precipitation across the snowpack surface (W/m²)
Q_{gnd}: Ground heat flux across the snowpack base (W/m²)

with

$$Q_{rad} = Q_{is}\,(1-\alpha) + Q_{il} + Q_o \quad (2.2)$$

Q_{is}: Incoming short-wave radiation (W/m²)
α: Surface albedo (-)
Q_{il}: Incoming long-wave radiation (W/m²)
Q_{ol}: Outgoing long-wave radiation (W/m²)

The energy conducted by solid or liquid precipitation and the soil heat flux can also be taken into account even if their contribution is rather small (Zappa et al., 2003). The primary advantage of using physically based models is that they have applicability in a wide range of conditions and environments. Their big disadvantage is the large amount of input data which are necessary to run the model (Fox, 2003).

2.1.2 Temperature-index models

These models lump all components of the surface energy balance discussed in section 2.1.1 into a degree-day factor, which is a proportionality coefficient that calculates melt rates on the basis of air temperature (normally in excess of some threshold value). Air temperature is considered to be representative for the main terms of the energy balance. A recent overview of this approach is given by Hock (2003) and the physical basis is discussed by Ohmura (2001).

2.1.3 Hybrid models

These types of snow- and icemelt models attempt to keep the simplicity of the degree-day approach, but also explicitly represent other important components of the surface energy balance, in particular by solar radiation (Fox, 2003). The most common addition to temperature-index-type models has been the incorporation of measured short-wave radiation or net radiation (Martinec, 1989; Brubaker et al., 1996; Cazorzi and Fontana, 1996). Hock (1999) proposed the extension of the temperature-index approach under consideration of the daily potential direct radiation variations. This approach was found to considerably improve simulations of spatial and temporal variations in melt rates compared with a model using a single degree-day melt factor, and only little additional improvement in model performance was achieved using a fully distributed energy balance model (Fox, 2003; Zappa, 2003).

2.2 PCRaster

PCRaster is a geographic information system (GIS), which combines classical GIS applications with dynamic modelling. The programme package was developed at the Department of Physical Geography, Faculty of Geosciences, at the University of Utrecht, The Netherlands (PCRaster, 2004). PCRaster provides a variety of tools to store, manipulate and analyse spatial and temporal information. PCRaster is used as an environmental programming component for the modification of TAC^{d}.

2.2.1 Concepts of PCRaster

PCRaster provides a high-level linkage between GIS and the dynamic section of a modelling system. Hence PCRaster is called a dynamic GIS (van Deursen, 1995) and different ways of combining GIS and dynamic modelling are shown in Figure 2.1.

The high-level linkage of PCRaster makes the use of an external data conversion programme unnecessary. Here the dynamic model is one of several tools within the development environment of PCRaster, which is directly linked to the spatial GIS database. This approach enables the spatial distributed treatment of temporal variable data, such as time series. Other approaches like low- or medium-level linkage consider the dynamic model as a separate tool with spatial input data provided by an external GIS. Data exchange usually happens manually or by an automatic external conversion programme. The PCRaster environmental modelling language (EML) is specially designed for the tasks of modelling dynamic environmental systems in spatial and temporal resolutions. Therefore, a function library provides operators and functions from which many are especially designed for hydrological modelling. Further, it is possible to develop functions in Delphi or C++. These functions can be implemented into the model script in form of a dynamic link library. Thus, PCRaster allows a flexible treatment of individual questions.

The handling of data types is very strict in order to avoid forbidden map operations. Typical data types of maps, tables or time series are boolean, scalar, nominal or ordinal.

The spatio-temporal conceptionalisation of PCRaster is shown in Figure 2.2. Rectangular cells are used to describe the natural system. Attributes like storage levels or altitudes are assigned to each cell of a raster map. Lateral information exchange between cells is realised by neighbourhood relations, which are also expressed in raster maps or can be calculated via GIS

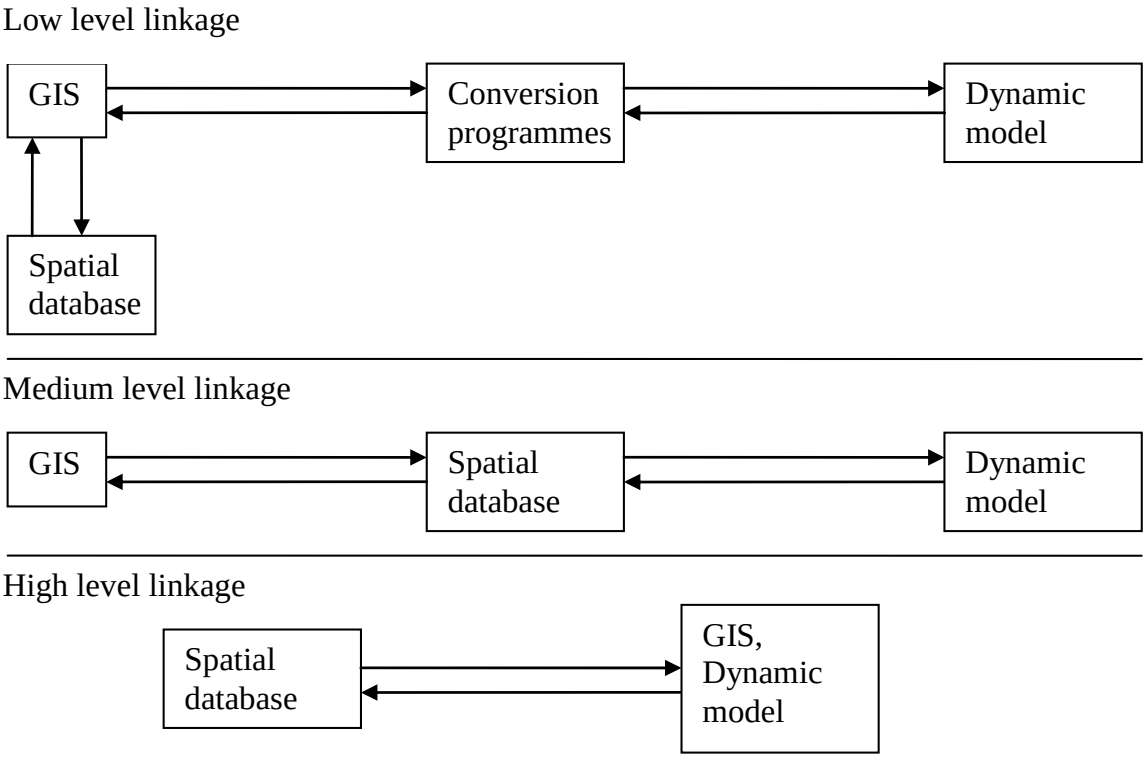

Figure 2.1: Level of linkage between GIS and dynamic modelling (taken from Ott (2002), according to van Deursen (1995))

operations. Neighbourhood relations enable the simulation of lateral and vertical fluxes, e.g. of water, within a catchment. In Figure 2.2 time-dependent attributes (variables) are assigned to the vertically arranged cells. Depending on the number of vertically layered maps a 3-dimensional structure can be simulated via 2-dimensional map stacks. The information exchange conditions are saved in each cell as attributes. This approach is referred to as 2.5-dimensional (PCRaster, 2004).

Input and output of a PCRaster model can be single raster maps or time series. Input raster maps or time series are read in for each time step, whereas specific time steps (e.g. monthly values) can be chosen for the creation of output files (maps, time series). Output files can be used in other programmes for further treatment.

2.2.2 Dynamic modelling with PCRaster

PCRaster operations can be executed in a DOS shell. The model script summarises single operations and can be called with a batch file. The script consists of five major sections with different responsibilities towards data management within the model. The first section is the **binding** section. Here variables are defined and assigned to the respective data type (boolean, scalar, nominal, ordinal). In this section external time series are read in as well as raster maps like the digital elevation model (DEM). The **areamap** section contains the name of the clone map, which consists of the information about the spatial discretization for all maps produced in the model. Further, all input maps have to correspond with the information of the clone map. The **timer** section defines the time step discretization and the number of time steps in a model run. The initial values of the variables are assigned in the **initial** section. This section

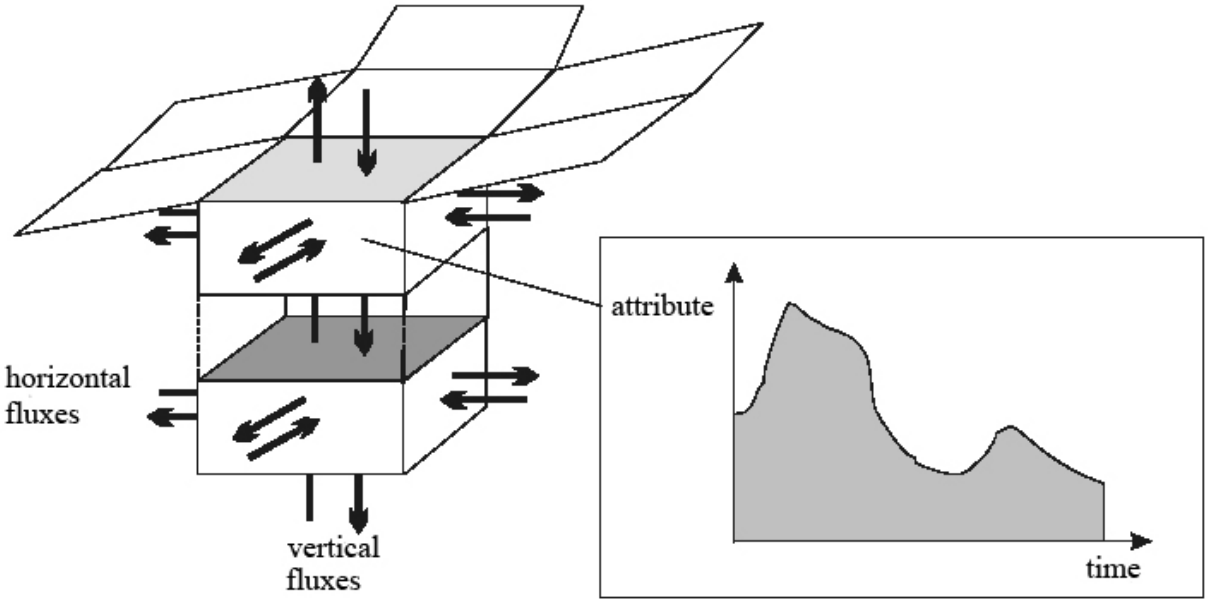

Figure 2.2: Spatial fluxes and time-variable cell attributes (taken from Roser (2001), according to van Deursen (1995))

might contain functions to calculate the initial values or specific values e.g. for initial storage levels. The **dynamic** section is the core of the model where the sequential definition of model operations for each time-step is realised. At time-step i variable values are used that were calculated in time-step i-1 and at the end of time-step i the values of variables for the time-step i+1 are available. All variables and their values are saved as raster maps.

The dynamic modelling language enables mathematical and analytical map operations and provides conditional structures (if…else) and an iterative section (repeat…until). PCRaster (2004) provides an excellent documentation of the dynamic GIS with comments and explanations of all functions and operators. Thus, the description of PCRaster in this work is limited to the main ideas and concepts of the development environment, which are necessary to understand the further descriptions of model development.

2.3 Methodology of model modification

2.3.1 The internal water balance

As stressed in Wissmeier (2005) the main criterion for the soundness of a catchment model is the internal water balance. Input and output fluxes as well as stored water are calculated for each time step and than cumulated over the simulation period. The internal water balance summarises the storages and fluxes. Thus, input fluxes are added while output fluxes are subtracted. Due to the integral structure of the internal water balance fundamental errors in the model script result in a continuously rising or declining water balance. Water is “produced” in the model if the balance is negative, whereas a positive balance indicates that water “disappears” during simulation. The internal water balance is a calculation of the internal mass conservation of the model and must therefore be balanced out. This can be seen as the fundament of a precipitation-runoff model (Wissmeier, 2005).

$$Balance = \sum_{i=1}^{n}\left(\sum_{j=1}^{k} Input_{i,j} - \sum_{j=1}^{k} Output_{i,j} + \sum_{j=1}^{k} Storages_{1,j} - \sum_{j=1}^{k} Storages_{i,j}\right) \quad (2.3)$$

Balance: Internal water balance of simulation period (mm)
$Input_{i,j}$: Input of water fluxes at actual time step (mm)
$Output_{i,j}$: Output of water fluxes at actual time step (mm)
$Storages_{1,j}$: Sum of storage levels of all storages at first time step of simulation period (mm)
$Storages_{i,j}$: Sum of storage levels of all storages at actual time step (mm)
n: Number of time steps (-)
k: Number of grid cells (-)
i: Time step (-)
j: Raster cell (-)

Glaciermelt water and precipitation is considered as input into the model. Output fluxes are calculated for water that is entering the river network or losses due to evaporation. Storages are snowpack, water content of snowpack, soil moisture, upper and lower storage, storage of water in flat parts of the glaciers and valley bottom storage (Chapter 5.5).

One needs to keep in mind that numerical models always suffer from inaccuracies related to time and spatial discretization and rounding. Minimal fluctuations of the internal balance are therefore expected even if the script is fully debugged. Earlier applications of the internal water balance as a diagnostic tool (e.g. Wissmeier 2005) have shown that the internal water balance can be considered sufficiently accurate if the value stays within a millionth of the input amount. Further, no systematic decline or increase should be evident.

2.3.2 The virtual test site

Virtual test sites are synthetic small catchments with the same topographical features as the real catchment to which the model should be applied. In this study it is necessary to create a test site with an altitude range of several thousand metres and a significant glacier cover. The test site is used for testing the newly developed subroutines. Figure 2.3 shows the virtual test site of 10 x 10 grid cells with glacier-covered parts and the local drainage direction (ldd).

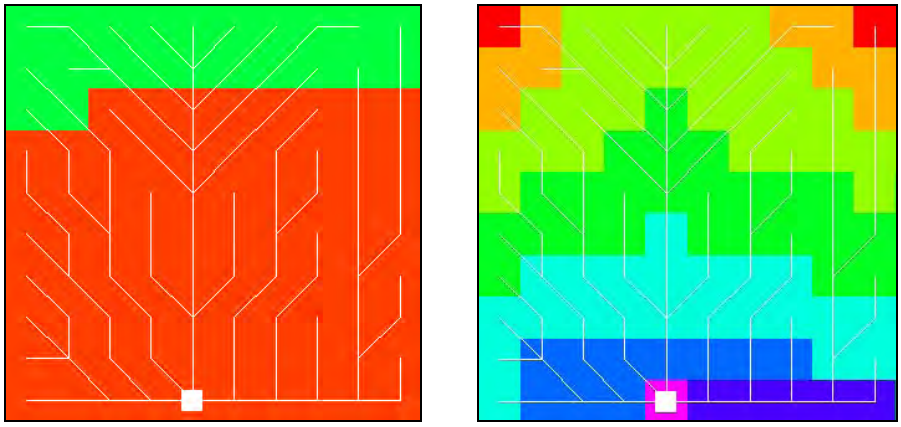

Figure 2.3: Virtual test site. Glacier map with ldd (left) and digital elevation model with ldd (right)

With a virtual test site interconnected effects are manageable in order to observe specific catchment reactions. Processes can be observed with only short computation times. Thus, parameter tuning becomes clearer and the effects of changes in catchment characteristics and climatic input data become more obvious.

2.4 Conclusions

PCRaster combines GIS with dynamic modelling which avoids intensive data conversion between both systems. The GIS provides classical tools for spatial analyses. In the dynamic section spatial and temporal input data can be processed with the help of special hydrological tools. Output files of all attributes can be created at any time step as a map or time series. The dynamic modelling language is easy to understand and to learn and therefore no specialist knowledge in computer sciences is necessary. A limitation for model application is the guideline that a model run has to start at time step ”1”. Therefore new formatting of input data is necessary if the modelling time is to be changed.

The internal water balance is used as a diagnostic variable to evaluate the soundness of the model code which is tested in a virtual test site.

3 Areas of investigation

Three high mountain headwater catchments in the Annapurna, Langtang and Khumbu regions were selected for the model application (Figure 3.2). These are the catchments which extend from the Modi Khola river to the gauging station at 3470 m a.s.l., the Langtang Khola river to the gauging station at 3800 m a.s.l., and the Imja Khola river to the gauging station at 4355 m a.s.l. (Table 3.1, Figures 3.1 and 3.2). The development work of the TAC[d] model was conducted using the data for the Langtang Khola catchment, and this catchment was investigated in detail based on an extensive literature study. In the other two catchments both the HBV-ETH and the TAC[d] model were applied without changes in the conceptual structure of the models. It was not the primary goal of this study to provide a comprehensive description of the Modi Khola and the Imja Khola catchments. The catchments are located in Nepal's most famous national parks and tourist regions with an infrastructure that includes lodges and trails. The distance between the Modi Khola and Langtang Khola catchments is 200 km, and 120 km between the Langtang Khola and Imja Khola catchments. Hydrological and meteorological stations are operated by the Snow and Glacier Hydrology Unit (SGHU) of the Department of Hydrology and Meteorology (DHM) in Kathmandu. Table 3.2 contains detailed information about the glaciers with numbers in Figure 3.2. Table 3.1 gives the altitude range of the catchments as published in the DHM yearbooks.

Table 3.1: Main characteristics of the investigated catchments

		Imja Khola	**Modi Khola**	**Langtang Khola**
Investigation period		1988-1995	1991-1994	1987-1998
Area				
Total	(km²)	141.4	160.6	360.0
Glacierized	(km²/%)	53.4/37.7	76.6/47.7	166.1/46.1
Debris-covered glacier	(km²/%)	24.0/45.0*[1]	6.96/9.1*[1]	32.1/19.3*[1]
Altitudes				
Range	(m a.s.l.)	4355-8501	3470-8091	3800-7234
Average	(m a.s.l.)	5500	5327	5169
Exposition				
North *[2]	(%)	17.9	12.7	21.3
South *[3]	(%)	37.0	38.0	26.8
East, West, Horizontal *[4]	(%)	45.1	49.3	51.9
Mean slope	(°)	28.6	34.9	26.7
Land cover				
Glacier	(km²/%)	53.4/37.7	76.6/47.7	166.1/46.1
Barren land	(km²/%)	67.8/48.0	66.81/41.6	183.8/51.1
Forest	(km²/%)	-	0.7/0.4	2.1/0.6
Grass land	(km²/%)	17.6/12.5	15.0/9.3	3.4/0.9
Others	(km²/%)	2.6/1.8	1.4/0.9	4.6/1.3

*[1] in percent of glacier-covered area
*[2] 315° - 45°
*[3] 135° - 225°
*[4] 45° - 135° and 225° - 315°

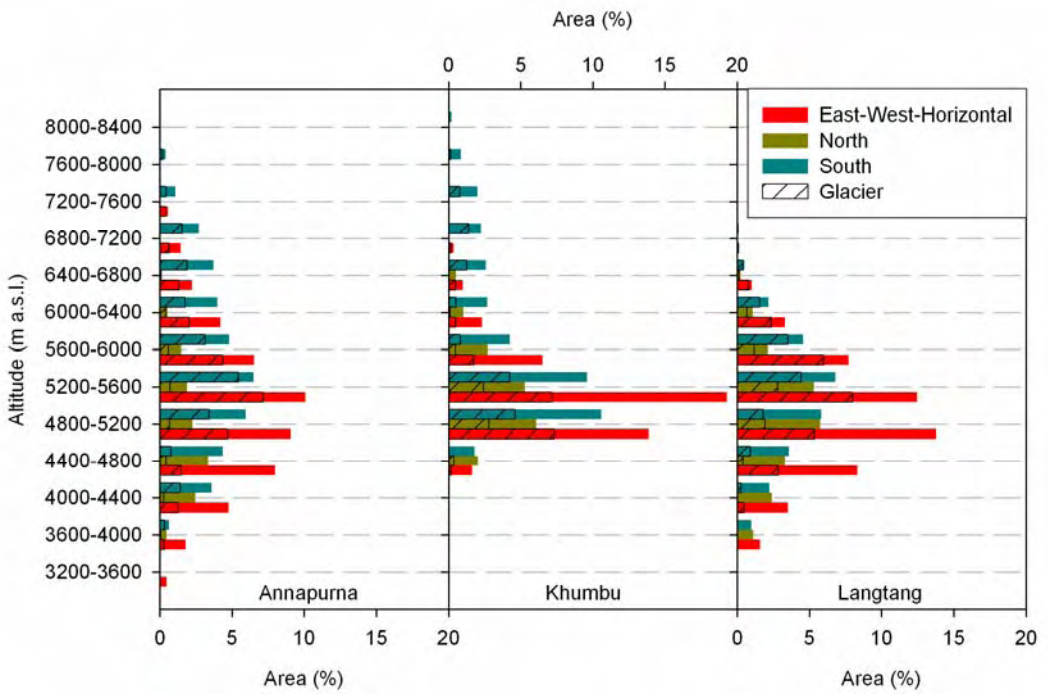

Figure 3.1: Area altitude distribution of the three investigated catchments with proportion of glacier-covered area

Table 3.2: Main glaciers of the investigated catchments

Name of station and catchment	Glaciers of catchment map no.	Area (km²)	Mean length (m)	Mean elevation (m)	Orientation of ablation	Orientation of accumulation
Langtang Khola Langtang	1	12	6580	5522	S	SE
	2	6	5830	5136	SW	SW
	3	5	1520	5841	SW	SW
	4	16	11590	4991	SE	SE
	5	68	17740	5833	S	S
	6	4	2150	5737	SW	SW
	7	26	1580	5243	SW	SW
Modi Khola Annapurna	1	5	2530	5685	NE	NE
	2	8	5060	5105	SE	SE
	3	3	2720	5441	SE	SE
	4	10	12670	5876	S	S
	5	1	1200	5547	W	W
	6	1	1450	5151	SW	SW
	7	2	3140	5486	SE	SE
	8	12	8260	5429	S	S
	9	4	3800	5898	S	S
	10	15	6970	5830	SW	SW
	11	3	3160	5395	NW	NW
	12	1	1900	5319	W	W
	13	3	3215	5471	W	W
Imja Khola Khumbu	1	5	6330	5349	S	S
	2	2	4110	5349	S	S
	3	9	8870	5465	SW	SW
	4	19	10770	6431	W	SW
	5	4	4110	5508	NW	NW
	6	6	5060	5525	N	N

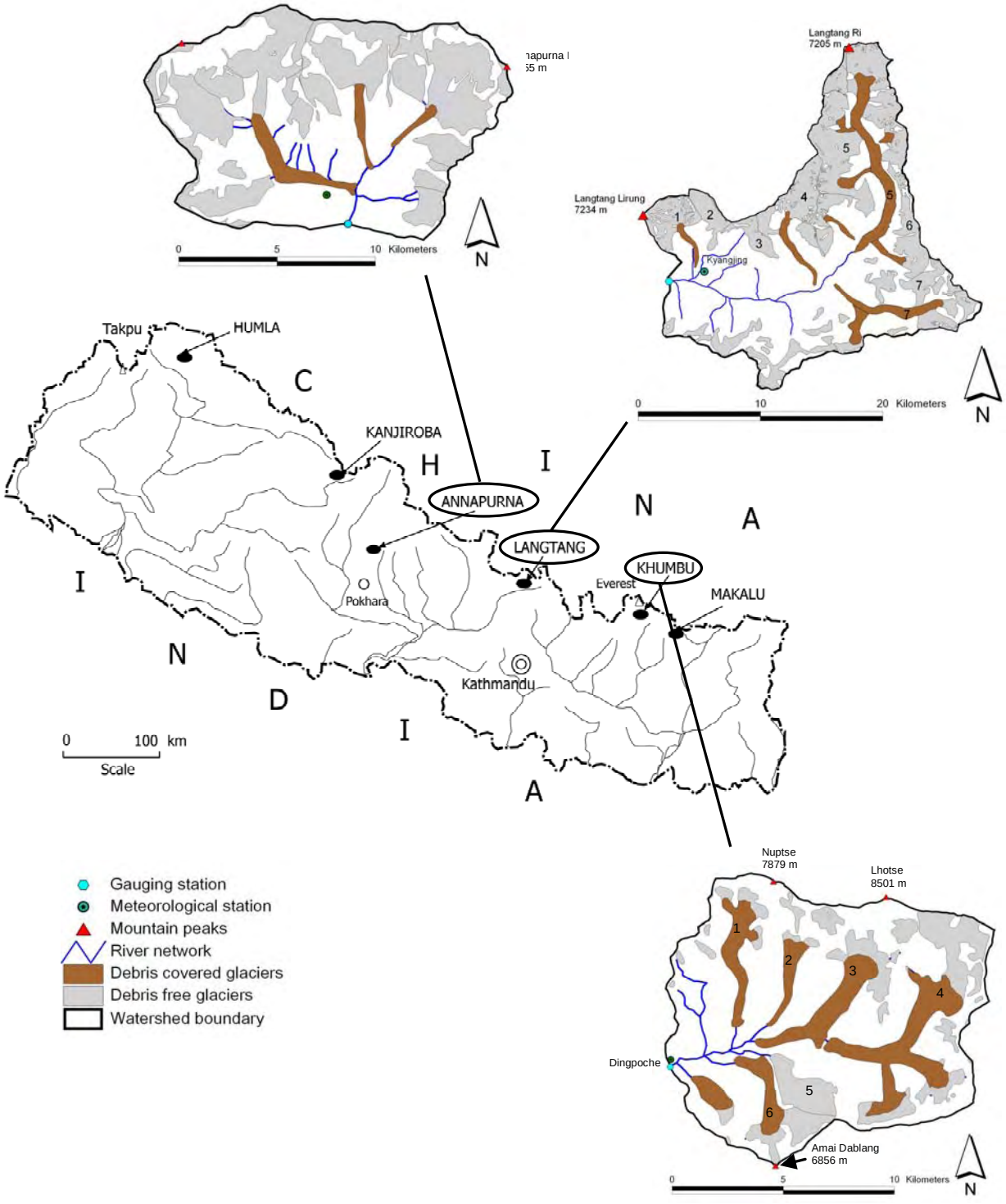

Figure 3.2: Map of Nepal with SGHU stations and detailed maps of Annapurna, Langtang and Annapurna catchment. The basins of Humla, Kanjiroba and Makalu were originally also instrumented (Grabs et al., 1993), but not used due to a poor data base.

3.1 Morphology, topography and land cover

3.1.1 Langtang Khola catchment

The 360 km² large catchment is located in the Langtang National Park and extends from 3800 m a.s.l. up to the Langtang Lirung at 7234 m a.s.l.. Two further peaks reach above 7000 m. The maximum altitude range is 3434 m with an average altitude of 5169 m a.s.l. (Table 3.1). The average steepness of the slopes of 27° reflects the high potential relief energy of the catchment. The valley is dissected by the Langtang Khola and is typically U-shaped. Table 3.1 summarises the main characteristics of the area studied. Several sets of moraines occupy the valley bottom, which have been correlated to the Little Ice Age, the Neoglacial, the younger and older Late Glacial periods and the pre-Late Glacial advance (Heuberger et al., 1984; Ono, 1986 quoted in Watanabe et al., 1989). Boulders and scree cover the steep slopes and high plateaus, while the occurrence of forest and grassland in the lower altitudes with no steep inclination along the river is limited to 1.5% of the entire catchment area. The riverbed consists of sand and gravel. The geology of this area is part of the Main Central Thrust Zone, which consists of granite, gneiss and schist.

Himalayan glaciers are summer accumulation type glaciers, which means that both accumulation and ablation occur primarily during the summer monsoon season. The glaciers are categorised into two types according to the surface conditions of the ablation zone: debris-free glaciers and debris-covered glaciers (Moribayashi, 1974). 166 km² of the 360 km² catchment area are occupied by glaciers, of which 32 km² (19%) are covered by debris, especially the glacier tongues below 5200 m. The Yala glacier and the Lirung glacier have been studied in detail in terms of glacier fluctuations. Fujita et al. (1998) conducted a survey of the Yala glacier terminus in September 1994, May and October 1996 and found that the retreat rate and surface lowering has accelerated in recent years. Repeated surveys of transverse surface profiles of the Lirung glacier from 1987 to 1999 revealed that the glacier surface has lowered from 1996 to 1999 (Naito et al., 2002). Photographs taken at different times show clearly the retreat of the glacier and there is an indication that the upper steep part and the lower flatter part of the Lirung glacier will separate in the near future (Shrestha and Shrestha, 2004).

3.1.2 Modi Khola and Imja Khola catchments

The Modi Khola catchment is located in the Annapurna region and covers an area of 160 km², 48% of which is covered by glaciers. Its altitude ranges from 3470 to 8091 m a.s.l. with a mean altitude of 5327 m (Table 3.1). Most of the glaciers are located at about 5400 m a.s.l. and 9.1% of the ice area is covered by a debris layer. The high mountain Himalayan Imja Khola catchment is located in the Khumbu region close to Mt. Everest (Sagarmatha, 8848 m). 38% of the 141 km² large catchment area is covered by glaciers, of which 45% are covered by debris. The catchment altitude ranges from 4355 to 8501 m a.s.l. with Mount Lhotse (8501 m) as the highest peak in the catchment. Yamada et al. (1992) observed a constant glacier retreat in the period from 1978 to 1989 at different glaciers in the Khumbu region with annual retreat rates of 2.28 m/a to 4.6 m/a. Surface lowering of the debris-covered Khumbu glacier, located close to the Imja Khola catchment, accelerated from 1995 to 1999 (about 2 m/a) compared to the period from 1978 to 1995 (about 1 m/a) as reported by Kadota et al. (2002).

3.2 Climate

The characteristic mark of the climate of Nepal is the monsoon circulation with predominant easterly winds in the summer and westerly winds from October to May (Kraus, 1966). The summer monsoon with large precipitation amounts from June to September does not break out at once. A gradual change from the dry winter season to the summer monsoon results from the pre-monsoonal convective precipitation events which are often accompanied by thunderstorms (Ueno et al., 1993). Every summer between June and July, the sun moves northwards and heats up the mountains creating a massive convection cell. The subsequent rising air produces a vacuum that draws the moisture-laden air of the Bay of Bengal. This air moves into the Himalayan barriers, cools as it rises and condenses in the form of rain. This is the start of the monsoon season, which brings three to four months of high humidity with overcast skies and gentle rain. About 70–80% of annual precipitation falls during this period.

In winter, western Nepal experiences a reverse monsoon caused by a shift in the jet stream. This phenomenon, which draws weather patterns from the west of the Arabian Sea, brings moisture to the region in the form of snow. The oscillation of the jet stream occurs between November and March (ICIMOD/UNEP, 2002).

The three catchments represent the various climatological conditions of the Nepalese Himalaya with decreasing precipitation amounts from the west (Modi Khola catchment) to the east (Imja Khola catchment).

3.2.1 Air temperature

The pre-monsoon season, from March to mid-June, is characterised by a gradual increase in air temperature. The monsoon season, from mid-June to the end of September, is dominated by positive values of air temperature. In this season, the diurnal variation of the air temperature is generally very small due to a thick cloud cover (Shiraiwa et al., 1992). The monsoon season is finished at the end of September and is followed by the post-monsoon season, from October to December, which is characterised by fine weather. The air temperature decreases in this period and the winter season begins in January. Figure 3.3 compares the mean monthly air temperature values calculated for the respective investigation periods of the catchments studied.

3.2.1.1 Langtang Khola catchment

The mean daily air temperature at the SGHU station is 0.2°C in the dry season from October to June and 8.4°C in the monsoon season. The long-term mean air temperature from 1987 to 1998 was 1.8°C. Shiraiwa et al. (1992) reported a mean monthly air temperature of approximately −10.0°C during the winter period at three stations in the valley at an altitude of between 5090 m a.s.l. and 5180 m a.s.l. during their study period June 1989 to March 1991. Air temperature shows distinctive altitude dependence with a mean annual air temperature from June 1989 to March 1991 of 1.9°C at the SGHU station and −3.5°C at 5090 m a.s.l.. Based on the measurements conducted by Shiraiwa et al. (1992) a mean annual gradient can be calculated as −0.46°C/100 m. Sakai et al. (2004) give a lapse rate of −0.5°C/100 m for the monsoon season 1996.

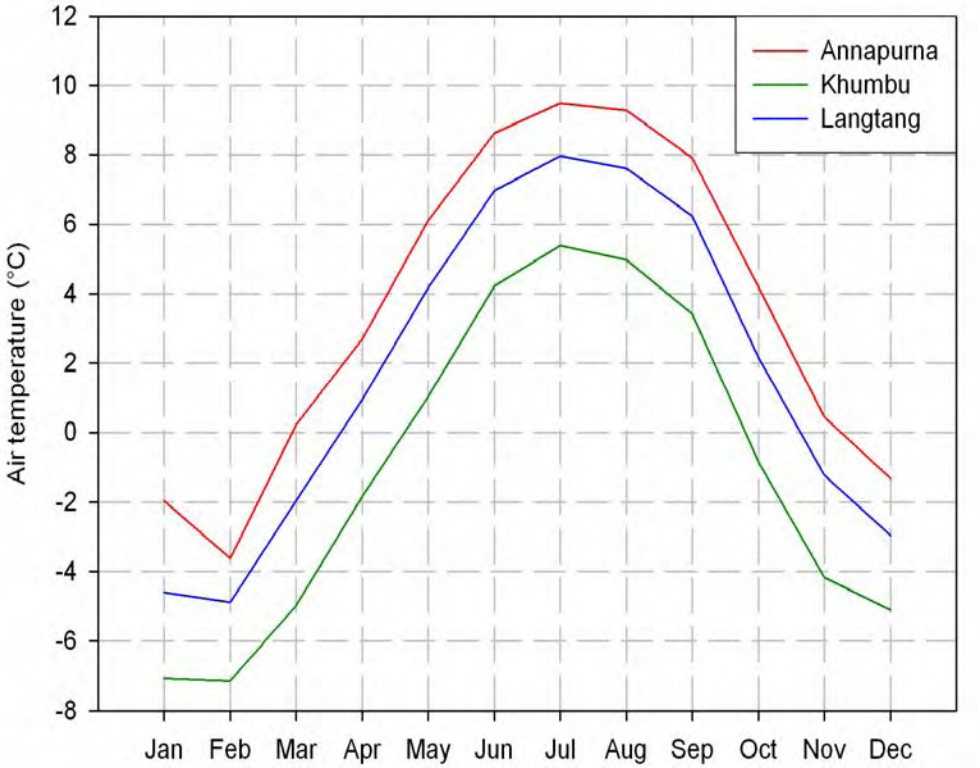

Figure 3.3: Mean monthly air temperature of the investigated catchments

3.2.1.2 Modi Khola and Imja Khola catchments

Air temperature at the SGHU station in the Modi Khola catchment is slightly higher than in the Langtang Khola catchment with an annual mean of 3.5°C. Mean daily air temperature in the dry season is 0.8°C while it is 8.9°C during the monsoon season.

The SGHU station in the Imja Khola catchment is the highest station in the Nepalese Himalaya. Thus, mean annual air temperature is the lowest of the three stations with –0.9°C. The mean air temperature of the dry season is –3.7°C and 4.6°C during the monsoon season.

3.2.2 Precipitation

Precipitation is primarily influenced by the monsoon with the highest daily occurrence probability of precipitation in July and August, as shown in Figure 3.4. An exception is the Annapurna catchment with a second high value in April. However, data quality is questionable in this catchment. Data availability does not allow the calculation of daily occurrence probabilities in this catchment either. Precipitation in the summer monsoon period is triggered mainly by convective clouds. In the pre-monsoon season, the maximum daily amount of precipitation becomes smaller compared to the winter season, while the number of days with precipitation increases month by month. From June to August precipitation is high in total and occurs almost every day. In the later part of the monsoon season (September to October) the maximum daily amount is considerably greater, while the number of rainy days decreases gradually. In winter, precipitation is produced by the occasional passage of westerly troughs, which are called ‘western disturbances’ (Ramage, 1971). Precipitation occurs on only a few days. However, the maximum daily precipitation is rather high. The altitudinal

dependence of precipitation is strongly controlled by the characteristics of cumulus clouds and mountain-valley circulation. Only a few studies exist which examine the seasonal variation in altitudinal dependence of precipitation in the catchments studied. The western part of the Nepalese Himalaya receives more precipitation than the eastern part, as shown in Figure 3.4.

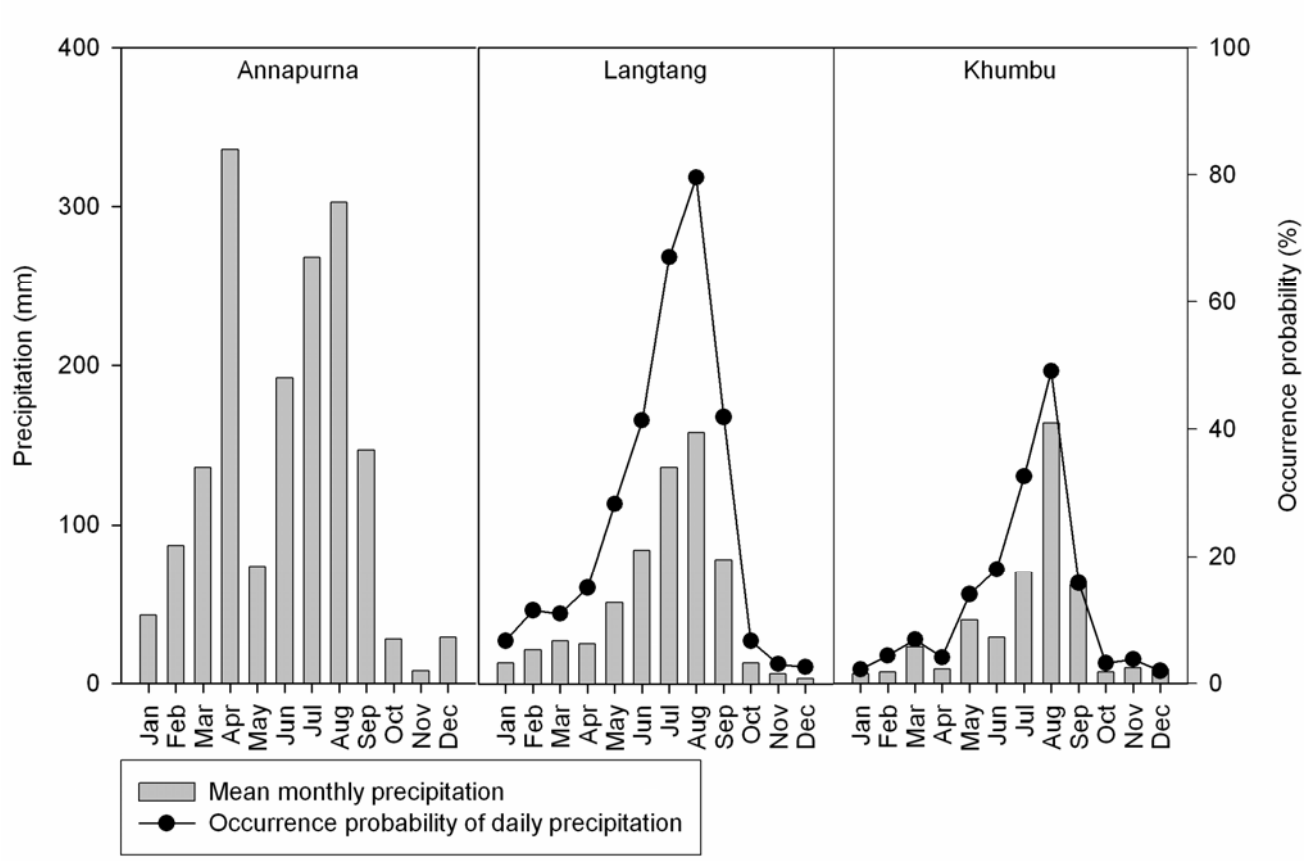

Figure 3.4: Mean monthly precipitation amounts and occurrence probabilities of daily precipitation of the investigated catchments

3.2.2.1 Langtang Khola catchment

In the period from 1988 to 1998, 74% of the annual precipitation fell during the monsoon season (Figure 3.4). Mean annual precipitation at the SGHU station can be estimated as 615 mm. The SGHU station is located at the bottom of the valley at an altitude of 3920 m a.s.l., where less precipitation falls from the cumulus clouds as compared to stations along the mountain slopes as reported by Seko (1987) and Ueno and Yamada (1990).

Seko (1987) and Shiraiwa et al. (1992) observed that the amount of precipitation at an altitude of 5090 m a.s.l. is almost 1.5 times higher than at the SGHU station (3920 m a.s.l) during the monsoon periods of 1986 and 1990. From June to September precipitation amounted to around 820 mm at 5090 m a.s.l. and to 540 mm at the SGHU station in 1990. From December to March the amount of precipitation at 5090 m a.s.l. was twice as high as at 3920 m a.s.l. in 1986. Based on these findings, a linear precipitation gradient can be estimated as 4.4%/100 m (related to the amount at 3920 m a.s.l.) as an annual mean (Ueno et al., 1993). Precipitation amounts generally decrease from the west to the upper parts of the valley in the north-east. The upper parts of the valley at an altitude of 5300 m a.s.l. receive almost the same amount of precipitation as the SGHU station. This is because less moist air is conveyed to the upper part

of the valley by monsoonal circulations prevailing from the south. A mountain barrier running west-east at the southern side of the valley prevents moisture from penetrating into the uppermost reaches of the valley. The upper part of the valley receives approximately two-thirds of the precipitation of the middle reaches (Shiraiwa et al., 1992). Relatively small differences in the amount of precipitation are reported for the south- and north-facing slopes of the valley. The described altitudinal and spatial distribution of precipitation was found to be valid for liquid as well as for solid precipitation.

3.2.2.2 Modi Khola and Imja Khola catchments

The Modi Khola catchment receives the most precipitation of the catchments studied. Data availability, however, is the worst in this catchment. Therefore, only data from 1991 to 1994 were used for model application and for statistical analyses. The daily occurrence probability of precipitation cannot be calculated due to the high number of missing values and cumulated precipitation amounts. Mean annual precipitation amounts equal 1647 mm, whereas only 55% falls during the monsoon season. There is a secondary precipitation peak in April but the reliability of the data base is questionable for this month.

The driest catchment is the Imja Khola catchment with a mean annual precipitation of 320 mm (at 4355 m a.s.l.) in the period from 1987 to 1995. 67% of the annual precipitation falls during the monsoon season. Bollasina et al. (2002) observed an annual average precipitation amount of 465 mm from 1994 to 1999 at their station at 5050 m a.s.l. in the close vicinity of the Imja Khola catchment. Further, they found that 90% of precipitation falls between June and September.

3.2.3 Evapotranspiration

Evapotranspiration was measured at the Lirung glacier and at the SGHU station in the Langtang Khola catchment at altitudes of 4190 m a.s.l. and 3920 m a.s.l. respectively. Sakai et al. (2004) observed an average daily actual evaporation of 4.5 mm/day at the SGHU station and 1.99 mm/day at the Lirung glacier from July to August 1996. Observations were carried out with lysimeters, which are plastic cylinders 10 cm in depth and 16.7 cm in diameter. The edge was set at the same level as the ground surface. It was filled with debris or soil. Evaporation was obtained from precipitation and percolated water, which was collected in another cylinder below the lysimeter. During the observation period, 59% of precipitation evaporated at the SGHU station while evapotranspirated water accounted for 25% at the Lirung glacier. However, only 14.6% of the entire catchment area is below 4500 m and as evaporation generally decreases with elevation and with the presence of snow and ice covers, this term plays a minor role in the water balance (Lang, 1981). There are no data available from the other catchments.

3.3 Hydrology

The Snow and Glacier Hydrology Unit (SGHU) has collected gauge height data in the three catchments. Discharge is estimated from gauge height and rating curves as described in Section 6.2. Table 3.3 summarises the discharge characteristics of Langtang Khola, Modi Khola and Imja Khola.

Table 3.3: Runoff characteristics of the catchments for the periods given in Table 3.1

		Modi Khola	Imja Khola	Langtang Khola
Easting *		83 57 00	86 56 40	85 33 00
Northing *		28 31 00	27 53 40	28 13 00
Altitude *	(m a.s.l.)	3470	4355	3800
HQ	(m^3/s)	27	16	23
MHQ	(m^3/s)	24	13	19
MQ	(m^3/s)	10	4	7
MNQ	(m^3/s)	4	1	2
NQ	(m^3/s)	2	0.5	1

* of gauging station

Several instantaneous floods occurred in the catchments. They have the typical flash flood characteristic with a fast rise and decline, usually without a corresponding precipitation event, such as a glacier lake outburst flood (GLOF). In the last half-century, several glacial lakes have developed in the Hindu Kush Himalayas and the Tibetan Himalayas. This can be attributed to the effect of recent global warming. The glacial lakes have formed at the glacier terminus due to the recent retreat of glaciers. The majority of these glacial lakes are dammed by unstable moraines, which were formed by the glaciation of the Little Ice Age. Occasionally a lake bursts releasing large amounts of its stored water, which causes serious floods downstream along the river channel. This phenomenon is recognised to be a common problem in Hindu Kush Himalayan countries such as Nepal, India, Pakistan, Bhutan, and China (Tibet) (ICIMOD/UNEP, 2002). The sudden break of a moraine may generate the discharge of large volumes of water and debris, causing floods.

In order to distinguish the hydrological seasons from a full year's discharge, accumulated values of mean daily discharge (m^3/s) for the respective observation period of the catchments are plotted against time as shown in Figure 3.5 for the Langtang Khola and the Imja Khola catchments. The figure shows a rapidly increasing rate of the accumulated values in the monsoon season and a comparatively slowly increasing rate in winter. The discharge regimes can be classified as glacial with maximum discharge from July to August and minimal discharge in winter (Figure 3.5). These analyses were conducted for the Langtang Khola and Imja Khola catchments because discharge data availability of the Modi Khola catchment is not appropriate for such analyses.

3.3.1 Langtang Khola catchment

During the winter season precipitation falls as snow and therefore it is stored until melting starts, usually in March. From the beginning of June to the end of September 65% of the annual discharge is observed, while in July and August it is 37%. This is quite low compared to glacierized catchments in the European Alps and can be explained by the high winter runoff. In the Rofenache catchment (Austria) 56% of the discharge occurs in July and August (Schulz, 1999). Both catchments have nearly the same extent of glacier cover, 46% and 41% respectively. For the same reason the Pardé coefficients for July and August are relatively low for a glacierized catchment. Motoyama et al. (1987) determined a constant decreasing rate of the winter recession curve, with a recession rate of 0.01 day^{-1}. The half-value period of decreasing discharge is 67 days, from late December to late March, when the catchment is covered by snow. The constant rate implies that runoff processes are maintained throughout

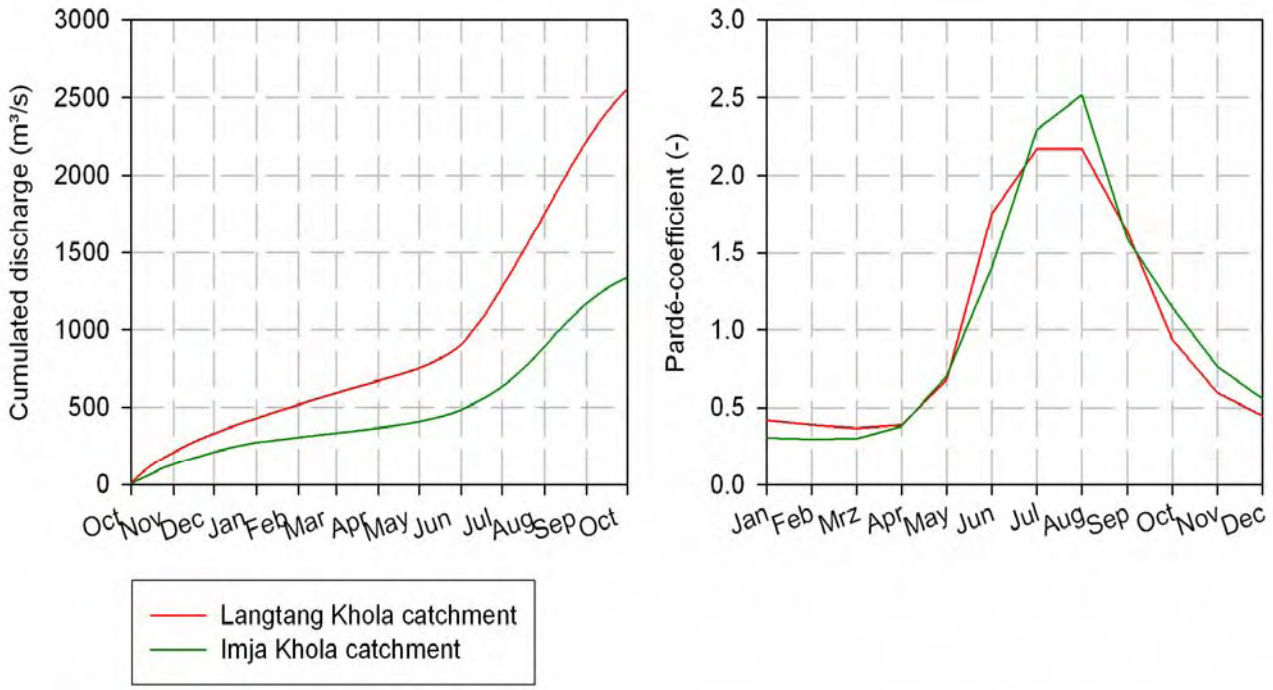

Figure 3.5: Accumulated mean discharge values (left) and runoff regimes of Langtang Khola (1987-1998) and Imja Khola (1988-1995) after Pardé (MQ_{month}/MQ_{year}) (right)

the winter. Consequently, winter runoff is characterised by a constant recession rate with no inflow of rainwater and meltwater under the condition of air temperature below melting point. The mean discharge from December to the end of April is 2.8 m³/s. About 16.6% of annual discharge occurs in this period. Motoyama et al. (1987) estimated the minimum runoff as 1.3 mm/day, referring to the glacier area in their observation period from July 1985 to July 1986. The winter discharge is attributed to the outflows of englacial water stored during the monsoon season and to meltwater from the glacier bottom due to geothermal heat. Paterson (1969), however, determines maximum icemelt caused by geothermal heat as 6 mm per year. The generated runoff of the glacier area of the Langtang Khola catchment would amount to less than 0.007 mm/day (ice density = 0.91 g/cm³). This amount can be neglected compared to the minimum runoff of 1.3 mm/day. It is therefore reasonable to assume a rather significant water storage mechanism in glaciers as postulated by Tangborn and Rana (2000). Drilling results during the post-monsoon season in the ablation zone of the Yala glacier revealed the existence of abundant water in the glacier body (Iida et al., 1984).

3.3.2 Imja Khola catchment

The hydrological characteristics are quite similar to those of the Langtang Khola catchment. Here, 64% of the annual discharge occurs from June to September and 40% of the annual discharge is observed in the monsoon months of July and August.

Winter discharge is also relatively high and amounts to 15% of the annual discharge. The mean discharge from December to April is 1.3 m³/s.

3.4 Conclusions

The three catchments show different climatic conditions and for this reason were chosen for the application of the hydrological models. Data availability and quality are the most appropriate in the Langtang Khola catchment and the development work of the TAC^d model was done using this data base.

Detailed hydrogeological or geological maps are not available, thus the knowledge about the catchments is limited to topographical maps, field visits and catchment descriptions in literature which concentrate mainly on the climatological characteristics of the catchments. The primary demands on model development must therefore be the integration of physiographic and topographic information in the mathematical description of the melt and runoff generation processes. The conceptualisation of the runoff generation routine of TAC^d has to account for the distribution of water within a year. Limited knowledge about runoff generation processes of the catchments implies the delineation of the hydrological response units based on topographical and land cover maps. The dominant land cover types are glaciers and barren land which are considered in the modification of TAC^d. Glaciers are covered by debris layers which affect meltwater production. Regionalisation of meteorological input data must be adapted to the altitude range of the catchments studied.

4 The catchment models TAC^d and HBV-ETH

In this study two models were used for runoff simulation: HBV-ETH and TAC^d. The HBV-ETH precipitation-runoff model is a version of the widely used HBV model with special features to calculate the runoff of glacierized catchments. The development of the HBV model began in 1973 at the SMHI (Swedish Meteorological and Hydrological Institute) (Bergström, 1976 and 1992) and was further refined at the ETH Zurich (Braun and Renner, 1992; Hottelet et al., 1993). Altitude belts and orientation classes (North, South, East, West) are used for spatial discretization of the snow and glacier routine. The glacier area is considered as a percentage of the area of each altitude belt and orientation class. A temperature-index method is used for the calculation of melt as in TAC^d, whereas debris-covered glaciers are not considered specifically in the version of the HBV-ETH model applied here.

The soil routine and the runoff generation routine are not spatially distributed. An upper and a lower storage simulates the runoff generation. HBV-ETH has been successfully applied in various Alpine and Himalayan catchments (Braun et al., 2000).

The catchment model TAC (tracer-aided catchment model) was developed by Uhlenbrook and Leibundgut (2002) as a semi-distributed model. It belongs to the group of conceptual or grey box models. The model was developed further by Roser (2001), who introduced the raster-based distributed structure of the model (TAC^d) (Uhlenbrook et al., 2004; Uhlenbrook and Sieber, 2004). TAC^d was applied successfully to catchments in different climatic regions (Beek, 2004; Ott and Uhlenbrook, 2004; Johst et al., 2005). Wissmeier (2005) implemented solute transport to the model structure.

Model structure and conceptual ideas of the routines are described with the help of TAC^d with parameter names as used in the model script. The concepts of HBV-ETH are quite similar and therefore not described separately. The main differences are the runoff generation routine and the spatial discretization of both models. Table 4.1 compares selected features of TAC^d with those from the HBV-ETH model. Detailed information about the HBV-ETH model can be found in Konz (2003). Modifications of routines of TAC^d and specific adaptations to the conditions of Himalayan catchments are explained in Chapter 5.

Table 4.1: Comparison of TAC^d with the HBV-ETH model

	TAC^d	**HBV-ETH**
Regionalisation of meteorological input data	Horizontal and vertical gradients	Vertical gradients
Calculation of potential evapotranspiration	Calibrated sinusoidal course	Calibrated sinusoidal course
Calculation of snow and icemelt	Temperature-index method	Temperature-index method
Spatial distribution of snow and glacier routine	Raster-based	Altitude belts and orientation classes
Debris-covered glaciers	Considered	Not considered
Spatial distribution of soil routine	Raster based, HRUs	lumped
Spatial distribution of runoff generation routine	Raster based, HRUs	lumped

4.1 Concepts and structure of TAC^d

The conceptual structure of TAC^d consists of individual routines (Figure 4.1). The sequentially linked routines represent the main parts of the land phase hydrological cycle and are mostly adopted from other conceptual models (WaSiM ETH: Schulla, 1997; HBV: Bergström, 1976 and 1992).

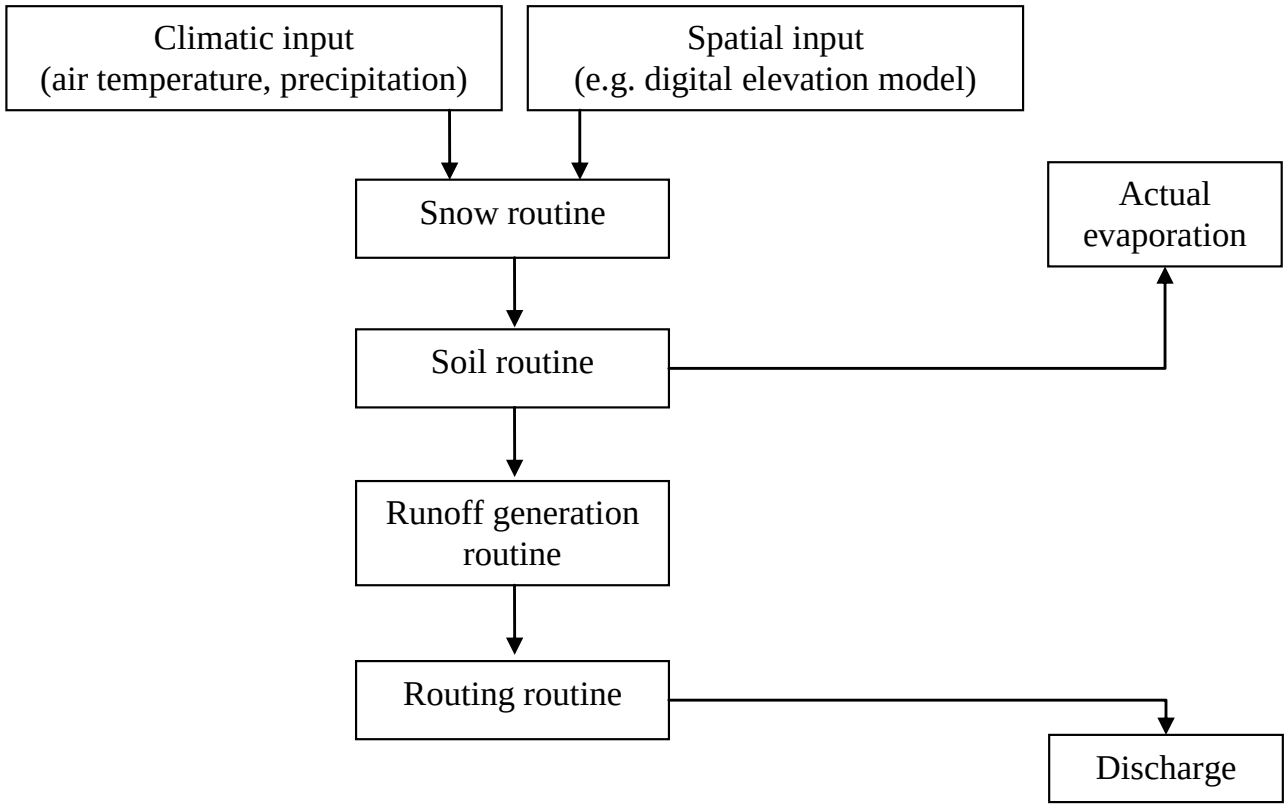

Figure 4.1: Schematic model structure of TAC^d

The model consists of a snow routine to calculate snow accumulation and ablation and it contains a soil routine to determine soil moisture and actual evaporation. The runoff routine is the core of the model. It was developed based on tracer experiments and it attempts to simulate the dynamic of the runoff generation processes with simple linear storages. The routing routine simulates the wave propagation in the channel network. Apart from the main result, which is the simulated discharge, the model also yields intermediary results such as storage terms, soil moisture and snow cover.

4.2 Routines of TAC^d

4.2.1 Snow routine

The snow routine was mainly adopted from the HBV model (Bergström, 1976 and 1992). The TAC^d model uses a temperature-index method to calculate the snowmelt. Input data are daily

values of air temperature and precipitation. The output is the effective precipitation (InSoil), consisting of liquid precipitation and snowmelt. It is the input into the soil routine.

The following processes are considered:

a) Differentiation between liquid and solid precipitation
b) Correction of solid precipitation
c) Estimation of snowmelt
d) Estimation of storage and refreezing of liquid water in the snow cover.

a) Differentiation between liquid and solid precipitation

Precipitation is considered to be solid if air temperature is below the threshold value TT. TT is an empirical parameter which has to be determined by calibration. This parameter is also used in the degree-day method as a general temperature correction.

b) Correction of solid precipitation

The amount of a day's solid precipitation is corrected by the parameter SFCF. Systematic errors, such as unsatisfactory representativity of the climatic station or measuring errors of solid precipitation, can be corrected with the help of the precipitation correction factor (Sevruk, 1985):

$$Prec = PrecStation \cdot SFCF \quad \text{if air temperature} < TT \tag{4.1}$$

Prec:	Corrected solid precipitation (mm/time step)
PrecStation:	Measured precipitation (mm/time step)
SFCF:	Snowfall correction factor (-)

Solid precipitation is added to the snowpack storage (SnowPack) in units of millimeter water equivalent.

c) Estimation of snowmelt

The TAC^d model uses a temperature-index method, the so-called degree-day method (Zingg, 1951), and the energy for snowmelt is derived directly from the air temperature. The required energy available for meltwater production, however, is best determined via the energy balance as approximately 60 to 80% of the energy originates from radiation absorption (Paterson, 1969). Energy balance methods to calculate snowmelt require data which are not available in the Himalayan catchments. The calculation of snowmelt amount (MeltWaterSnow) is carried out as the product of the degree-day factor and the difference between air temperature and the threshold value TT, if the air temperature is above TT (Uhlenbrook, 1999):

$$MeltWaterSnow = Cfmax\ (Temp - TT) \tag{4.2}$$

MeltWaterSnow:	Amount of snowmelt (mm/time step)
Cfmax:	Degree-day factor (mm/(°C day))
Temp:	Mean daily air temperature (°C)
TT:	Threshold temperature or general temperature correction (°C)

d) Estimation of storage and refreezing of liquid water in the snow cover

The snow cover is able to store liquid water due to its porous structure. The water content of snow cover (WaterContent) is calculated with the parameter CWH (coefficient of

water-retention capacity) as a fraction of the water equivalent of the actual snowpack (Uhlenbrook, 1999):

$$WaterContent = CWH \cdot SnowPack \tag{4.3}$$

WaterContent: Water content of snow cover (mm)
CWH: Coefficient of water-retention capacity (-)
SnowPack: Water equivalent of snowpack (mm)

The water content of snow cover is the second storage in the snow routine. In the case of the presence of a snow cover and air temperature above the threshold temperature, calculated meltwater and rain is added to the water content until the water-retention capacity is reached. Additional water, either as rain or meltwater, enters the following routine directly.

If the air temperature is below the threshold temperature, liquid water stored in the snow cover refreezes. Refreezing (Refreeze) is controlled by the parameter CFR (refreezing coefficient) and, together with meltwater (MeltWaterSnow), is the linkage between the two storages of the snow routine (Uhlenbrook, 1999; Wissmeier, 2005):

$$Refreeze = CFR \cdot Cfmax \cdot (TT - Temp) \tag{4.4}$$

Refreeze: Refreezing water in snowpack (mm/time step)
CFR: Refreezing coefficient (-)

4.2.2 Soil routine

The output of the snow routine is the input into the soil routine (InSoil) which was adopted from the HBV model (Bergström, 1976 and 1992).

The following processes are conceptualised:

a) Calculation of soil moisture storage, infiltration and percolation through the soil
b) Calculation of actual evaporation

a) Calculation of soil moisture storage, infiltration and percolation through the soil

The maximum storage capacity of the soil moisture storage is determined by the parameter FC (field capacity). Infiltration is calculated dependent on the ratio between actual soil moisture (SoilMoisture) and field capacity (FC) by a non-linear function. The parameter BETA accounts for different infiltration characteristics of soils. The smaller the BETA, the more water is sent to the next routine even when soil moisture is small compared to field capacity (Uhlenbrook, 1999):

$$\frac{ToRunoffGeneration}{InSoil} = \left(\frac{SoilMoisture}{FC} \right)^{BETA} \tag{4.5}$$

ToRunoffGeneration: Infiltration into runoff generation routine as fraction of the actual soil moisture (mm/time step)
InSoil: Input into soil routine (mm/time step)
SoilMoisture: Soil moisture storage (mm)
FC: Maximum of soil moisture storage (mm)
BETA: Empirical parameter (-)

This conceptualisation of the infiltration and percolation process is an important prerequisite for calculating infiltration in high alpine soils where macropores and preferential pathways are common. Due to the spatially variable parameterisation of BETA and FC, different soil reactions can be simulated for each cell.

b) Calculation of actual evaporation

Actual evaporation is calculated within the soil moisture routine dependent on the parameter LP. LP defines the fraction of FC above which actual evaporation is supposed to be equal to the potential evaporation. If the actual soil moisture (SoilMoisture) is below the product of LP and FC, a linear reduction of potential evaporation is initialized (Figure 4.2) (Uhlenbrook, 1999):

$$ActET = PotET \qquad \text{if SoilMoisture} \geq LP \bullet FC \qquad (4.6)$$

$$ActET = PotET \cdot \frac{SoilMoisture}{LP \cdot FC} \qquad \text{if SoilMoisture} < LP \bullet FC \qquad (4.7)$$

ActET: Actual evaporation (mm/time step)
PotET: Potential evaporation (mm/time step)
LP: Reduction parameter of field capacity (-)
FC: Field capacity (mm)

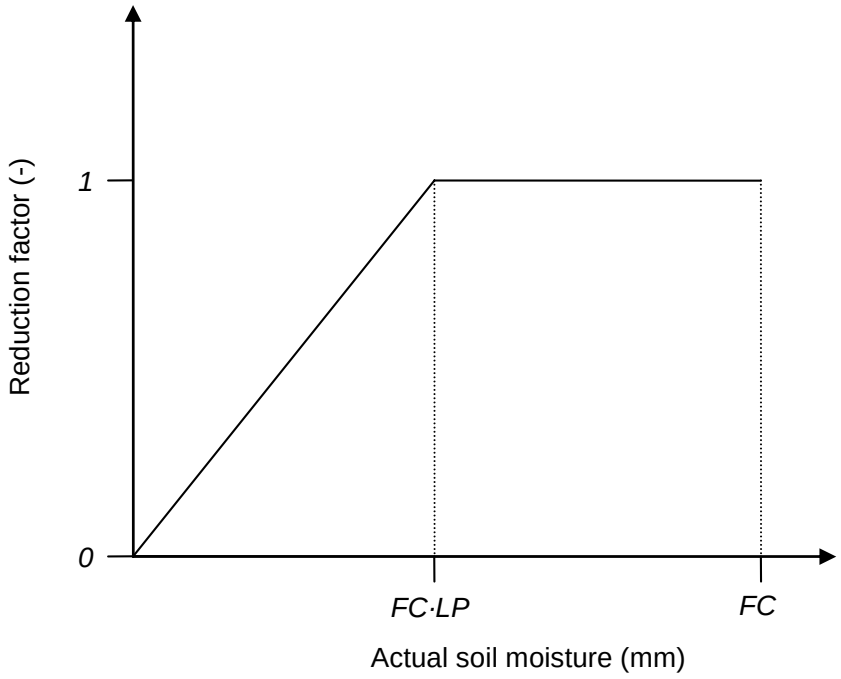

Figure 4.2: Reduction of potential evaporation depending on soil moisture (according to Uhlenbrook, 1999)

Actual evaporation is subtracted from the soil water storage (Equation 4.8).

$$SoilMoisture = SoilMoisture - ActET \qquad (4.8)$$

There is no evaporation if a snow cover exists. This assumption is justified as over snow evaporation and condensation generally cancel each other out over longer time periods. Evaporation can be an important factor, as regards energy, over a short period, but as a

mass balance component the amount of evaporation is small compared to, for instance, precipitation in high alpine areas (Lang, 1981). The output of the soil routine (ToRunoffGeneration) is directed to the runoff generation routine.

4.2.3 The runoff generation routine

In this section the general ideas behind the conceptualisation of the runoff generation routine are explained, and generalised parameter names are used in the description and in the equations. Parameter names of the runoff generation routine consist of a specific part and a general part. The star (*) replaces the specific part of the parameter name.

The runoff generation routine of the TAC[d] model refers to the hydrological classification of the catchment according to hydrogeologic and physiographic basin characteristics. This divides the catchment into different hydrological response units (HRU) and enables a process-oriented runoff simulation. The runoff generation processes of each HRU are conceptualised differently by linear storage concepts. Each cell consists of either a simple linear storage or a vertically arranged storage cascade, interconnected via vertical and lateral fluxes. The water content of each storage (*_box) is determined by the output of the soil routine (ToRunoffGeneration), lateral fluxes and by the storage characteristics. These are defined by an upper limit of storage capacity (*_H), by a storage coefficient (*_K) and, in the case of a storage cascade, vertical fluxes are controlled by a percolation parameter (*_P). The conceptual idea for storage outflow is the simple differential equation of a linear reservoir (Equation 4.9).

$$-\frac{dV}{dt} = k \cdot V = Q \tag{4.9}$$

V: Storage level (mm)
t: Time step (time step)
k: Storage coefficient (1/time step)
Q: Flux (mm/time step)

With the integral solution for an instantaneous Dirac impulse at time t = 0:

$$V(t) = V_0 \cdot e^{-kt} \tag{4.10}$$

V(t): Storage level at time t (mm)
V_0: Storage level at time t = 0 (mm)

Figure 4.3 shows a linear reservoir and the graphical visualisation of its response function (Equation 4.10).

These parameters and the arrangement of storage forms are assigned separately for the cells of each hydrological response unit. Runoff (Q_*) from these storages at time t is meant to be proportional to the water level of the respective storage (Equation 4.11).

$$Q\_* = *\_box \cdot *\_K \tag{4.11}$$

Q_*: Runoff of storage (mm/time step)
*_box: Water content of storage (mm)
*_K: Storage coefficient (1/time step)

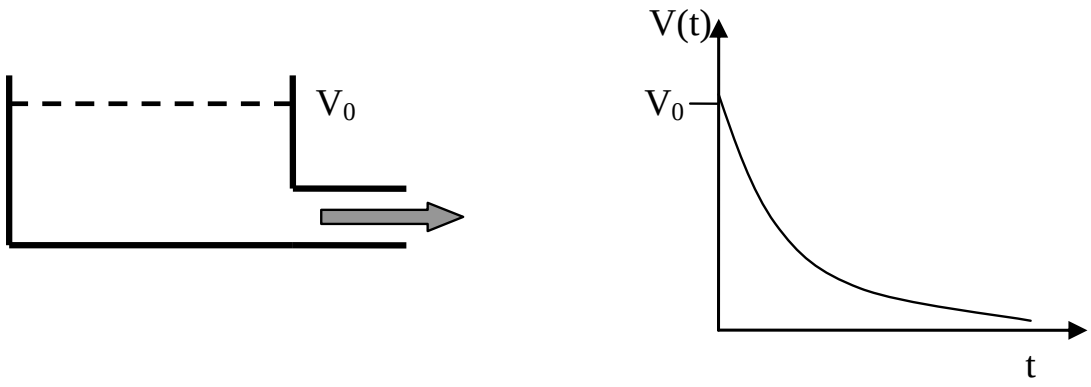

Figure 4.3: Linear reservoir and its response function to an instantaneous Dirac impulse (according to Seibert 2002, revised)

If the upper limit of the storage is reached the additional water is added to Q_* (Equation 4.12). The process of saturated overland flow and the temporary extension of saturated zones can be simulated by an overflowing storage. This mainly happens at convergent cells like valley bottoms.

$$Q\_* = Q\_* + Overflow \tag{4.12}$$

Overflow: Overflow of the storage (mm/time step)

The direction of lateral flows is given by a local drain direction network (ldd). This drainage network can be created in PCRaster based on the digital elevation model. For the creation of the ldd a common D8 algorithm is used, where flows can be directed in eight different orthogonal and diagonal directions, depending on the steepest slope between the central cell (ldd code 5) and the neighbouring cells (ldd code 1 to ldd code 9) (PCRaster 2004).

Fluxes are redistributed into the storages according to the respective runoff generation type of the downstream cell. Thus, lateral fluxes are additional inputs to the storages (*_box) of each cell and therefore contribute to their filling.

4.3 Conclusions

The catchment model TAC^d is designed for process-oriented runoff simulation. Based on the distributed structure of TAC^d the catchment is discretized into cells of equal hydrological response, which are dominated by specific runoff generation processes. Storage analogies with different vertically and horizontally arranged and linked storages can be parameterised differently referring to the specific characteristics of the hydrological response unit. Lateral flow forms a storage cascade.

The modular structure of TAC^d enables an easy adaptation to regional catchment characteristics. Due to its complex distributed structure, especially of the runoff generation routine, thorough knowledge of runoff generation processes of a meso-scale catchment is a prerequisite for the application of TAC^d. Thus the reliable identification of runoff generation types via topographical, geological and pedological maps, aerial photography, remote sensing and personal user knowledge is essential (Wissmeier, 2005).

The HBV-ETH model is a well-known catchment model and most of the modifications of TAC^{d}, described in the following chapter, are taken from the conceptual ideas of this model. The main differences between both models are the runoff generation routine and the spatial discretization.

Interaction between routines in the case of error compensation is a well-known problem (Braun and Aellen, 1990) and must be considered in the calibration procedure. For this reason, sensitive parameters should be taken from the literature if available and ratios between storage parameters of the HRUs fixed before calibration. Over-parameterisation is to be avoided as far as possible and plausibility of parameters taken into account during the calibration procedure.

5 Modifications of TAC^d

The catchment model TAC^d was developed for the lower alpine conditions of the Black Forest, Germany (Uhlenbrook et al., 2004). The sophisticated routines for calculation of potential evaporation or for regionalisation of climatic data require input data which are not available in the Nepal Himalayas. Therefore it was necessary to simplify or replace routines of TAC^d for application to the Himalayan catchments. The development work focuses on incorporating as much physiographic information as possible to provide a physical base for process-oriented simulation of runoff generation as well as of snow and ice ablation or accumulation. In addition to Chapter 4, only the recent modifications of the TAC^d routines are explained in this chapter. The equations are written in PCRaster programming language with original variable names.

5.1 Regionalisation of meteorological data

Daily data of air temperature and precipitation are available at one meteorological station in the catchments studied (Chapter 3). For this reason, regionalisation of these data is based on vertical and horizontal gradients taken from the literature.

5.1.1 Regionalisation of precipitation

Measuring precipitation is a challenging task, especially in alpine regions. Nevertheless, precipitation data are a key element of runoff simulation as they are the main input to the model aside from glaciermelt. Systematic measurement errors occur and have to be corrected. The following components are responsible for these errors:

1. Deformation of wind field over the precipitation gauge orifice
2. Evaporation losses and splash losses
3. Interception losses of measuring instrument
4. Observer errors (e.g. variation in observation time)
5. Instrument errors (e.g. poor calibration, technical problems)

The list is not considered to be complete but shows the main sources of errors. Due to these errors precipitation is usually underestimated. Sevruk (1985) pointed out that, in the case of the Hellmann precipitation gauge, points one and three are the most important. Various methods to correct these errors are discussed in the literature (Sevruk, 1985; Richter, 1995) and mainly depend on wind speed measurements. These data are not available in the catchments studied. Another problem is the representativity of the climatic station. In a high alpine catchment this might be the major problem in the determination of basin precipitation. As shown in section 3.2.2.1, there are considerable differences in precipitation amounts in different parts of the catchment. In order to compensate for systematic errors and the lack of representativity of the climatic station, an empirical precipitation correction factor (PCF) similar to the snowfall correction factor (SFCF) was introduced:

$$PrecCor = PrecStation \cdot PCF \quad \text{if air temperature} \geq TT \tag{5.1}$$

PrecCor: Corrected liquid precipitation (mm/time step)
PrecStation: Measured precipitation at climatic station (mm/time step)
PCF: Precipitation correction factor (-)

Shiraiwa et al. (1992) observed an increasing amount of precipitation with altitude in the Langtang Khola catchment. These observation results imply the application of an altitude-dependent correction of precipitation via a vertical gradient for solid and liquid precipitation. This gradient reflects the increasing amount of precipitation in comparison to the measured value at an altitude of 3920 m (Equation 5.3). According to Shiraiwa et al. (1992) there is also a horizontal gradient. Thus, the measured amount of precipitation at the SGHU station is corrected for each cell depending on the horizontal distance between target cell and climatic station (Figure 5.1).

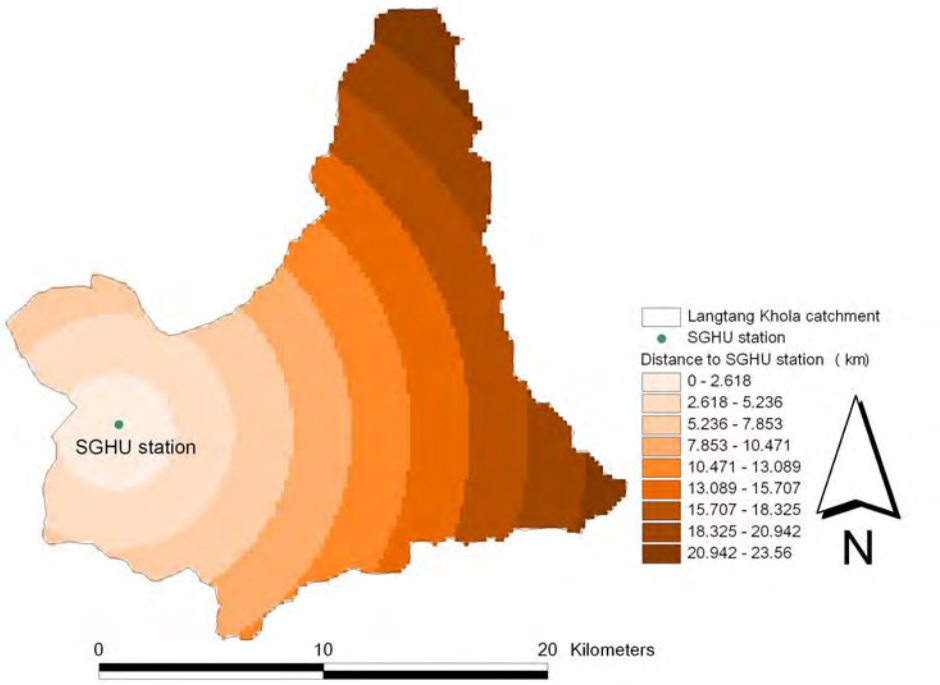

Figure 5.1: Horizontal distance between SGHU station and target cell at Langtang Khola catchment

Precipitation declines towards the upper reaches of the catchment (Shiraiwa et al., 1992) with a negative horizontal gradient (PHorizGrad) in percent of the actually measured value at the climatic station per 1000 m distance (Equation 5.2).

$$PrecHorizontal = PrecCor \cdot (1 + (PHorizGrad \cdot DistToClim) \quad (5.2)$$

PrecHorizontal: Horizontally corrected precipitation (mm/time step)
PHorizGrad: Horizontal gradient ((%/1000m)/100)
DistToClim: Horizontal distance between target cell and climatic station (km)

Vertical correction is conducted after the horizontal correction.

$$PrecAltitude = PrecHorizontal \cdot (1 + (PGrad \cdot AltDiff) \quad (5.3)$$

PrecAltitude: Altitude-corrected precipitation (mm/time step)
PGrad: Vertical gradient ((%/100m)/100)
AltDiff: Vertical distance between target cell and climatic station (m)

PrecAltitude or PrecHorizontal is set at zero if Equations 5.3 and 5.2 become negative. Horizontal and vertical gradients are constant for the entire simulation period.

The amount of precipitation cannot increase constantly with altitude due to the declining water-retention capacity of the air caused by decreasing air temperature. Therefore, PrecAltitude is considered to be constant at altitudes above 5000 m.

5.1.2 Regionalisation of air temperature

Air temperature is distributed with elevation by applying a fixed lapse rate (TGrad) as follows:

$$Temp = TempStation + (AltDiff \cdot TGrad) \quad (5.4)$$

Temp: Altitude-corrected air temperature (°C)
TempStation: Measured air temperature at climatic station (°C)
TGrad: Vertical air temperature gradient (°C/100m)

5.2 Calculation and regionalisation of potential evapotranspiration

Previous versions of TAC[d] calculated potential evapotranspiration using approaches such as Penman-Monteith (Ott and Uhlenbrook, 2004) or Turc-Wendling (Uhlenbrook and Leibundgut, 2002; Johst et al., 2005). In the Himalayan catchments, neither method is applicable due to the absence of data. Braun (1985) applied a triangular function to calculate potential evapotranspiration. The parameter ETmax is considered a free parameter defining the maximum amount of potential evapotranspiration. A more realistic calculation of potential evapotranspiration can be achieved by a sinusoidal function (Hottelet et al., 1993). Maximum potential evapotranspiration is defined by the parameter (ETmax) peaking on 1 August (Figure 5.2). ETmax is the amplitude of the sinusoidal function with a minimum on 1 February.

$$PotET = (ETmax \cdot 0.5) \cdot (1 + \sin((l/MaxDay \cdot 360) - (360/MaxDay \cdot CounterDay)) \quad (5.5)$$

PotET: Potential evapotranspiration (mm/time step)
ETmax: Maximum of potential evapotranspiration (mm/time step)
l: Day of maximum potential evapotranspiration (1 August = day 304 or 305)
MaxDay: Maximum days of the year (365 or 366)
CounterDay Day (starting from 1 October = day 272)

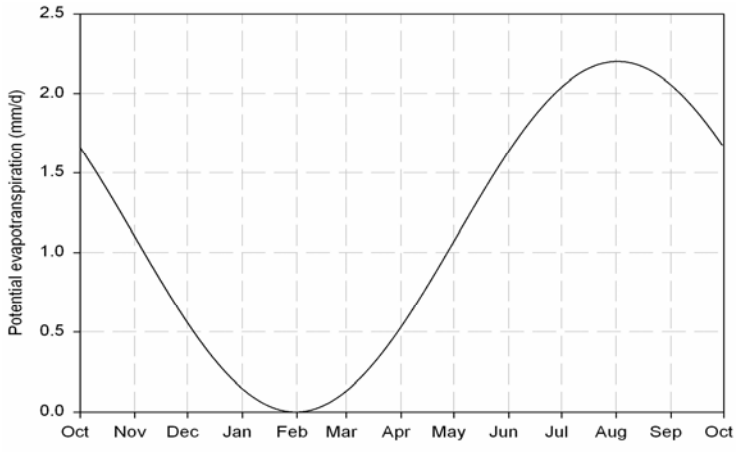

Figure 5.2: Potential evapotranspiration as a sinusoidal function

Detailed measurements of evapotranspiration reported in Gronowski (1992) justify the sinusoidal temporal distribution of potential evapotranspiration (Figure 5.3). Compared to Gronowski (1992), a shift of maximum potential evapotranspiration was necessary to adapt the function to high alpine climatic situations where a maximum of potential evapotranspiration usually occurs in August (Weber, 2004). Evapotranspiration of grassland in particular shows a strong correlation to net radiation (Figure 5.3).

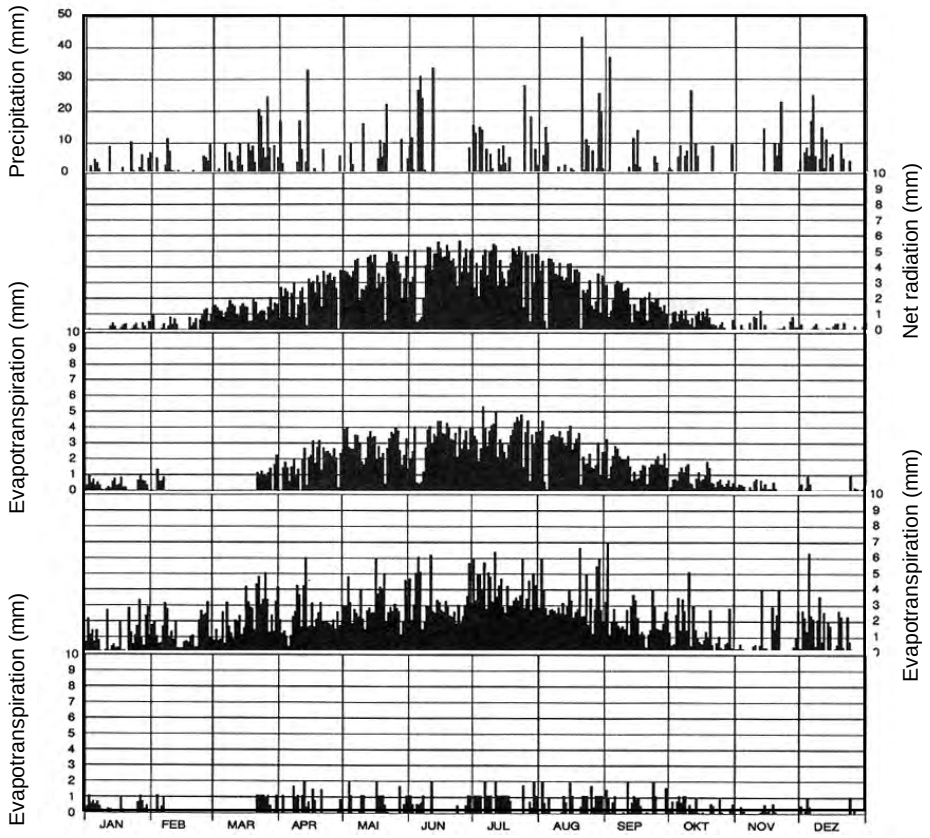

Figure 5.3: Comparison of daily evapotranspiration of different surfaces in the lower alpine region in Switzerland (Gronowski, 1992)

Potential evapotranspiration is regionalised via an altitude gradient. This altitude-dependent correction of potential evapotranspiration takes the temperature dependence of evapotranspiration into account. As temperature decreases with altitude, less energy is generally available for evapotranspiration. This implies an altitude-dependent correction of potential evapotranspiration as well.

$$PotETAltitude = PotET \cdot (1 + ETGrad \cdot AltDiff) \quad (5.6)$$

PotETAltitude: Altitude-corrected potential evapotranspiration (mm/time step)
ETGrad: Vertical gradient of potential evapotranspiration ((%/100m)/100)

5.3 The snow and glacier routine

5.3.1 Sunshine duration correction factor for temperature-index method

Glaciers are a form of long-term water storage. When snow does not melt completely, multi-year-old snow or firn is formed which is eventually transformed into ice. The melting of ice during the summer months then contributes to runoff, especially during times when snow has already melted. The amount of snow or ice meltwater is calculated here on the basis of the temperature-index method. Computations using air temperature as the sole index of melt energy stem from Zingg (1951), who introduced the degree-day factor. Air temperature measured at a station located downwards of the glacier provides more information about melting processes on the glacier surface than that which is measured at a station located directly on the glacier (Lang, 1968; Ohmura, 2001; Weber, 2004). Temperature measurements on the glacier yield lower values due to the cooling effect of the melting ice surface. A station which lies within the katabatic wind system of the glacier but not on the glacier itself is not exposed to these energy losses and is therefore more representative of the energy actually available. This prerequisite for the application of the degree-day method is fulfilled in all three Himalayan catchments.

Meltwater production in alpine regions, however, depends primarily on radiation as an energy source. Short-wave radiation balance over glaciers supplies up to 90% of available melt energy on Vernagtferner, Austrian Alps (Weber, 2004). Thus, short-wave radiation balance plays the most important role in meltwater production on alpine glaciers (Paterson, 1969). The intensity of short-wave radiation input for a single cell in the raster-based distributed catchment is strongly influenced by astronomical and physiographic parameters such as the diurnal and annual course of the sun, the steepness and orientation of the slopes, and the shadowing effects of surrounding mountains (Escher-Vetter, 2000). Therefore, emphasis is placed in this study on modelling the spatial distribution of meltwater production as a function of the sunshine duration of a day per cell. Consequently, the degree-day factor needs to be diversified according to sunshine duration. Cazorzi and Fontana (1996) suggested a radiation index based on clear sky radiation as an approach to fully distributed snowmelt modelling. They produced maps of mean monthly energy indices and incorporated a so-called “combined melt factor” to calculate snowmelt with air temperature as the only input variable. The “combined melt factor” is a modification of the classical degree-day factor. Hock (1999) proposed a further development of this idea, varying the melt factor on an hourly basis for each DEM cell according to temporal and spatial variation of clear sky direct radiation, calculated using standard solar algorithms. Braun et al. (1993) applied a sinusoidal course of the degree-day factor in the HBV-ETH model defined by two parameters for the minimum and the maximum of the sinusoidal function. This approach accounts for the longer periods of sunshine duration during the summer causing higher incoming short-wave radiation values; thus more energy for melting is available during summertime. Hottelet et al. (1993) introduced a parameter Rexp which is applied to the results of the degree-day method as a multiplicative factor in order to simulate different meltwater production rates of the exposition classes: northern-, southern-, eastern- or western-oriented slopes or horizontal planes. Meltwater production usually increases on south-facing slopes whereas it decreases on north-facing slopes, as compared to eastern- and western-oriented slopes or horizontal planes. Thus, the parameter Rexp is larger than one to simulate the increased melting of south-facing slopes. For north-facing slopes, the inverse value of Rexp (1/Rexp) is used because this value is smaller than one and therefore diminishes the meltwater production. Meltwater production on eastern- and western-oriented slopes and horizontal planes is not modified by Rexp (Rexp = 1.0). In the semi-distributed HBV-ETH model, only the above-mentioned orientation

classes are used to modify the meltwater production. The distributed spatial discretization of TAC^d allows the specific manipulation of the degree-day method for each cell. The modification of the classical temperature-index method can be seen as the combination of the above-mentioned approaches for distributed snowmelt modelling. Based on the digital elevation model (DEM), the potential sunshine duration is calculated by POTRAD 5 (Potential Radiation Equator Model; van Dam, 2004) taking into account the aspect of cells and sun position as well as the shading effects of mountains. Externally derived potential sunshine duration maps (Shade) are a further input to TAC^d and are used to derive cell-specific correction factors (RexpMap) for the degree-day method. Cells with long sunshine duration receive more short-wave radiation and thus can produce more meltwater than cells with less sunshine. Thirteen hours per day is, for instance, the maximum sunshine duration in Langtang Khola catchment; by contrast, there are periods of the year during which northern-oriented cells at the bottom of the valley receive no direct sunlight at all due to shading effects.

The calibration parameter Rexp in TAC^d is used to define the range of the temporal and spatial variable RexpMap. Rexp is assigned to cells with maximum sunshine (13 h) and therefore defines the maximum possible value of RexpMap. The minimum of RexpMap is determined using the inverse value of Rexp (1/Rexp) which is assigned to cells with minimum sunshine duration (0 h). The inverse value of Rexp as the minimum of RexpMap is justified because this value is less than one and therefore diminishes the meltwater production and no further calibration parameter is necessary. A linear relation between Shade and RexpMap is assumed (Equation 5.7, Figure 5.4) for the calculation of the maps of the correction factor.

$$RexpMap = ((Rexp-(1/Rexp))/(MaxShade-MinShade))\cdot(Shade-MinShade)+(1/Rexp) \quad (5.7)$$

RexpMap: Map stack of correction factor for degree-day method (-)
Rexp: Correction factor for cells with maximum potential sunshine duration (-)
MaxShade: Maximum potential sunshine duration (h/day): 13 h in the Langtang Khola catchment
MinShade: Minimum potential sunshine duration (h/day): 0 h in the Langtang Khola catchment
Shade: Map stack of potential sunshine durations (h/day)

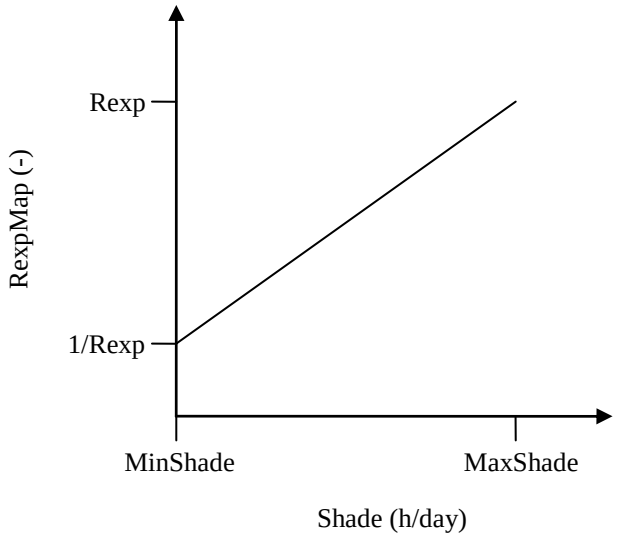

Figure 5.4: Linear relation between potential sunshine duration and the correction factor for the degree-day method

Maps of the correction factor are calculated for each day. This simple method enables a spatial and temporal discretized simulation of snow- and icemelt to be made.

The annual course of RexpMap of each cell equals a sinusoidal function and according to Equation 5.8 this causes a sinusoidal annual course of the degree-day factor with its maximum at the end of June and its minimum at the end of December, as suggested by Braun et al. (1993). The advantage compared to Braun et al. (1993) is that the sinusoidal course of the degree-day factor is derived separately for each cell based on physiographic properties of the catchment. The approach combines the ideas of Braun et al. (1993) and Hottelet et al. (1993) based on a more physical background.

5.3.2 Accelerated melting of ice compared to snow

Ice shows an accelerated melting due to a reduced reflection compared to snow (Table 5.1). More short-wave radiation can be absorbed and therefore more energy for melting is available (Escher-Vetter, 1980). Further, latent and sensible heat fluxes over snow are reduced due to the lower roughness length of snow as compared to ice (Ambach, 1972). For simulation of icemelt of snow-free parts of glaciers, the parameter Rmult (>1) is introduced to the degree-day method (Equation 5.9).

Table 5.1: Reflection of snow and ice surfaces (Paterson, 1994)

	Range (%)	**Mean (%)**
Dry snow	80-97	84
Melting snow	66-88	74
Firn	43-69	53
Clean ice	34-51	40
Slightly dirty ice	26-33	29
Dirty ice	15-25	21
Debris-covered ice	10-15	12

5.3.3 Reduction of icemelt under debris layers

Melt conditions of ice under the debris-covered parts of glaciers must be considered separately from the conditions of clean glaciers. On the one hand, a rather thick debris cover protects the ice from direct solar and long-wave radiation, resulting in a reduction of melt as indexed by the current air temperature. On the other hand, the debris cover is darker than ice which increases absorption if the debris layer is thin (Table 5.1, dirty ice). Depending on the thickness of the debris cover, melting is decoupled from the current meteorological situation. This finding is reported by many researchers, but results vary as to the thickness required before ablation is accelerated or suppressed. The values of debris thickness required for an enhanced melting are typically 7-8 cm (Popovnin and Rozova, 2002). Figure 5.5 shows a generalised spectrum of debris thicknesses and their impact on meltwater production.

Nakawo and Young (1981) explained the discrepancies, found by different researchers, in the thicknesses required before ablation is accelerated or suppressed with different thermal properties of debris and the different meteorological conditions prevailing at the time the experiments were carried out. Thus, not only debris thickness has to be considered for examining ablation under a debris layer (Nakawo and Takahashi, 1982) but also the thermal

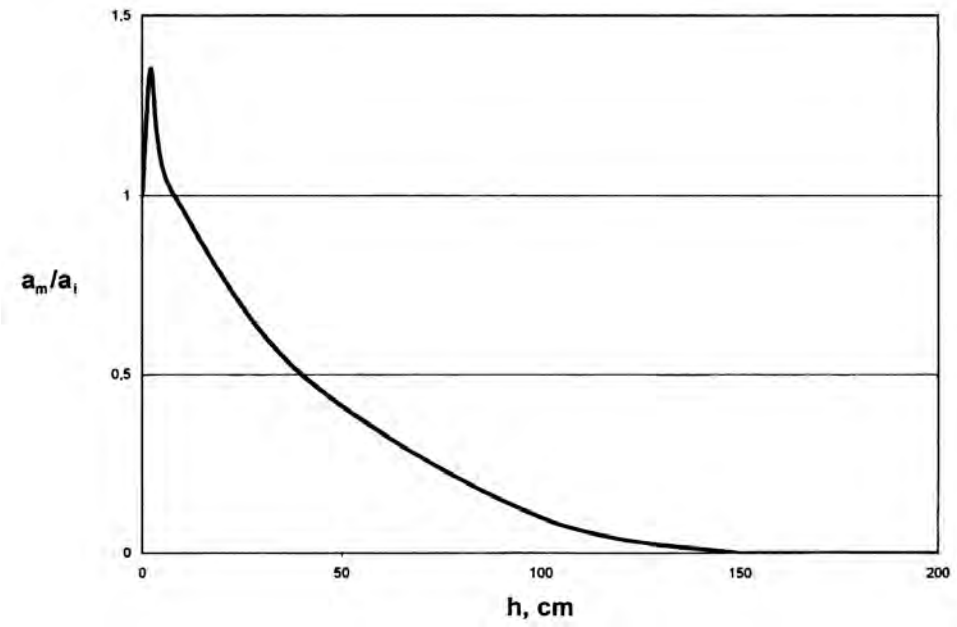

Figure 5.5: Non-dimensional ablation rate a_m/a_i dependence on moraine-cover thickness h (cm) for the Djankuat glacier. A_m is the ablation rate under the debris layer (mm/day) and a_i the ablation rate of bare ice (mm/day) (taken from Popovnin and Rozova, 2002)

properties of debris and the meteorological conditions. However, it is very difficult to measure debris distribution in the field, partly because it varies between geographical areas, and partly because collecting such data is dangerous and it is sometimes impossible to assess the entire surface of debris-covered glaciers (Rana et al., 1997). Rana et al. (1996) suggested an average thickness of debris cover of 0.5 - 1 m for the ablation area of the Lirung glacier and the Langtang glacier in the Langtang Khola catchment. In the 1997 study, Rana et al. showed a considerable overestimation of ablation if debris-covered areas are treated the same way as debris-free glaciers and an underestimation if no melt is assumed for these areas. The average thermal resistance of the debris cover has been estimated from surface temperature obtained from Landsat 5 (TM band 6) images. Their simulation results revealed that the debris cover of the Lirung glacier nearly halves the meltwater production compared to a virtual glacier tongue of the Lirung glacier which is assumed to be debris-free. Thus, the additional parameter Rmuld in Equation 5.10 was introduced following Braun et al. (1993). Rmultd is given a value below 1.0 in order to reduce the meltwater production under debris layers.

The revised equations for snow- and icemelt are as follows:

$$MeltWaterSnowPack = Cfmax \cdot (Temp - TT) \cdot RexpMap \quad (5.8)$$

MeltWaterSnowPack: Meltwater of the snowpack (mm/time step)

$$MeltWaterGlacierClean = Cfmax \cdot (Temp - TT) \cdot RexpMap \cdot Rmult \quad (5.9)$$

MeltWaterGlacierClean: Meltwater of the debris-free glaciers (mm/time step)
Rmult: Parameter for accelerated melt of ice compared to snow (-)

$$MeltWaterGlacierDebris = Cfmax \cdot (Temp - TT) \cdot RexpMap \cdot Rmult \cdot Rmultd \quad (5.10)$$

MeltWaterGlacierDebris: Meltwater of the debris-covered glaciers (mm/time step)

Rmultd: Parameter for reduced meltwater production under debris cover (-)

5.3.4 Annual mass balance of glaciers

The annual mass balance at a given point of a glacier is defined as the sum of water accumulation in the form of snow and ice and the corresponding ablation over the whole year (Paterson, 1994):

$$b_a = a_a + c_a = \int_{t_0}^{t_1} [c(t) + a(t)]dt \tag{5.11}$$

b_a: Specific annual mass balance at a given point (m)
a_a: Annual ablation (m)
c_a: Annual accumulation (m)
c(t): Accumulation rate over time t, e.g. 1 day (m/day)
a(t): Ablation rate over time t, e.g. 1 day (m/day)
t_0: First day of the measurement year (usually 1 October)
t_1: Last of measurement year (usually 30 September of the following year)

The annual mass balance of the glacier corresponds to the integration of the specific point balances b_a over the whole glacier area (Paterson, 1994):

$$B_a = \int_{s_g} b_a ds = \int_{s_{ac}} b_a ds + \int_{s_{ab}} b_a ds \tag{5.12}$$

B_a: Total annual mass balance of the glacier (m^3)
s_g: Area of the glacier (m^2)
s_{ac}: Accumulation area of the glacier (m^2)
s_{ab}: Ablation area of the glacier (m^2)

Different methods exist to determine the annual mass balance at a set of points in the accumulation area and the ablation area (Paterson, 1994). Total annual mass balance of the entire glacier is obtained via spatial interpolation. TAC^d enables the estimation of the annual mass balance based on the hydrological simulation outputs. For each cell with glacier cover (nRGType 2, 3), the mass balance is calculated on the basis of the simulated snow accumulation and the simulated snow- and icemelt (Schaefli et al., 2005):

$$MassBalance = SnowpackforBalance - MeltWaterGlacierforBalance - MeltWaterSnowpackforBalance \tag{5.13}$$

MassBalance: Annual glacier mass balance (mm)
SnowpackforBalance: Annual snow accumulation (mm)
MeltWaterGlacierforBalance: Annual meltwater of glaciers (mm)
MeltWaterSnowpackforBalance: Annual meltwater of snow (mm)

The annual mass balance of the entire glacier is the arithmetic mean of the mass balances of single cells belonging to the same glacier. Further, the equilibrium line altitude, which is the altitude where accumulation and ablation balances out, is calculated in the model.

5.4 Soil routine

The concepts of the soil routine (section 4.2.2) were not revised in this study. However, different parameters can be used to simulate different hydrological response units (HRUs). Generally, soil is rare in the catchment, thus the main function of the soil routine is to calculate actual evaporation before water reaches the runoff generation routine.

5.5 Runoff generation routine

The arrangement of the linear storages (section 4.2.3) had to be adjusted to simulate the runoff generation processes of a high alpine catchment. In order to yield a more precise process simulation, four HRUs were defined according to their specific runoff generation types (nRGType). Each of the HRUs has a specific conceptual composition of the storages within a cell. The storage characteristics are defined by parameters such as storage coefficients, maximum storage levels and values for vertical fluxes (section 4.2.3). The HRUs are as follows:

- Non-glacier area (nRGType 1)
- Glacier area (nRGType 2)
- Glacier area with an inclination of less than 3° and debris cover (nRGType 3)
- Valley bottom with an inclination of less than 8° (nRGType 4)

In partly glacierized catchments, runoff consists of liquid precipitation and meltwater (Menzies, 2002). NRGType 1 represents the ice-free parts of the catchment except for the glacial gravel beds in the main valley of the catchment. Two forms of storage are chosen to represent fast and slow runoff components. The fast components can be interpreted as preferential pathways like macropore flow which is common in areas covered by gravel and boulders. Retardation of flow can be caused by depressions and by micropores in the finer debris under the gravel or boulders. The slow runoff components are attributed to drainage of water in fissures of the rocks which drain slowly.

Several runoff components in glaciers can be described (Moser et al., 1986). The drainage system of glaciers can be subdivided into supraglacial, intraglacial and subglacial drainage systems (Figure 5.6).

In the firn area water infiltrates the unsaturated porous snow and firn. Usually, snow and firn have a high storage capacity due to the connected pores (Colebeck, 1972). Storage capacity is determined by the metamorphism of the snow (Male, 1980). The ice represents the impermeable layer on which meltwater drains supraglacial on the ice surface. A supraglacial drainage network develops during the ablation period consisting of connected channels, ending in crevasses or moulins. The storage capacity of ice is lower than the storage capacity of snow and firn (Nesje and Dahl, 2000). However, water can be stored in fissures (“water-veins”) and small pools (Mader, 1992). Water is usually directed vertically through the intraglacial drainage system. The subglacial drainage system develops during the ablation period to a channel network (Nye, 1976). While doing so, meltwater extends the channels because of mechanical friction and friction heat causing thermal erosion (Röthlisberger, 1972; Shreve, 1972). Meltwater drainage through a glacier can be compared with runoff generation of a karst aquifer (Hooke, 1989). According to Röthlisberger (1972) water fluxes concentrate in main channels due to decreasing pressure in the ice channels with increasing water drainage. Water pressure works against ice pressure and prevents the closing of the channels. As water pressure diminishes, ice pressure becomes more important and constricts the

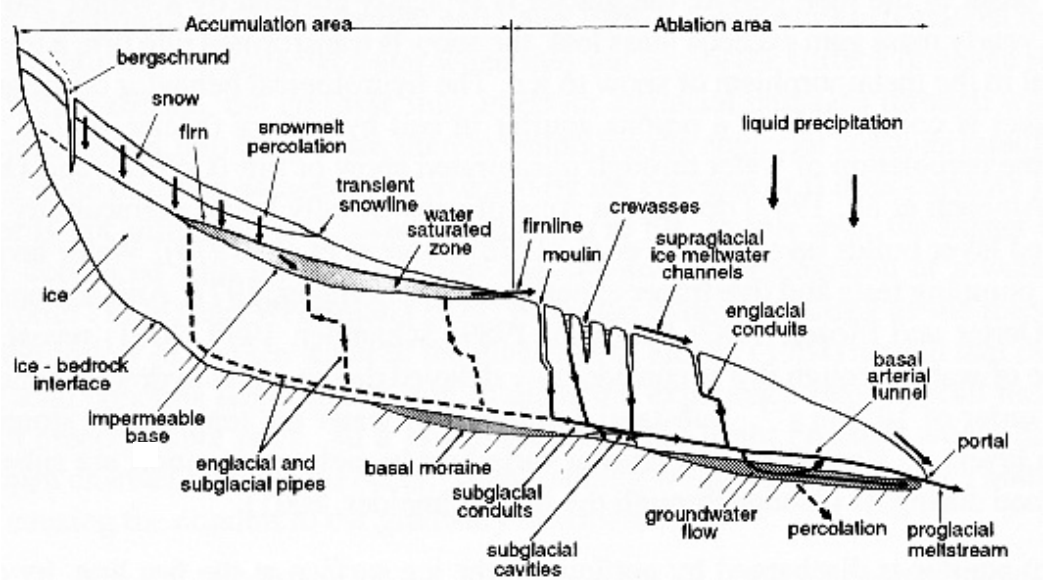

Figure 5.6: Schematic diagram of supraglacial, intraglacial and subglacial drainage pathways of a temperate glacier (according to Röthlisberger and Lang (1987), taken from Schuler, 2002)

channels. These processes adjust the channels to the meltwater amount in time scales of weeks and months. Water leaves the glacier through the glacier terminus. Moser et al. (1986) subdivided runoff of glacierized catchments according to its origins: runoff from ice area and runoff from firn and snow areas (Figure 5.7).

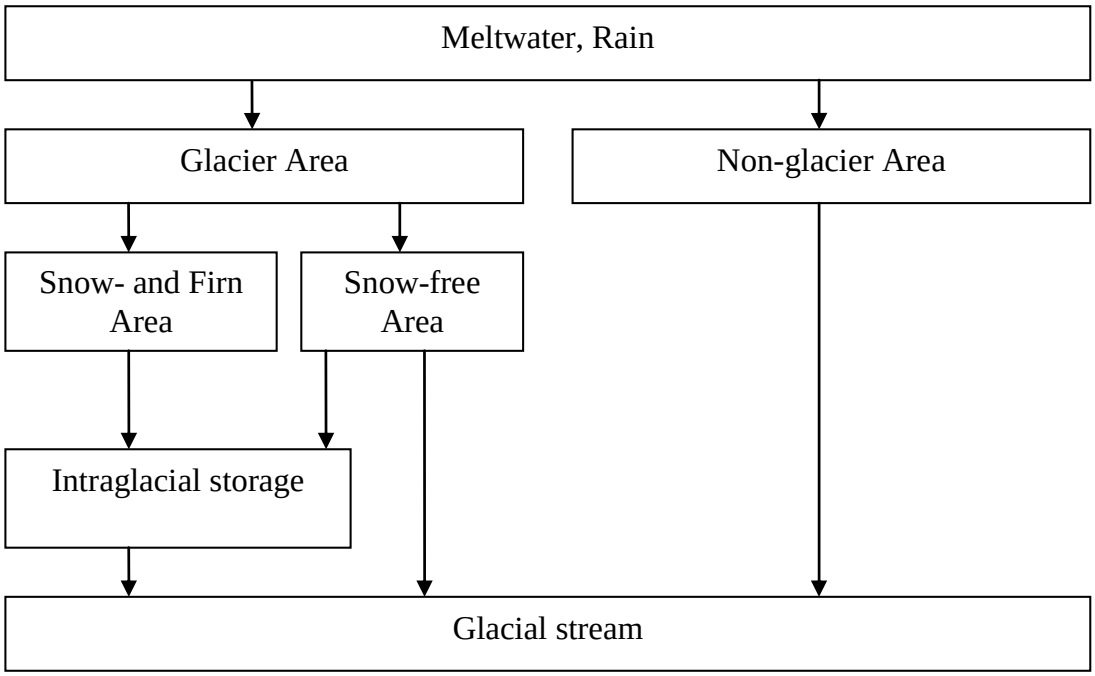

Figure 5.7: Runoff scheme of glacierized catchments (taken from Moser et al. 1986, revised)

In line with these considerations, glacier-covered parts of the catchment (nRGType 2), except for the valley glaciers with an inclination of less than 3° and debris cover, are treated with the same concepts as nRGType 1 but with different parameter values.

Input from the soil routine (ToRunoffGeneration) fills the upper storage box (US_box) and controlled by the parameter US_P it finally contributes to the filling of the lower storage box (LS_box). Fast runoff components and interflow are simulated by the upper storage with limitation of storage capacity. If the upper limit of the upper storage (US_H) is reached, water flows directly to the next downstream cell without retardation. In this case, runoff from the upper storage is composed of the outflow of the storage, determined by the storage content (US_box) and the storage coefficient (US_K), and of the additional water which exceeds the storage capacity (US_box-US_H). Percolation into the lower storage occurs via a constant value (US_P). The outflow from the lower storage is also defined by the storage content (LS_box) and the storage coefficient (LS_K) and represents the slow baseflow component. There is no upper limit of this storage. Figure 5.8 shows the conceptualisation of the runoff generation routine of nRGTypes 1 and 2.

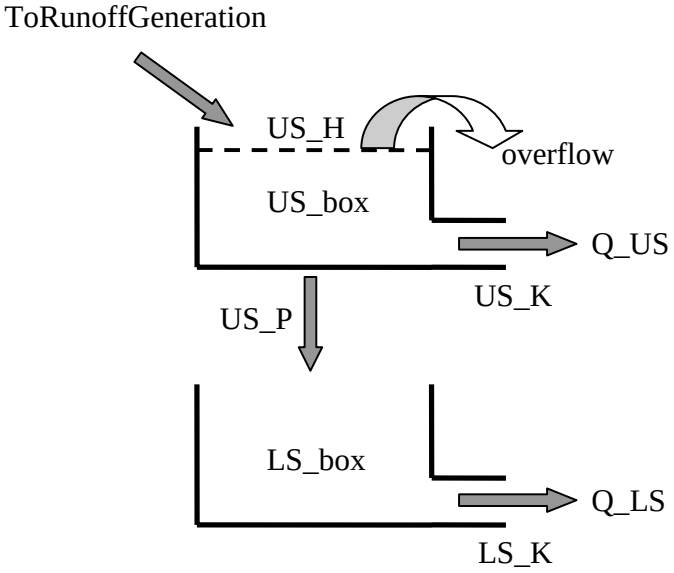

Figure 5.8: Conceptualisation of the runoff generation routine of nRGType 1 and 2

The third HRU are the glacier tongues with an inclination of less than 3° and debris cover (nRGType 3). Glacier storage is a widely used term applied to different processes and time scales by different disciplines in hydrology and glaciology (Jansson et al., 2002). Three time scales can be identified where storage occurs: long-term storage concerns storage of ice and firn as glaciers on time scales of years to centuries and longer, intermediate-term storage is applicable to processes such as storage and release of snow and water in and on a glacier on a seasonal time scale, and the short-term storage concerning diurnal effects of drainage through the glacier (Jansson et al., 2002). Figure 5.9 summarises the forms of glacier storage and the corresponding time scales.

Water can be stored in various ways: in surface snow and firn, surface pools, intraglacial pockets, subglacial cavities, crevasses, intraglacial and subglacial drainage networks and in basal sediments. As shown in section 3.3, winter discharge is quite high in the catchments

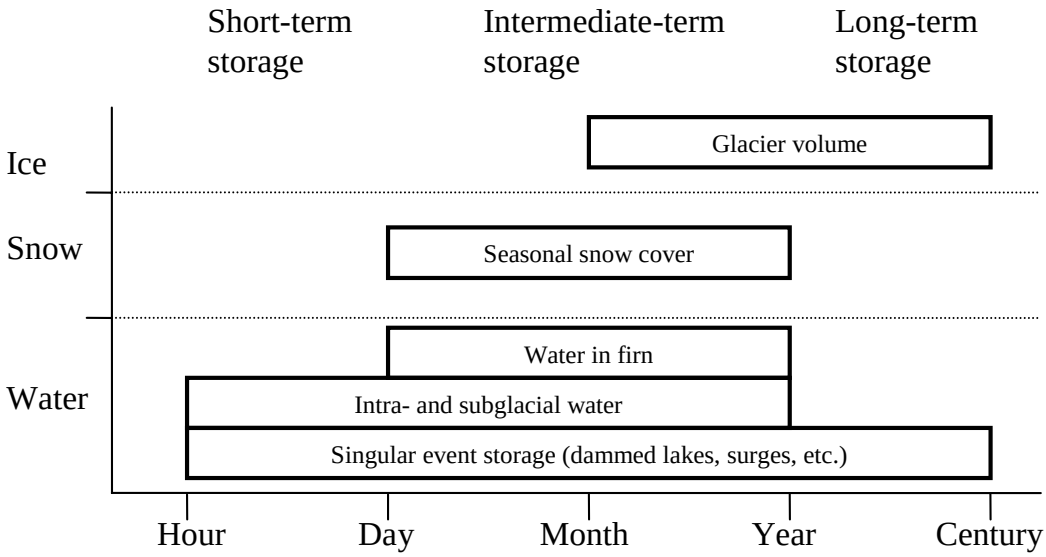

Figure 5.9: Forms of glacier storage and the corresponding time scales (taken from Jansson et al. 2002, revised)

studied although there are neither liquid precipitation nor melting conditions from post-monsoon to pre-monsoon season. Motoyama et al. (1987) argued that the winter discharge of the Langtang Khola is supplied from the outflow of englacial water and from bottom meltwater of the glaciers. This hypothesis is supported by drilling results on the Yala glacier revealing the existence of abundant water in the glacier body which flows in the post-monsoon season in the accumulation and ablation zone of the Yala glacier (Iida et al., 1984). Winter discharge has been observed from many temperate glaciers (e.g. Vallon et al., 1976; Östling and Hooke, 1986; Kohler, 1995). For conceptualisation of the runoff generation processes of the third HRU, only one storage is used. Storage capacity is limited by an upper limit (GlacierLS_H). Runoff of this storage (GlacierQ_LS) is computed by applying a storage coefficient (GlacierLS_K) with additional water if the storage content (GlacierLS_box) exceeds GlacierLS_H. This conceptualisation is based on the assumption that the large valley glaciers can store a great amount of water in pools or small sub- and supraglacial lakes. Thus, GlacierLS_H is larger than the upper limits of the storages of nRGType 1, 2 or 4.

A fourth HRU (nRGType 4) was identified on the basis of information acquired during field visits and from area photographs. The valley bottom with an inclination of less than 8° is considered to be an aquifer consisting of glacial gravel beds where water can be stored. The same structure of storage as in nRGType 3 is used to simulate the hydrological processes but with different parameterisation for different flow dynamics. Figure 5.10 shows the conceptualisation of nRGType 3 and 4. The threshold inclinations of 3° and 8° for the delineation of nRGType 3 and 4 are used because hydraulic properties of glaciers with inclinations of more than 3° or glacial gravel beds with inclinations greater than 8° are considered to be inadequate to store large amounts of water. Due to the assumed well-developed subglacial drainage systems the threshold inclination of nRGType 3 must be smaller. Sub- or supraglacial pools or lakes cannot develop in steeper parts of the glacier tongues. Supraglacial lakes have only been observed on debris-covered glaciers in the Himalayan catchments.

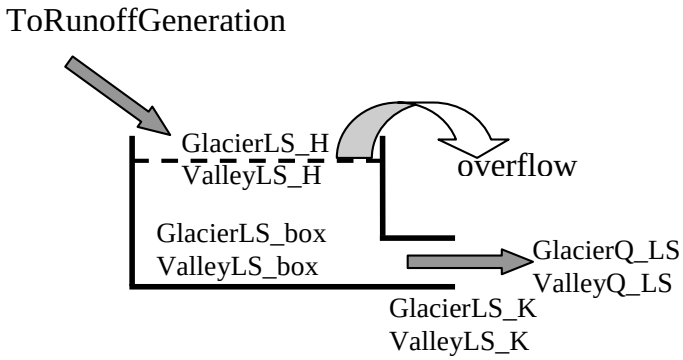

Figure 5.10: Conceptualisation of the runoff generation routine of nRGType 3 (Glacier*) and 4 (Valley*)

5.6 Lateral flows

The distributed structure of TAC[d] enables the simulation of lateral flows from one cell to the next cell. Based on the local drain direction network (ldd), flow directions are determined according to the steepest slope between the cells (PCRaster, 2004). Figure 5.11 gives an overview of the lateral connection of the HRUs. Within nRGType 1, 2 and between both nRGTypes, runoff from the upper storage is directed laterally to the US_box of the next

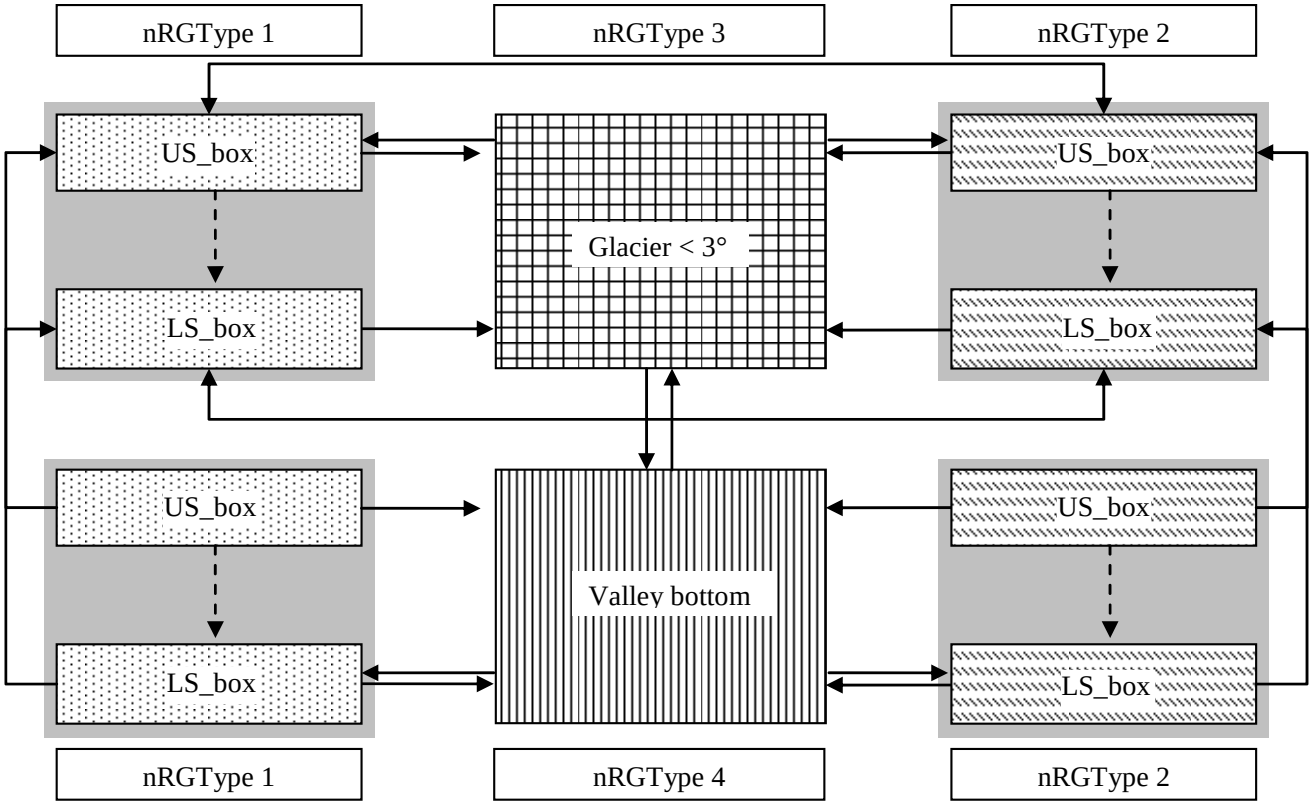

Figure 5.11: NRGTypes and their lateral connection. Solid arrows are lateral fluxes, dotted arrows are vertical fluxes between the storages.

downstream cell, whereas runoff from the lower storage is directed laterally to the LS_box of the corresponding cell. Runoff of US_box and LS_box of nRGType 1 or 2 is directed to GlacierLS_box of nRGType 3 and into ValleyLS_box of nRGType 4. Outflow of nRGType 3 flows into the upper storage of nRGType 1 or 2 or, if the next downstream cell belongs to nRGType 4, into the ValleyLS_box. NRGType 4 drains into LS_box if nRGType 4 and 1 or 2 are neighbouring cells or into GlacierLS_box of nRGType 3. All fluxes are directed to the river network if a cell is identified as a stream cell.

5.7 Routing routine

Once water fluxes have reached stream cells, the generated runoff from one time step is distributed on the following days using one free parameter (MaxBas), which determines the base in an equilateral triangular weighting function (Seibert, 2002):

$$Q_{sim}(t) = \sum_{i=1}^{MaxBas} c(i) \cdot Q_{beforerouting}(t-i+1) \tag{5.14}$$

with the weighting function:

$$c(i) = \int_{i=1}^{i} \frac{2}{MaxBas} - \left| u - \frac{MaxBas}{2} \right| \cdot \frac{4}{MaxBas^2} du \tag{5.15}$$

$Q_{sim}(t)$: Simulated discharge at time t (m^3/s)
c(i): Weight (-)
$Q_{beforerouting}$: Simulated discharge before routing at time t (m^3/s)
t: Time (day)
i, u: Time steps (day)
MaxBas: Empirical parameter (-)

It is assumed that water remains in the river network for less than one day due to the high flow velocity of alpine rivers. Therefore the parameter MaxBas is set at 1.0 a priori.

5.8 Initialization of storages

Compared to previous applications of TAC^d, the high Himalayan headwater catchments have a permanent snow cover at high elevations. The two types of storage of the snow and glacier routine are the snowpack (SnowPack) and the water content of the snowpack (WaterContent). In previous versions of TAC^d these storage types were initialized as empty storages because there was no snow cover at the beginning of the hydrological year in the respective lower alpine catchments. If the storage types of the snow and glacier routine are initialized at zero, the snow cover of the first simulated hydrological year consists only of solid precipitation having fallen during the winter season which precedes the first simulated monsoon season. This causes, on the one hand, a significant underestimation of snowmelt in the monsoon season and, on the other hand, an overestimation of icemelt. If there is no snow cover on the glaciers and temperature is above the threshold temperature (TT), ice starts melting. Depending on the meteorological situation of the simulation period, this problem could affect more than just the first hydrological year. For this reason, additional initialization maps of SnowPack and WaterContent were introduced in this version of TAC^d.

Maps of the storage levels produced during initialization runs were used for the initialization of the simulation period (Section 7.2).

The initialized storages are:

- Snowpack (SnowPack)
- Water content (WaterContent)
- Upper storage (US_box)
- Lower storage (LS_box)
- Glacier storage (GlacierLS_box)
- Valley bottom storage (ValleyLS_box)
- Soil moisture (SoilMoisture)

5.9 The internal water balance

Figure 5.12 shows the internal water balance of the modified TAC^d model for the Langtang Khola catchment for a simulation period of 2200 time steps. The cumulated precipitation input, as shown in the upper part of the graph, adds up to nearly 45 million millimetres. The maximum amplitude of the internal water balance, lower part of the graph, ranges from +31 mm to −17 mm. Neither an increasing nor a declining trend is evident. Therefore, the prerequisite described in section 2.3.1 to consider the internal water balance as accurate is fulfilled. The increasing fluctuation with increasing time steps might be a result of rounding errors but the inaccuracies still stay within millionths of the amount of input.

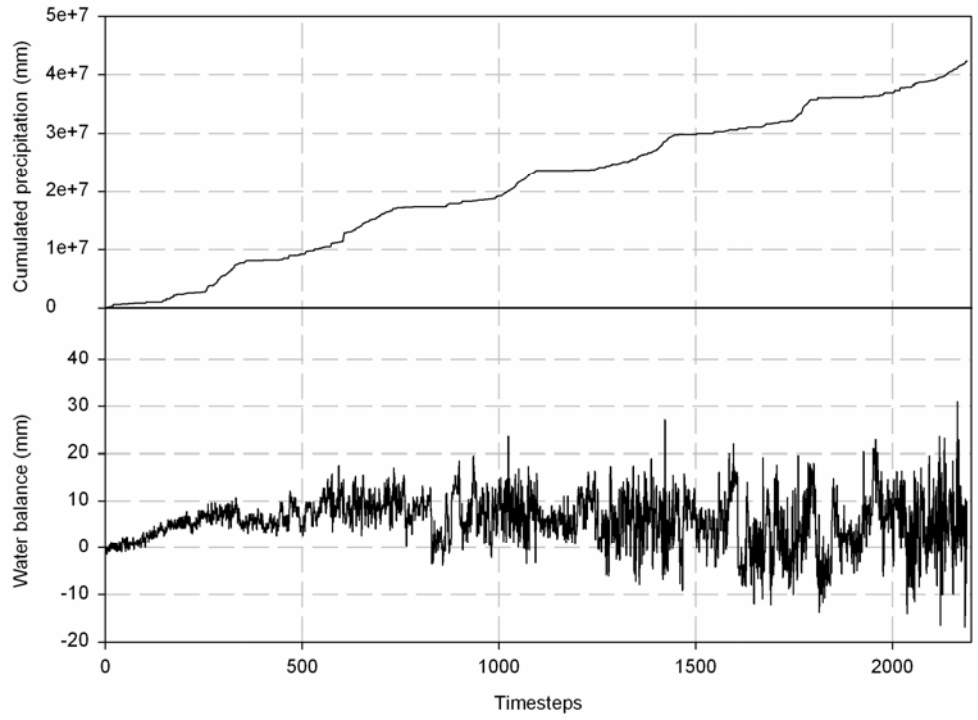

Figure 5.12: Internal water balance and cumulated precipitation input for 2200 time steps for the Langtang Khola catchment (here: 1 time step = 1 day)

5.10 Conclusions

Numerous modifications were carried out in order to adjust the model to the climatologic and physiographic conditions of the Himalayan catchments studied. No significant violations of mass conservation of the modified TAC^d could be detected.

As far as possible the conceptual ideas behind the routines remained untouched. Implementation of glaciermelt was essential for simulations of the highly glacierized catchments such as the Langtang Khola, Modi Khola and Imja Khola catchments. Modifications of the temperature-index method allow a more realistic calculation of snow- and icemelt based on physiographic and topographic characteristics and astronomic parameters. Glacier mass balances can be simulated for each glacier and these can be used for model evaluation or calibration if measured values are available.

A sinusoidal function is implemented for calculating potential evapotranspiration, which seems to yield a realistic temporal distribution.

The runoff generation routine identifies the main hydrological response units and considers differences of runoff dynamics between them. The routing routine is quite rudimentary but adequate for this application as water leaves the catchment quickly once the river network is reached. Thus a complex wave routing is not necessary. Figure 5.13 gives an overview of the structure of TAC^d and the sequential order of routines either modified or taken from previous versions of TAC^d.

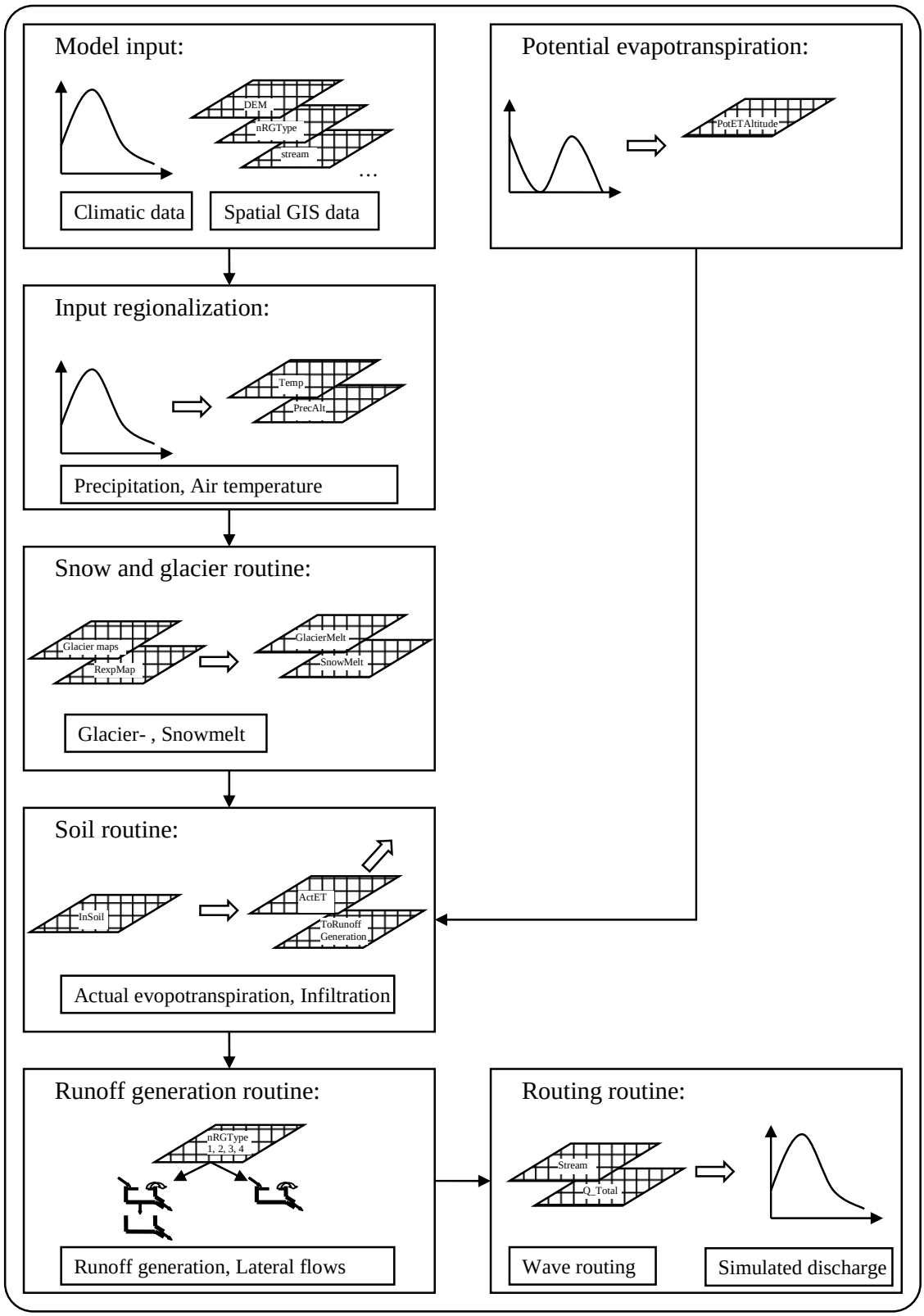

Figure 5.13: Structure of TAC[d] with the most important input and output maps or time series of each routine

6 Preprocessing: Data base and data processing

The preprocessing section in hydrological modelling contains the data processing of climatological input data and spatial data. In the case of distributed modelling various digital maps need to be produced to provide spatial information in an adequate resolution and in the correct format demanded by the respective programme environment used for the development of the model. Complete time series of meteorological input data are a prerequisite for the model application. This information has to be transformed into a specific format as well. In this study an intensive quality check of meteorological data was necessary, and gaps in time series of daily mean air temperature and daily sums of precipitation had to be bridged with appropriate methods. This chapter describes the extrapolation methods and the processing of spatial data with the help of the Langtang Khola catchment; these procedures were also applied to the Imja Khola and Modi Khola catchments.

6.1 Data collection at stations of the Snow and Glacier Hydrology Unit (SGHU)

Snow and glacier hydrological studies were started in 1987 by the Department of Hydrology and Meteorology (DHM) in collaboration with the German Agency for Technical Cooperation (GTZ) within the framework of a special fund provided by the government of Germany (Grabs and Pokhrel, 1993). During this period three hydrometeorological stations were established in the Annapurna, Langtang and Khumbu regions with the purpose of systematically collecting hydrological and meteorological data. Up to now three further stations have been established and the project is carried out by His Majesty's Government of Nepal, DHM.

Daily mean discharge is derived from 4-hourly gauge height measurements and stage-discharge relationship. Rating curves are calculated using dilution techniques for discharge measurements. Air temperature is measured with thermohydrographs, and charts are evaluated at 6-hourly intervals and the maximum, minimum and mean daily air temperatures are made available. Precipitation is read manually and the daily totals are published.

Data are published in yearbooks by His Majesty's Government of Nepal, Ministry of Science and Technology, Department of Hydrology and Meteorology, Snow and Glacier Hydrology Unit, Kathmandu, Nepal. Pictures in Figures 6.1 and 6.2 show the meteorological station of the Langtang Khola catchment and the position where the gauge height is measured.

Most of the stations of the Snow and Glacier Hydrology Unit (SGHU) are situated in the higher Himalayan regions. Access to these Himalayan catchments is rather difficult and the stations are a long way from Kathmandu. Due to this fact data collection at the SGHU stations has been outsourced to local staff living close to the stations. These data observers are primarily farmers or mountain guides and are often not familiar with the scientific demands for a reliable data basis. The environmental conditions in the high alpine Himalayas are rough. As a result, the time series of precipitation, air temperature and gauge height show data gaps caused by measurement errors, avalanches, hail, thunderstorms or heavy rainfall during the monsoon season. These harsh weather conditions cause considerable damage to the stations and the instruments. Vandalism by local people and animals is also a reason for data loss. SGHU has made a great effort to improve data collection and to keep the stations operational throughout the whole year. Emergency field visits in addition to regular field visits and the training of local staff are some of these endeavours to provide more reliable

data. Despite this, the remoteness and inaccessibility of stations during the monsoon and winter season sometimes delay the maintenance work of the stations. Figure 6.3 shows the availability of precipitation, air temperature and gauge height data of the Langtang Khola, Modi Khola and Imja Khola catchments. More details are summarised in Tables A1, A2, A3 (Appendix) for each hydrological year.

Figure 6.1: Outlet of Langtang Khola catchment where water level is measured at 3800 m a.s.l.

Figure 6.2: Meteorological station of Langtang Khola catchment situated in Kyangjing at 3920 m a.s.l.

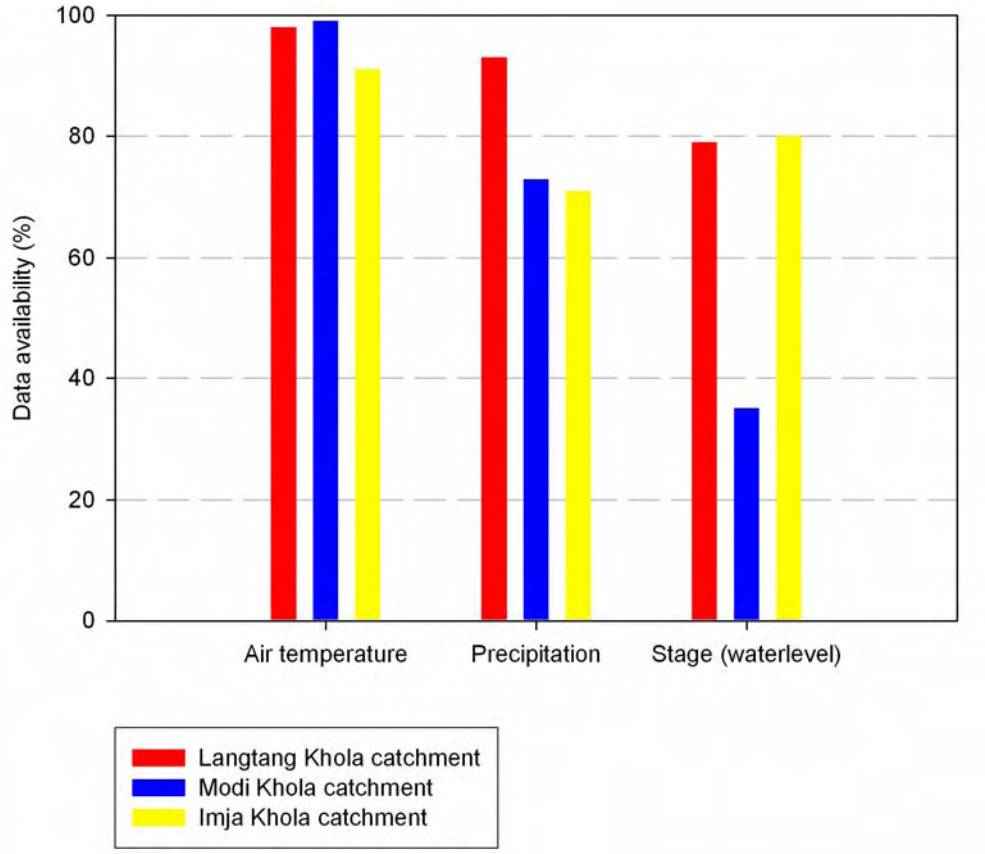

Figure 6.3: Data availability at the three investigated catchments of the respective investigation periods

6.2 Daily discharge data

Discharge data are derived from gauge height readings and stage-discharge calibration measurements executed by SGHU staff during their field trips throughout the year. Tracer dilution methods are used to measure discharge as described by Spreafico and Grabs (1993). Based on these measurements SGHU derives rating curves to calculate daily discharge values. In this study additional stage-discharge relationships were calculated applying various regression functions like exponential, potential and linear regression functions and the calculated discharges were evaluated and corresponding R^2-values given. Table 6.1 shows the equations of the rating curves of the catchments under investigation.

Table 6.1: Equations of rating curves of investigated catchments and corresponding R^2-values

Catchment	Rating curve equation	R^2-value
Modi Khola	$8.109 \cdot (\text{gauge height})^{2.039}$	0.98
Imja Khola	$16.561 \cdot (\text{gauge height} + 0.076)^{2.364}$ *	0.99
Langtang Khola	$8.409 \cdot (\text{gauge height} - 0.078)^{1.334}$ *	0.92

* rating curve derived by SGHU

Intensive data analysis was necessary to ensure the reliability of the discharge data. Daily gauge height data were plotted and checked for consistency. A typical error detected by this procedure is demonstrated in Figure 6.4. The red line is the discharge of the Langtang Khola

catchment calculated with original gauge height values as published in SGHU yearbooks, which is obviously inconsistent. Compared with other years it seems that the original values of gauge heights were recorded, where 1 m was erroneously subtracted (0.40 m instead of 1.40 m). In that case the original yearbook values were adjusted by adding 1.0 m to each daily value of the respective period in accordance with original staff gauge data sets (handwritten). The blue line shows the discharge calculated from revised gauge height. The revised discharge data are used for model evaluation and calibration.

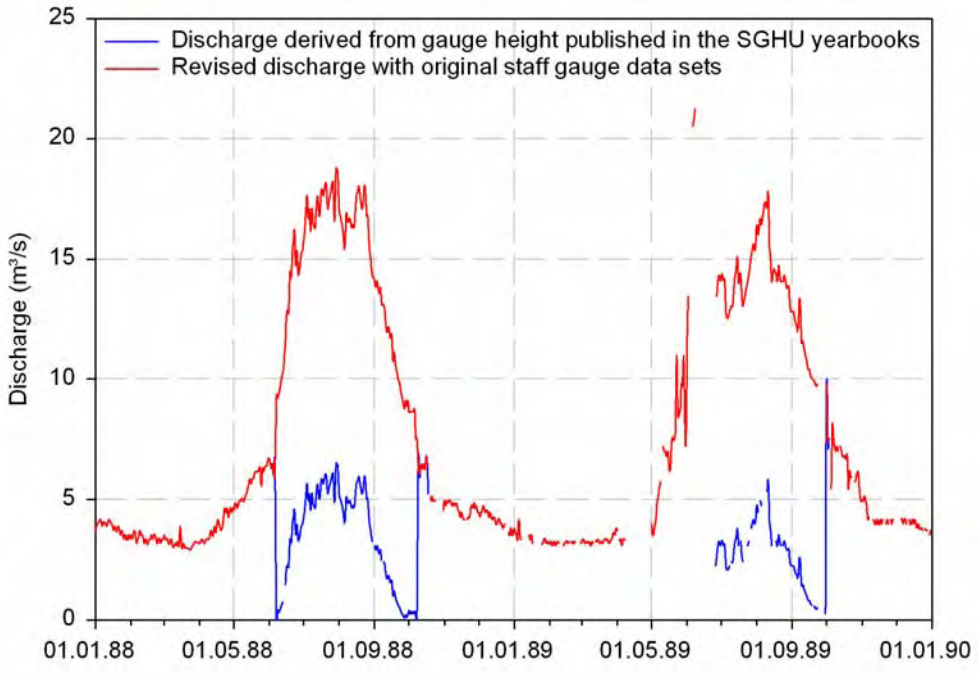

Figure 6.4: Typical error in discharge data calculated from gauge height as published by SGHU and the revised discharge data of the Langtang Khola catchment. In the erroneous discharge data, water levels were recorded that were 1.0 m too low

Another inconsistency was detected for the hydrological year 1997/98 of the Langtang Khola catchment when the low flow period seems to show inaccurate values. Again, the original staff gauge data were used to revise the published data as shown in Figure 6.5.

These are two examples of the data consistency analysis procedure which was applied to all three catchments if necessary.

6.3 Daily air temperature data

Daily air temperature data are available for 91% to 98% of the investigation periods in the catchments. This can compete with European standards. However, hydrological models require data sets without gaps. Thus, an appropriate procedure to bridge the gaps in air temperature time series had to be found on the basis of air temperature data of reference stations of the Standard Data Meteorological Service Network of DHM in the vicinity of the catchments studied. Table 6.2 summarises the reference stations with elevation, conducted measurements and the schematic map in Figure 6.6 shows the location of the stations.

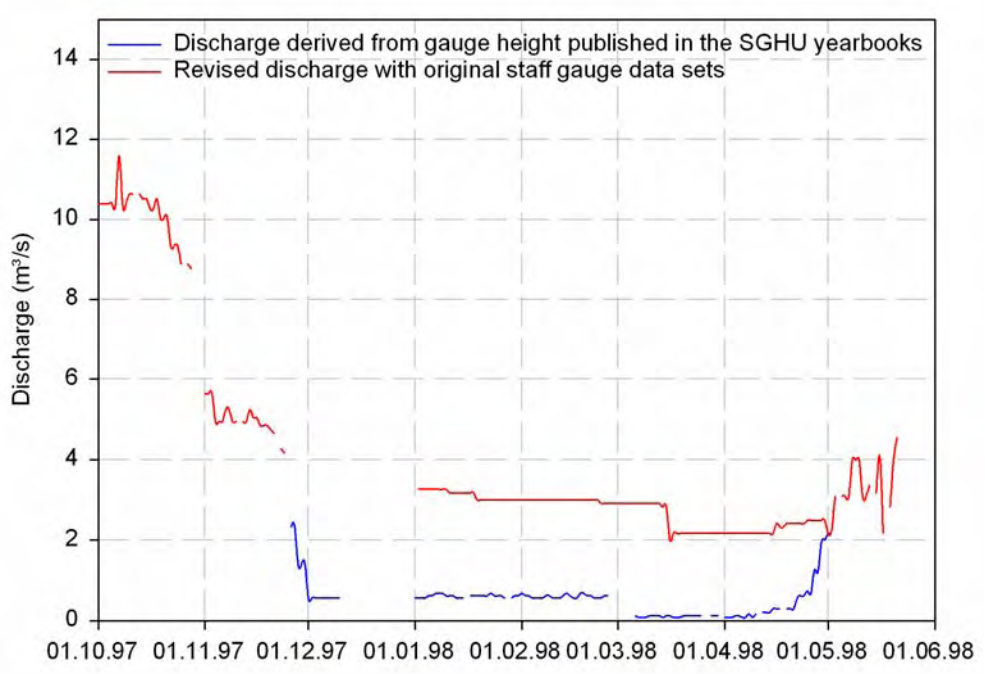

Figure 6.5: Original and revised discharge data of the low flow period of the hydrological year 1997/98, Langtang Khola catchment

Table 6.2: Summary of DHM reference stations used for data processing (P: precipitation, T: temperature)

Region	Station	Elevation (m a.s.l.)	Measurements
Annapurna	Pokhara Airport	827	TP
Annapurna	Malepatan (Pokhara)	856	TP
Annapurna	Bhadaure Deurali	1600	P
Annapurna	Lumle	1642	TP
Annapurna	Lamachaur	1070	P
Annapurna	Ghandruk	1960	P
Annapurna	Siklesh	1820	P
Langtang	Timure	1900	P
Langtang	Sarmathang	2625	P
Langtang	Kathmandu Airport	1336	TP
Langtang	Thamachit	1847	P
Langtang	Dhunche	1982	TP
Langtang	Tarke Ghyang	2480	P
Langtang	Paigutary	unknown	TP
Khumbu	Chaurikharka	2619	P
Khumbu	Pakarnas	1982	P
Khumbu	Aisealukhark	2143	P
Khumbu	Okhaldhunga	1720	TP
Khumbu	Khumjung	3750	P
Khumbu	Salleri	2378	P
Khumbu	Chialsa	2770	TP

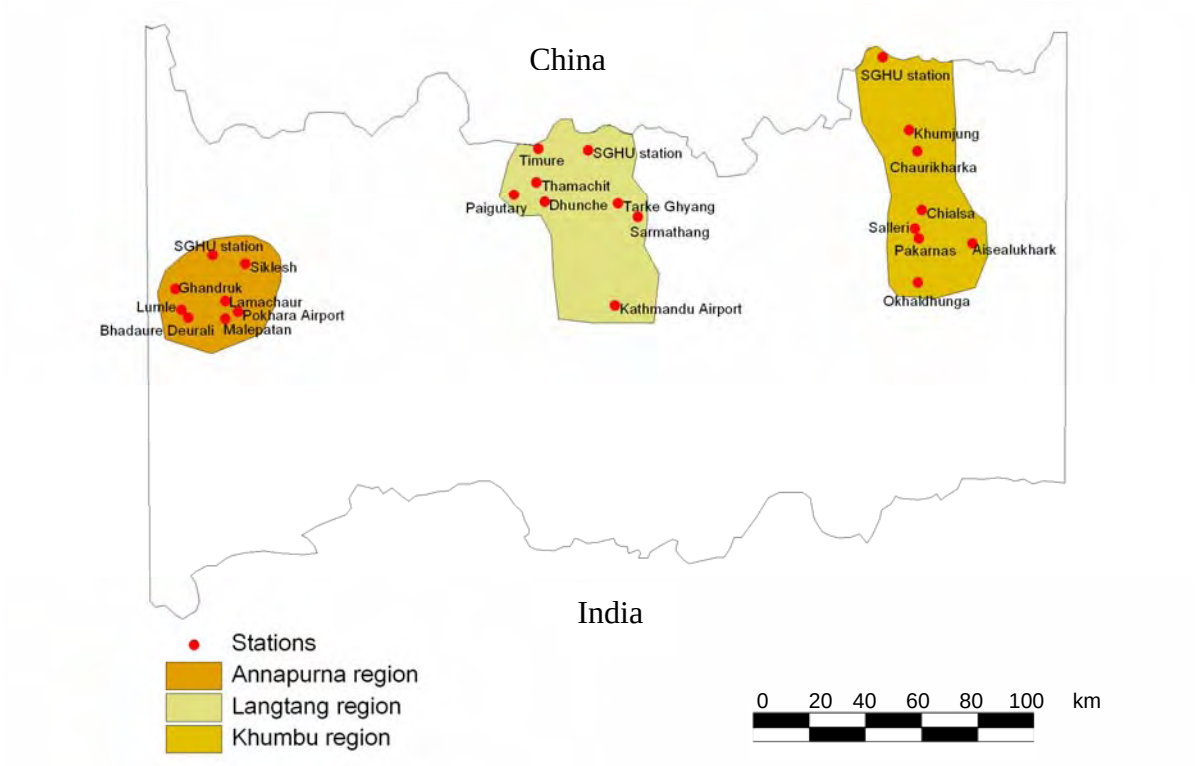

Figure 6.6: Schematic map of SGHU stations and DHM reference stations in the Annapurna, Langtang and Khumbu regions

6.3.1 Correction of inconsistencies in the measured air temperature time series

The time series of measured daily mean air temperature of the Langtang Khola catchment shows inconsistencies from January 1995 onwards (Figure 6.7). The mean air temperature from 1988 to 1995 is 1.79°C, whereas it is 4.40°C for the period from 1995 to 2000.

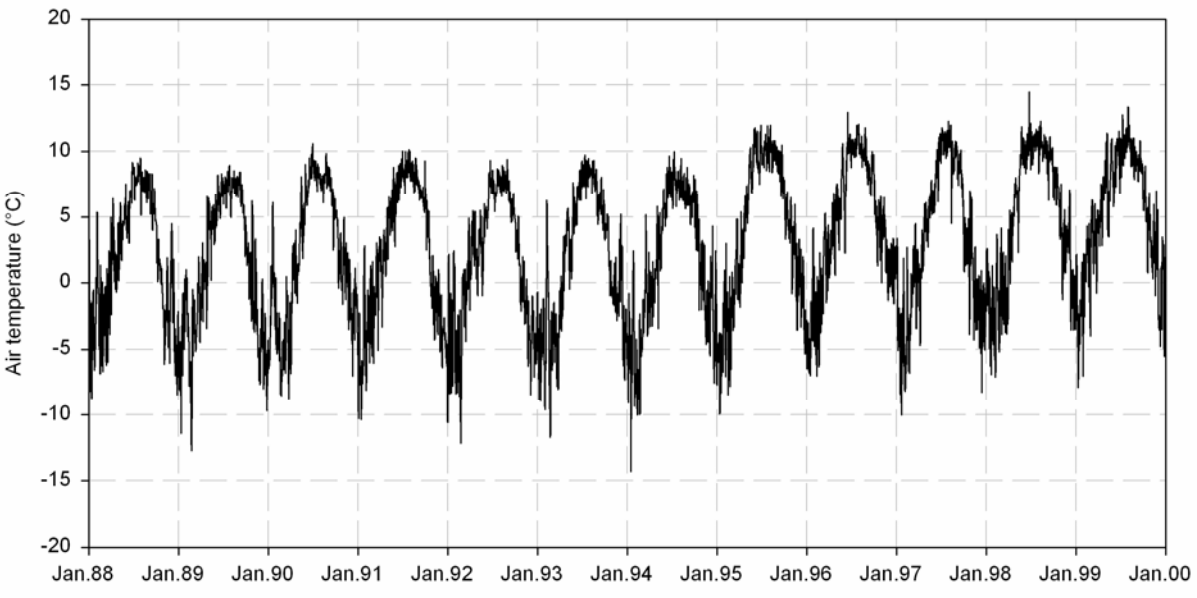

Figure 6.7: Inconsistencies in the time series of air temperature from 1988 to 2000. There is a 2.6°C shift from 1995 onwards

This shift of approximately 2.6°C has a significant impact on the discharge simulation and had to be corrected. It is assumed that the shift is caused by a systematical error in the measurement of the air temperature. Thus, the difference between both average air temperature values was subtracted from each daily value from 1995 onwards and the revised time series was taken for the simulation.

6.3.2 Extrapolation of air temperature data

The entire procedure of data processing in the case of daily mean air temperature data is described with data of the year 1997 of the Langtang Khola catchment and is based on Weber (1997). The method was applied to each catchment where data gaps occurred.

6.3.2.1 General remarks and data analyses

The current value of air temperature (generally measured 2 m above ground) does not only depend on the entire synoptic situation and the altitude above sea level but also on local vertical and horizontal exchange conditions. Horizontal processes can be all advective processes like local wind systems or passing fronts; vertical distribution of air temperature near the surface is connected to the surface energy balance.

Local air temperature measurements at different stations cannot be transferred directly from one station to another due to the different specific microclimatic conditions at the meteorological station like albedo, heat conductivity of soil, water content of soil and vegetation as well as the surface roughness (Kraus, 1966; Weber, 1997). This list of impacts on local air temperature measurements is not complete but it can be seen that even in a small area significant differences of microclimatic conditions occur. Air temperature graphs of different stations in the Langtang region are given in Figure 6.8.

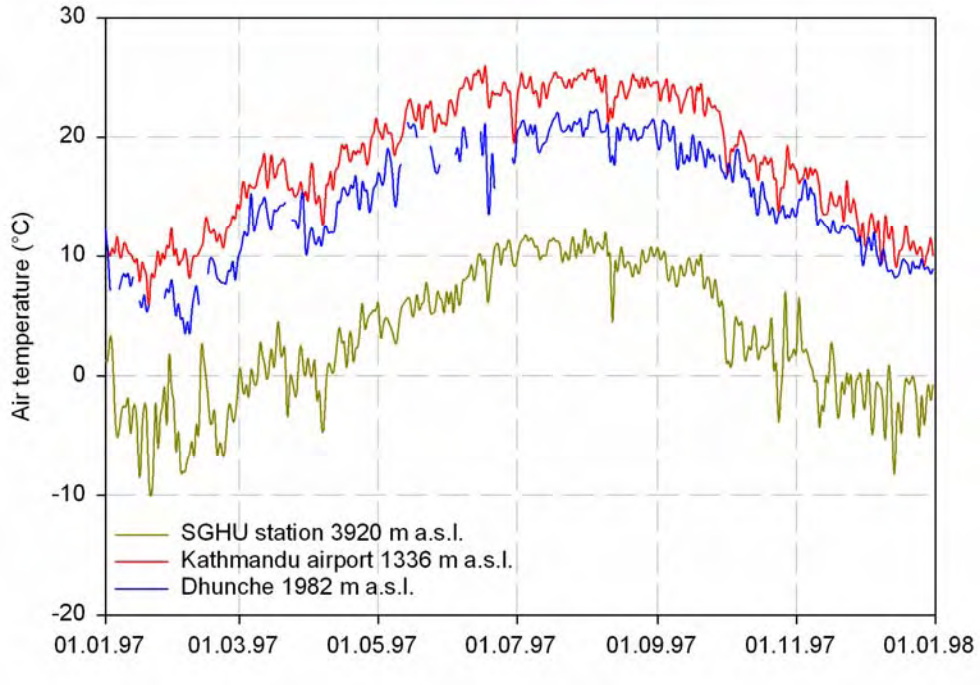

Figure 6.8: Comparison of daily air temperatures at Kathmandu airport (1336 m a.s.l.), Dhunche (1982 m a.s.l.) and SGHU station (3920 m a.s.l.) in the Langtang region, 1997

Dhunche is located at an altitude of 1982 m a.s.l. around 6 km down valley from the SGHU station. It is situated on a plateau on a west-oriented slope of a steep valley. Kathmandu is about 60 km south of the Langtang catchment at an altitude of 1336 m a.s.l and surrounded by mountains up to 2000 m a.s.l. Both reference stations show nearly the same structure in their air temperature variations with a balanced variance all year round. A reason for this fact could be equal terrain properties of both reference stations. The day-to-day variability of air temperature increases with altitude (SGHU station) due to the rough climate at higher elevations. Weber (1997) explains the increasing variance with the influences of surface and orography. The variance becomes more pronounced during the dry season (October to May) at the SGHU station. In Figure 6.9 daily air temperature values of reference stations are plotted linearly versus SGHU data. The data of Dhunche or Kathmandu can explain 85% and 87% respectively of the temperature information of the SGHU station. The reference stations have a higher correlation among each other with $R^2 = 0.93$. The slope of the regression line is below 1.0 due to the high variance of the air temperature data of the SGHU station. The y-axis section of the regression line corresponds well with the mean temperature differences between the SGHU station and the reference stations and therefore with the mean vertical temperature gradients shown in Table 6.3.

Table 6.3: Mean air temperature differences between the SGHU station and the reference stations in the Langtang region and the y-axis section of the regression line of Figure 6.9 for the year 1997

	Mean temperature difference (°C)	**Mean vertical temperature gradient (K/100m)**	**y-axis section of the regression line (-)**
SGHU – Kathmandu	14.8	-0.57	15.0
SGHU – Dhunche	11.6	-0.59	12.2

Furthermore, scattering around the regression line is larger at low temperatures (0°C and below at the SGHU station) than at higher temperatures, which can be explained with the higher variance of the SGHU data during the dry season.

6.3.2.2 Procedure of extrapolation of daily mean air temperature values

Literature (e.g. Hormann, 1994) provides various methods of temperature regionalisation in high alpine regions, most of them being regressive approaches. These methods mostly require a remarkable station density which is not available in the Nepal Himalayas. Therefore, the regionalisation method applied here is derived from the vertical gradient as follows:

$$T_{SGHU} = T_{Ref} + grad \cdot \Delta z \qquad (6.2)$$

T_{SGHU}: Temperature at SGHU station (°C)
T_{Ref}: Temperature at reference station (°C)
grad: Vertical temperature gradient (K/100m)
Δz: Altitude difference (m)

Not taking into account the horizontal information can be justified with the use of daily mean temperature values which make the specific synoptic impacts at the stations negligible in such a small area under investigation. More arguments can be found in Weber (1997). A linear regression like Equation 6.2 does not consider seasonal variation of regression parameters.

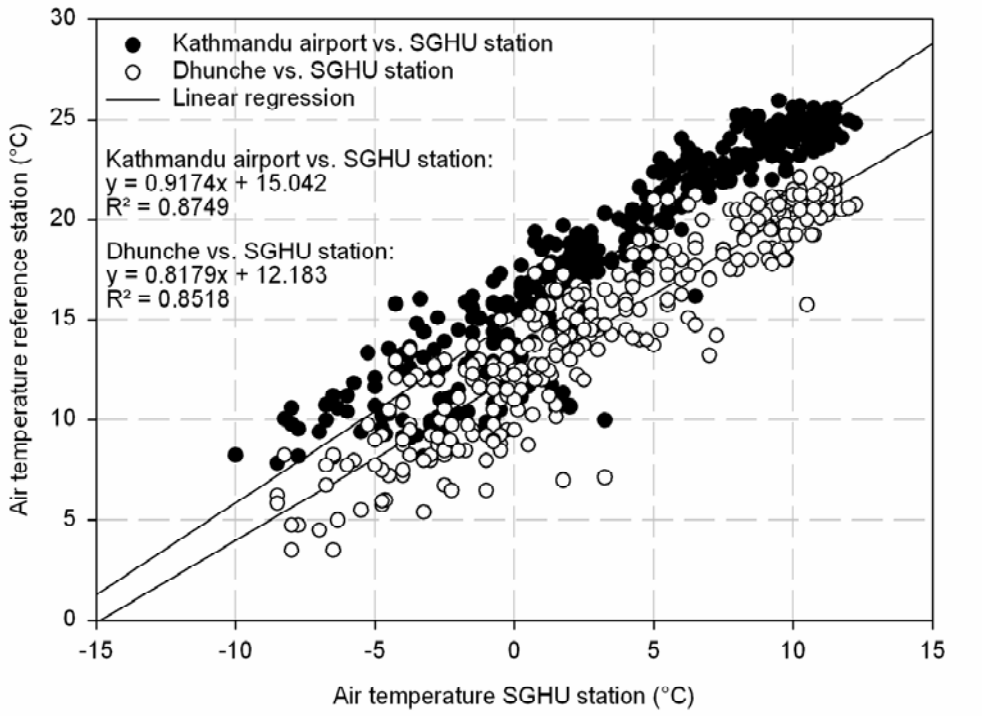

Figure 6.9: Comparison of daily mean air temperature values of the SGHU station (3920 m a.s.l.) with the Kathmandu (1336 m a.s.l.) and Dhunche (1982 m a.s.l.) meteorological stations, 1997

However, Figure 6.10 shows a significant difference of the vertical air temperature gradients between the monsoon and dry periods.

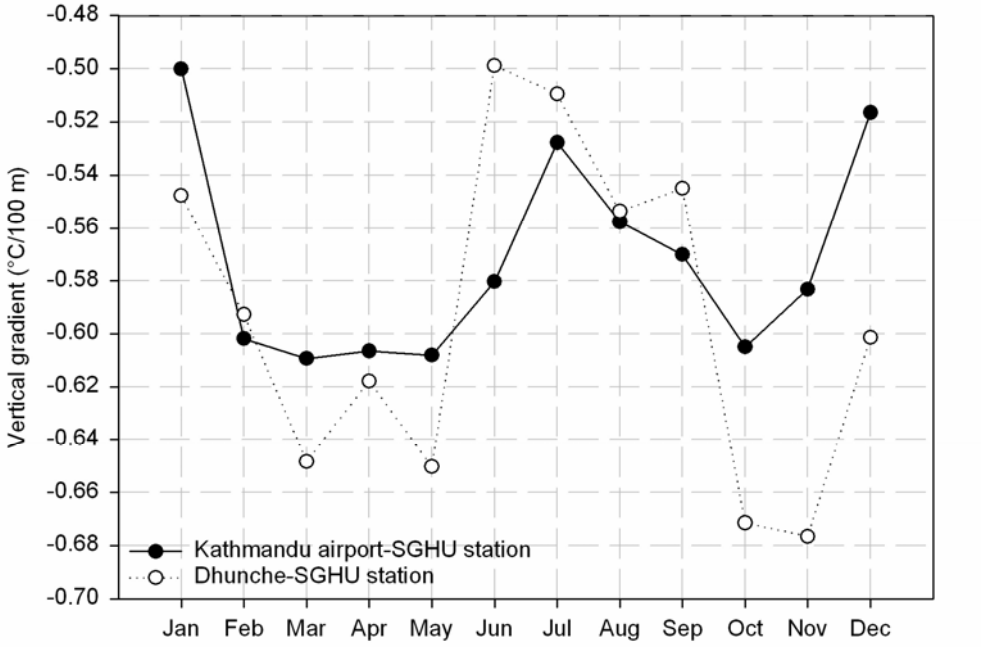

Figure 6.10: Vertical monthly air temperature gradients between the SGHU station (Langtang Khola catchment) and Kathmandu, and between the SGHU station and Dhunche, 1997

As a conclusion of the analysis of temperature gradients it can be stated that a constant mean gradient would overestimate the air temperature at the SGHU station in winter and underestimate the air temperature in summer.

Figure 6.9 shows that an extrapolation of air temperature data of the SGHU station with a temperature-dependent linear regression with the data of either Kathmandu or Dhunche is more accurate for higher temperatures than for temperatures at freezing level. In the precipitation-runoff model high temperatures are responsible for snow- and icemelting, while temperatures around freezing are responsible for the distinction of melting or refreezing of water in the snowpack and for the distinction between snowfall or rain. Thus, air temperature around freezing level is of great importance for the simulation of the snowpack.

Temperature values of the Langtang Khola catchment only show gaps of a few days of the respective years (Table A1, Appendix) except in October and November 1987. Therefore, it is useful to derive air temperature values with a method based on annual data and not on average values of the entire period. This takes into account the specific synoptic situation of each year.

For the extrapolation of temperature values a universal regression method is useful, analogue to the linear regression, which depends only on the temperature values of the reference stations. Weber (1997) suggests a second order polynomial function:

$$T_{Ref} = A \cdot T^2_{SGHU} + B \cdot T_{SGHU} + C \qquad (6.3)$$

A,B,C: Coefficients (-)

The coefficients A, B, C are regressively determined from mean monthly air temperature values as shown in Figure 6.11.

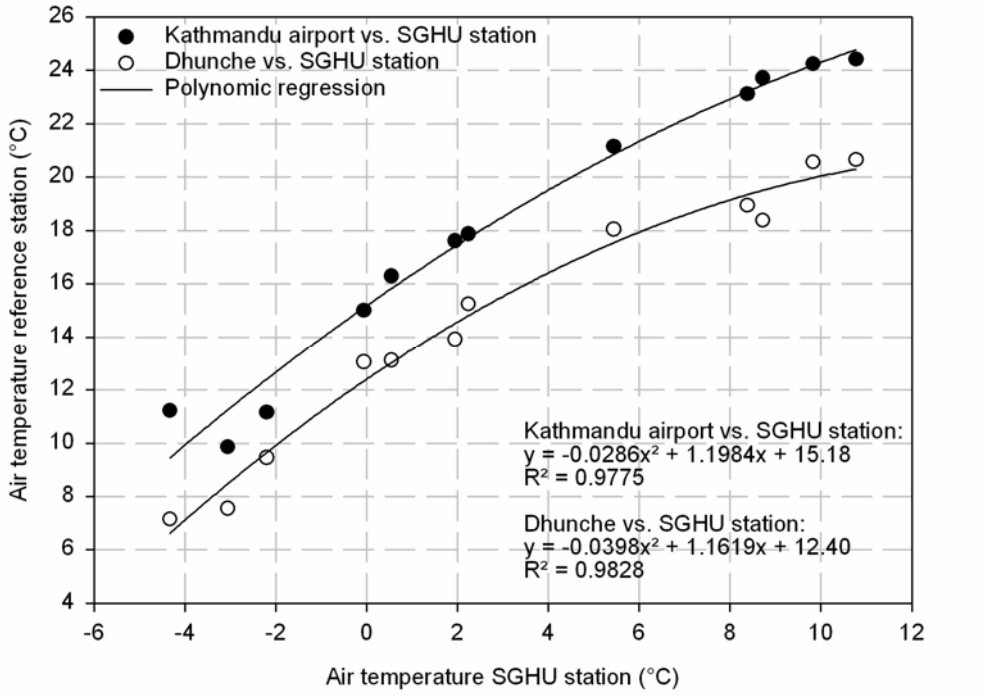

Figure 6.11: Empirical relation between the reference stations and the SGHU station in the Langtang region with a second-order polynomial function, 1997

Weber (1997) states that the value of C gives approximately the mean annual temperature difference between the stations. The B value should be near 1 and A describes mainly the impact of atmospheric stratification. Usually this value is negative with a magnitude of around –0.03. If the coefficients differ significantly from these values, the simulation might be unrealistic. Furthermore, it is essential that the regression is performed with the values of the reference station as the independent variable to cover the entire range of values of the SGHU station. Only within the range of values of the SGHU station has the curve the appropriate curvature. If the curvature increases above A = |0.05| (Weber, 1997), the range of values of the function for T_{Ref} will be limited unrealistically for higher temperature values. A larger curvature could be the result of a wrong representation of parts of the range of values of the stations due to many missing data in a specific period, e.g. in the monsoon season. This is not a problem in the Langtang Khola catchment because of good data availability. The application of the second order polynomial function improves the fit as compared to a linear function (Table 6.4).

Table 6.4: Comparison of regression analysis between monthly mean air temperature values of the SGHU station and reference stations in the Langtang region with different regression models

Reference station	R^2-value for polynomial function	R^2-value for linear function
Kathmandu	0.9775	0.9656
Dhunche	0.9828	0.9539

This finding corresponds well with the results of temperature extrapolation at Vernagtferner, Austria (Schulz, 1999). The curvature lies within the intended magnitude for all years. The only exception is the year 1987 where October and November show gaps of more than 10 days. The curvature is A = –0.0466 in that year. Weber (1997) and Schulz (1999) found for the Annapurna region (Nepal) and the Vernagtferner (Austria) respectively that the coefficients only vary slightly from year to year and can be considered as nearly constant for a station. The same can be stated for the Langtang Khola catchment in periods when data availability is appropriate. Therefore an average of each coefficient (A, B, C) was calculated for the period 1988 to 1998 and applied for extrapolation of the air temperature values of the year 1987 where the number of missing data is too large to derive representative coefficients. The Kathmandu reference station is a station at an airport and therefore complete data sets are available from 1987 to 1998. Thus, for data extrapolation Kathmandu was taken as a reference station to derive the required coefficients.

6.4 Daily precipitation data

Daily sums of precipitation are available for 71% to 93% of the observation periods of the catchments (Tables A1, A2, A3, Appendix). Low-level reference stations in the vicinity of the SGHU stations (Table 6.2) are used for extrapolation to bridge the gaps. The filling of data gaps is necessary if observations are missing or only sums over several days were recorded instead of daily readings (Braun et al., 1998). These sums had to be redistributed over the previous days. The analyses described here with the help of the Langtang Khola catchment were processed for all years within the observation period of all three catchments.

6.4.1 General remarks

Nepal's precipitation regime is of a continental type and predominantly convective (section 3.2.2). There are distinctive dry seasons and rainy seasons where precipitation events are short but very intensive. In the dry season precipitation is quite rare and there are days without precipitation in the rainy season. These characteristics enable an approach to reconstruct daily values of precipitation at a SGHU station with adequate reliability.

If precipitation is solid, it will be assigned to the snow storage of the hydrological model and contributes to runoff maybe weeks or months later when the snow cover is melting. Therefore, it is more important to get the total amount of snowfall rather than the correct temporal distribution. Stricter rules must be set in the case of rainfall. If storages are filled, liquid precipitation contributes to runoff directly, therefore it is important to get the correct timing of daily rain events.

Hydrological models consider numerous processes which are important for runoff calculation and the exact assignment of amount and time of precipitation is only one factor. Also important for runoff calculation is the correct timing of meltwater production, which is, however, directly related to temperature. In any case, it is important to derive representative time series of precipitation and air temperature to simulate short-term fluctuation in runoff.

6.4.2 Procedure of extrapolation of daily sums of precipitation

The procedure of extrapolation of daily sums of precipitation is a statistically based method developed by Weber (1997), which takes different reference stations of the corresponding region into account. An intensive statistical analysis of the time series of the SGHU station and the reference stations revealed that none of the reference stations in the regions under investigation corresponds well with the SGHU station.

Precipitation data of the SGHU station and the reference stations were analysed according to the following criteria:

a) Determination of the occurrence probability of precipitation events for each station for each month

b) Determination of the joint probability of precipitation occurrence at the SGHU station and the DHM reference stations

c) Determination of the mean ratio of monthly sums of precipitation at the SGHU station and the DHM reference stations

d) Determination or estimation of the "true" monthly sums of precipitation at the SGHU station.

The criterion for a) is the number of days per month with precipitation of more than 1 mm. The number of days with or without joint precipitation at the SGHU and reference stations is the criterion for b). The ratio of c) provides a dimension of the amount of precipitation which can be expected during a precipitation event at the target station (SGHU station). In high alpine regions precipitation increases with altitude. Local upwind-downwind effects are dominant and the theoretically possible amount of precipitation cannot increase constantly with altitude due to the declining water-holding capacity of air because of decreasing air temperature. The value of d) is used to match the synthetic precipitation data to a more

realistic value. This point is quite delicate because of data gaps in the SGHU time series. If no data are available, this value must be estimated subjectively.

There is no reference station that shows precipitation patterns similar to those of the SGHU station. Therefore, extrapolation methods like the one for temperature extrapolation cannot be applied. Thus, all reference stations are considered to derive event probability and amount of precipitation at the SGHU stations. The daily amount of precipitation at the SGHU station is calculated on the basis of this information with following equation (Weber, 1997):

$$P_{SGHU} = \frac{1}{N} \cdot \sum_{r=1}^{N} \left(P_r \cdot F_{r,m} \cdot W_{r,m} \right) \tag{6.4}$$

P_{SGHU}: Daily sum of precipitation at SGHU station (mm/day)
P_r : Measured precipitation at reference station r (mm/day)
$F_{r,m}$: Mean ratio of amount of precipitation between station r and SGHU station of the month m (-)
$W_{r,m}$: Weighting of station r according to the joint occurrence probability of precipitation at target station and reference stations for the month m (-)
N: Number of reference stations

The matrix of the mean ratio of monthly sums of precipitation at the reference stations and SGHU station in the Langtang region is derived from the mean monthly sums of precipitation of the period 1988 to 1998 as shown in Figure 6.12. Table 6.5 shows the $F_{r,m}$ values of Equation 6.4.

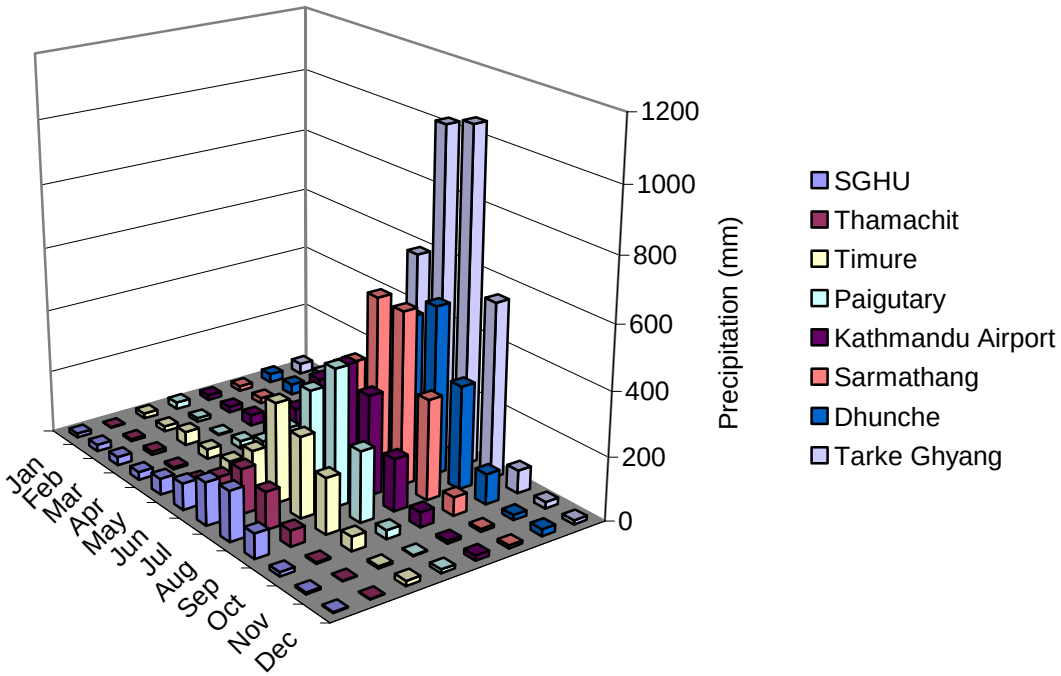

Figure 6.12: Mean monthly sums of precipitation at the SGHU station and reference stations in the Langtang region from 1988 to 1998

Table 6.5: Mean ratio of amount of precipitation between the reference station r and the SGHU station in the Langtang region of the month m ($F_{r,m}$) from January to December

SGHU	Timure	Thamachit	Paigutary	Dhunche	Tarke Ghyang	Sarmathang	Kathmandu Airport
1.00	0.80	2.00	0.59	0.47	0.38	0.82	0.84
1.00	1.19	2.00	1.77	0.61	0.49	1.13	1.07
1.00	0.62	2.00	2.00	0.43	0.43	0.91	0.79
1.00	0.83	2.00	1.00	0.41	0.37	0.67	0.45
1.00	1.34	2.00	0.72	0.34	0.32	0.49	0.35
1.00	0.72	1.22	0.54	0.32	0.14	0.27	0.30
1.00	0.43	0.96	0.42	0.29	0.13	0.25	0.37
1.00	0.62	1.33	0.37	0.30	0.15	0.29	0.50
1.00	0.45	1.57	0.35	0.24	0.14	0.25	0.47
1.00	0.29	2.00	0.47	0.14	0.18	0.22	0.28
1.00	0.87	2.00	1.82	0.37	0.28	0.66	0.63
1.00	0.19	1.57	0.26	0.14	0.25	0.37	0.19

Variation of $F_{r,m}$ is low during the monsoon season while it increases during the winter season and the factors become more uncertain. However, occurrence probability of precipitation is small and therefore $F_{r,m}$ plays a minor role in Equation 6.4 during the winter season. Dhunche, Tarke Ghyang, Sarmathang and Kathmandu airport receive much more precipitation than the SGHU station. In the case of Tarke Ghyang the mean annual precipitation amount is approximately six times the amount of the SGHU station. These stations are located on the south-west flank of the Himalaya where condensation of moisture-laden air starts due to orographic lifting. This is also the reason for higher precipitation intensities at these stations. Figure 6.13 shows the number of days with precipitation amounts greater than 1.0 mm, 5.0 mm, 10.0 mm, 20.0 mm and 50.0 mm for the year 1997. Days with precipitation amounts of more than 50.0 mm only occur at Dhunche, Tarke Ghyang, Sarmathang and Kathmandu airport.

Timure and Thamachit correspond better with the SGHU station, but Thamachit usually receives half the precipitation of the SGHU station while Timure gets about 1.5 times more precipitation than the SGHU station in a year. Thamachit is located in the inner Himalayan region in a lee position and therefore receives the smallest precipitation amount of all the reference stations.

Figure 6.14 shows the mean daily occurrence probability of precipitation in the Langtang region. The occurrence probability is given as a percentage. It can also be interpreted as a percentage of days with precipitation per month. Thus, it rains nearly every day at Tarke Ghyang in July and August while the SGHU station receives rain on 22 of 31 days. The highest occurrence probabilities of precipitation can be found in July for all the reference stations with more than 75%. At the SGHU station, however, occurrence probability is higher in August with 80% for the observation period 1988 to 2000. Generally, the occurrence probabilities of precipitation are high during the monsoon season and low during the winter. Precipitation disposition during the dry season is higher from February to April than from November to January. Tarke Ghyang receives the most precipitation with the highest occurrence probability.

Figure 6.15 illustrates the probability of joint occurrence of precipitation events at the SGHU station and the reference stations in percent. The matrix values of the joint occurrence

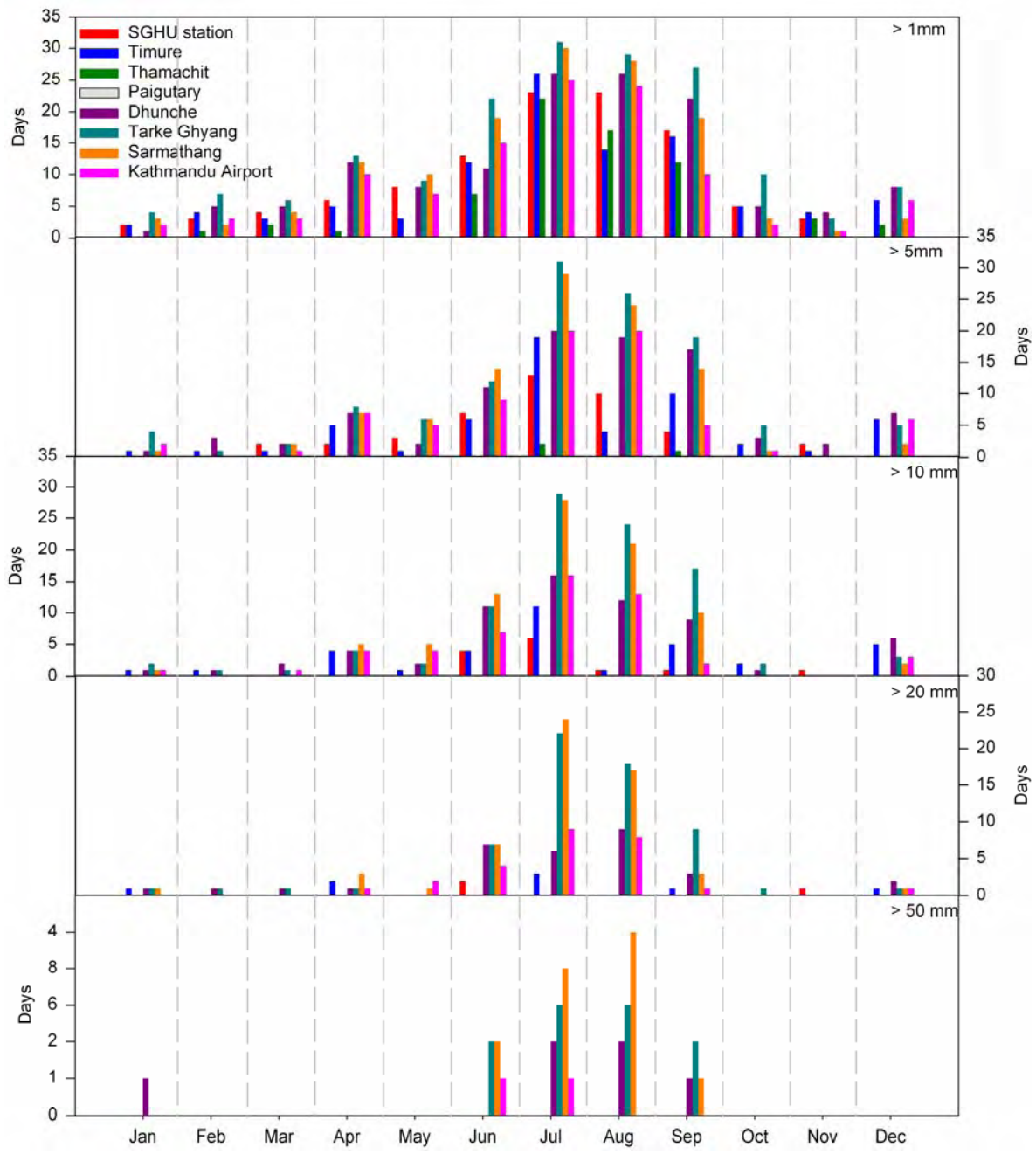

Figure 6.13: Number of days with precipitation amount of more than 1.0 mm, 5.0 mm, 10.0 mm, 20.0 mm and 50.0 mm at the SGHU station and reference stations in the Langtang region, 1997

probability of precipitation (given in absolute numbers) serve as weights ($W_{r,m}$) in Equation 6.4. None of the reference stations reflects the situation at the SGHU station adequately for the whole year. Good correspondence can be found only in August (Tarke Ghyang) and during the dry season especially in November and December when nearly no precipitation events occur. For the rest of the year corresponding events can only be expected every second or third day. In most of the years Dhunche, Tarke Ghyang, Sarmathang and Kathmandu airport show a slightly higher joint probability than Timure and Thamachit.

With all this information, synthetic daily sums of precipitation can be calculated. Equation 6.4 usually overestimates the real sums of precipitation at the SGHU station. If only a few days

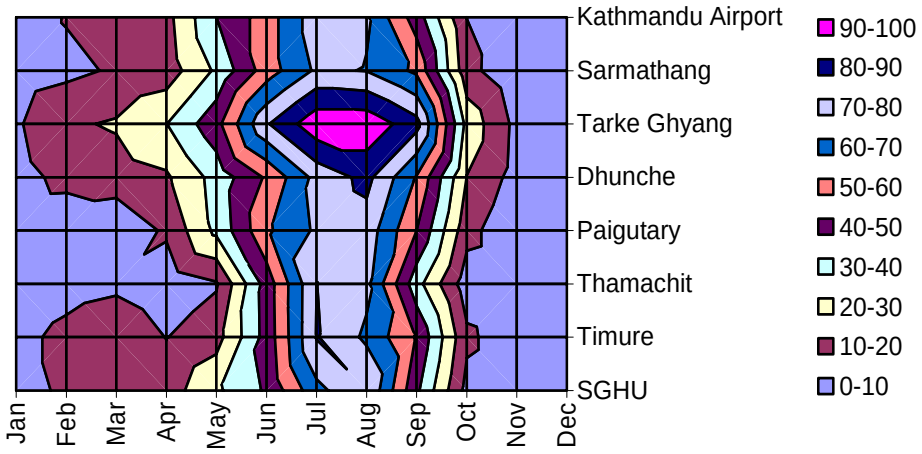

Figure 6.14: Mean daily occurrence probability of precipitation (in %) of the SGHU station and reference stations in the Langtang region (1988-1998)

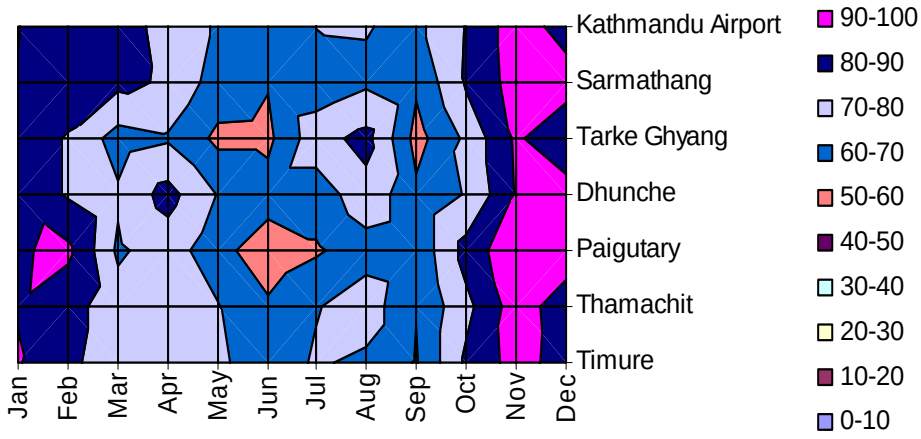

Figure 6.15: Probability of joint occurrence of precipitation events (precipitation yes or no) (in %) at the SGHU station and reference stations situated in the Langtang region (1988-1998)

are missing, the determination or estimation of the "true" monthly sums of precipitation at the SGHU station is possible for the respective month. The ratio of measured monthly sums of precipitation and extrapolated values is taken for the adjustment of the synthetic daily values to the current meteorological situation at the SGHU station. If too many days of a month are missing, mean monthly sums of precipitation of measured values of months without gaps are taken for the adjustment. In this case a mean ratio is calculated for the respective month as shown in Table 6.6.

Table 6.6: Extrapolated and measured monthly sums of precipitation and their ratio of years without gaps in March at the SGHU station in the Langtang Khola catchment

Year	Extrapolated	Measured	Ratio
1988	130.7	56.2	2.3
1989	81.7	31.0	2.6
1992	47.1	14.0	3.4
1993	50.3	27.4	1.8
1994	50.5	13.2	3.8
1997	37.0	21.5	1.7
1998	184.5	40.8	4.5
1999	5.0	21.8	0.2
Mean ratio			2.6

In the case of March 1991 there are 30 days without measurements and therefore it is impossible to estimate the "true" monthly sum of precipitation based on measurements. Thus, the mean ratio of Table 6.6 is taken. A subjective criterion to check the reliability of the ratio is the percentage deviation of monthly sums of precipitation of the SGHU station and reference stations from the long-term mean. These deviations show whether the respective month is wetter or dryer than the long-term mean. Table 6.7 and Figure 6.16 show that in March 1991 some stations are wetter (Timure, Dhunche, Kathmandu Airport) than the long-term mean and others are dryer (Tarke Ghyang, Sarmathang, Paigutary). Months with gaps in the daily time series have not been considered in this statistical analysis. These months give no deviation values in Table 6.7. Timure and Paigutary are close to the SGHU station and both stations are located in the inner Himalayan region like the SGHU station. Timure receives about twice as much (102% more) precipitation in March 1991 as the long-term mean, while Paigutary gets no precipitation at all. March 1991 is therefore considered as a month with balanced precipitation patterns compared to the long-term mean. An example for a dryer month than the long-term mean is October 1991 where all stations show a negative deviation. Therefore, the long-term mean ratio for March (2.6) seems to be quite reliable because it gives a modified extrapolated sum of 27 mm which is exactly the same as the long-term mean value of March. This criterion is only subjective but it gives some support to judge the reliability of the ratio and thus the reliability of the extrapolated values. The ratio is now used to adjust the daily precipitation data.

Table 6.7: Deviation of monthly sums of precipitation from the long-term mean of precipitation in 1991 at the SGHU station and reference stations in Langtang region

month	SGHU	Timure	Thamachit	Paigutary	Dhunche	Tarke Ghyang	Sarmathang	Kathmandu Airport
Jan	-	-	0	-100	-	-12	25	31
Feb	-	-	83	-100	-18	-	-83	-42
Mar	-	102	-	-100	2	-47	-97	32
May	48	-	-33	-100	-32	-26	-97	89
Apr	29	13	-	-11	-	-	-69	-
Jun	-	42	-	71	-	-	-84	-
Jul	-45	-	-31	40	-	-22	-94	-49
Aug	-	-	-3	37	-	-14	-62	-11
Sep	-	-	-	8	-	3	-45	-
Oct	-77	-93	-60	-100	-	-	-64	-100
Nov	50	-57	-100	233	-	-	-89	-100
Dec	400	0	100	92	-	38	-	56

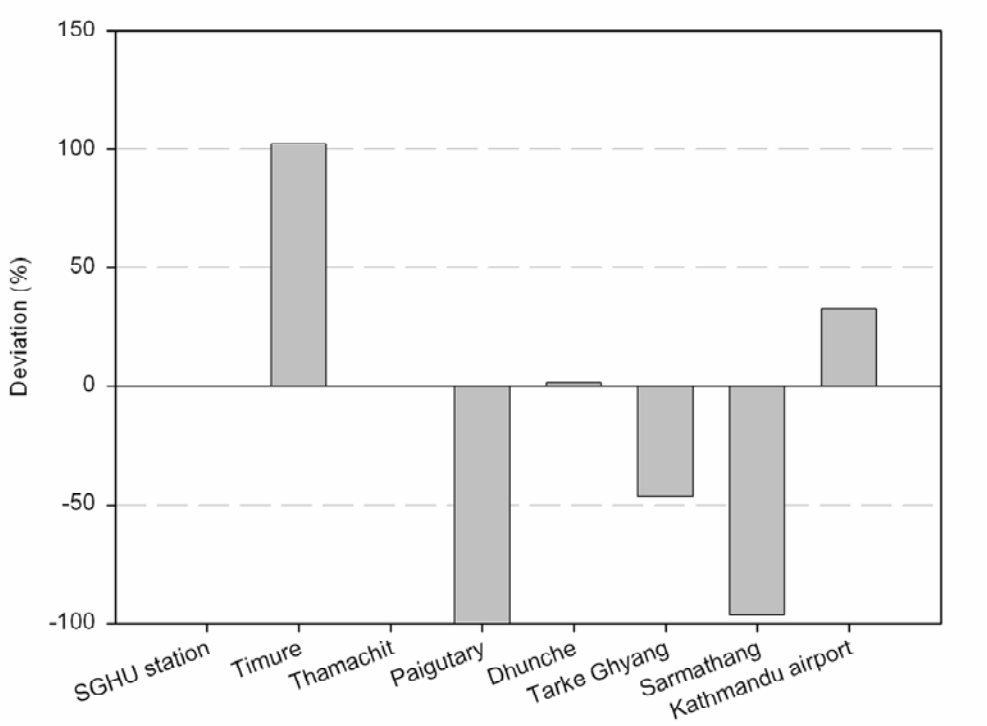

Figure 6.16: Deviation of sums of precipitation in March 1991 from mean monthly sums of precipitation (period 1988-1998) at the reference stations and SGHU station in the Langtang region

Data of the extrapolated time series are only used to fill gaps in the original time series of the SGHU station or to redistribute cumulated values over the previous days. Figure 6.17 summarises the steps of the extrapolation method.

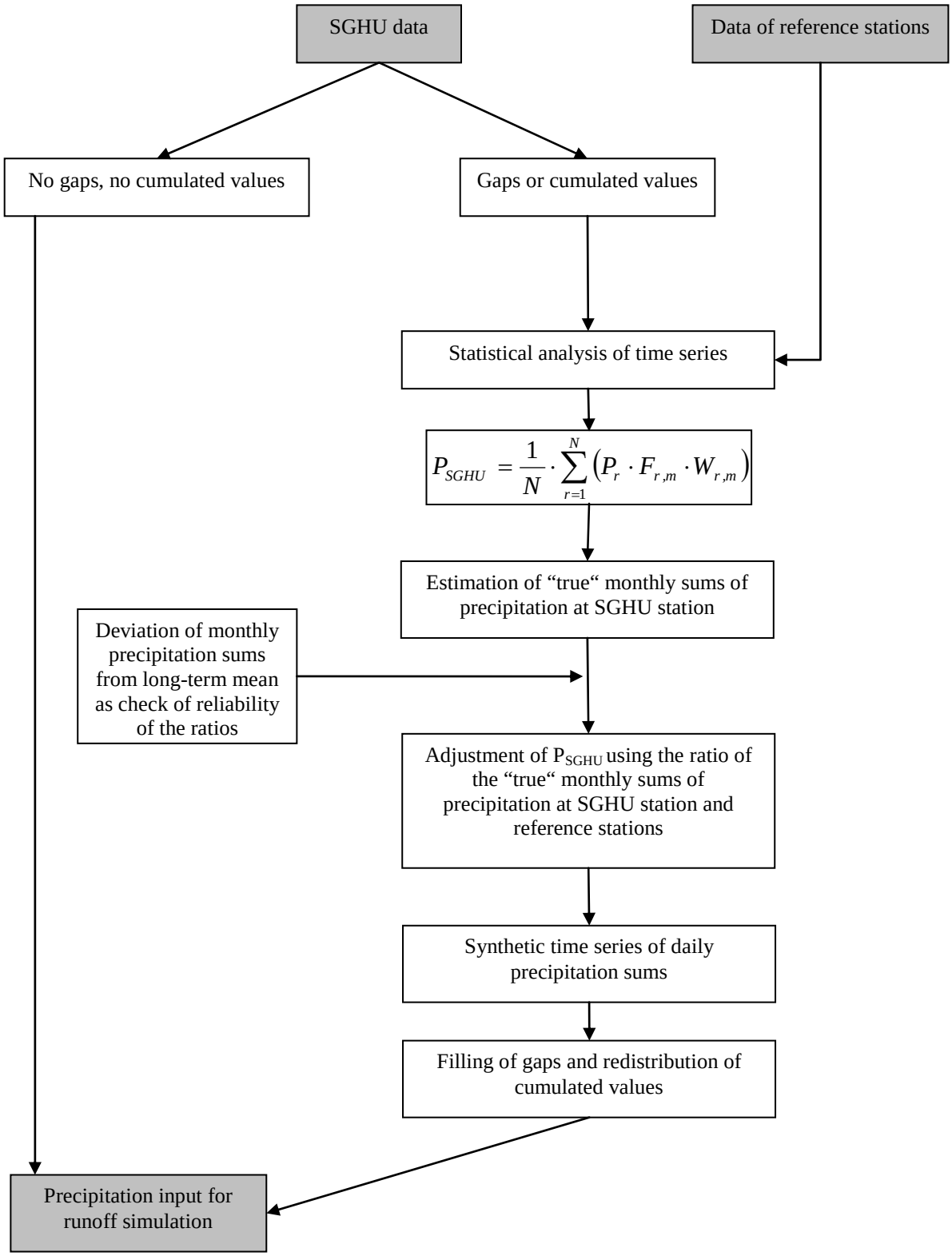

Figure 6.17: Steps of the extrapolation method for daily sums of precipitation

6.5 Spatial data

6.5.1 Data base

Areal information was derived from digital maps of the Survey Department of His Majesty's Government of Nepal. The digital maps were produced by the Survey Department in co-operation with the government of Finland. Table 6.8 shows the digital maps that were used in the study. They contain GIS layers with altitude, land use, river system and glacier information as vector-based polygons or lines. The glacier-covered area was taken from maps published in ICIMOD's glacier inventory (ICIMOD/UNEP, 2002).

Table 6.8: Digital maps of the Survey Department used to derive area information

Catchment	Sheet No.	Date of aerial photography	Date of field validation	Scale
Langtang	2885 11	1992	1996	1:50,000
Khola	2885 15	1992	1996	1:50,000
	2885 16	1992	1996	1:50,000
Modi Khola	2883 08	1996	2000	1:50,000
Imja Khola	2786 04	1992	1996	1:50,000

In the case of Langtang Khola catchment digital maps of the Survey Department do not cover the whole catchment area. The north-western part is located in China, therefore the map of the German Alpine Club (DAV) was used to complete the digital maps. The following Table 6.9 gives the data of the additional DAV map called "Langthang Himal-Ost".

Table 6.9: Additional topographic map that covers the Chinese part of the Langtang catchment

Sheet No.	Date of aerial photography	Date of field validation	Scale
DAV 0/11	1973	-	1:50,000

The glacier distribution is derived from the digital maps of ICIMOD's glacier and glacier lake inventory. This inventory was realised in co-operation with the United Nations Environmental Programme (UNEP) (ICIMOD/UNEP, 2002). Digital data sets of the Land Observation Satellite (LANDSAT)-5 Thematic Mapper (TM) and of the Indian Remote Sensing Satellite Series 1D (IRS1D) were used mostly for the inventory. Some data sets of Système Probatoire d'Observation de la Terre (SPOT), Multi-Spectral (XS) and SPOT Panchromatic (PAN) were also used. The topographic maps were published by the Survey of India in the period from the 1950s to the 1970s on a scale of 1 inch to 1 mile (i.e. 1:63,360) and by the Survey Department of His Majesty's Government of Nepal in 1996 on a scale of 1:50,000. The topographic maps of the Survey Department were based on aerial photographs from 1992 and field validation in 1996. The aerial photographs (scale 1:50,000) used for ICIMOD's glacier inventory were taken in 1992 for eastern Nepal and in 1996 for western Nepal. Prints of the satellite images in the form of planimetric maps on a scale of 1:250,000 published by the Remote Sensing Centre of Nepal in 1984 were used for the inventory of glaciers and glacial lakes. Landsat MSS data in digital format from March–April 1994, resampled in 50 m pixel size, are

available at ICIMOD in Kathmandu, Nepal. These glacier maps do not contain debris layers; therefore, additional printed maps were taken to derive information about debris-covered glaciers (Table 6.10). The maps for the Modi Khola and Imja Khola catchments were produced by the "Arbeitsgemeinschaft für Vergleichende Hochgebirgsforschung", Munich and the DAV map was used for the Langtang Khola catchment.

Table 6.10: Printed maps that contain information about debris-covered glaciers

Catchment	Sheet No.	Date of aerial photography	Date of field validation	Scale
Modi Khola	No. 9	-	1989-1991	1:100,000
Imja Khola	No. 2	-	1955-1963	1:50,000
Langtang Khola	DAV 0/11	1973	-	1:50,000

6.5.2 Spatial discretization and transformation of vector-based maps into raster maps

As described above, the Survey Department provides vector maps of land use, contour lines and river systems. These vector maps have to be converted into raster maps. A cell size of 200 x 200 m² is considered to be appropriate in view of computation time and temporal discretization. Larger cell sizes are not appropriate in relief-dominated areas like mountain valleys when applying process-oriented modelling. Ott (2002) found a significant information loss with increasing cell size which is especially problematic in mountainous catchments. Various methods to derive the raster maps from the vector-based maps were tested and are presented here with results of the Langtang Khola catchment. The first method (method I) is the conversion of the vector map into a 10 x 10 m² grid. This grid is aggregated to a 50 x 50 m² grid and then to the final 200 x 200 m² raster map using average values. Aggregation from a 10 x 10 m² to a 200 x 200 m² raster map is the second method (method II). The third method (method III) is the direct conversion from the vector map to the 200 x 200 m² raster map without aggregation. Results of methods I to III are evaluated using the deviation of the area distribution of each altitude belt (400 m) of the 200 x 200 m² raster map from the 10 x 10 m² raster map (Figure 6.18, upper graphic). The 10 x 10 m² raster map is considered to be the one providing the most reliable area distribution. Figure 6.18 (upper graphic) shows that the area distribution of altitude belts of raster maps calculated by method III deviates the least from the area distribution of the 10 x 10 m² raster map. Methods I and II overestimate the area of the higher altitude belts significantly whereas method I delivers no values for the altitude belt from 6800 to 7200 m. Method III underestimates the area of the highest altitude belt. 0.23% of the catchment area is located in this altitude belt, i.e. 0.84 km² of 360 km². Method III covers 0.64 km² for this altitude belt.

Another evaluation criterion is the deviation of the area distribution of slope classes (10°) of the 200 x 200 m² raster map from the 10 x 10 m² raster map (Figure 6.18, lower graphic). Slopes were derived from the 200 x 200 m² digital elevation models which were calculated using methods I-III. The differences between the results of the three methods are not as significant as in Figure 6.18 (upper graphic). The area distribution of slope class 51°-60° is highly underestimated by all three methods. This effect is caused by the dominance of flat areas in raster maps with low resolution (200 x 200 m²) and is therefore independent from the method applied to derive the 200 x 200 m² raster map. Method III is taken to calculate the raster maps from the vector maps.

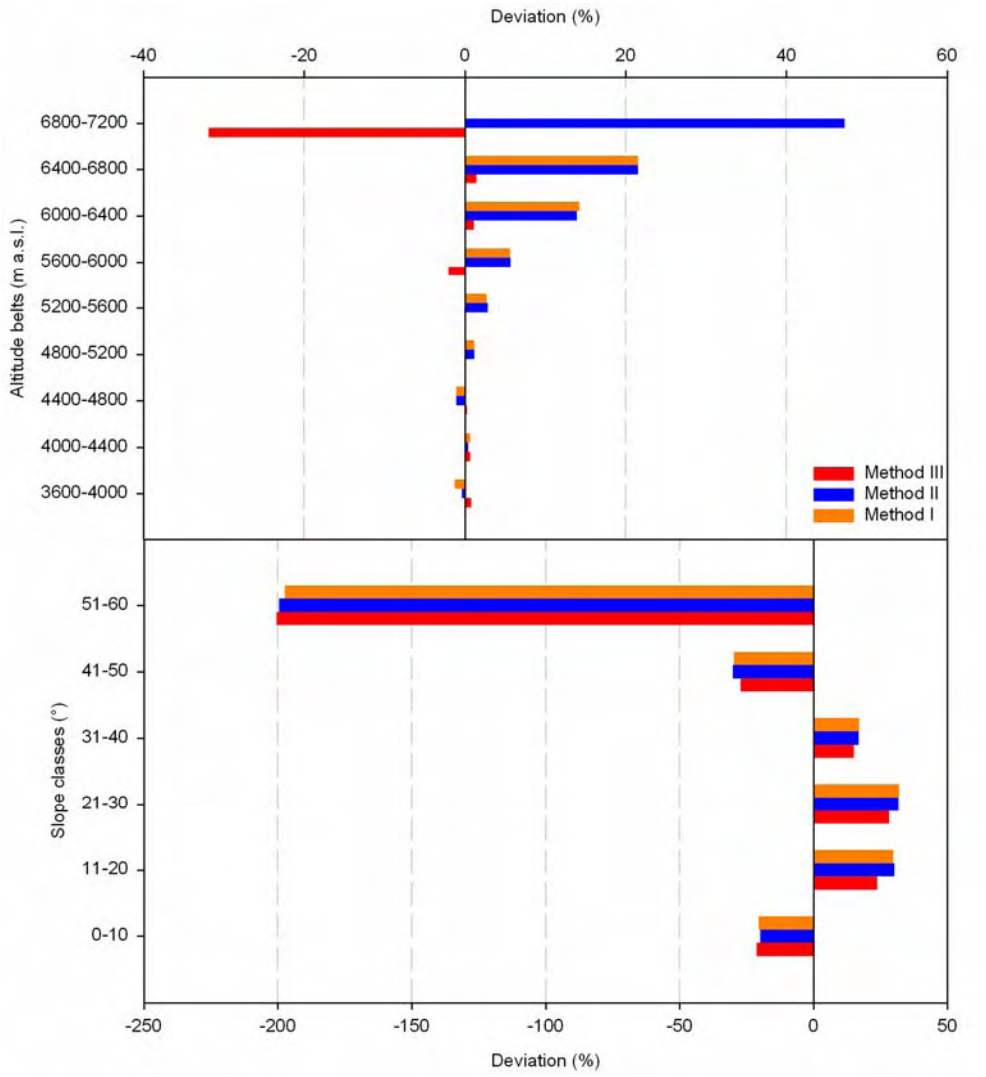

Figure 6.18: Deviation of area distribution of altitude belts (400 m) and of area distribution of slope classes (10°) of the Langtang Khola catchment of the 200 x 200 m² raster maps calculated using methods I-III from the 10 x 10 m² map

6.5.3 Digital elevation model

The digital elevation models of the three catchments were derived from the digital topographic vector maps of the Survey Department with contour intervals of 40 m. A triangular irregular network (TIN) was used to convert the contour lines into a 3D elevation model on vector basis. This elevation model consists of polygons which can be converted into raster cells using method III. The 200 x 200 m² digital elevation models serve as fundamental maps for spatial modelling.

6.5.4 River network

The river network was digitised from the DAV topographic map or from maps of the "Arbeitsgemeinschaft für vergleichende Hochgebirgsforschung" (Table 6.10) and converted

into the raster format. The river network layer of the digital maps of the Survey Department clearly overestimates the stream density and the river network shows many gaps. Field visits revealed that in these digital maps water-free channels in the flanks of the mountains are defined as rivers.

The meandering of the streams in the catchment causes an overestimation of stream cells in the raster format. The unrealistic accumulation of stream cells in the area of meanders was corrected manually to achieve a more realistic river network. The river network covers the glacier-free part of the catchment and all streams end at the glacier tongues (Figure 6.19, left).

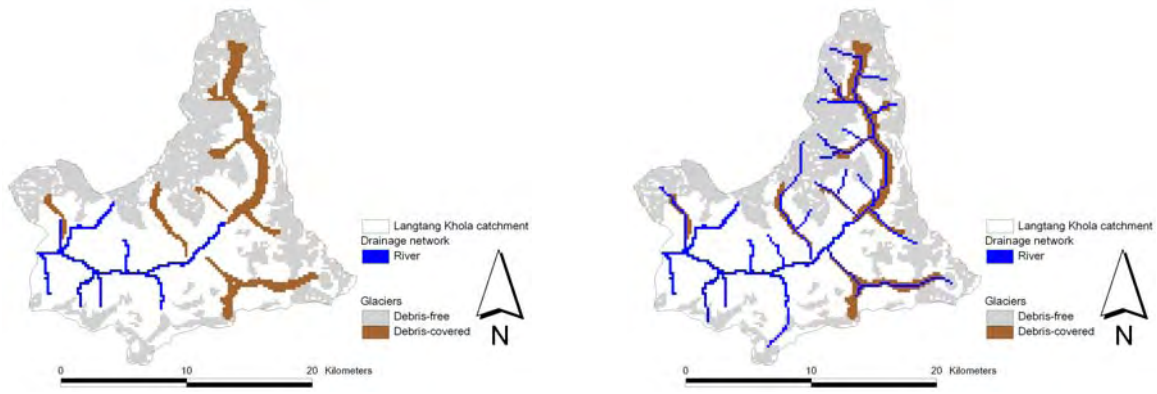

Figure 6.19: River network derived from DAV topographic map (left) and revised river network (right) of the Langtang Khola catchment

It can be assumed that a subglacial channel network exists (section 5.5). Field visits have substantiated this assumption (Figure 6.20).

Figure 6.20: Stream beneath the debris-covered glacier in the Modi Khola catchment

Therefore the river network was extended below the glaciers manually as shown in Figure 6.19 (right). Subglacial channel networks exist mainly in the ablation area of valley glaciers, therefore the channel network was extended only in the areas of these glaciers. The range of the extension is hard to define but actually no liquid water is produced in the model in the higher altitudes of the catchment, and thus no lateral fluxes occur in these areas. An overestimation of the river network in the higher altitudes therefore causes no significant error in the simulation. It is much more important to get a realistic river network in the ablation area of the glaciers where liquid precipitation and meltwater occurs. The extension of the river network is necessary to get a more realistic simulation of the discharge dynamics. Water in the river network is directed to the outlet of the catchment during one time step (here taken to be 1 day) while lateral fluxes are only directed from one cell to the next downstream cell during one time step. With the river network derived from the DAV map or from maps of the "Arbeitsgemeinschaft für vergleichende Hochgebirgsforschung" unrealistic residence times of water in the glacier-covered parts of the catchment would cause wrong simulations of discharge dynamics. The river network obtained (Figure 6.19, right) was not concordant with the local drainage direction network (ldd), which was derived from the DEM (section 4.2.3). Thus, it was necessary to "burn" the revised river system into the DEM to match the ldd to the river network. All river network cells of the DEM were deepened by 100 m, and the ldd was calculated using the revised DEM. This DEM is not used for spatial regionalisation of meteorological data because it would yield wrong information at the revised cells due to the altitude dependence of the regionalisation methods. No sinks or pits were observed while creating the ldd.

6.5.5 Land use

The land use 200 x 200 m² raster maps were derived from the land use map of the Survey Department, the DAV map, maps of the "Arbeitsgemeinschaft für vergleichende Hochgebirgsforschung" and from the glacier maps of ICIMOD. Three units were distinguished (Figure 6.21): non-glacier-covered parts (Survey Department), glacier-covered areas (ICIMOD) and debris-covered glaciers (DAV, "Arbeitsgemeinschaft für Vergleichende Hochgebirgsforschung").

6.5.6 Runoff generation type units

As described in section 5.5 four runoff generation type units were identified on the basis of topographic maps and field surveys. The units are (Figure 6.22): non-glacier-covered parts (nRGType 1), glacier-covered areas (nRGType 2), glacier tongues with an inclination of less than 3° and debris cover (nRGType 3), and the valley bottom with an inclination of less than 8° (nRGType 4). A more detailed differentiation was not possible on the available data base. NRGTypes 1 and 2 dominate in the catchment (Table 6.11).

Table 6.11: Area of the runoff generation type units

		Langtang Khola	Imja Khola	Modi Khola
nRGType		**Area (km²/%)**	**Area (km²/%)**	**Area (km²/%)**
1	Non-glacierized	189.7/53	81.4/58	83.6/52
2	Glacier	162.1/45	48.4/34	76.3/47
3	Glacier tongue	3.2/1	4.4/3	0.4/0.2
4	Valley bottom	4.8/1	6.6/5	0.3/0.2

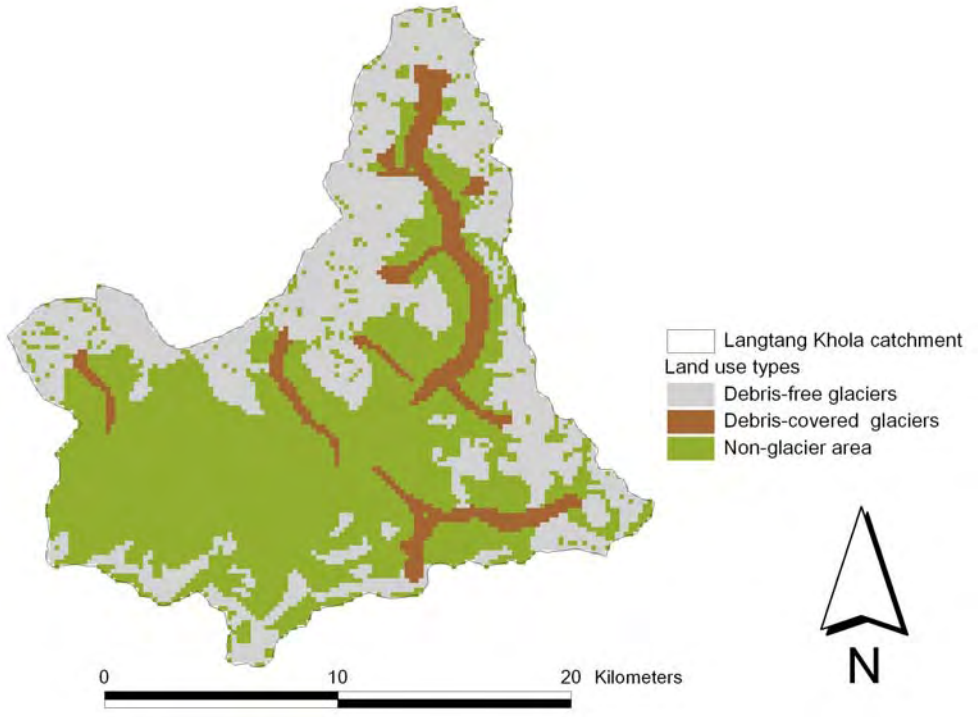

Figure 6.21: Land use map of the Langtang Khola catchment

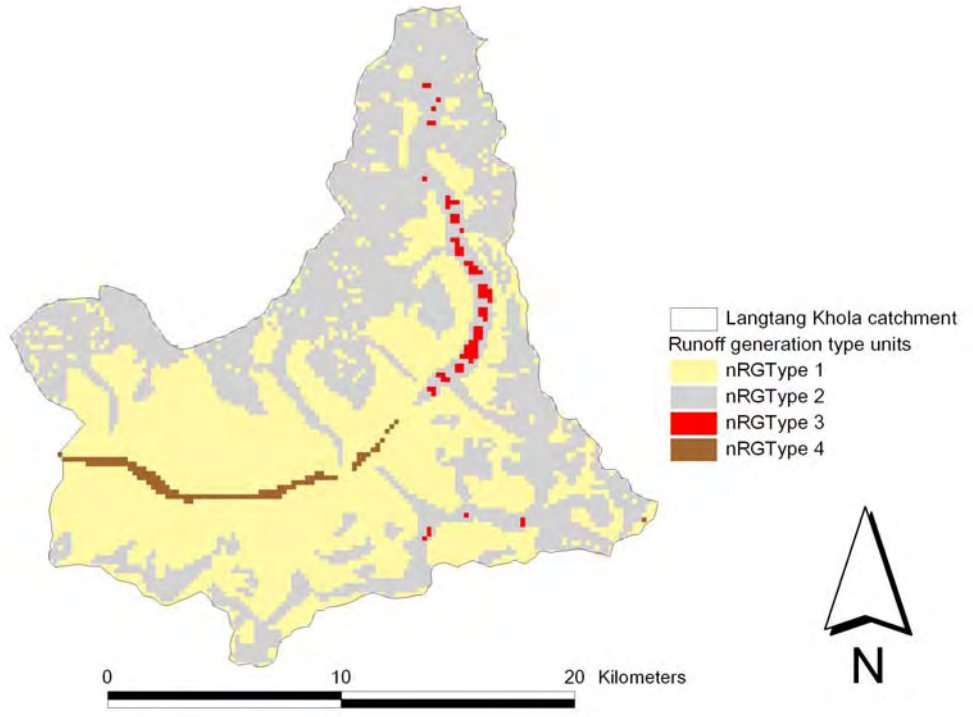

Figure 6.22: Runoff generation type units of the Langtang Khola catchment

6.6 Conclusions

The quality of the meteorological input data is considered to be appropriate for discharge simulation in daily resolution after the described corrections and extrapolations whereas the quality of the measured discharge data strongly varies between the investigated catchments. It is therefore proposed to take the visual inspection of the simulated hydrograph as an important evaluation criterion beside the objective evaluation criteria for the calibration of the model.

Various ways to transfer the vector maps into raster maps were tested and the method with the smallest information loss was taken. The spatial resolution of 200 x 200 m² seems to be quite high compared to the temporal resolution of daily time steps regarding lateral flow simulations. However, the extension of the river network partly compensates these errors and the spatial resolution of 200 x 200 m² is essential for realistic melt simulations.
The runoff generation type units are derived subjectively from the digital elevation models, from the available land use maps and from topographical maps under consideration of observations during field trips.

7 Processing

The processing section contains details of the model application. The available input data sets were subdivided into a calibration and a validation period (Table 7.1). The models were tested in the validation period with the optimal parameter set obtained in the calibration period.

Table 7.1: Calibration and validation periods

Catchment	Calibration period	Validation period
Langtang Khola	1993-1998	1987-1993
Modi Khola	-	1991-1994
Imja Khola	1991-1995	1988-1991

7.1 Model evaluation

In addition to the visual inspection of the simulated hydrograph in comparison with the measured one, four different objective evaluation criteria were used. The most common criterion is the model efficiency according to Nash and Sutcliffe (1970):

$$R_{eff} = 1 - \frac{\sum_{i=1}^{n}(Q_{i,obs} - Q_{i,sim})^2}{\sum_{i=1}^{n}(Q_{i,obs} - \overline{Q_{obs}})^2} \quad (7.1)$$

R_{eff}: Model efficiency (-)
$Q_{i,obs}$: Observed runoff at time step i (mm/time step)
$Q_{i,sim}$: Simulated runoff at time step i (mm/time step)
$\overline{Q_{obs}}$: Mean observed runoff for the whole observation period (mm/time step)
i: Time step
n: Duration of simulation period (number of time steps)

Model efficiency is dimensionless and ranges from -∞ to 1. A perfect fit is achieved if the value is 1. The logarithmic model efficiency emphasises the weighting of low discharges and therefore can be used to evaluate the simulated low flows (Uhlenbrook, 1999):

$$R_{log\,eff} = 1 - \frac{\sum_{i=1}^{n}(log(Q_{i,obs}) - log(Q_{i,sim}))^2}{\sum_{i=1}^{n}(log(Q_{i,obs}) - \overline{log(Q_{obs})})^2} \quad (7.2)$$

R_{logeff}: Logarithmic model efficiency (-)
$\overline{log(Q_{obs})}$: Mean logarithmic observed runoff for the whole observation period (mm/time step)

Another criterion is the coefficient of determination which is defined as the ratio of explained sum of squares and total sum of squares (Yamane, 1964):

$$R^2 = \frac{\left(\sum_{i=1}^{n}((Q_{i,obs} - \overline{Q_{obs}})(Q_{i,sim} - \overline{Q_{sim}}))\right)^2}{\sum_{i=1}^{n}(Q_{i,sim} - \overline{Q_{sim}})^2 \cdot \sum_{i=1}^{n}(Q_{i,obs} - \overline{Q_{obs}})^2} \quad (7.3)$$

R^2: Coefficient of determination (-)
$\overline{Q_{sim}}$: Mean simulated discharge for the whole observation period (mm/time step)

The coefficient of determination ranges from 0 to 1 where 1 is the optimal correlation between measured and simulated discharge. The fourth criterion is the volume error, which is the standardised cumulated difference between simulated and measured discharge of a defined period:

$$VE = \sum_{i=1}^{n}(Q_{i,obs} - Q_{i,sim}) \quad (7.4)$$

VE: Volume error (mm)

In this study the volume error has been calculated for each hydrological year (mm/a).

The evaluation criteria were calculated in an external statistics programme. Missing values in the measured discharge data were considered, and only complete data pairs of simulated and measured discharge of a time step were used for the calculation of the evaluation criteria.

7.2 Initialization

The initialization of storage values is of great importance for realistic simulations of discharge and other components of the hydrological cycle. Initial storage levels have to be adjusted to the conditions at the beginning of the simulation by initialization runs (section 5.8). Wissmeier (2005) found that simulations with TAC^d are extremely sensitive to their initial conditions. Thus climatic input data of the validation period were taken to calculate the initialization maps containing storage levels of the beginning of the calibration period. These maps have to be calculated during initialization runs of TAC^d with given starting values for storage levels for the first initialization run. Depending on parameterisation, initialization maps are produced at the end of each initialization run. The calculated storage values are used as new starting values for storage levels. This procedure has to be repeated until constant storage levels are achieved (Figure 7.1).

Six initialization runs were performed to achieve stable storage levels. Wissmeier (2005) recommended repeating the initialization procedure for each calibration run. This is not appropriate due to the long computation time. Here, the initialization procedure was repeated if significant changes in the objective evaluation criteria occurred or if storage parameters of the runoff generation routine were calibrated. These parameters mainly determine the storage characteristics and therefore they have the greatest impact on the initialization maps. If, for example, the upper limit of the storages is reduced during a calibration run and therefore the initial storage levels are higher than the upper limit, fast drainage would occur and discharge would be highly overestimated at the beginning of the simulation period. Figure 7.2 shows a section of an initialization map of the upper storage levels (US_box) with the ldd. Highest storage levels occur at convergent points like valley bottoms or nodes of the ldd.

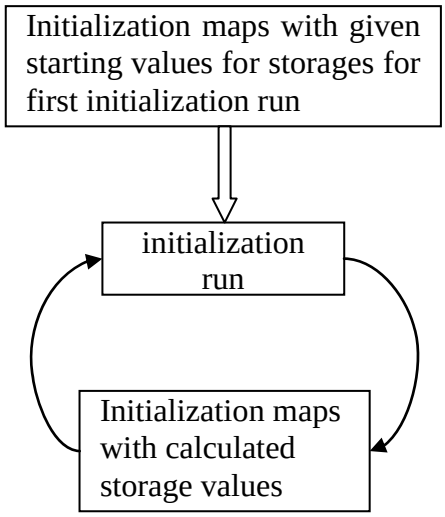

Figure 7.1: Initialization procedure

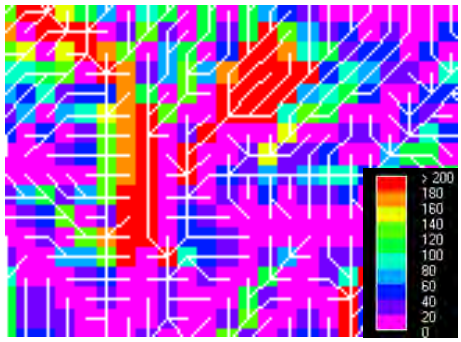

Figure 7.2: Section of the initialization map for upper storage levels (US_box) with ldd

The validation period was initialized with the same initialization maps as used for the calibration period. These maps represent the situation at the end of the validation period; therefore, the levels are not the realistic values of the beginning of the validation period. The simulation error caused by this assumption affects only the first year of the validation period until the storage levels have adjusted to the situation at the beginning of the validation period. This adjustment takes place quickly because the magnitude of the storage levels does not vary that much from one post-monsoon season to another.

7.3 Calibration of the model

The aim of the calibration procedure is the optimal adaptation of model parameters to achieve the best simulation results. The models were calibrated to the Langtang Khola catchment and the obtained parameter set was taken as the starting point for calibration to the Imja Khola and Modi Khola catchments. Optimization of parameters of TAC^{d} and HBV-ETH was realised by a so-called inverse modelling technique where simulated values were compared with measurements and the results were evaluated by visual inspection of the hydrographs and by

statistic evaluation criteria (section 7.1). Good simulation of measured discharge was the main optimization criterion. Additionally, glacier mass balances or water equivalents of snow cover can be taken for the optimization of the model parameters. Snow water equivalent measurements were not available in the catchments. Sporadic measurements of glacier mass balances of the Langtang Khola catchment were used as an additional calibration criterion.

Due to the long computation time, sophisticated parameter estimation techniques cannot be applied. However, a systematic approach consisting of three phases was chosen to yield the optimal parameter set. The first parameter set was created in phase I using guide numbers from literature. Braun et al. (1993) and Hagg (2003) applied the HBV-ETH model in various highly glacierized catchments in Central Asia. Parameters of the snow and glacier routine were derived from this study because the snow and glacier routine of TAC^d is comparable to the HBV-ETH model.

The magnitudes of the parameters of the soil and runoff generation routine of the different HRUs are intended to reflect the different hydrological responses of each HRU. Thus, mainly the expected relations between the HRUs were considered in the parameterisation of these routines. NRGType 3, for example, was expected to have the highest storage capacity of all HRUs and therefore the parameter GlacierLS_H was assumed to be at least 10 times higher than US_H2 of nRGType 2. Retardation of the upper storage is generally considered to be lower than retardation of the lower storage. This relation can be expressed with higher K-values of the upper storages. The parameters of the soil and runoff generation routine were chosen on the basis of calibration experiences with TAC^d in other catchments and of process understanding as shown in the examples above (Uhlenbrook 2005, personal conversation).

The values of this parameter set deliver magnitudes of the parameters for further calibration. Parameters were varied by a manual trial-and-error technique in phase II. Mainly, parameters of the snow and glacier routine and the precipitation correction factors were changed during this phase. The ratios between the storage parameters of the soil and runoff generation routine were not changed in this phase. If GlacierLS_H was reduced, all other upper limits of storages had to be reduced proportionately. The manual trial-and-error technique revealed the behaviour of the parameters and showed the occurrence of optima after only a few calibration runs. Based on this experience, calibration in pairs of the most sensitive parameters was performed in calibration phase III. This phase is often referred to as fine-tuning. Parameters of the soil and runoff generation routine remained untouched in this phase. The following pairs of model parameters were selected, based on previous modelling exercises with HBV-ETH by Renner and Braun (1990):

1) PCF-SFCF
2) Cfmax-TT
3) Cfmax-Rexp
4) Cfmax-CRFR
5) Cfmax-SFCF
6) SFCF-TT

The 5x5 Matrix of R_{eff} identifies the optimal constellation of the parameter pairs (Figure 7.3). The optimization runs in pairs were repeated until simulation results could not be improved any more.

Calibration of conceptual rainfall-runoff models in highly glacierized catchments is quite tricky. Glaciers are sources of water whose contribution to runoff generation is hard to estimate from discharge data. An overestimation of meltwater production can for, instance,

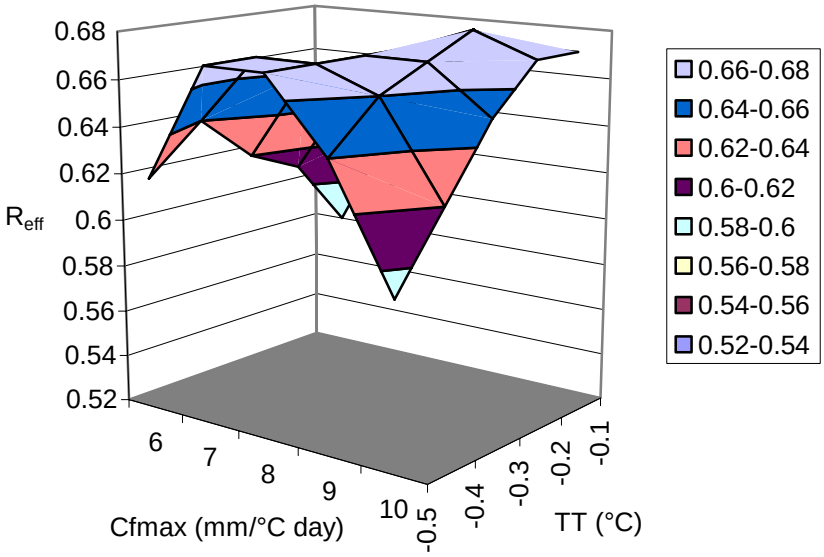

Figure 7.3: Example of 3D visualisation of the results of calibration in pairs (TT vs. Cfmax) of TAC^d for the Langtang Khola catchment

compensate for underestimated basin precipitation or vice versa. In this way, good simulation results can occur for the wrong reasons. In order to improve the process simulation a multi-criteria calibration can be applied instead of a single criteria calibration (Hottelet et al., 1994; Seibert, 2000). Information about the glacier mass balances in addition to discharge were considered in the calibration procedure to find the optimal parameters of the snow and glacier routine. Table 7.2 shows the available measurements of glacier mass balances in the Langtang Khola catchment.

This second optimization criterion enables a more realistic simulation of glaciermelt and therefore a more realistic discharge simulation.

The optimal parameter sets of the TAC^d and HBV-ETH models for the investigated catchments are shown in Tables A4 and A5 (Appendix). Red numbers indicate the changed parameters compared to the parameter set of the Langtang Khola catchment. Approximately 350 model runs of TAC^d were performed in the calibration procedure for the Langtang Khola catchment.

7.4 Results of the calibration period of the Langtang Khola catchment calculated with TAC^d

Comparative studies of conceptual precipitation-runoff models (Rango, 1992) have shown that for the simulation of daily values of discharge in high alpine catchments R_{eff}-values over 0.8 can be assessed as good. The first two hydrological years of the calibration period show a good adaptation of the simulated to the measured discharge. The dynamics of the hydrograph is reproduced satisfactorily in these years. From the hydrological year 1995/96 onwards the discharge is consistently overestimated by the model. In these years the measured discharge data show many gaps and inconsistencies which seem to be measuring errors. Measured discharge in the monsoon period in 1996/97 varies between 14.08 m³/s and 16.69 m³/s and remains on the same level for several days. Furthermore, measured discharge values in the

post-monsoon season 1997 show unrealistic high values until the beginning of November. In 1997/98 many data gaps occur and again, unrealistic plateaus of the discharge values can be observed. Due to these inconsistencies the hydrological years 1996/97 and 1997/98 were not considered for calibration. Table 7.3 summarises the evaluation criteria.

Table 7.2: Glacier mass balances in the Langtang Khola catchment

Glacier	Altitude of point measurement (m a.s.l.)	Mass balance (mm)	Observation period	Study
Yala	5150	-2300	May-October 1996	Fujita et al. (1998)
	5190	-2100	May-October 1996	Fujita et al. (1998)
	5230	-1700	May-October 1996	Fujita et al. (1998)
	5280	-1500	May-October 1996	Fujita et al. (1998)
	5350	-300	May-October 1996	Fujita et al. (1998)
	5380	300	May-October 1996	Fujita et al. (1998)
	5390	900	May-October 1996	Fujita et al. (1998)
	Areal average	-357	May-October 1996	Fujita et al. (1998)
Yala	5240	-2240	March 1991-March 1992	Braun et al. (1993)
	5580	510	March 1991-March 1992	Braun et al. (1993)

Table 7.3: Evaluation criteria of simulation results calculated with TAC^d (calibration period)

Hydrological year	R_{eff} (-)	log R_{eff} (-)	R^2 (-)	VE (mm/a)
1993/94	0.85	0.75	0.89	57
1994/95	0.87	0.80	0.88	-8
1995/96	0.53	0.31	0.72	92
1996/97	0.46	0.84	0.76	-8
1997/98	0.28	0.49	0.83	-43

The winter discharge is simulated well in the years 1993/94, 1994/95 and 1996/97 with logarithmic model efficiencies (log R_{eff}) from 0.75 to 0.84. The years 1995/96 and 1997/98 show unreliable equal values in the low flow season which could be reading errors or errors in digitising the handwritten data.

Generally, the calculated onset of discharge in May and June is delayed by some 10 days or more and, consequently, discharge is underestimated at the beginning of the melt/monsoon period. On the other hand, discharge is generally overestimated in the second half of the

melt/monsoon period. This causes an underestimation of measured annual discharge of 57 mm in 1993/94 and 92 mm in 1995/96. In 1994/95 there is a significant overestimation of the discharge in the pre-monsoon season. This overestimation is compensated over the year and the volume error is minimal in this year. Figure 7.4 compares the simulated discharge with the measured discharge.

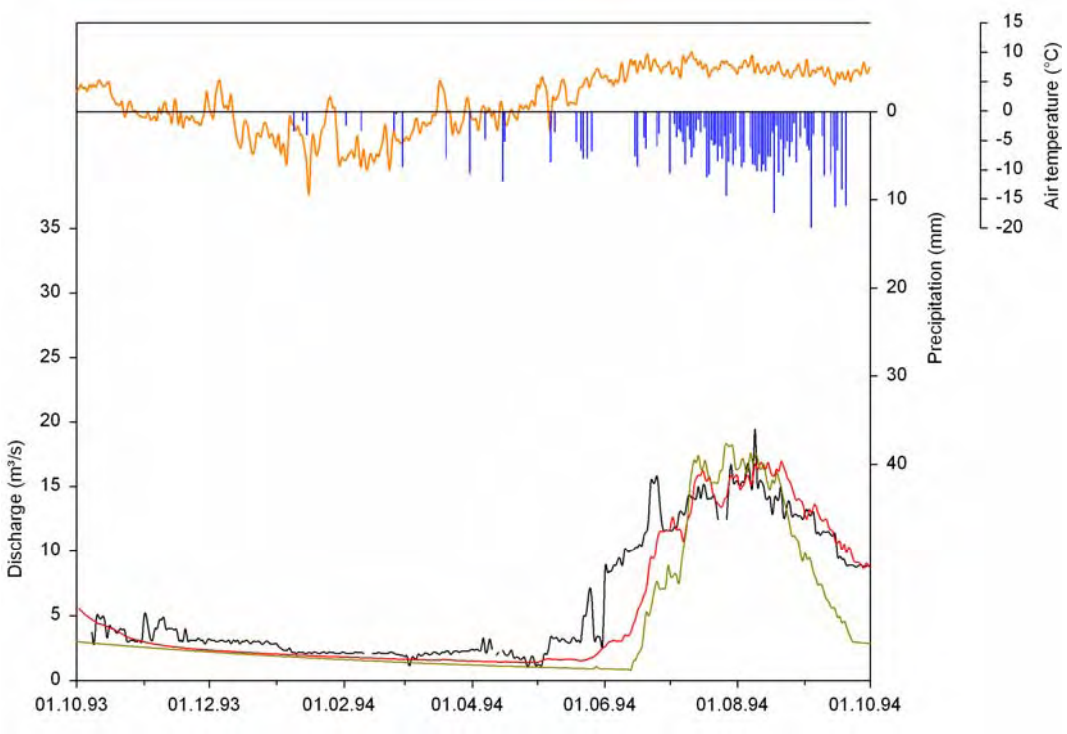

Figure 7.4: Measured (black) and simulated (red: TAC[d]; green: HBV-ETH) discharge of the hydrological year 1993/94 of the Langtang Khola catchment with measured air temperature (orange) at the SGHU station and calculated basin precipitation (blue)

Glacier mass balances were observed from 19.5.1996 to 6.10.1996 by Fujita et al. (1998) at altitudes from 5150 m a.s.l. to 5390 m a.s.l. on the Yala glacier (Table 7.2). The mass balances are calculated for the cells in which the point measurements took place. Figure 7.5 shows that the balances generally are underestimated either in the ablation area or in the accumulation area. However, the magnitudes are in the right order of magnitude. A reason for the differences of the simulated and measured balances is the cell size of 200 x 200 m². That means that point measurements are compared with simulated mass balances of an area of 40,000 m². The altitudes of the cells and of the point measurements differ and therefore different meteorological conditions prevail at the cells and at the observation points. Further, microbial production on the surface of the Yala glacier was observed by Kohshima et al. (1993). The surface of the ablation area was covered with a dark-coloured mud-like material which mainly consisted of algae and bacteria. This thin layer reduces the surface albedo of the glacier and accelerates glacier melting (Figure 5.5 in section 5.3.3). The study revealed that the melting rates on the covered surface were about three times higher than on the uncovered surface. This could be a reason for the underestimation of the ablation.

Fujita et al. (1998) determined the areal average mass balance of the Yala glacier for the observation period as –357 mm. The simulated mass balance for the entire Yala glacier is –332 mm for the same period, which compares favourably.

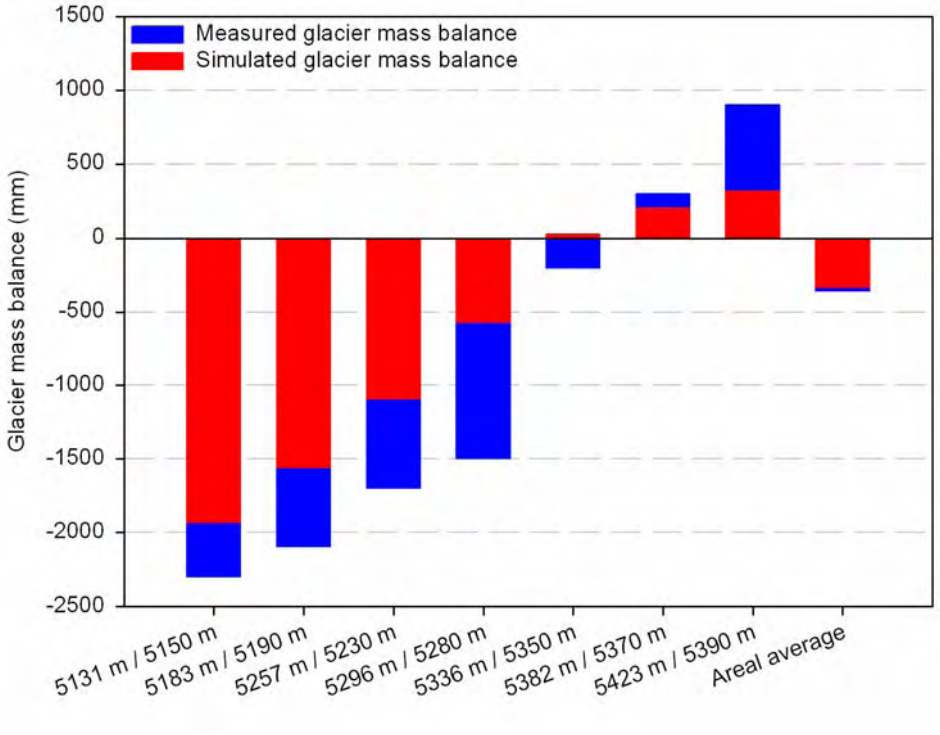

Figure 7.5: Comparison of simulated glacier mass balances with the TAC[d] model and measured glacier mass balances at different altitudes on the Yala glacier from 19.05.1996 to 6.10.1996. The blue bars are behind the red bars and both start at 0.00 mm. First numbers of x-axis are the altitudes of the 200 x 200 m² cells in which the balance was measured. Second numbers show the altitudes of the observation points.

7.4.1 Water balance of the Langtang Khola catchment for the calibration period calculated with TAC[d]

7.4.1.1 Annual basin precipitation

The aggregational state of precipitation was determined at each cell using the extrapolated air temperature at the given cell and the threshold air temperature (TT). The basin precipitation was derived from the daily precipitation amounts at the SGHU station using vertical and horizontal gradients (section 5.1.1). About 47% of the basin precipitation falls as snow and 53% as rain (Table 7.4). This result shows the important role of snow and ice storage in controlling the water balance.

Table 7.4: Annual basin precipitation (mm/a) and its aggregational state for the calibration period calculated with the TAC[d] model

	1993/94	**1994/95**	**1995/96**	**1996/97**	**1997/98**
Solid precipitation	184	384	212	267	278
Liquid precipitation	248	284	309	309	350
Total over catchment	432	668	520	576	628
Measured precipitation at SGHU station	461	689	551	611	656

7.4.1.2 Annual water balance

The following main components of the annual water balance can be distinguished:

$$Q = P_b + G_{melt} - ET - \Delta S \quad (7.5)$$

Q: Discharge (mm/a)
P_b: Basin precipitation (mm/a)
G_{melt}: Glaciermelt (mm/a)
ΔS: Changes in storages, here primarily in form of snow accumulation which feeds the glaciers (mm/a)

Table 7.5 and Figure 7.6 show the values of the individual terms as calculated by the model. Basin precipitation (432 to 668 mm/a) and discharge (470 to 694 mm/a) are by far the largest components, followed by glaciermelt (274 to 422 mm/a). Basin precipitation and glaciermelt are the input into the system. The storage term summarises water storage in groundwater, snowpack and soil. Actual evapotranspiration accounts for 12 to 17% of the input.

Table 7.5: The main terms of the water balance of the Langtang Khola catchment as assessed by the TAC^d model for the calibration period in mm/a

	1993/94	**1994/95**	**1995/96**	**1996/97**	**1997/98**
Discharge	470	605	532	556	694
Actual ET	122	134	126	112	127
Glaciermelt	295	313	316	274	422
Precipitation	432	668	520	576	628
Storage change	135	242	179	182	229
Balance	0	0	0	0	0

7.5 Results of the validation period of the Langtang Khola catchment calculated with TAC^d

The hydrological years from 1987/88 to 1992/93 were simulated for model validation with the optimal parameter set shown in Table A4 (Appendix). There are gaps in the measured discharge data in this period which partly complicate the interpretation of the results (Table A1, Appendix). Hardly any reliable data are available for June 1989 and September 1991. This was considered in the calculation of the evaluation criteria. The evaluation criteria are shown in Table 7.6.

Table 7.6: Evaluation criteria of simulation results calculated with TAC^d (validation period)

Hydrological year	**R_{eff} (-)**	**log R_{eff} (-)**	**R^2 (-)**	**VE (mm/a)**
1987/88	0.58	0.05	0.87	97
1988/89	0.72	0.32	0.90	40
1989/90	0.68	0.45	0.84	50
1990/91	0.20	0.40	0.88	-30
1991/92	0.30	0.59	0.82	-9
1992/93	0.76	0.68	0.91	37

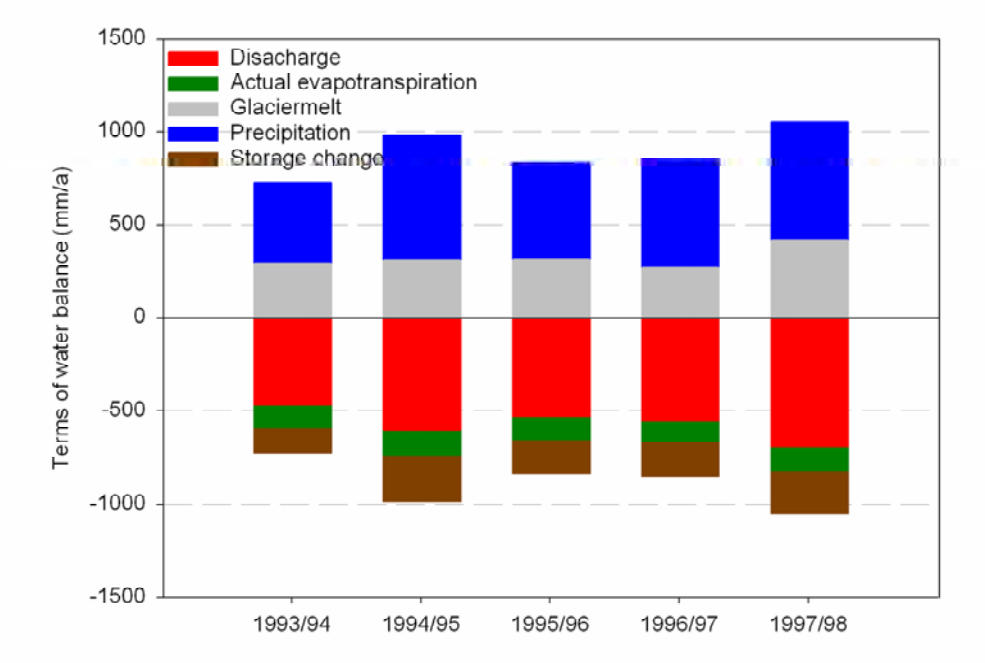

Figure 7.6: Main terms of the water balance of the calibration period of the Langtang Khola catchment calculated with TAC^{d}. Added components with a positive sign are the input into the system whereas the added values with a negative sign are the output of the system and the storage change.

Measured winter discharge is higher in this period, with an average from November to the end of April of 3.35 m³/s compared to the average of 2.73 m³/s in the calibration period. TAC^{d} systematically underestimates the winter discharge in all hydrological years of the validation period and overestimates discharge in the melt/monsoon period (Figure 7.7). These compensating effects are the reason for the relatively small volume errors (Table 7.6). R_{eff} and log R_{eff}, however, show a drop in performance compared to the calibration period whereas the coefficient of determination implies a strong connection between the measured and simulated hydrograph.

In the validation period there is one glacier mass balance observation available from 28.03.1991 to 17.03.1992 (Braun et al., 1993). This observation is again a point measurement which causes the same problems as described for the comparison of measured and simulated mass balances of the calibration period. However, the agreement is satisfactory and shows that the parameterisation of the snow and glacier routine is representative for the entire simulation period (Figure 7.8).

7.5.1 Water balance of the Langtang Khola catchment for the validation period

7.5.1.1 Annual basin precipitation

In the validation period approximately 50% of the precipitation is solid. Table 7.7 summarises the results of the single hydrological years.

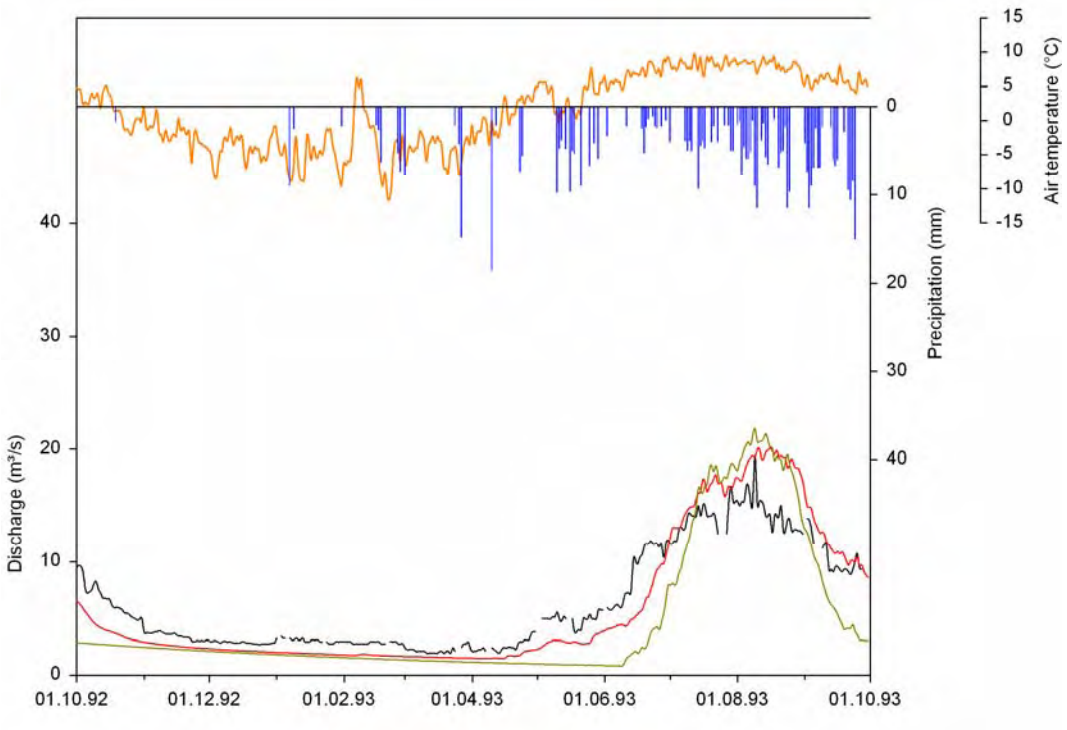

Figure 7.7: Measured (black) and simulated (red: TAC[d]; green: HBV-ETH) discharge of the hydrological year 1992/93 of the Langtang Khola catchment with measured air temperature (orange) at the SGHU station and calculated basin precipitation (blue)

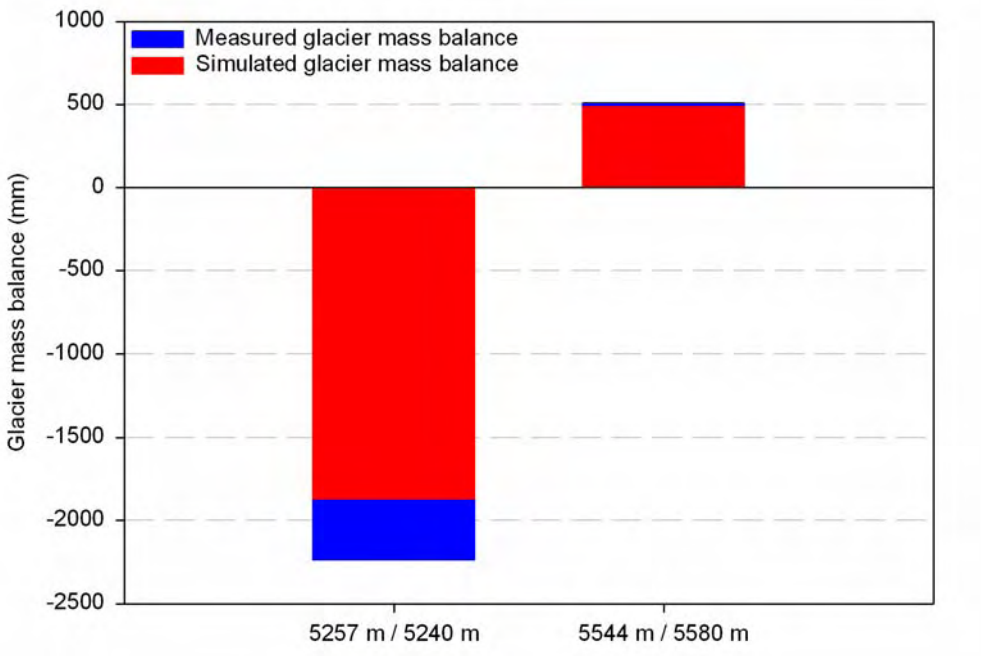

Figure 7.8: Comparison of simulated and measured glacier mass balances at different altitudes on Yala glacier from 28.03.1991 to 17.03.1992. The blue bars are behind the red bars and both start at 0.00 mm. First numbers of x-axis are the altitudes of the 200 x 200 m² cells in which the balance was measured. Second numbers show the altitudes of the observation points.

Table 7.7: Annual basin precipitation (mm/a) and its aggregational state of the validation period calculated with the TAC[d] model

	1987/88	1988/89	1989/90	1990/91	1991/92	1992/93
Solid precipitation	355	469	222	213	254	280
Liquid precipitation	337	265	353	337	284	229
Total over catchment	691	734	575	551	539	509
Measured precipitation at SGHU station	733	769	609	585	569	537

7.5.1.2 Annual water balance

The water balances (Equation 7.5) of the validation period show nearly the same patterns as the water balances of the calibration period. However, discharge and precipitation is higher in the validation period, with an average annual discharge of 602 mm compared to 571 mm in the calibration period and an average annual precipitation of 600 mm in the validation period and 565 mm in the calibration period. Table 7.8 and Figure 7.9 summarise the components of the water balance.

Table 7.8: The main terms of the water balance of the Langtang Khola catchment as assessed by the TAC[d] model for the validation period in mm/a

	1987/88	1988/89	1989/90	1990/91	1991/92	1992/93
Discharge	593	567	656	715	559	522
Actual ET	117	109	136	141	110	112
Glaciermelt	255	222	412	445	291	317
Precipitation	691	734	575	551	539	509
Storage change	236	279	195	140	160	192
Balance	0	0	0	0	0	0

7.6 Results of the Langtang Khola catchment calculated with HBV-ETH

A detailed comparison of simulation results of both models can be found in section 8.8. Discharge at the beginning and at the end of the monsoon season is constantly underestimated by the HBV-ETH model. This is the reason for relatively small R_{eff} and log R_{eff} values as shown in Table 7.9. The underestimation is expressed in positive volume errors (VE) from 20 mm to 258 mm per year.

HBV-ETH simulates glacier mass balances for altitude belts of 500 m and the orientation classes East-West-Horizontal, South and North. The comparison with the areal average glacier mass balance of the south-facing Yala glacier as given in Fujita et al. (1998) for the monsoon season of 1996 shows a good correspondence between measured and simulated glacier mass balances (Figure 7.10).

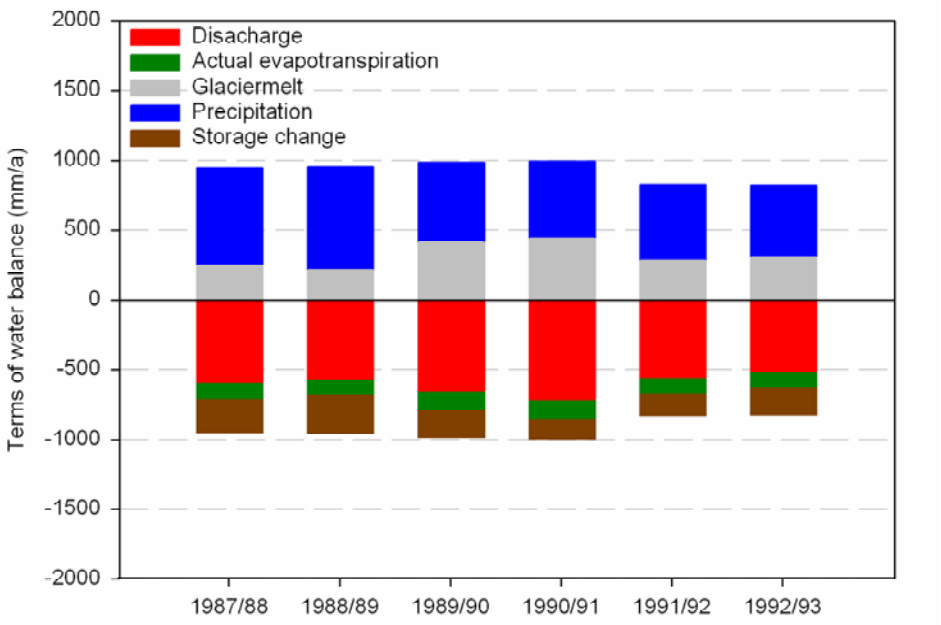

Figure 7.9: Main terms of the water balance of the validation period of the Langtang Khola catchment calculated with TAC[d]. Added components with a positive sign are the input into the system, whereas the added values with a negative sign are the output of the system and the storage change.

Table 7.9: Evaluation criteria of the simulation results calculated with HBV-ETH

	R_{eff}	Log R_{eff}	R^2	VE
1987/88	0.26	-2.83	0.78	258
1988/89	0.37	-1.45	0.81	161
1989/90	0.37	-0.49	0.77	20
1990/91	-0.33	-0.38	0.80	-136
1991/92	-0.05	-0.44	0.68	80
1992/93	0.40	-0.60	0.76	107
1993/94	0.59	0.07	0.75	123
1994/95	0.83	0.63	0.91	126
1995/96	0.29	-0.38	0.62	81
1996/97	0.18	0.15	0.63	46

Simulated glacier mass balances of the validation period also correspond well with the measured balances of the Yala glacier (Figure 7.11).

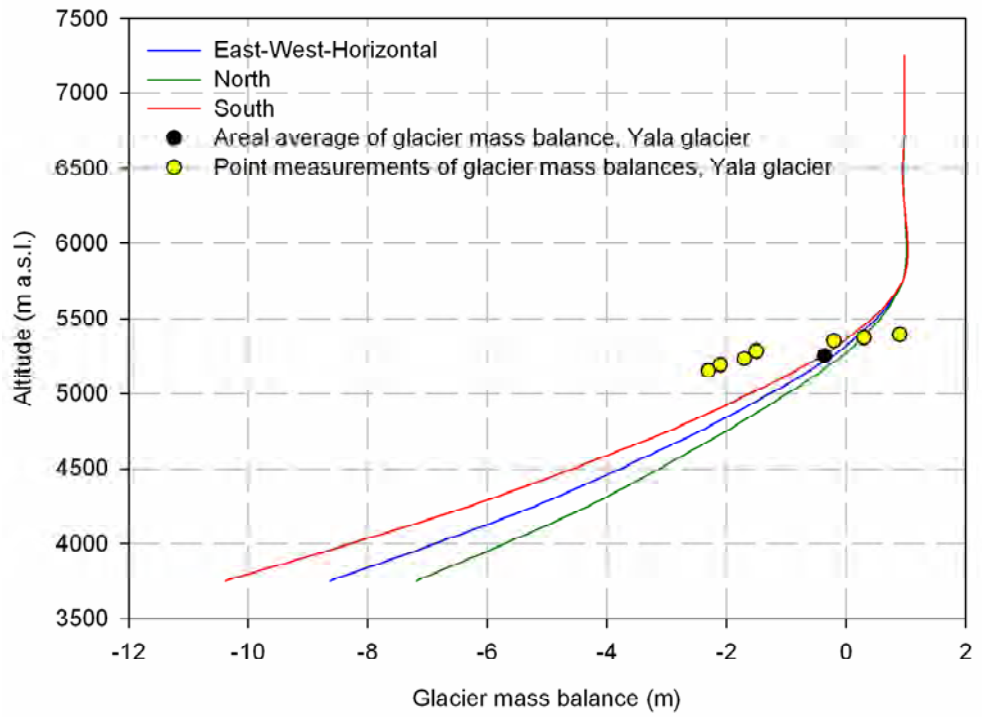

Figure 7.10: Comparison of measured and simulated glacier mass balances of the calibration period (hydrological year 1995/95) of the Langtang Khola catchment as calculated by the HBV-ETH model

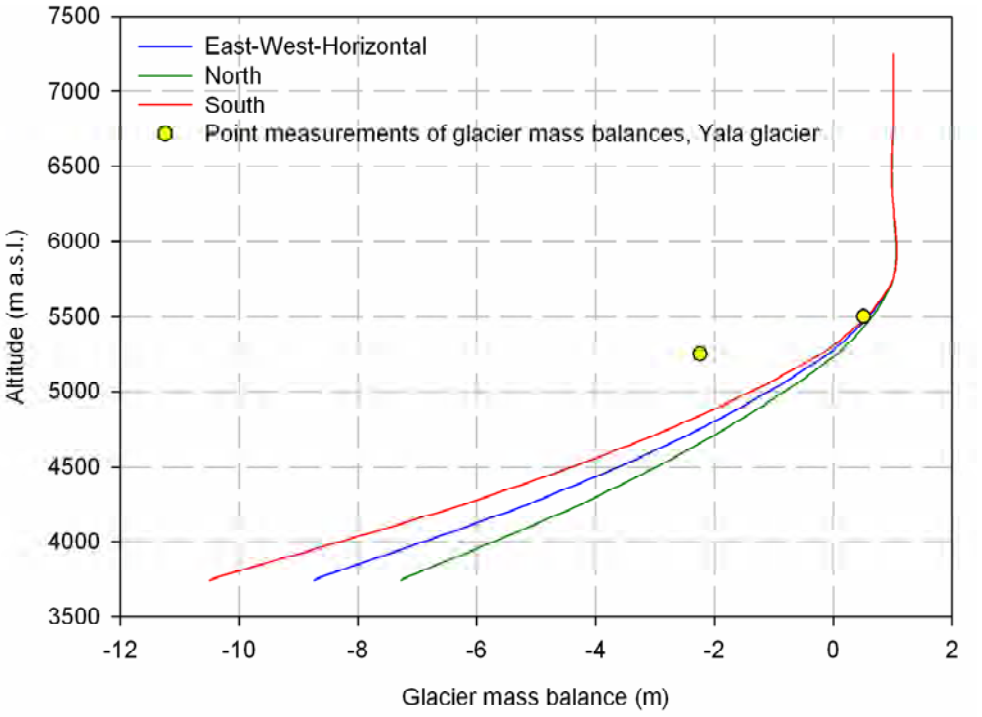

Figure 7.11: Comparison of measured and simulated glacier mass balances of the validation period (hydrological year 1991/92) of the Langtang Khola catchment as calculated by the HBV-ETH model

7.7 Results of the Modi Khola catchment

For the Modi Khola and Imja Khola catchments the presentation of simulation results is not subdivided into calibration and validation periods. Generally, the data availability and the quality of available data is worst in the Modi Khola catchment and the application of a hydrological model is a prerequisite for achieving a reliable assessment of the hydrological conditions of such a catchment.

The availability of discharge data in the Modi Khola catchment is low and the quality of the available measurements is questionable. Therefore, the catchment was treated as an ungauged basin and it was simulated with the unchanged parameter set of the Langtang Khola catchment. Only the horizontal precipitation gradient of the TAC^d model was set at 0.00 because there is no information about horizontal variability of precipitation in the catchment (Table A4, Appendix). The RCF of the HBV-ETH model was set at 1.2 (Table A5, Appendix). The visual inspection of the simulated hydrographs reveals that the basic pattern of the measured hydrograph can be reproduced by both models, especially during the monsoon season of 1991/92 (Figure 7.12; Figure A2, Appendix). The negative values of R_{eff} (log R_{eff}) for all three simulated hydrological years do not, however, satisfy the objective evaluation criteria. It seems that both models strongly underestimate winter discharge in the first two hydrological years but these measured discharge data are not sufficient for a reliable evaluation. In the third hydrological year measured discharge during the winter season is much smaller compared to the first two years. The available discharge data show that the simulated hydrographs are in the right magnitude and therefore no further calibration attempts were conducted.

Table 7.10: Evaluation criteria of the Modi Khaola catchment for simulation results calculated using TAC^d and HBV-ETH

	TAC^d				**HBV-ETH**			
	R_{eff}	**log R_{eff}**	**R^2**	**VE**	**R_{eff}**	**log R_{eff}**	**R^2**	**VE**
1991/92	-1.41	-9.21	0.42	289	-2.40	-21.12	0.38	508
1992/93	-1.20	-3.86	0.45	-68	-1.91	-4.43	0.29	20
1993/94	0.37	0.12	0.86	-31	0.69	0.19	0.83	36

Braun et al. (1998) achieved better simulation results regarding the objective evaluation criteria but they calibrated the model to the available discharge data using independent parameter sets. Their model is furthermore only calibrated for the monsoon season because they give a fixed runoff amount for the glacier-covered area which maintains the winter discharge (GBASE in Braun et al., 1998).

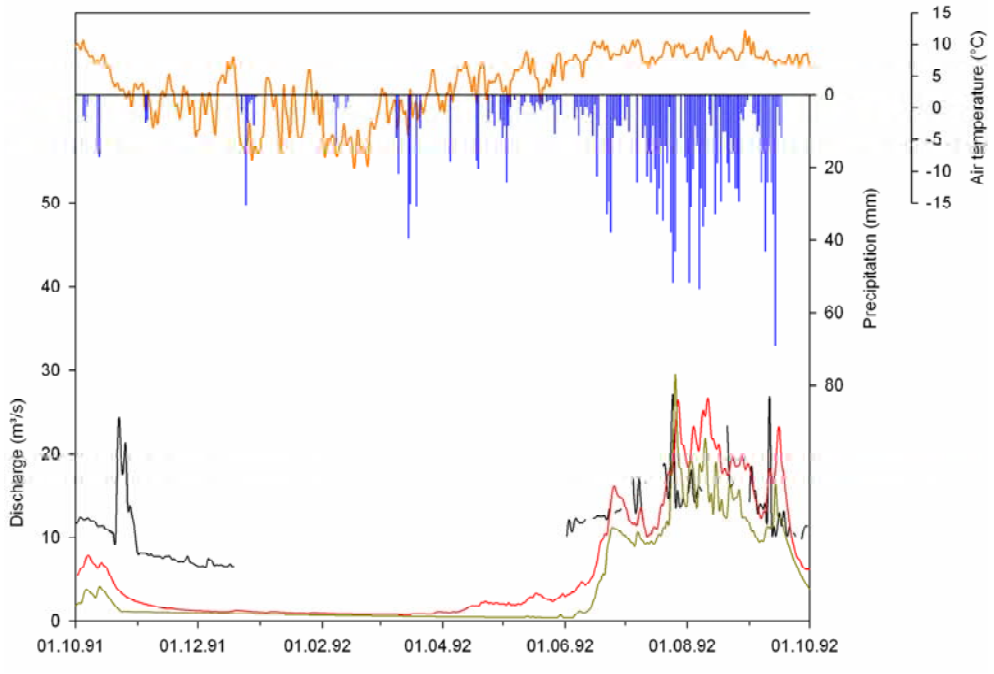

Figure 7.12: Measured (black) and simulated (red: TAC^d; green: HBV-ETH) discharge of the Modi Khola catchment (1991/92) with measured air temperature (orange) at the SGHU station and calculated basin precipitation (blue)

7.7.1 Water balance of the Modi Khola catchment calculated with the TAC^d model

7.7.1.1 Annual basin precipitation

76% of basin precipitation falls as snow (Table 7.11) due to the large precipitation amounts in the winter season (Figure 3.4).

Table 7.11: Annual basin precipitation (mm/a) and its aggregational state calculated with the TAC^d model

	1991/92	1992/93	1993/94
Solid precipitation	1314	1861	2126
Liquid precipitation	768	882	680
Total over catchment	2082	2743	2807
Measured precipitation at SGHU station	1194	1542	1577

7.7.1.2 Annual water balance

The Modi Khola catchment receives the most precipitation of the three catchments studied and the annual water balance is dominated by precipitation (2080 to 2800 mm/a) (Figure 7.13). Glaciermelt (290 to 390 mm/a) is in the same order of magnitude as in the Langtang Khola catchment, but in the Modi Khola catchment it plays a minor important role with relation to precipitation. Evapotranspiration ranges from 80 to 110 mm/a and is considered somewhat too low; more sophisticated methods should be investigated. Discharge (1190 to 1500 mm/a) and the storage term of the water balance (1190 to 1600 mm/a) are in the same order of magnitude. The storage term is dominated by the accumulation of

precipitation (snow) in the upper parts of the catchment whereas the glacier mass balances of the lower parts are negative in all the years (Figure 7.14).

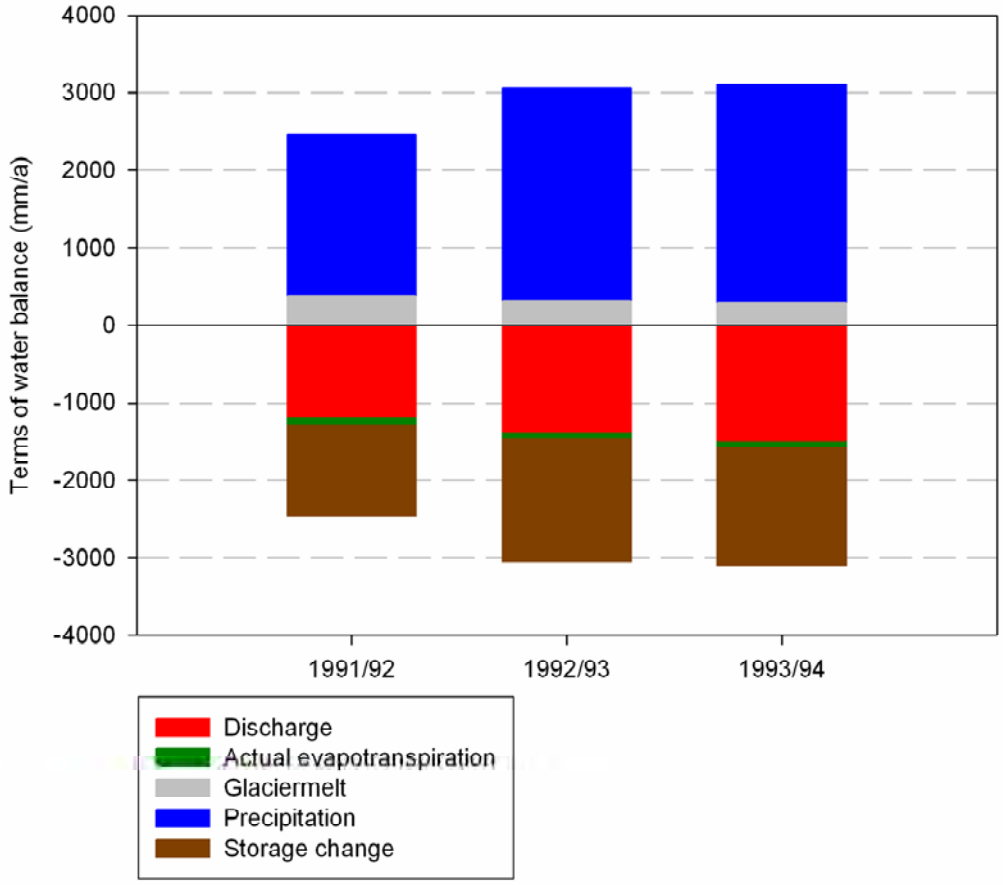

Figure 7.13: Water balance of the Modi Khola catchment as calculated by the TAC^{d} model

The increasing mass losses in the altitude belt 4400 to 4800 m a.s.l. can be explained by the declining extent of debris-covered glaciers above 4400 m a.s.l. Below this altitude nearly all glaciers are covered by debris which reduces ablation, and thus the mass losses are relatively low in the lower altitudes. The glacier mass balances of the entire glacier area are positive in all the simulated hydrological years, which should result in an increasing ice area (Table 7.12). There are no glacier mass balance data available in the catchment, but Fujita et al. (2001) measured the glacier mass balance of the Rikha Samba glacier in Hidden Valley, approximately 10 km north of Mount Dhaulagiri, which is located 35 km north-west of the Modi Khola catchment. Mass balance during 1998/99 is largely negative and the equilibrium line altitude is at 5800 m a.s.l.. They further observed an increased retreat rate of the glacier terminus in the 1990s. Although these observations were not conducted directly in the catchment, it becomes obvious that the positive mass balances over the entire glacier area as calculated by the TAC^{d} model are unlikely. The equilibrium line altitude is calculated at about 5000 m a.s.l. which seems to be too low. In cases where both meteorological data and discharge data are questionable, as in the Modi Khola catchment, glacier mass balance data are highly important for the calibration of conceptual models.

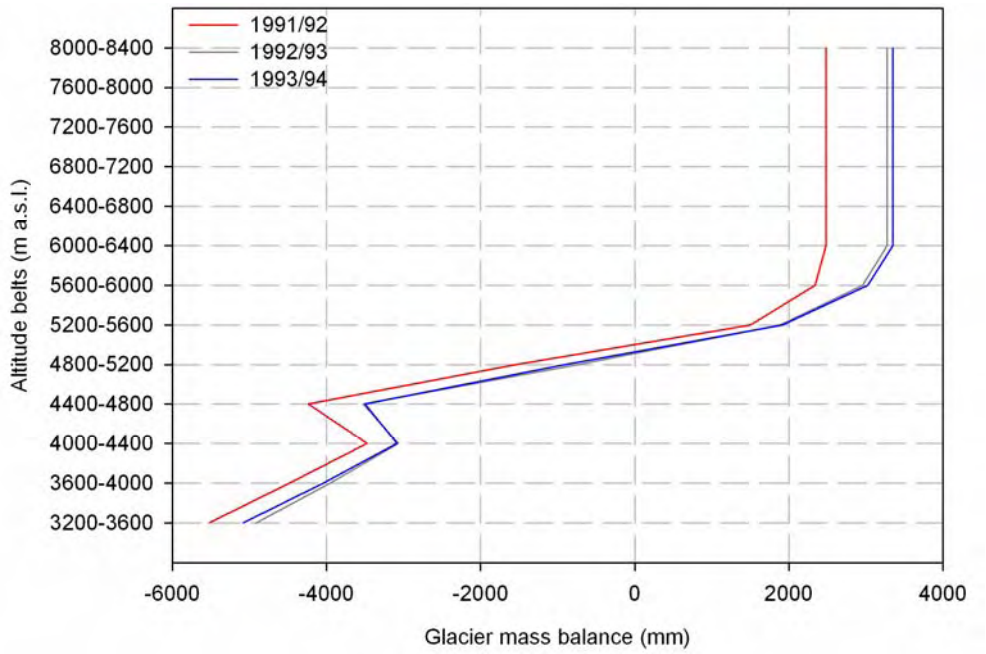

Figure 7.14: Altitude-dependent glacier mass balances as calculated by the TAC^{d} model

Table 7.12: Glacier mass balances and change of snow cover over the entire catchment area

	Glacier mass balance (mm)	**Change in snow cover (mm)**
1991/92	558	837
1992/93	1176	1127
1993/94	1178	1094

7.8 Results of the Imja Khola catchment

The optimal parameter set of Langtang Khola catchment was taken to simulate discharge of the Imja Khola catchment. An underestimation of discharge in all simulated hydrological years could be observed using the unrevised parameter set. For the adaptation to the conditions of the Imja Khola catchment, parameters of the snow and glacier routine were calibrated, whereas the parameters of the soil and runoff generation routine remained unchanged except CPERC of the HBV-ETH model (Tables A4 and A5, Appendix). The results presented here were achieved with only five calibration runs. Kayastha et al. (2000) observed a positive degree-day factor of 16.9 mm day^{-1} °C^{-1} from 21 May to 1 June 1999 on the Khumbu glacier. The simulated degree-day factor on bare ice amounts to 16.38 mm day^{-1} °C^{-1} in the pre-monsoon season.

In most of the years the TAC^{d} model delivers better results than the HBV-ETH model (Table 7.13). Figure 7.15 shows the simulated and measured hydrographs of the hydrological year 1993/94. Further simulation results can be found in Figure A3 (Appendix). The hydrological years 1991/92 and 1992/93 show unreliable discharge measurements and were not taken for model calibration.

Table 7.13: Evaluation criteria of simulation results of Imja Khola catchment calculated with TAC[d] and HBV-ETH

	TAC[d]				HBV-ETH			
	R_{eff}	log R_{eff}	R^2	VE	R_{eff}	log R_{eff}	R^2	VE
1988/89	0.74	0.65	0.87	261	0.43	-1.45	0.78	461
1989/90	0.46	0.42	0.57	-69	0.61	-0.58	0.67	94
1990/91	0.75	0.71	0.86	30	0.73	-0.28	0.86	268
1991/92	0.37	0.00	0.80	323	-0.05	-1.47	0.70	435
1992/93	0.03	-0.80	0.56	317	-0.54	-3.79	0.50	458
1993/94	0.79	0.8	0.80	38	0.62	0.47	0.72	137
1994/95	0.70	0.77	0.76	26	0.71	0.09	0.71	177

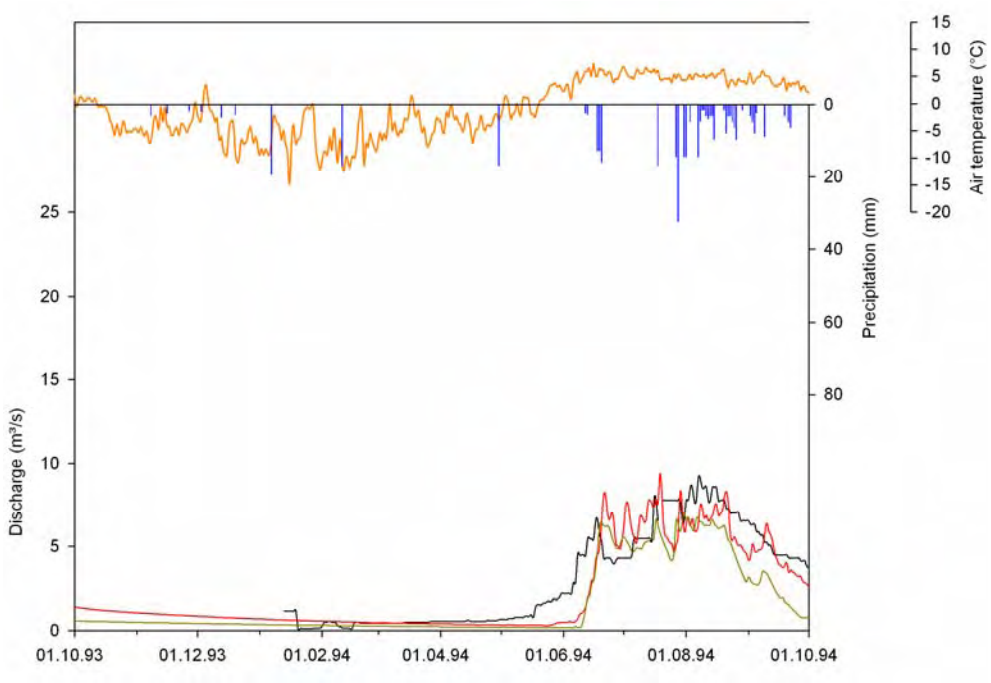

Figure 7.15: Measured (black) and simulated (red: TAC[d]; green: HBV-ETH) discharge of the Imja Khola catchment in the hydrological year 1993/94 with measured air temperature (orange) at the SGHU station and calculated basin precipitation (blue)

7.8.1 Water balance of the Imja Khola catchment calculated using the TAC[d] model

7.8.1.1 Annual basin precipitation

Based on the TAC[d] model application the portion of solid precipitation is calculated to be 61% and liquid precipitation amounts to 39% (Table 7.14).

Table 7.14: Annual basin precipitation (mm/a) and its aggregational state calculated with the TAC[d] model

	1988/89	1989/90	1990/91	1991/92	1992/93	1993/94	1994/95
Solid precipitation	487	271	216	291	144	198	207
Liquid precipitation	243	202	117	155	64	145	202
Total over catchment	730	472	333	446	208	343	409
Measured precipitation at SGHU station	448	289	204	272	126	209	251

7.8.1.2 Annual water balance

The terms of the water balance as outlined in Equation 7.5 are visualised in Figure 7.16. Glaciermelt (330 to 700 mm/a) is the largest source of water in most of the hydrological years, whereas precipitation (200 to 1000 mm/a) dominates the years 1987/88 and 1988/89. Discharge (420 to 850 mm/a) is the largest component of the water balance. Actual evapotranspiration ranges from 80 to 120 mm/a. Storage change varies from 40 to 570 mm/a.

Changes in snow and ice storage are calculated over the non-glacierized catchment area and over the glacierized area of the Imja Khola catchment (Figure 7.17). Over the non-glacierized parts of the catchment these terms are always positive (70 to 430 mm/a), which should result in the formation of further glaciers. However, observation shows that this snow is redistributed by wind and avalanches, feeding the valley glaciers, and this process is not accounted for by the model. The glacier mass balance term varies from about –410 to –1300 mm/a. The calculation of changes in snow and ice storage over the entire catchment area show negative values for all the years of the investigation period (Figure 7.17). It seems that there were constant mass losses, which is supported by the findings of Yamada et al. (1992) and Nakawo et al. (1997), who measured a general retreat and mass losses of various "clean" and debris-covered glaciers in the Nepalese Himalaya.

7.9 Conclusions

The application of the TAC[d] and HBV-ETH models in the Langtang Khola catchment was successful in most of the simulated years with model efficiencies from –0.33 to 0.87. The dynamics of the hydrograph can be reproduced satisfactorily, considering the reliability of the measured discharge and climatological data. Not only discharge but also glacier mass balances can be simulated well. However, the simulation of the onset of discharge in the pre-monsoon season is delayed in most of the simulated hydrological years. The soundness of the model code is proven by a balanced water balance.

The calibration procedure is still subjective compared to automatic calibration techniques, but the advantage of using this method is that the modeller becomes familiar with the sensitivity of the parameters. The compliance of the fixed ratios between the storage parameters of the soil and runoff generation routine in particular, as well as the decoupling of these parameters from the calibration procedure in phase three reduce the risk of over-parameterisation. The multi-criteria calibration with additional mass balance data as a further calibration criterion in addition to discharge enables a more realistic discharge simulation.

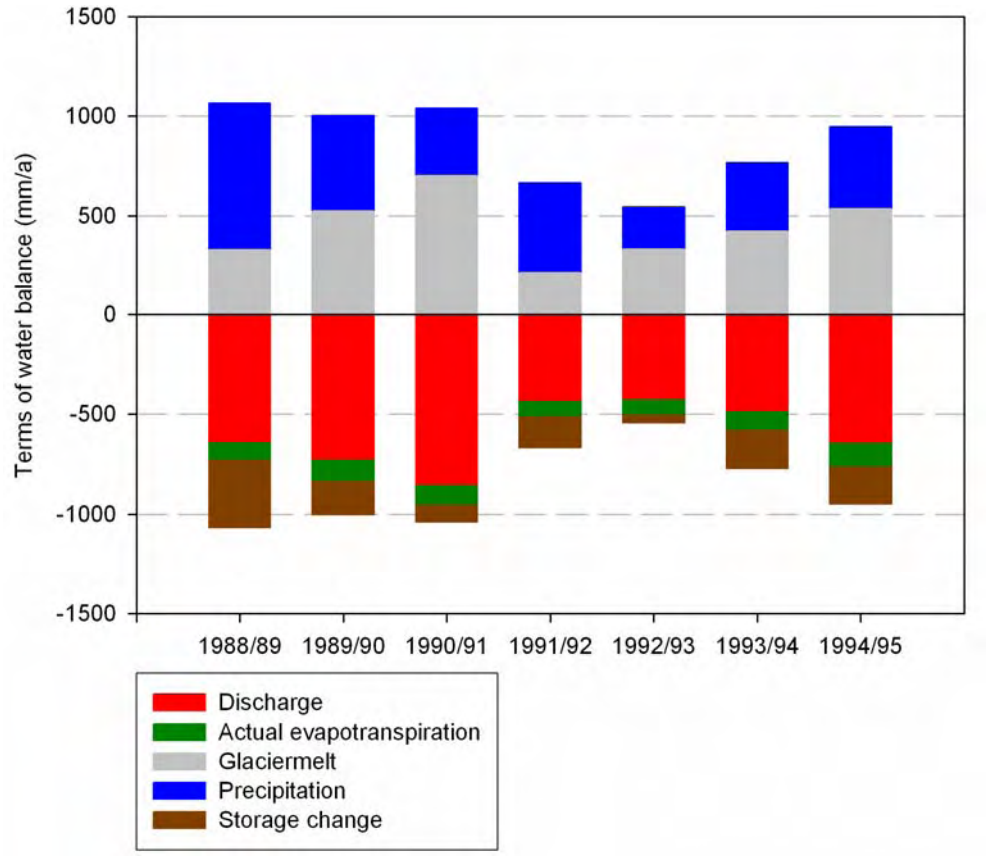

Figure 7.16: Water balances of the Imja Khola catchment as calculated using the TAC[d] model

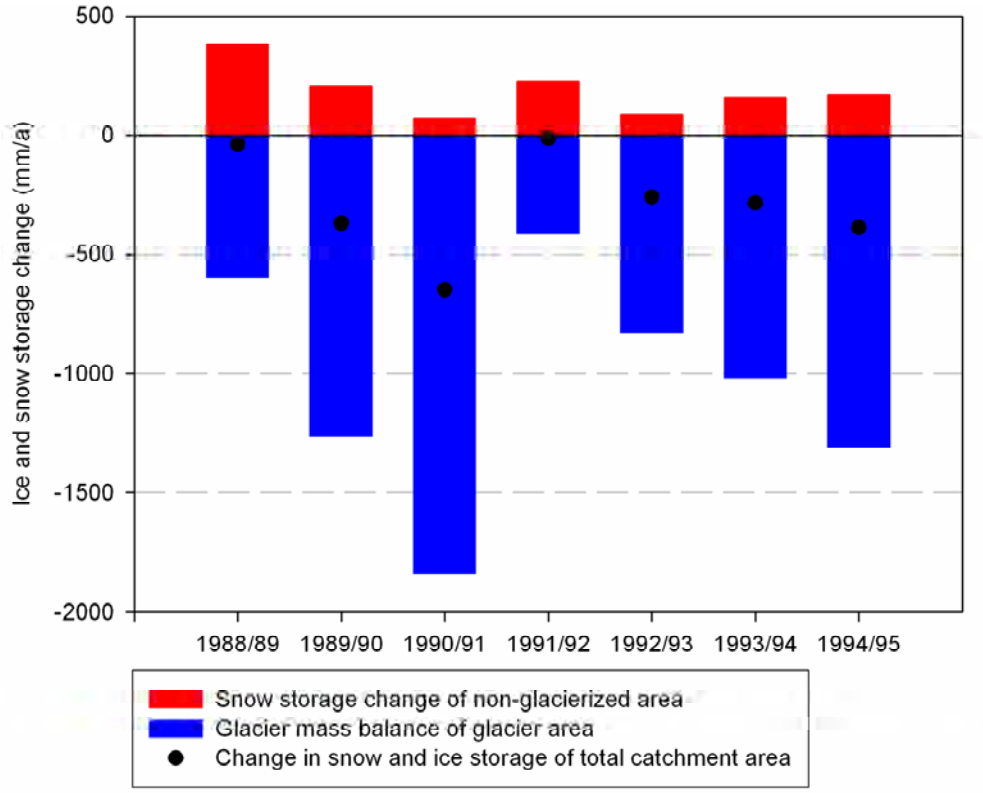

Figure 7.17: Changes in snow and ice storages of the Imja Khola catchment as calculated using the TAC[d] model

The parameter set of the Langtang Khola catchment was taken for the simulation of the discharge of the Modi Khola and Imja Khola catchments. In the case of the Modi Khola catchment, the data availability is very scarce and the measurements are of questionable reliability. Therefore, no further calibration of the models was conducted in this catchment. The visual inspection of the hydrographs shows that the simulated discharge is in the right order of magnitude, whereas single patterns are not reproduced satisfactorily. TAC^d simulates most of the precipitation as snow, which results in positive glacier mass balances above 5000 m a.s.l. Glacier mass balance measurements are highly significant for the validation of these simulation results.

Good simulation results of the Imja Khola catchment were achieved with only a few adaptations to the parameter set of the Langtang Khola catchment and only five calibration runs were computed. The glacier mass balances are negative in all hydrological years.

Both conceptual precipitation runoff models require a rather modest data input, and if one or more years of discharge measurements are available, these models can be applied in Himalayan catchments. Additional snow and glacier mass balance measurements are important for the calibration of the snow and glacier routine and measurement programmes should be established in all three catchments.

8 Model analysis and discussion

This section contains a detailed analysis of the model structure and the simulation results of the further developed distributed catchment model TAC^d as well as a comparison with the semi-distributed HBV-ETH model. The analyses were performed using data of the Langtang Khola catchment because its data availability is the most reliable of the three investigated catchments.

8.1 Extrapolation of input data

Complete time series of daily mean air temperature and daily precipitation amounts are the prerequisite for the simulation of daily discharge with TAC^d and HBV-ETH. Statistical methods were used to bridge gaps in the time series and to redistribute cumulated precipitation amounts. The extrapolation results and their impacts on discharge simulation are discussed in the following chapters.

8.1.1 Temperature extrapolation

The comparison of measured and extrapolated air temperature is shown in Figure 8.1 for the year 1997. The annual measured temperature course was reproduced well by the extrapolation and even single structures were modelled realistically. The simulation of the monsoon season is generally better than the simulation of the dry season. The R_{eff} is 0.88 for the year 1997.

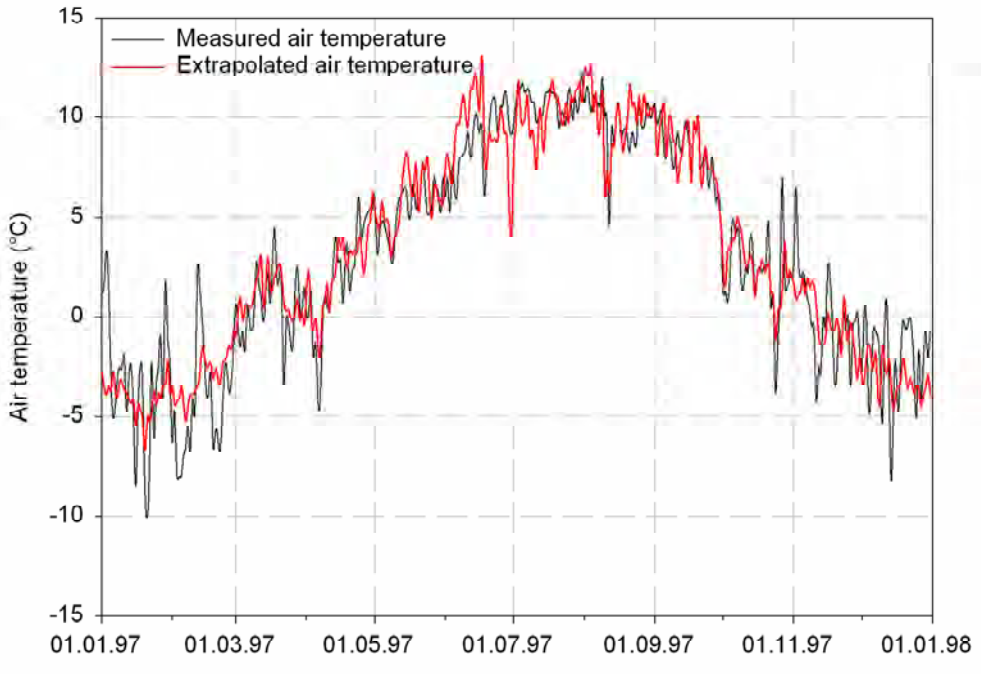

Figure 8.1: Comparison of measured and extrapolated air temperature, 1997, Langtang Khola catchment

A more objective visualisation is shown in the scatter plot in Figure 8.2 (left). The parameters of the linear regression line still deviate from a 1:1 ratio and errors of several °C occur in isolated cases. However, an improvement compared to the simple linear regression as an

extrapolation method can be observed (Figure 8.2, right). 90% of the observed daily mean air temperatures can be explained with the extrapolation using the second order polynomial function while only 87% can be explained with the simple linear regression in 1997.

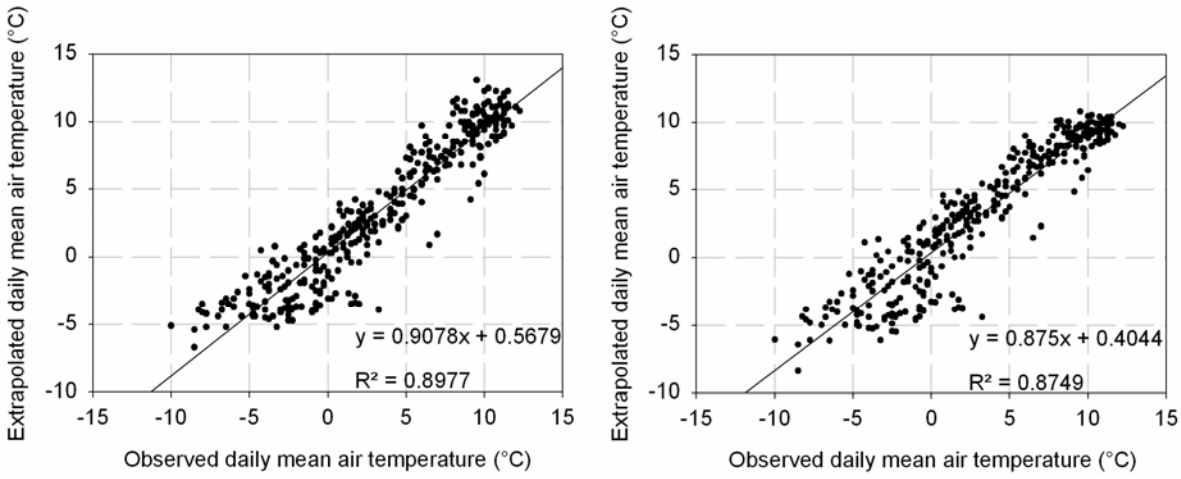

Figure 8.2: Scatter plots of observed and simulated daily mean air temperature. Extrapolation with second order polynomial function (left) and simple linear regression (right), 1997

Table 8.1 summarises the R^2 values of the years in which the extrapolation method was applied in the Langtang Khola catchment.

Table 8.1: Coefficients of determination for the years of the Langtang Khola catchment in which gaps in the air temperature time series were filled using the extrapolation method

Year	**R^2**
1987 (18.6. to 31.12.)	0.70
1988	0.75
1989	0.86
1991	0.91
1997	0.90
1998	0.85

The extrapolated values were used only to bridge the gaps in the time series. For 98% of the time, measured values were available in the Langtang Khola catchment and therefore only single values of the extrapolated time series were used. The extrapolated values are considered as "first guess" of the order of magnitude of the values which were used for bridging the gaps. The final values have to fit in the course of the measured values and can be adjusted subjectively if the calculated values seem to be unreliable and do not fit in the course of the measured time series. Thus, the course of the inserted values is determined by the course of the extrapolated values as well as by the course of the measured values. Figure 8.3 shows an example for the mode of operation where extrapolated values were used to bridge the gaps in the time series.

The combination of extrapolation and subjective evaluation of the extrapolated values in relation to the course of the measured time series reduces the error of the inserted value. The

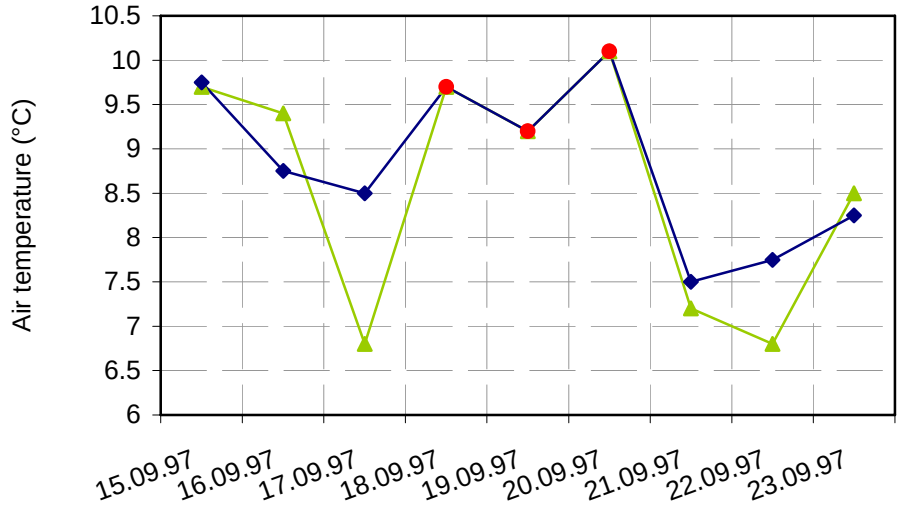

Figure 8.3: Example for the mode of operation of data extrapolation of air temperature time series, 1997, Langtang Khola catchment. Red points are the values inserted to bridge the gaps in the time series, blue squares are the measured values and the green triangles are the extrapolated values

error is not zero but should be below 1°C in most cases. Further, most of the gaps are single missing days or, at the most, series of 3 to 4 days during periods where air temperature is above the threshold temperature for melting (TT). This simplifies the adjustment of the extrapolated values to the course of the measured values and the error of the inserted values becomes minimal. Longer series of missing values occur mainly in November and December when air temperature is below TT. If air temperature is clearly below TT, the impact of possible extrapolation errors on the discharge simulation results is minimal because no meltwater production occurs. Correct extrapolation results are therefore most important for temperature levels above and around TT. Figure 8.1 shows that extrapolation results of air temperature above TT (in the monsoon season) are much better than those of air temperature below TT.

8.1.2 Precipitation extrapolation

The measured precipitation values are compared with the synthetic values of June and July 1997 in Figure 8.4 for the visualisation of the precipitation extrapolation results. Some of the precipitation amounts are reproduced well, e.g. around 27 July 1997; others are redistributed over several days, e.g. around 29 June 1997. However, there are some significant deviations between the measured and the simulated precipitation amounts. The reconstruction of the precipitation amounts is based on probabilities and it is not an extrapolation like the temperature extrapolation where reliable correlations between the SGHU station and the reference stations are a prerequisite (Section 6.4.2). Nevertheless, the synthetic time series are able to describe the actual situation adequately. Figure 8.4 shows that the main patterns of the measured precipitation amounts are reproduced well by the algorithm.

The simulated daily precipitation amounts were adjusted to the actual precipitation amounts and therefore the deviations of the monthly amounts of precipitation are not significant. The temporal shift of the simulated precipitation amounts does not necessarily influence the

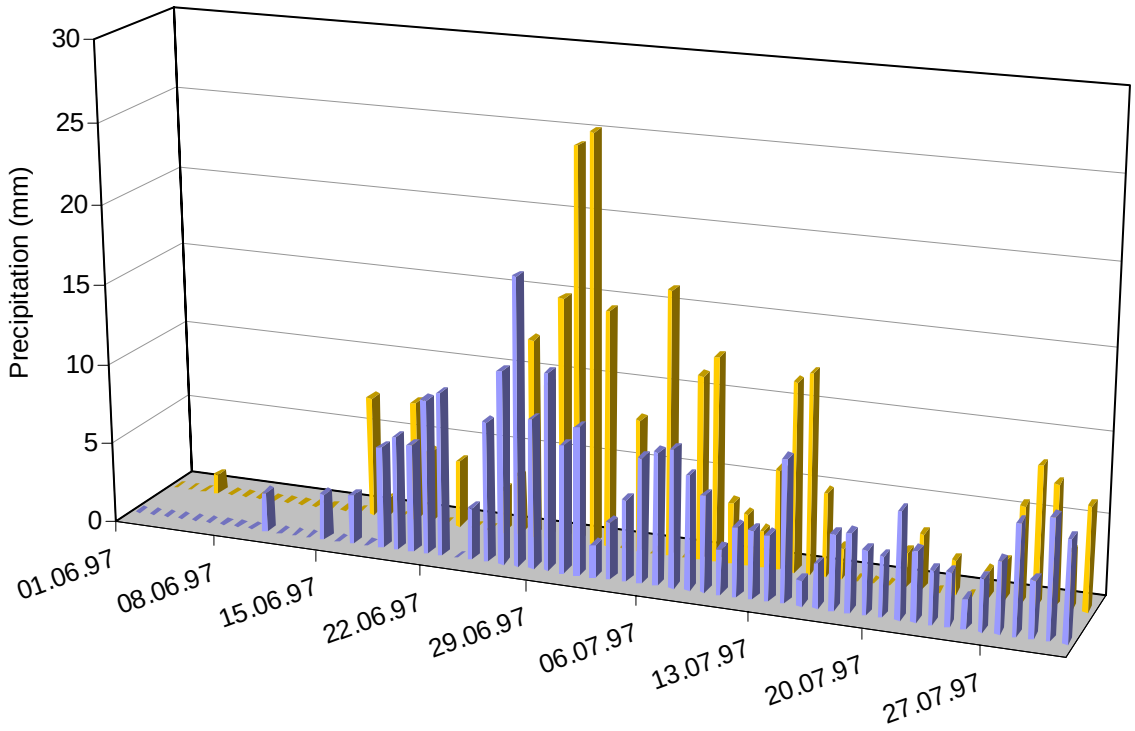

Figure 8.4: Comparison of measured daily precipitation amounts (yellow bars) and simulated daily precipitation amounts (blue bars) in June and July 1997, Langtang Khola catchment

discharge simulation. If the storage capacities of soil, snowpack or of the storages of the runoff generation routine are not exceeded, additional water is added to these storages and contributes to runoff generation with retardation. These retardation effects allow errors in temporal assignment in the magnitude of the errors of the simulated precipitation amounts. It must be considered further that precipitation events in the same region do not always occur at the same time or are stationary throughout the event. An event which was observed at several reference stations in the region can occur at the SGHU station earlier or later. If precipitation occurs at a reference station in the evening, the algorithm implies that there is rain or snowfall at the SGHU station on the same evening, whereas the precipitation event occurred in reality on the following morning at the SGHU station. This causes temporal shifts of the simulated precipitation amounts even if there is a strong coupling of the climatological conditions between the region and the target station (SGHU station).

The artificial coupling of the local conditions to the regional conditions might not necessarily be a disadvantage. There is only one station in the Langtang Khola catchment which is meant to represent the entire meteorological situation of the catchment and the absence of further data makes the evaluation of the representativity of this station impossible. It is possible that the more regionalised information of the simulated precipitation amounts are even more representative for the catchment than the measured values of a single station at the valley bottom.

A comparison of the simulated hydrographs calculated on the basis of measured daily precipitation amounts and extrapolated daily precipitation amounts in Figure 8.5 shows that the differences are minimal. The hydrological year 1995/96 was chosen for the comparison

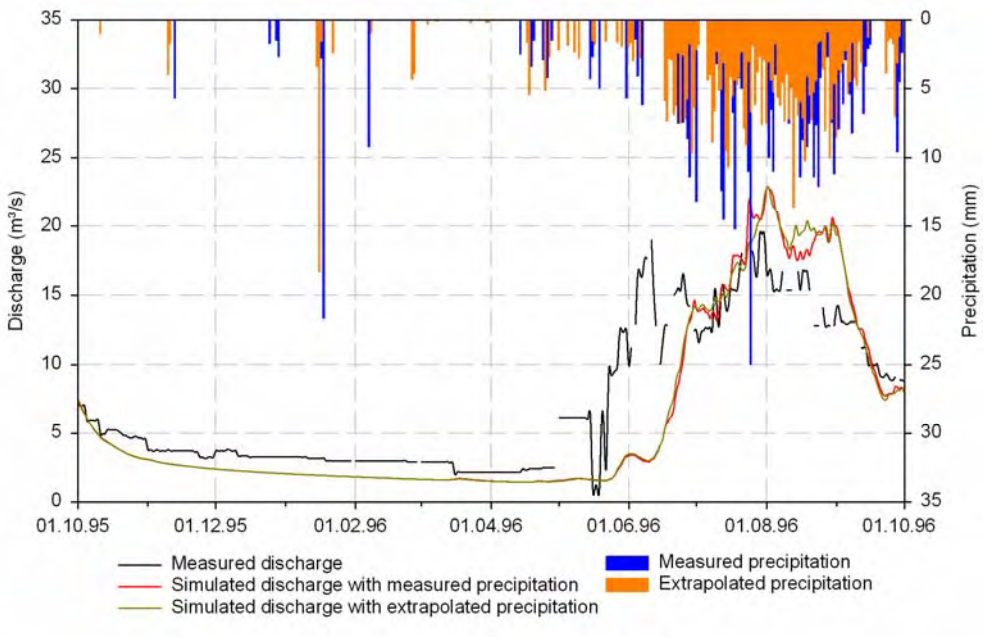

Figure 8.5: Comparison of the influences of different precipitation inputs on the discharge simulation. The hydrological year 1995/96 of the Langtang Khola catchment was chosen because there are no missing values or cumulated amounts of precipitation in the measured time series.

because this year shows neither gaps nor cumulated values and is therefore the most suitable for showing the influences of different precipitation inputs on the simulated hydrograph. The measured precipitation event of 25 July 1996 accounts for 25 mm while the extrapolation algorithm distributes this amount over previous days. The discharge peak calculated with the measured precipitation amounts is therefore not found in the simulated discharge with extrapolated precipitation input.

The extrapolated values are used only to fill gaps and to redistribute cumulated values. Plausible values of the measured time series were taken over unchanged in the newly generated time series. The new time series does not represent the real conditions for 100% but can be seen as an appropriate input for the simulation of daily discharge with TAC^{d}.

8.2 Regionalisation of input data

Two studies were found which provide spatial distributed information about air temperature and precipitation in the Langtang Khola catchment for the evaluation of the regionalisation of climatological input data. Figure 8.6 shows the location of the meteorological stations and the sites where precipitation, air temperature and maximum snow depth were measured. Shiraiwa et al. (1992) provide mean monthly air temperature data from June 1989 to March 1991 and precipitation data from June 1990 to April 1991 with maximum snow accumulation data from December 1989 to June 1990. Their stations were located at altitudes from 3920 m a.s.l. to 5300 m a.s.l.. Sakai et al. (2004) measured precipitation and air temperature at the Lirung glacier (4190 m a.s.l.) from 15 July to 29 August 1996. Table 8.2 summarises information on the meteorological stations and the conducted measurements.

Table 8.2: Meteorological stations in the Langtang valley and the measurements from Shiraiwa et al. (1992), Steinegger et al. (1993) and Sakai et al. (2004)

Station	Altitude (m a.s.l.)	Measurement	Observation period
1	5090	Precipitation	June 1990-September 1990
		Air temperature	June 1989-March 1991
2 (SGHU station)	3920	Precipitation	June 1990-September 1990
		Maximum snow depth	December 1989-June 1990
		Air temperature	June 1989-March 1991
3	5090	Precipitation	June 1990-September 1990
		Maximum snow depth	December 1989-June 1990
		Air temperature	June 1989-March 1991
4	4677	Maximum snow depth	December 1989-June 1990
5	5013	Maximum snow depth	December 1989-June 1990
6	4942	Maximum snow depth	December 1989-June 1990
7	5300	Precipitation	June 1990-September 1990
		Air temperature	June 1989-March 1991
8	4190	Precipitation	July 1996-August 1996
		Air temperature	July 1996-August 1996
9	5580	Snow accumulation	1980/81-1988/89
10	5350	Snow accumulation	1980/81-1988/89
11	5800	Snow accumulation	1980/81-1988/89

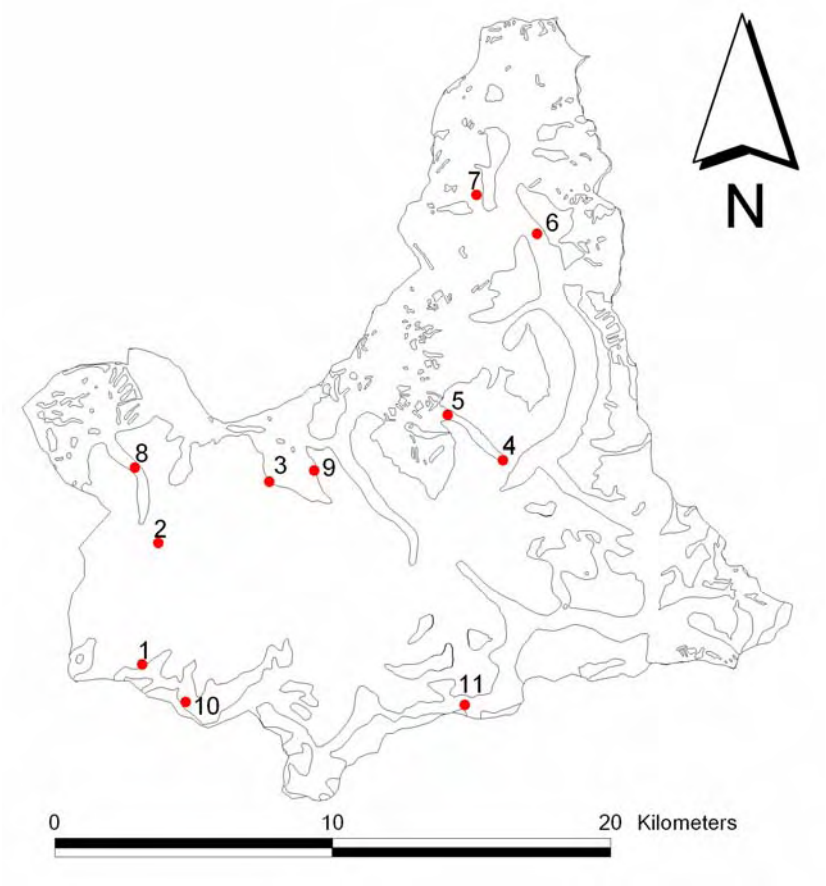

Figure 8.6: Langtang valley and the observation sites of the studies conducted by Shiraiwa et al. (1992), Steinegger et al. (1993) and Sakai et al. (2004)

8.2.1 Regionalisation of air temperature

The air temperature regionalisation is achieved using a fixed lapse rate as described in section 5.1.2. Calculated mean monthly air temperature values are compared with measurements at the stations described in section 8.2 for evaluation of the regionalisation method (Figure 8.7). Table 8.3 shows the coefficients of determination for the period from June 1989 to March 1991.

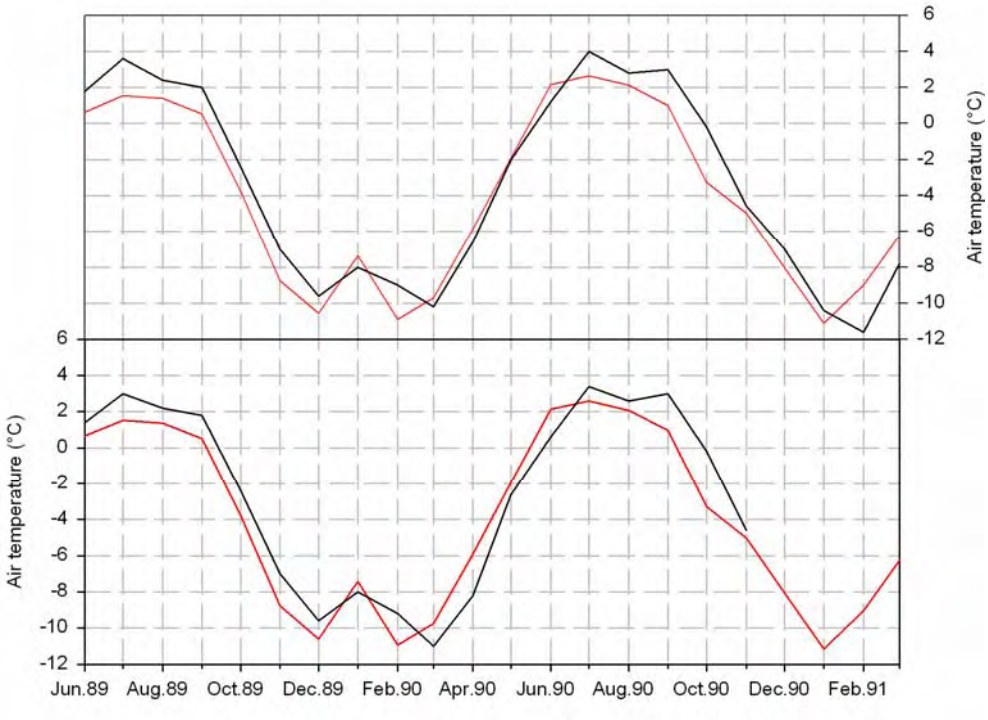

Figure 8.7: Comparison of simulated and measured air temperatures at Station 1 (upper graphic) and Station 3 (lower graphic), Langtang Khola catchment

Table 8.3: Coefficients of determination for the comparison of simulated and measured mean monthly air temperatures at different stations in the Langtang valley for the period from June 1989 to March 1991

Station	Altitude (m a.s.l.)	R^2
1	5090	0.94
3	5090	0.92

The R^2-values show a good simulation of the measured mean monthly air temperatures for both stations with the fixed lapse rate of –0.5°C/100 m. Visual inspection reveals, however, that air temperature during the monsoon season is underestimated at both stations. The mean air temperature at Station 8 from July to August 1996 (8.8°C) is also underestimated with 6.6°C as the simulated mean air temperature for that period.

The decline of air temperature with altitude during the monsoon season is less than the fixed rate. The seasonal variation in the vertical air temperature gradient between the SGHU station and Station 1 from June 1989 to March 1991 is shown in Figure 8.8.

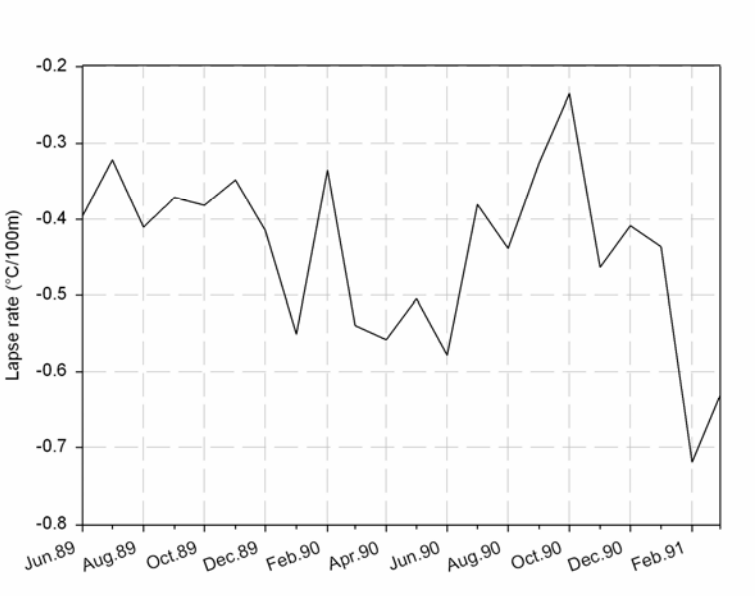

Figure 8.8: Seasonal variation in the vertical air temperature gradient between the SGHU station in the Langtang Khola catchment (3920 m a.s.l.) and Station 1 (5090 m a.s.l.)

The mean lapse rate from November to May is –0.54°C/100 m while it is –0.38°C/100 m from June to October. This seasonal change of the lapse rate cannot be considered when using a fixed lapse rate. In addition to that, the temperature gradient used in the model must be seen as an average value which has to be applicable to all simulated years and the measured air temperature at the SGHU station is considered to be representative for the entire catchment.

Air temperature is used for the calculation of snow- and icemelt in the temperature-index method. The threshold temperature TT in Equations 5.8, 5.9, 5.10 (section 5.3.3) is also a correction for the simulated temperature at the respective cell. TT is negative (–0.2°C; Table A4, Appendix) in this application which means that the daily air temperature is increased by the value of TT for the calculation of snow- and icemelt. This correction reduces the errors during the monsoon season caused by the fixed lapse rate. The regionalisation method does not consider the spatial variability of air temperature due to topographical shading effects. Shading effects are considered in the calculation of snow- and icemelt by the correction factor RexpMap (section 5.3.1). It is not necessary to include this information in the regionalised temperature values in order to obtain a realistic simulation of melt. The regionalisation of air temperature with a fixed gradient is considered to be an appropriate method for the available data base.

8.2.2 Regionalisation of precipitation

Horizontal and vertical gradients were used for the regionalisation of daily precipitation amounts. The horizontal gradient was introduced on the basis of observations made by Shiraiwa et al. (1992). Figure 8.9 compares the measured and simulated precipitation amounts from June to September 1990 at Stations 1, 3 and 7. The amounts over the four months were calculated with and without the horizontal gradient. The measured amounts were generally underestimated at Stations 1 and 3. By contrast, simulation without the horizontal gradient overestimates the precipitation amount at Station 7 and the calculated amount is even higher than the calculated amounts at Stations 1 and 3. The altitudes of the stations provide the

reason for this: Station 7 is the highest station. The measured precipitation amounts at Stations 1 and 3 are even more underestimated if the horizontal gradient is used for the simulation. However, the basic patterns of spatial distribution of basin precipitation are described more realistically. Station 7 receives less precipitation than Stations 1 and 3 (Section 3.2.2.1).

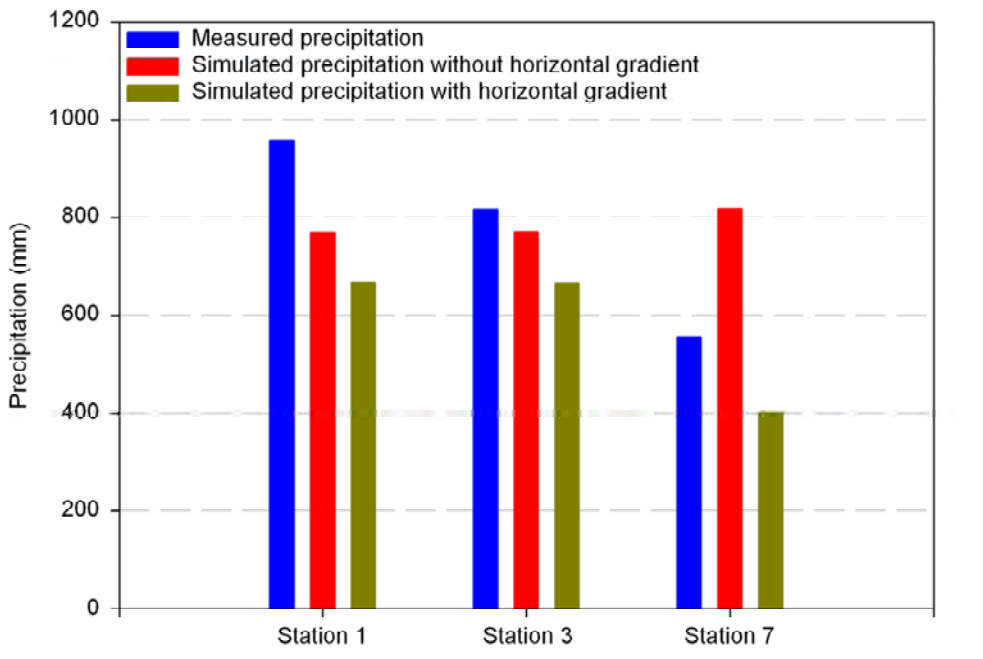

Figure 8.9: Comparison of measured and simulated precipitation amounts from June to September 1990 at three stations in the Langtang valley. The precipitation amounts were calculated with and without the horizontal gradient.

Figure 8.10 shows the influence of the horizontal gradient on annual precipitation distribution. Most of the annual precipitation falls in the upper reaches of the valley due to the higher elevations if the simulation is conducted without the horizontal gradient.

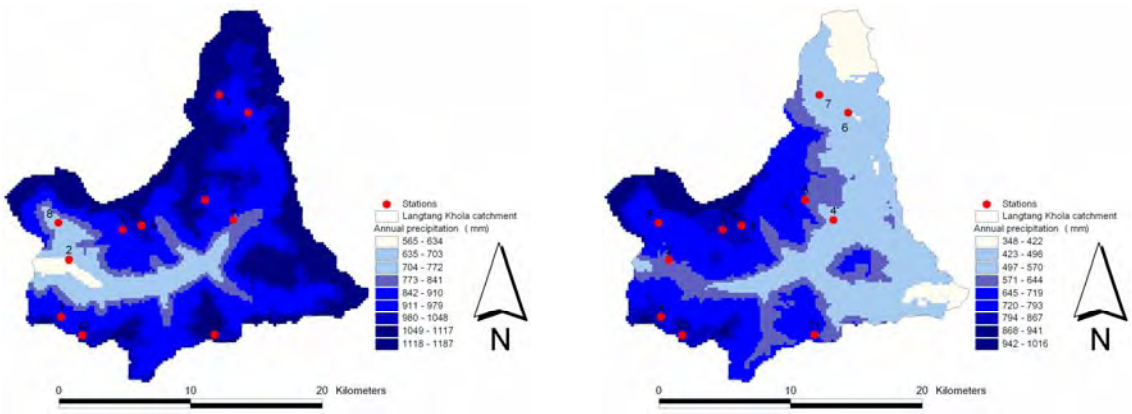

Figure 8.10: Distribution of annual precipitation amounts calculated without (left) and with (right) the horizontal gradient, Langtang Khola catchment

The measurements of maximum snow depth also show the declining amounts of solid precipitation in the upper reaches of the catchment. They cannot be compared with the simulated water equivalents because no snow density measurements were carried out.

Either the horizontal or the vertical gradient was determined from the measurements taken by Shiraiwa et al. (1992) as a magnitude for these parameters, but had to be changed slightly during the calibration procedure. The gradients in Table A4 (Appendix) are average values which were used for the entire simulation period. Deviations from measured events must therefore be expected.

8.3 Evapotranspiration

Actual evapotranspiration was measured at Stations 2 and 8 by Sakai et al. (2004) and given as an average from 15 July to 29 August 1996. The average value from Station 8 amounts to 1.99 mm/day and compares favourably with the simulated average value of 2.10 mm/day. The actual evapotranspiration at Station 2 is underestimated by the model with a simulated average of 2.01 mm/day compared to the measured average value of 4.5 mm/day.

The spatial distribution of the mean annual accumulated actual evapotranspiration from 1993 to 1998 in Figure 8.11 shows that the highest values occur at the valley bottom and at places where water is stored, e.g. glaciers.

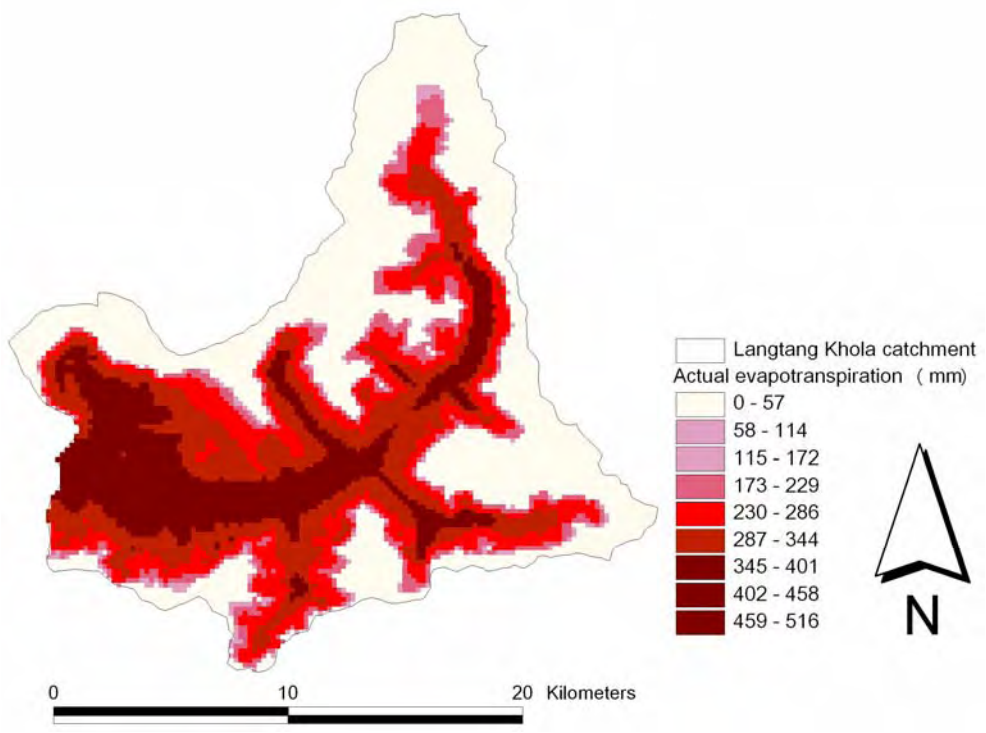

Figure 8.11: Spatial distribution of the mean annual accumulated actual evapotranspiration from 1993 to 1998, Langtang Khola catchment

Evapotranspiration can be an important factor, as regards energy, over a short period but as a water balance component the amount of evapotranspiration is small compared to, for example, precipitation in high alpine areas (Lang, 1981). Thus, the simple sinusoidal

approach for the calculation of potential evapotranspiration with a vertical gradient for regionalisation is considered to be appropriate for the available data base and the climatological conditions of the Langtang Khola catchment.

8.4 Snow and glacier routine

As Figure 8.12 shows, the integration of the algorithms for the calculation of glaciermelt brought the expected improvement in discharge simulation. There is a significant drop in performance if glaciermelt is neglected. The R_{eff}-values for the sample year 1994/95 are 0.88 for simulation including glaciermelt and 0.03 for simulation without glaciermelt. In general, the simulations without the extensions for glaciermelt greatly underestimate the observed runoff (VE is 297 mm/yr in 1994/95). Therefore, it is not possible to make reliable assumptions of the water balance of the catchment, mainly in the monsoon season, where a large amount of runoff originates from glaciermelt if glaciermelt is neglected.

TAC^d is able to reproduce the glacier mass balances satisfactorily as already shown in sections 7.4 and 7.5.

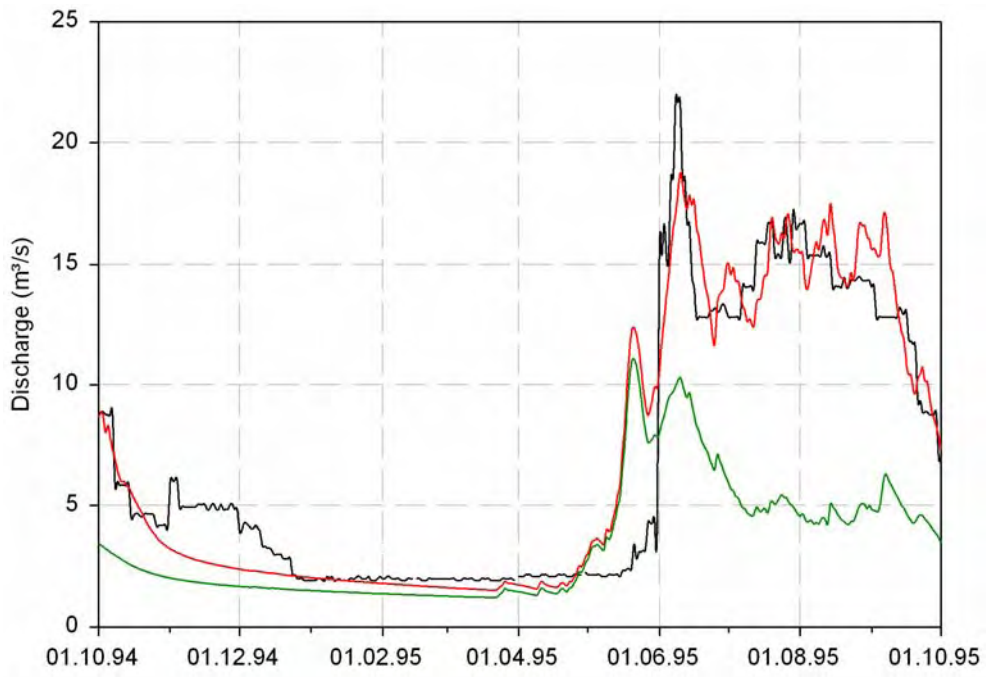

Figure 8.12: Comparison between observed discharge (black line) and simulated discharge (red line: with contribution of glaciermelt; green line: without contribution of glaciermelt), Langtang Khola catchment

The effects of the implemented extensions of the snow and glacier routine are discussed in the following chapters and evaluated as far as possible on the basis of measurements.

8.4.1 Seasonally and spatially distributed modelling of snow- and icemelt

The correction factor for the degree-day method (RexpMap) accounts for seasonal and spatial variations in the degree-day factor. Figure 8.13 shows the spatial distribution of RexpMap for the winter and the summer solstice as it is visualised in PCRaster.

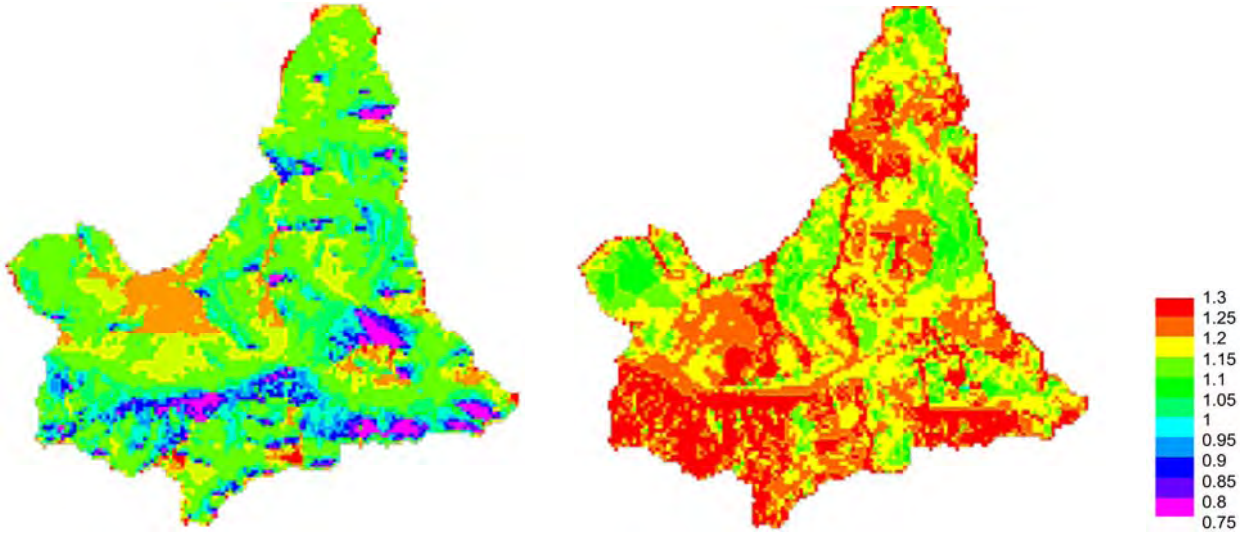

Figure 8.13: Spatial distribution of the correction factor for the degree-day method (RexpMap) at the winter solstice (21 December) (left) and the summer solstice (21 June) (right), Langtang Khola catchment

The spatial distribution of RexpMap shows realistic patterns. On 21 December the lowest values of RexpMap can be found at the north-oriented slopes at the valley bottom, whereas the highest values occur at the peaks and at highly elevated south-oriented plateaus. The zenith angle of the sun is close to 0° in the Langtang valley at the summer solstice due to its location close to the Tropic of Cancer (23.5° N). Thus, the map of 21 June shows the highest values at cells with northern and southern orientation and at the peaks or ridges. The lowest values are at east- or west-oriented slopes.

The temporal distribution of RexpMap follows a sinusoidal course with its maximum on 21 June and its minimum on 21 December. Figure 8.14 shows the average values of RexpMap of the Langtang valley for a hydrological year. The values are not less than 1.0, which indicates the dominance of cells with high RexpMap values in the catchment.

A sinusoidal annual course of the degree-day factor is proposed by Braun et al. (1993). They determined the sinusoidal oscillation of the degree-day factor with two parameters for the minimum and maximum of the curve. In this study the sinusoidal course of the degree-day factor is derived from astronomic and topographic information for each cell. This enables a more realistic temporal and spatial distributed simulation of melting processes.

This regionalisation method for meltwater calculation is linked with the potential sunshine duration and not with the actual sunshine duration. Thick clouds reduce the sunshine duration, especially during the monsoon season. The clouds are mainly convective, characterised by a large temporal and spatial variation (Kappenberger et al., 1993). For the most part, the sky is clear in the morning and clouds develop on the slopes during the day. Correction of the

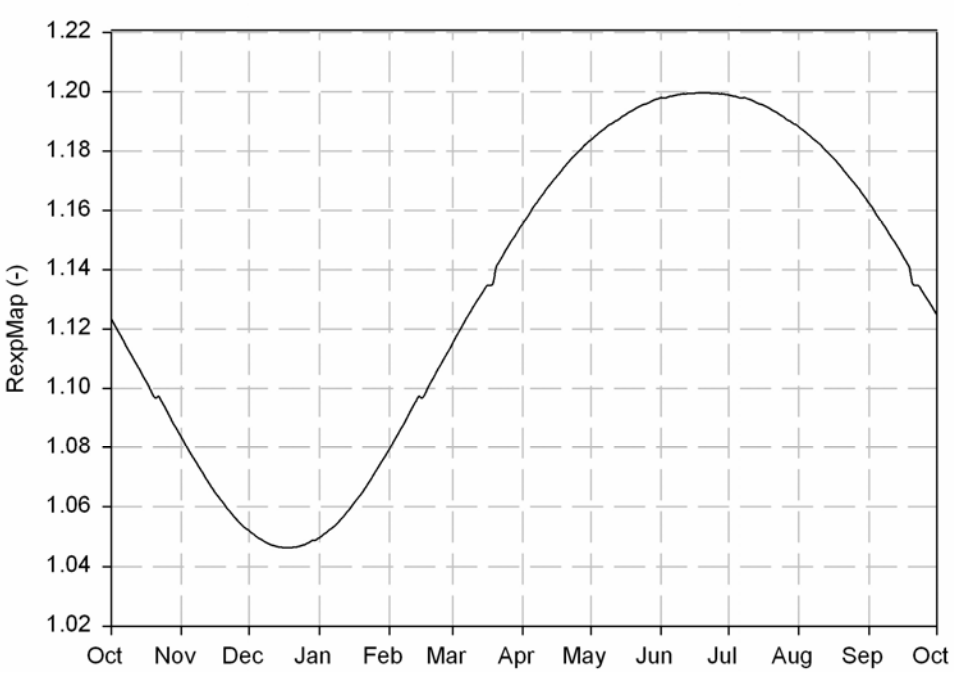

Figure 8.14: Sinusoidal course of the average correction factor for the degree-day method (RexpMap) of the Langtang valley for a hydrological year

potential sunshine duration using measurements of actual sunshine duration was not possible due to the lack of measurements.

The degree-day factor is about twice as large as in alpine applications (Braun and Aellen, 1990). Motoyama and Yamada (1989) observed surface glaciermelt rates of 12.7 mm/(°C day) for the Yala glacier at 5100 m a.s.l. for the period from 23 August to 3 September 1987. Further measurements of surface glaciermelt rates on the Khumbu glacier (Everest region) were even larger, with 16.9 mm/(°C day) for bare ice (Kayastha et al., 2000). The simulated degree-day factor for the area where the measurements on the Yala glacier were conducted amounts to 11.9 mm/(°C day). This value for bare ice is the product of Cfmax, RexpMap and the correction factor for accelerated melt of ice compared to snow (Rmult) (Equation 5.9). It can be considered as constant for the same period in different years because Cfmax and Rmult are constant values and the course of RexpMap is similar for all hydrological years. The simulated value can therefore be compared with the measured value of Motoyama and Yamada (1989) although their observation period does not lie within the simulation period. The values compare favourably.

The observed value at 5300 m a.s.l. on the Yala glacier, however, shows a very large difference as compared with the simulated degree-day factor. The value observed by Motoyama and Yamada (1989) for the period from 23 September to 3 October 1987 amounted to 19.2 mm/(°C day) and is more than twice as large as the simulated value of 8.5 mm/(°C day). When air temperature is measured over snow and ice surfaces as done by Motoyama and Yamada (1989), its information content with respect to energy availability for melt is greatly reduced. Air temperature measurements taken outside the glacierized area are considered to be more representative for the use of index methods in calculating snow- and icemelt (Section 5.3.1).

Figure 8.15 shows the spatial distribution of the snow cover at the end of the calibration period. The regions above 5500 m a.s.l. have a massive snow cover.

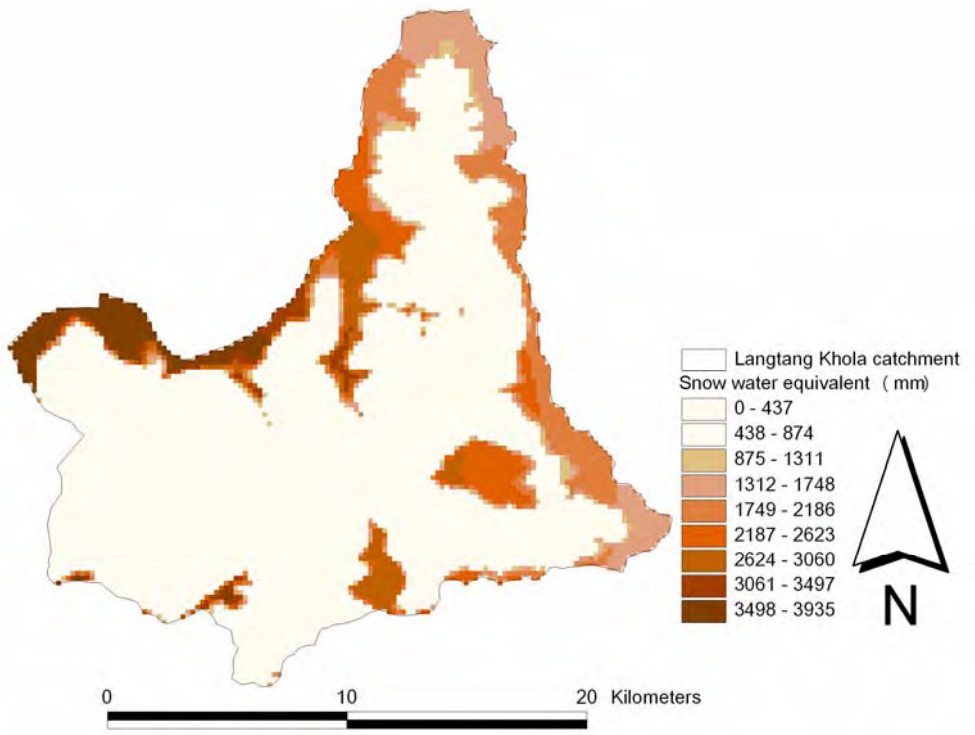

Figure 8.15: Spatial distribution of the snow cover at the end of the calibration period (30 September 1998), Langtang Khola catchment

Ablation in TAC^{d} is simulated as snow- or icemelt, whereas redistribution of snow via avalanches or wind is not considered by the model. Thus, no ablation is simulated for the areas above the altitude shown in Figure 8.16 where the air temperature is below the threshold temperature (TT).

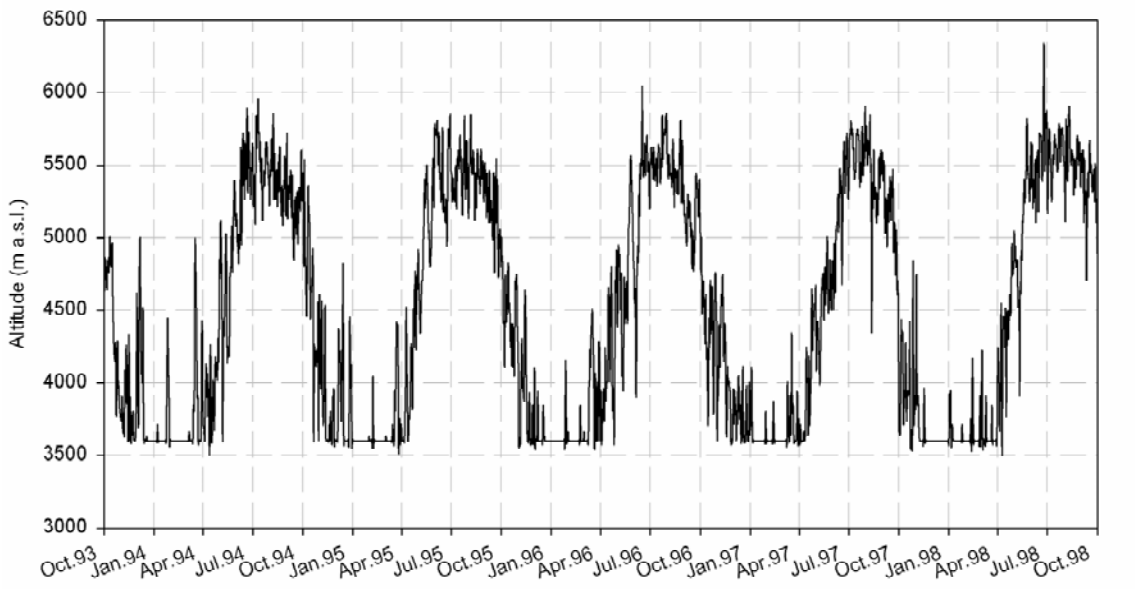

Figure 8.16: Altitude at which the air temperature equals TT, Langtang Khola catchment

This leads to an unrealistic snow cover simulation on the peaks and on steep slopes where snow is, in reality, redistributed via avalanches or wind, or where sublimation plays a significant role in the ablation process. Steinegger et al. (1993) measured stored precipitation in accumulation areas of glaciers from 1980/81 to 1988/89 and assessed the water equivalent of the individual snow layers. The variation in the annual accumulation is in the range of 600 to 1300 mm of water equivalent. For the assessment of the simulated snow accumulation the measured values are compared with the simulated ones in Table 8.4.

Table 8.4: Comparison of measured and simulated annual snow accumulation rates in the Langtang Khola catchment (Station numbers refer to sites shown in Figure 8.6.)

	Measured accumulation			**Simulated accumulation**		
	Station 9	Station 10	Station 11	Station 9	Station 10	Station 11
1987/88	638	133	723	847	490	700
1988/89	614	128	596	1219	947	743

Annual accumulation rates are overestimated at all stations except Station 11 in 1987/88. The impacts on the runoff generation are discussed in section 8.5.3.

Generally, the temperature-index method performs well if the air temperature is above TT because the air temperature is a representative diagnostic variable for the three major energy sources which determine snow- and icemelt, namely incoming net radiation, sensible and latent heat fluxes (Section 5.3.1). If the air temperature is below TT, no ablation can be calculated by the temperature-index method. This leads to an overestimation of accumulation rates in high altitudes where sublimation in addition to mechanical redistribution of snow contributes to ablation. Zappa et al. (2003) compared different approaches for snowmelt modelling. They found that the temperature-index-based methods are suitable if the interest is limited to simulations in daily resolution. Further, the classical temperature-index method as used in TAC^{d} performs very well compared to more sophisticated approaches, due to its robustness. The conceptual structure of the temperature-index method is less sensitive to the quality of the meteorological input than the physical-based approaches since the index method allows the calibration of more free parameters. This is a very important point for model applications in the Nepalese Himalayas.

8.4.2 Melt over debris-covered parts of the glaciers

About 19% of the glaciers in the Langtang Khola catchment are covered by debris, most of which lie in the lowest parts of the basin. Generally, glacier surfaces at these low elevations experience high melt rates and therefore constitute a strong water yield (Braun et al., 1993). However, the thickness of this debris layer may be up to several meters and, as mentioned in section 5.3.3, melt rates as a function of the current meteorological situation are reduced. The parameter Rmultd was introduced to account for this reduction. Rmultd ranges from 0.0 to 1.0. Rmultd = 0.0 means that melt is suppressed totally over the debris-covered parts of the glacier whereas melt rates are calculated as over clean ice if Rmultd is set at 1.0. Figure 8.17 shows the sensitivity of this parameter.

Discharge is generally underestimated if melt is suppressed totally and overestimated if debris-covered glaciers are treated the same way as clean glaciers. In the sample year 1994/95

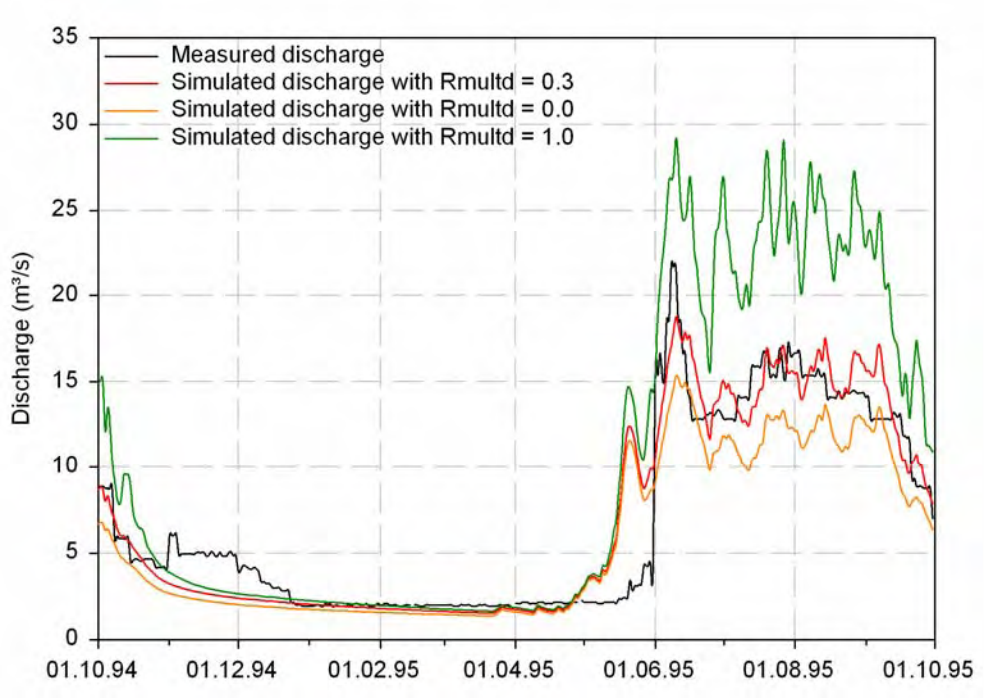

Figure 8.17: Sensitivity of the parameter Rmultd, Langtang Khola catchment

volume losses of 100 mm/a occur when setting Rmultd = 0.0; discharge is overestimated by about 269 mm/a if Rmultd = 1.0.

Sub-catchments of the Langtang Khola catchment are delineated for a scale-dependent analysis of the effects of Rmultd on discharge (Figure 8.18). Table 8.5 summarises the characteristics of the sub-catchments.

Table 8.5: The main characteristics of sub-catchments in the Langtang Khola catchment

	Area (km² / %*[1])	**Glacier area (km² / %*[2])**	**Debris-covered glacier area (km² / %*[3])**	**Altitude range of debris-covered glaciers (m a.s.l.)**
Lirung glacier	17.5 / 4.9	11.5 / 65.7	1.6 / 13.9	4000-4435
Langtang glacier	116.4 / 32.3	79.4 / 68.2	19.8 / 24.9	4477-5431
Langtang Khola	360.0 / 100.0	164.4 / 45.7	32.12 / 19.5	4000-5431

*[1] % of the Langtang Khola area
*[2] % of sub-catchment area
*[3] % of glacier area of the sub-catchment

The same two scenarios were calculated for the sub-catchments and the deviation from the discharge simulated with the calibrated parameter value (Rmultd = 0.3) was taken to show the consequences on the simulation results (Figure 8.19).

The Langtang glacier sub-catchment has the highest percentage of debris-covered glaciers and therefore shows the strongest reactions to changes in Rmultd. If Rmultd = 1.0, discharge in this sub-catchment increases by about 88% compared to the discharge simulated with the calibrated value of Rmultd. If Rmultd = 0.0, discharge is reduced by about 36%.

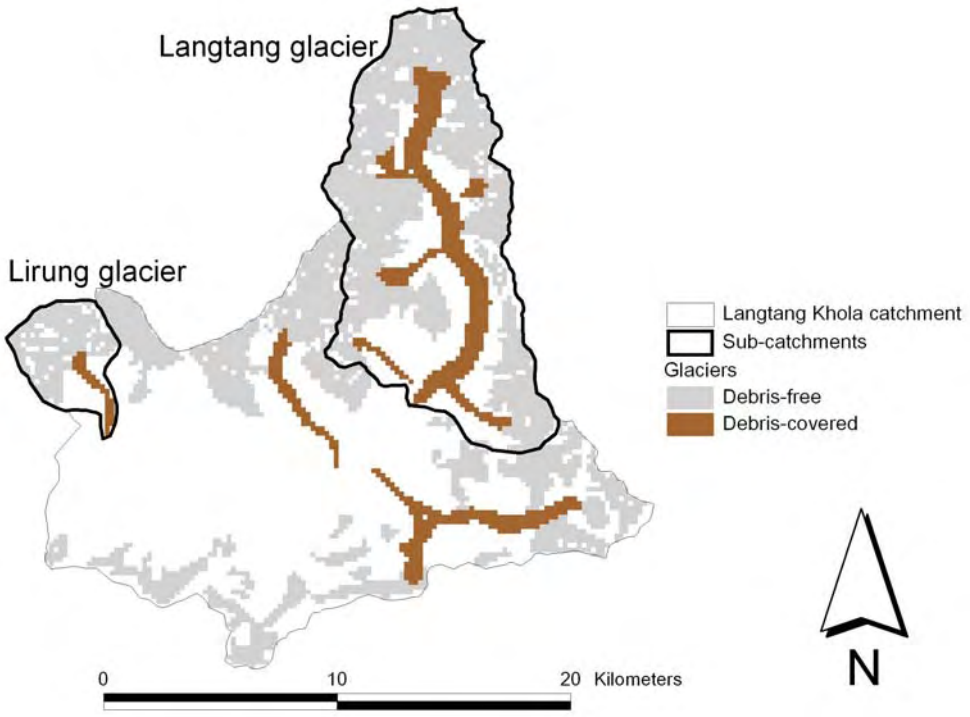

Figure 8.18: The Langtang Khola catchment with the Lirung glacier and Langtang glacier sub-catchments

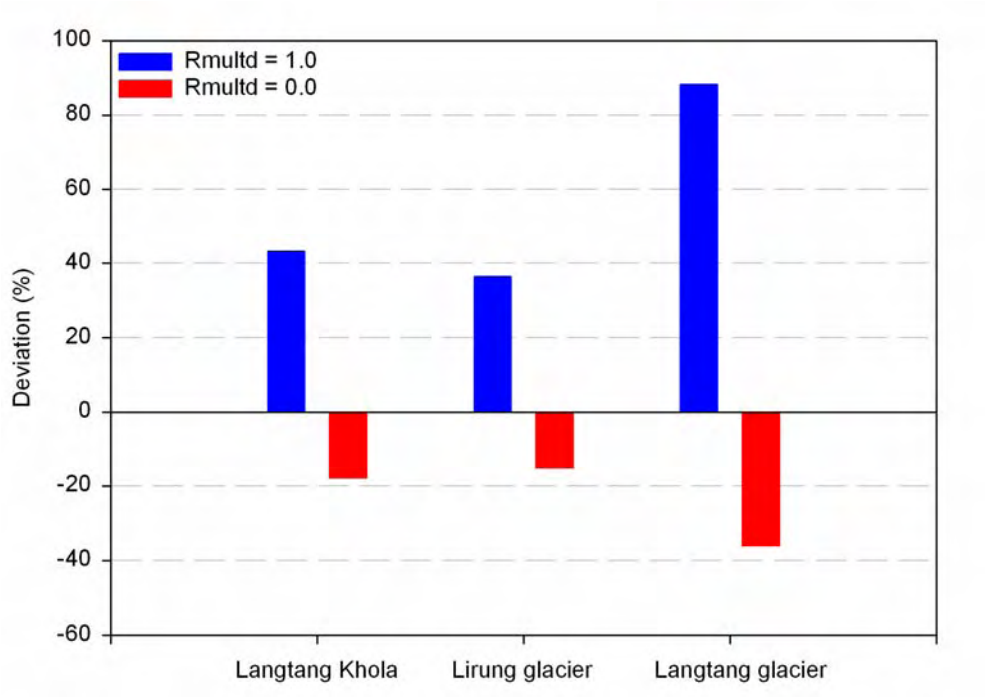

Figure 8.19: Deviation of scenarios results from discharge simulated with the calibrated value of Rmultd = 0.3 for the entire Langtang Khola catchment and the sub-catchments in the calibration period

The Langtang Khola catchment and the Lirung glacier sub-catchment show nearly similar reactions to changes in Rmultd although the difference in the debris-covered area between both catchments (5.6%) is the same as the difference between the Langtang Khola catchment and the Langtang glacier sub-catchment (5.4%). The debris-covered glacier tongue of the Lirung glacier ranges from 4000 m to 4435 m a.s.l. and is the lowest ice-covered area in the Langtang Khola catchment. Melting rates are therefore higher compared to the other debris-covered glacier tongues due to higher air temperatures at lower altitudes. The generally higher melting conditions compensate for the effects of a smaller debris-covered area of the Lirung glacier sub-catchment if Rmultd = 1.0.

If melt is suppressed over debris-covered glaciers, the altitudinal distribution of the clean glaciers of the respective sub-catchment is important for the assessment of the impact of suppression of melt on runoff generation. Figure 8.20 shows this altitudinal distribution of the clean glaciers in percent of the entire sub-catchment area. These glaciers constitute the water yield if there is no melt at the debris-covered glaciers. The absolute area of clean glaciers is much larger in the Langtang Khola catchment (132.28 km²) than in the Lirung glacier sub-catchment (9.9 km²). However, a larger proportion of the clean glaciers of the Lirung glacier sub-catchment is below 5000 m a.s.l. and experiences higher air temperatures. Thus, the deviations of the simulation results with Rmultd = 0.0 are quite similar for both catchments.

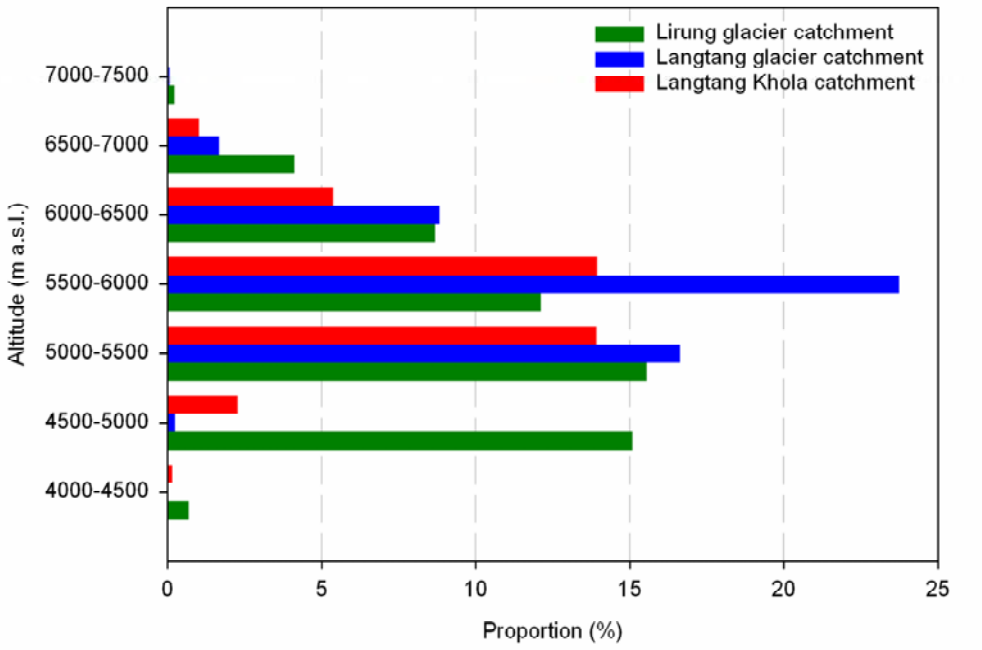

Figure 8.20: Altitudinal distribution of clean glaciers as a percentage of the entire sub-catchment area, Langtang Khola catchment

The value of Rmultd must lie between the two extremes, as shown above. Rmultd = 0.3 was chosen due to the experiences made by Popovnin and Rozova (2002) at the Djankuat glacier, Caucasus. They found a reduction of melt under debris layers of 50 to 70 cm of approximately 70% (Figure 5.5 in section 5.3.3) compared to the melt rate of bare ice.

These observations show that the impact of the debris-covered glaciers on icemelt mainly depends on the area of the debris layer within a catchment. The altitude of the glacier tongues and the spatial distribution of the clean glaciers, however, can cause compensating effects which complicates a general prediction of the scale-dependent impacts of debris-covered

glaciers on meltwater production. Analysis has shown that Rmultd is a very sensitive parameter and the approach supports the idea of distributed modelling to include different glacier surfaces.

8.5 The runoff generation routine

8.5.1 Composition of runoff in the river network

The composition of runoff shows seasonal variation (Figure 8.21). The high flow season is dominated by the outflow from the upper storages. The low flow is mainly a superposition of runoff of the lower storages of nRGType 1 and 2 and of the storages of nRGTypes 3 and 4. Outflow from the storages of nRGTypes 3 and 4 are important components for the maintenance of winter discharge although the area of these HRUs is small compared to the contribution areas of nRGType 1 or 2 (section 6.5.6, Table 6.11).

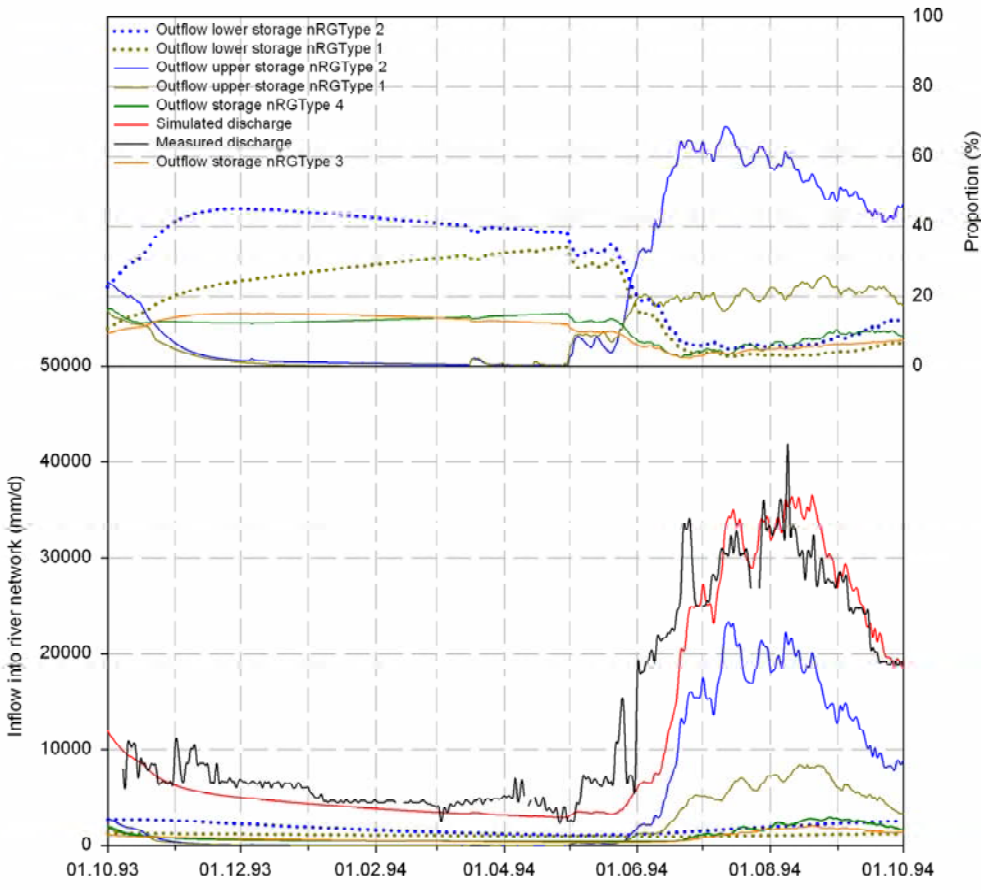

Figure 8.21: Contribution of each runoff component to the entire runoff in percent of the entire runoff (upper graphic) and as absolute values (lower graphic) for the hydrological year 1993/94, Langtang Khola catchment

8.5.2 Impact of the river network on the simulated discharge

The river network was derived from the DAV topographical map and had to be extended as described in section 6.5.4. The runoff composition of the simulated discharge with the unrevised river network is shown in Figure 8.22. A strongly reduced dynamic in the monsoon

season can be observed as well as a temporal shift of the simulated discharge in the monsoon season. The onset of the simulated discharge at the beginning of the monsoon season is much more delayed than the simulated discharge with the revised river network. The recession of the simulated discharge at the end of the monsoon season is also delayed by nearly one month.

It is noticeable that the outflow from the upper storage of nRGType 1 contributes more to the maintenance of the winter discharge than in the simulation with the revised river network. This can be explained with conceptualisation of the lateral fluxes. The cells which represent the glaciers are generally not directly connected to the unrevised river network and therefore do not directly contribute to the inflow into the river network. Figure 5.11 (section 5.6), however, shows that the outflow from the storage of nRGType 3 is directed to the upper storages of either nRGTypes 1 or 2, which are also connected laterally. Therefore, the outflows from nRGTypes 2 and 3 fill the upper storage of nRGType 1 and contribute to the maintenance of the winter discharge in that way.

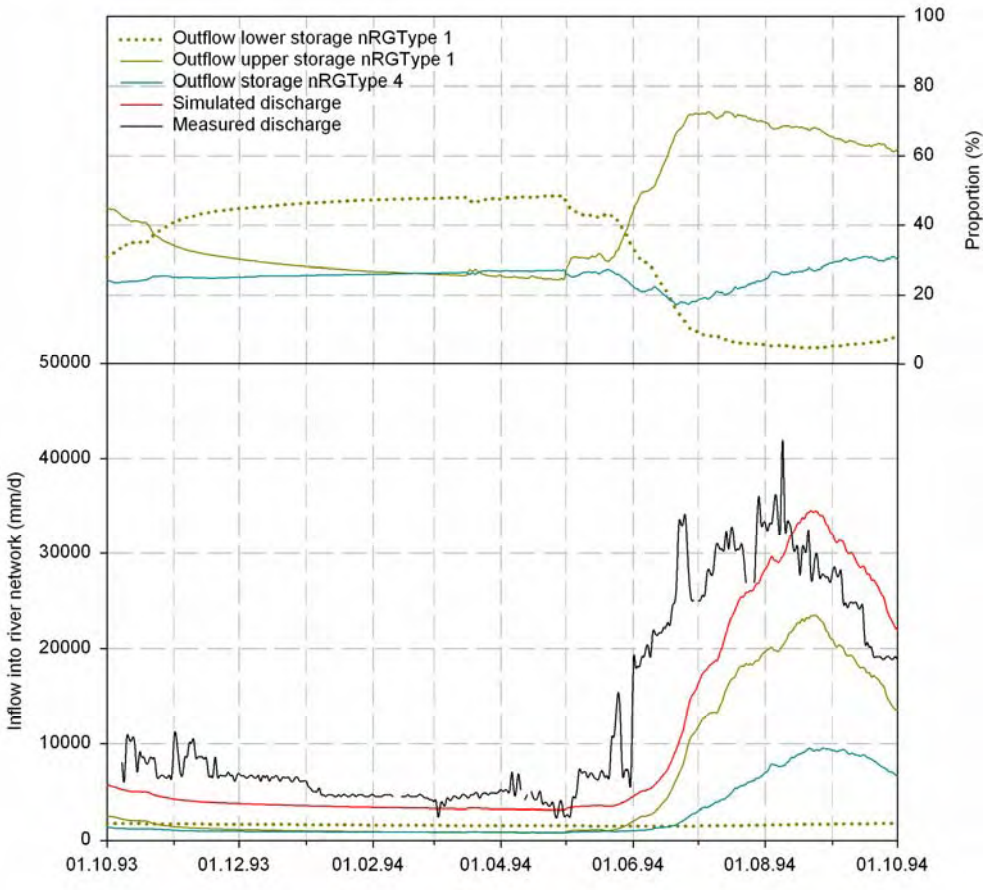

Figure 8.22: Contribution of each runoff component to the entire runoff in percent of the entire runoff (upper graphic) and as absolute values (lower graphic) for the hydrological year 1993/94 calculated with the unrevised river network, Langtang Khola catchment

The simulation results in Figure 8.22 show the importance of the modification of the river network. The subglacial drainage networks play an important role in the runoff generation but were not considered in the unrevised river network. The unrevised river network ended at the glacier tongues and therefore did not drain the upper reaches of the catchment which are covered mainly by glaciers. Runoff from a raster cell can flow through only one cell per time

step if the cell is not defined as a river network. This means that runoff which is generated in the upper reaches of the catchment needs many time steps until the unrevised river network is reached and therefore a delay of the simulated discharge is the result. The revised river network includes the glaciers and therefore accounts for the important role of the subglacial drainage network.

8.5.3 Simulation of the onset of discharge at the beginning of the monsoon season

The onset of discharge at the beginning of the monsoon season is delayed by some ten days or more in most of the simulated hydrological years. An exception is the year 1994/95 for which discharge at this time is overestimated by the model. A comparative analysis of the transformation of the output from the snow and glacier routine to discharge in the years 1993/94 and 1994/95 shows the reasons for these simulation errors (Figures 8.23 and 8.24).

For the comparison of the reactions of the outflows from the storages and of the storage levels on the input from the snow and glacier routine, all values were standardised on the catchment area. This means for instance that the storage levels of each cell of the same storage unit (e.g. GlacierLS_box, see section 5.5) were added and divided by the number of cells of the entire catchment (8996 cells). This standardisation allows the comparison of the sizes with respect to their importance to the turnover of water in the entire catchment.

Figures 8.23 and 8.24 show that the output from the snow and glacier routine of both years is directed to the runoff generation routine without retardation in the soil routine. In 1993/94 this input to the runoff generation routine fills the upper storages of the glacier and the non-glacier area (nRGType 1 and 2) until the end of June (Figure 8.23). The outflow from the storages is controlled by the respective storage levels and thus a constant rise of the outflow from both the upper storage of the glacier area (nRGType 2) and the upper storage of the non-glacier area (nRGType 1) can be observed in this period. Both outflows are responsible for the high flow simulation. The fluctuations in the input into the runoff generation routine are suppressed in the storages of the runoff generation routine which causes a strongly reduced dynamic of the outflow from the storages compared to the input.

At the end of June the upper storages are filled and the storage contents remain on nearly constant levels. Due to the conceptualisation of the upper storages, all additional water is directed to the next cell without retardation if the storages are filled completely. The dynamic of the outflow from both upper storages increases strongly from the end of June onwards. The fluctuations in the input are directly converted into fluctuations in the outflow. This fast reaction of the storages causes an improved discharge simulation during this period. In general, the dynamic of the output from the snow and glacier routine or the output from the soil routine agrees well with the dynamic of the measured discharge which proves that the underestimation of the measured discharge at the beginning of the monsoon season is caused by continuous saturation of the upper storages, ending in the suppression of the outflow dynamic.

In 1994/95 discharge is overestimated by the model at the beginning of the monsoon season. Figure 8.24 shows that this is caused by snowmelt. Solid precipitation from October 1994 to May 1995 amounts to 235 mm (water equivalent) compared to 44 mm during the same period in the previous year. This unusual snow cover causes a meltwater wave which quickly saturates the upper storages, especially of the non-glacier area. As Figure 3.1 in Chapter 3 shows, only a small part of the area below 4400 m a.s.l. is covered by glaciers. Therefore,

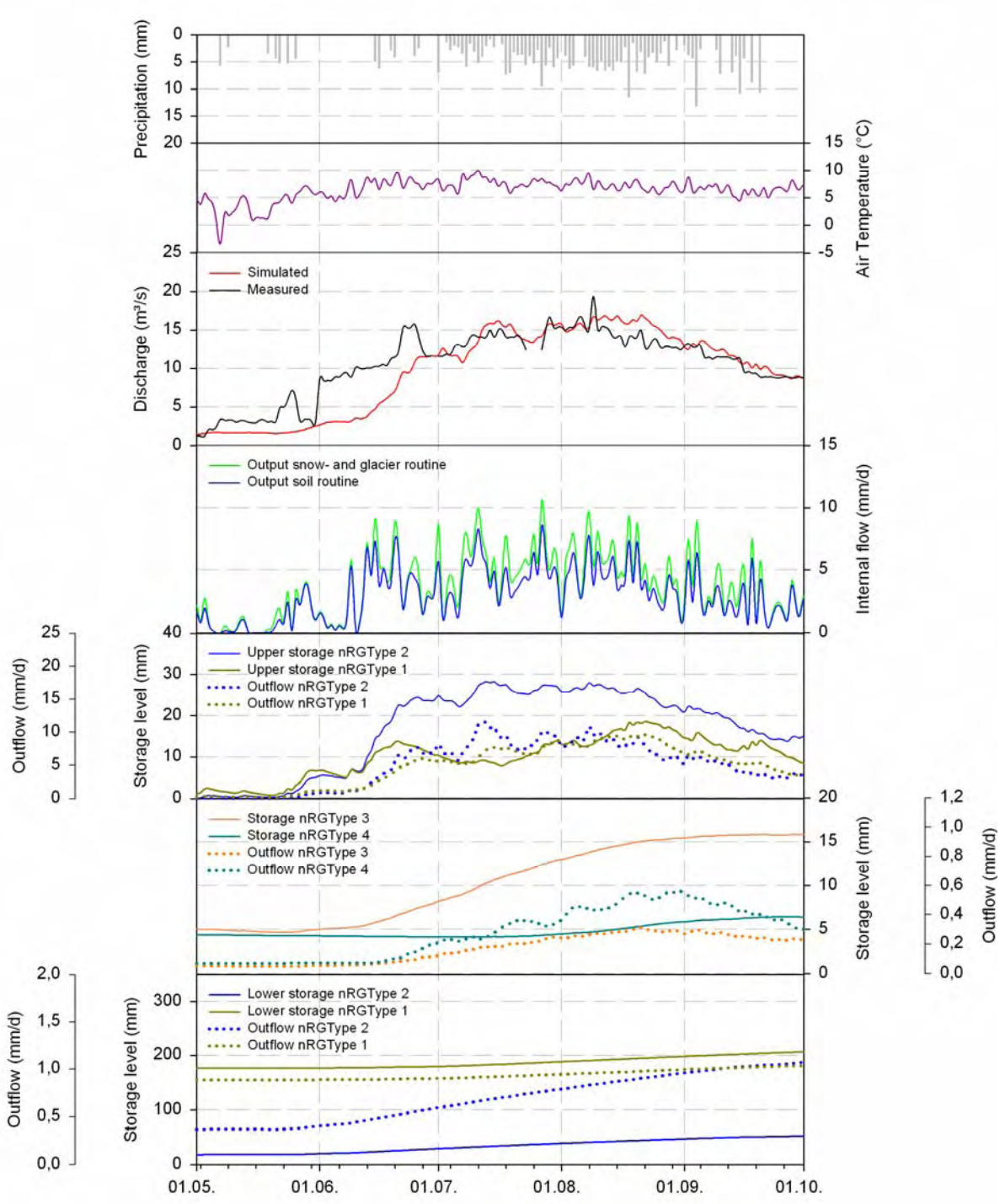

Figure 8.23: Transformation of snow- and glaciermelt and precipitation into discharge (hydrological year 1993/94). Intermediate results are average values per cell related to the entire catchment area, Langtang Khola catchment.

snowmelt at the beginning of the monsoon season mainly affects the storage levels of the non-glacier area in lower altitudes due to higher snowmelt rates.

Figure 8.25 shows the spatial distribution of the output of the snow and glacier routine as cumulated values from 1 October 1994 to 17 May 1995 when the output of the snow and glacier routine peaks.

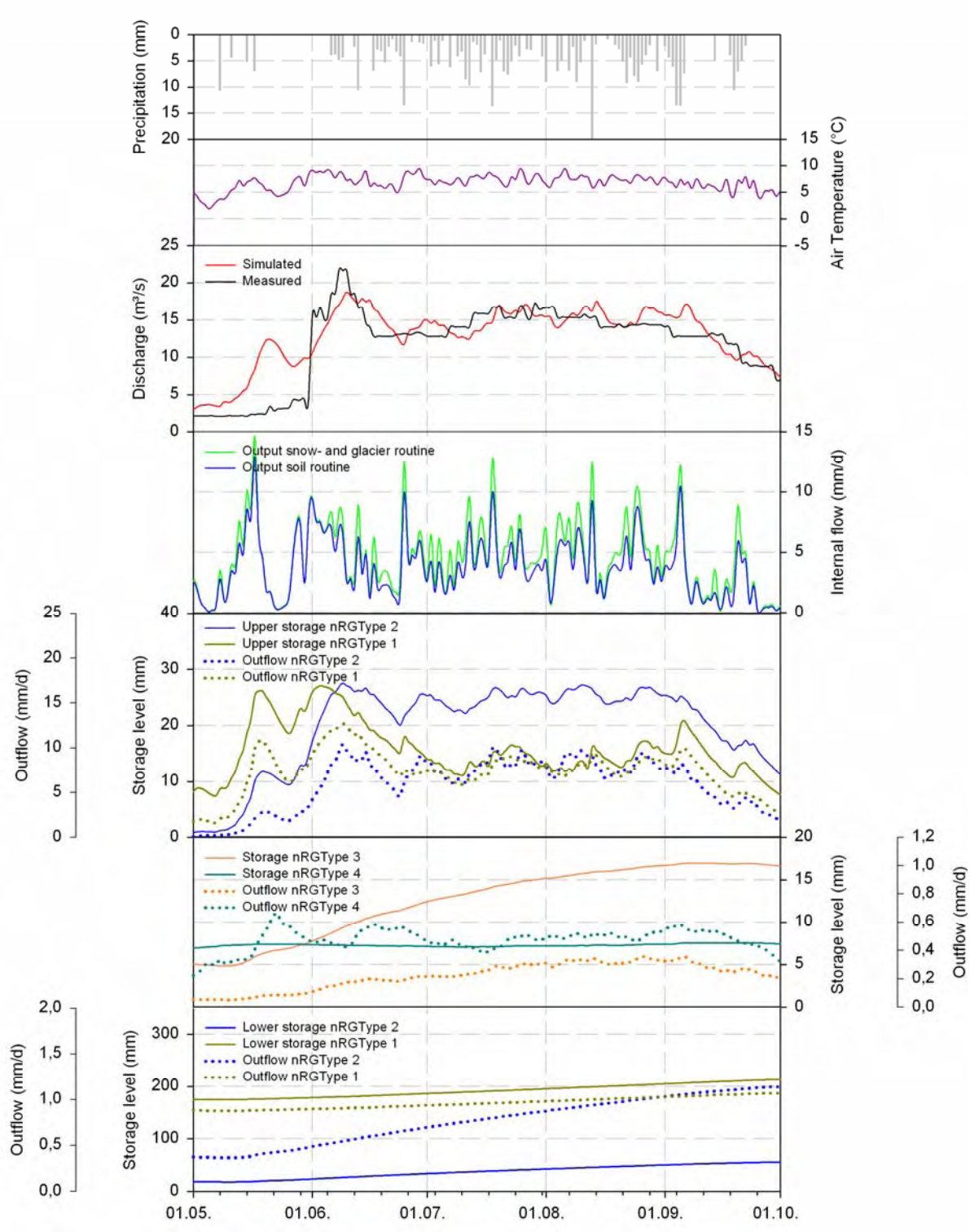

Figure 8.24: Transformation of snow- and glaciermelt and precipitation into discharge (hydrological year 1994/95). Intermediate results are average values per cell related to the entire catchment area, Langtang Khola catchment.

The storages of the non-glacier area are filled faster than the storages of the glacier area due to this spatial distribution and thus dominate the runoff generation at the beginning of the monsoon season in 1995. This fast saturation of the upper storages in May 1995 causes the same effects as observed at the end of June 1994. The dynamic of the outflow of the snow and

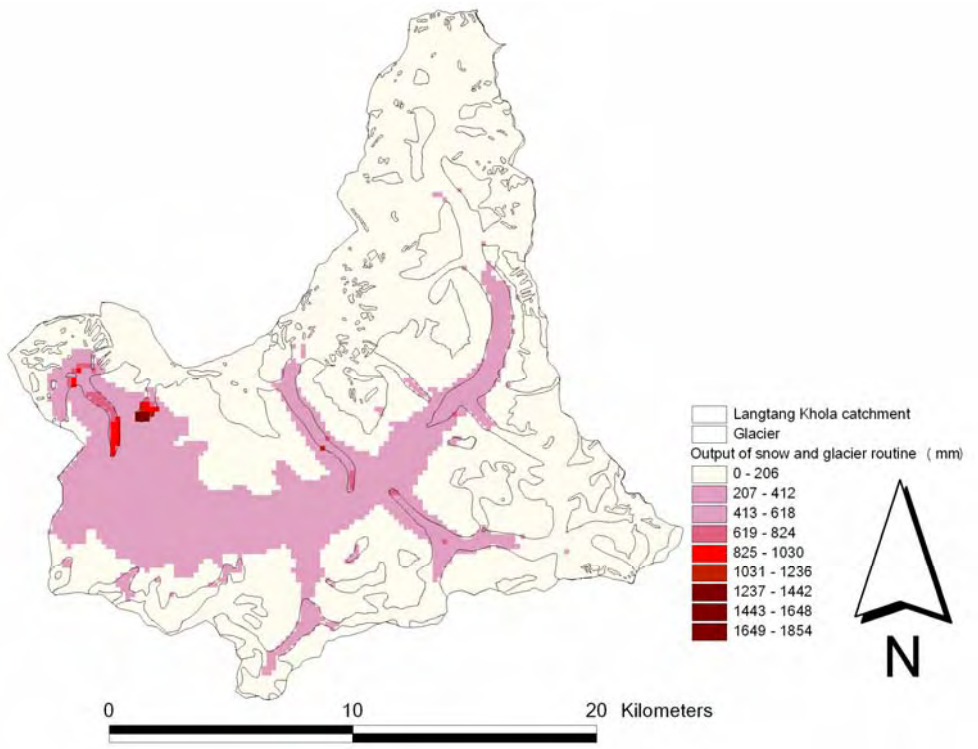

Figure 8.25: Spatial distribution of cumulated output of the snow and glacier routine from 1 October 1994 to 17 May 1995, Langtang Khola catchment

glacier routine is directly represented in the outflow of the upper storage of nRGType 1 whereas the outflow dynamic of the upper storages of the nRGType 2 is suppressed until mid-June 1995 compared to the outflow of the upper storage of nRGType 1.

The hydrograph is generally simulated well at the end of the monsoon season which proves that the parameterisation of the k-values of the upper storages is in order. The k-values control the drainage of the storages (section 4.2.3).

The comparison of the simulation results from these two monsoon seasons shows that the simulation of the onset of discharge strongly depends on the filling level of the upper storages. Meltwater mainly contributes to the saturation of the upper storages in the pre-monsoon season. The following could be the cause of the simulation problems at the beginning of the monsoon season:

- Wrong determination of solid precipitation, either measured or simulated. The distinction between solid and liquid precipitation is achieved by the TT parameter in the model.
- Measured air temperature is not representative for the energy input in the pre-monsoon season. A snow cover at the SGHU station could be the cause of cooling effects. The temperature-index method strongly depends on representative air temperature values for correct calculation of melt (section 5.3.1).
- Wrong storage concepts or parameterisation. It takes a long time until the upper storages are saturated due to nearly complete emptying during the winter season. This suppresses the dynamic of the outflow of the upper storages.

- Discharge was measured only once a day in the early afternoon. Discharge in glacierized catchments shows pronounced diurnal fluctuations especially if there is no further precipitation input. Discharge peaks in the early afternoon.
- Mass distribution due to avalanches causes an increased snow cover in the lower altitudes and thus an increase in meltwater production at the beginning of the monsoon season which cannot be calculated by the model.
- Temporal and spatial resolution does not fit. Water can flow only 200 m per day with a spatial resolution of 200 x 200 m². The residence times of fast runoff components are therefore unrealistically high.

8.6 Simulation results of the validation period

Winter discharge is underestimated in the validation period whereas discharge in the monsoon season is overestimated (section 7.5). A possible explanation could be that the storage capacity of the glaciers (of nRGType 2 and 3) was higher in the validation period. In the conceptualisation of the runoff generation routine these glaciers are considered to store most of the water during the monsoon season and maintain discharge in the dry season. The glacier map of the Langtang Khola catchment was derived from aerial photography shots taken between 1992 and 1996. Kappenberger et al. (1993) revealed with terrestrial photogrammetry that only small fluctuations in the glacier tongues occurred on south-facing glaciers from 1980 to 1991. Meanwhile, glaciers on north-facing slopes advanced in the same period. This observation was confirmed by measurements of annual surface lowering rates of the Lirung and Yala glaciers (Yamada et al., 1992; Fujita et al., 1998). The surface lowering has accelerated since the late 1980s on the Lirung glacier as well as on the Yala glacier (Asahi, 1998; Fujita et al., 1998; Naito et al., 2002). This means that the glacier map is representative for the calibration period but not necessarily for the validation period. If the storage capacity of the glaciers was higher in the validation period, more water could be retained during the melt/monsoon season and released during the winter season. This would reduce the discharge peaks in melt/monsoon season and increase discharge in the winter season.

The model was calibrated to the situation of the calibration period. The comparison of glacier mass balances in Figure 7.8 (section 7.5) shows that the parameterisation of the snow and glacier routine is representative for the entire simulation period (1987-1998). In Figure 8.26 only the upper storage limits of the glacier storages were increased and discharge was calculated using the same glacier map as for the calibration period. The simulated discharge with the revised optimal parameter set shows the expected tendencies. Discharge in the melt/monsoon season declined while winter discharge increased, especially in the post-monsoon season (September to October). The effect would be more pronounced if an increased glacier area were also used for the simulation of the validation period.

8.7 Multi-criteria calibration

The importance of a further calibration criterion beside measured discharge is presented in the following example.

Table 8.6 shows the optimal parameter set obtained from calibration (Table A4, Appendix) and another parameter set (parameter set 2) which mainly differs from the optimal parameter

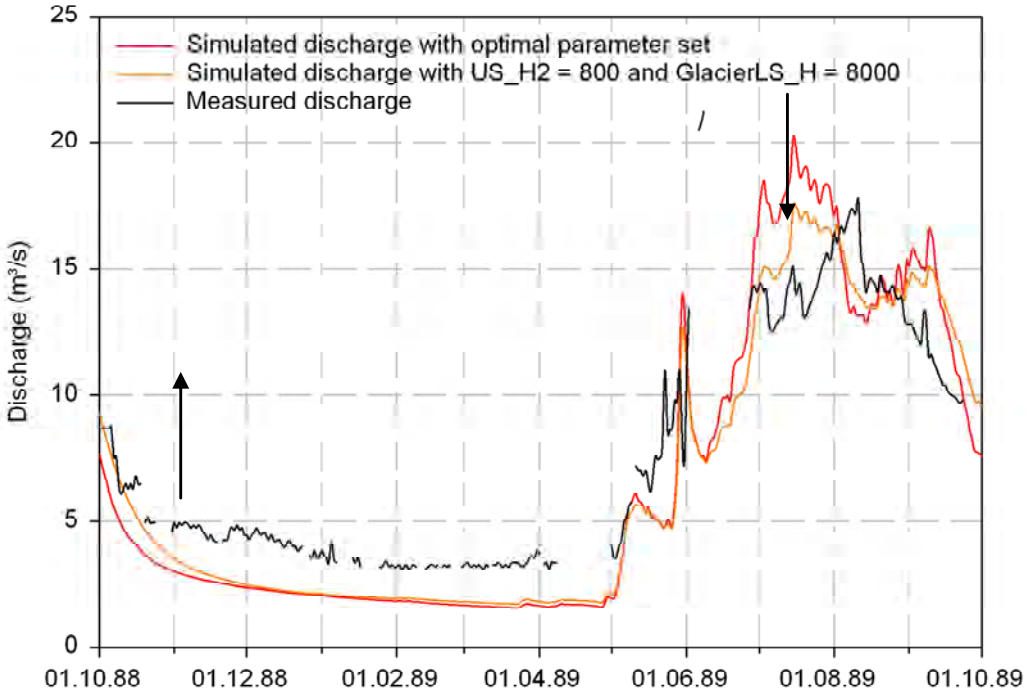

Figure 8.26: Simulation of the hydrological year 1988/89 with different parameter sets. The arrows indicate the tendency of the simulated hydrograph with the revised parameter set, Langtang Khola catchment.

set in the parameters of the snow and glacier routine and the parameters which control the calculation of the basin precipitation.

Table 8.6: Differences between the optimal parameter set and parameter set 2, Langtang Khola catchment

	Optimal parameter set	**Parameter set 2**
PCF	1.05	1.3
PGrad	0.04	0.045
PHorizGrad	-0.03	-0.02
TGrad	-0.5	-0.55
SFCF	1.2	1.4
Cfmax	7.0	4.0
Rmult	1.4	1.2
Rmultd	0.3	0.5

Both parameter sets give nearly the same simulation results as shown in Figure 8.27 and Table 8.7. The simulation using the optimal parameter set shows slightly better objective evaluation criteria but a visual inspection of the simulated curves reveals that the differences between the two simulation results are minimal for all hydrological years.

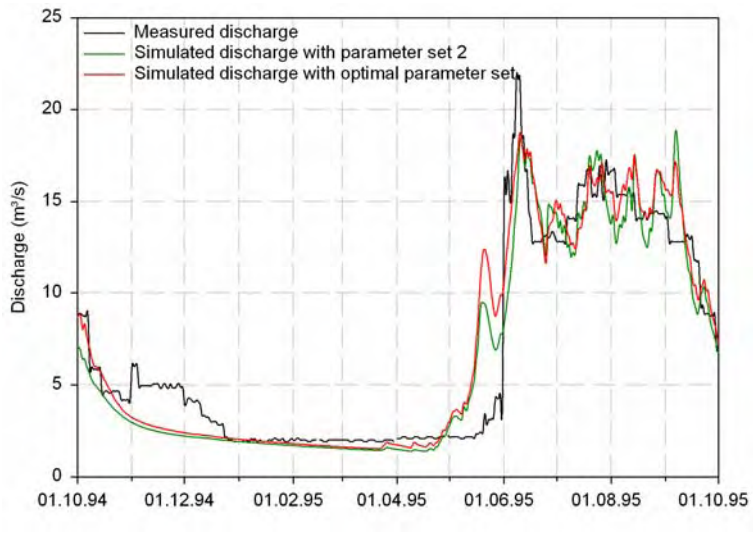

Figure 8.27: Comparison between measured and simulated discharge calculated using the optimal parameter set and parameter set 2, Langtang Khola catchment

Table 8.7: R_{eff}-values of simulation results with different parameter sets, Langtang Khola catchment

	R_{eff} of optimal parameter set	**R_{eff} of parameter set 2**
1993/94	0.85	0.72
1994/95	0.87	0.87
1995/96	0.53	0.48
1996/97	0.46	0.24

However, the comparison of simulated glacier mass balances in Figure 8.28 shows significant differences. It becomes obvious that ablation is underestimated, but this error is compensated for by an overestimation of basin precipitation and thus the differences in the simulated discharge are minimal.

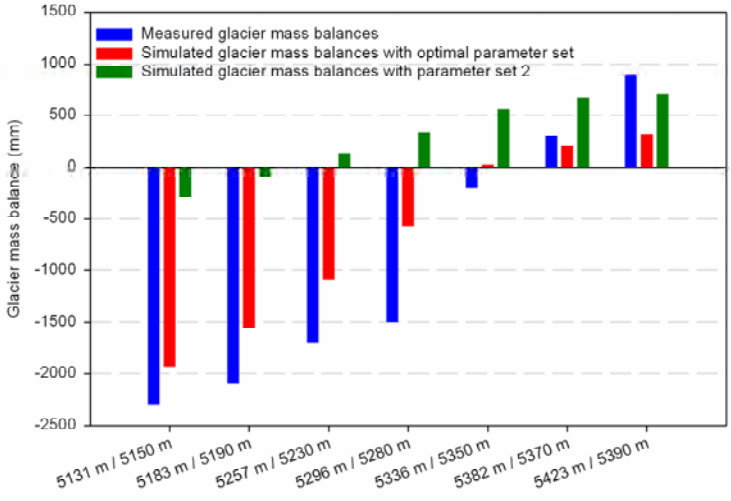

Figure 8.28: Comparison between measured and simulated glacier mass balances calculated using the optimal parameter set and parameter set 2, Langtang Khola catchment

8.8 Comparison of the TAC^d and HBV-ETH models

The simulation results of TAC^d are compared with the results of the HBV-ETH model for further evaluation of TAC^d.

The comparison of the evaluation criteria shows that TAC^d generally gives better simulation results (Table 8.9). Figure 8.29 shows that the monsoon season in July and August 1994 is simulated well by both models.

Table 8.9: Comparison of evaluation criteria of simulations with TAC^d and HBV-ETH, Langtang Khola catchment

	TAC^d				**HBV-ETH**			
	R_{eff}	Log R_{eff}	R^2	VE	R_{eff}	Log R_{eff}	R^2	VE
1987/88	0.58	0.05	0.87	97	0.26	-2.83	0.78	258
1988/89	0.72	0.32	0.90	40	0.37	-1.45	0.81	161
1989/90	0.68	0.45	0.84	50	0.37	-0.49	0.77	20
1990/91	0.20	0.40	0.88	-30	-0.33	-0.38	0.80	-136
1991/92	0.30	0.59	0.82	-9	-0.05	-0.44	0.68	80
1992/93	0.76	0.68	0.91	37	0.40	-0.60	0.76	107
1993/94	0.85	0.75	0.89	57	0.59	0.07	0.75	123
1994/95	0.87	0.80	0.88	-8	0.83	0.63	0.91	126
1995/96	0.53	0.31	0.72	92	0.29	-0.38	0.62	81
1996/97	0.46	0.84	0.76	-8	0.18	0.15	0.63	46

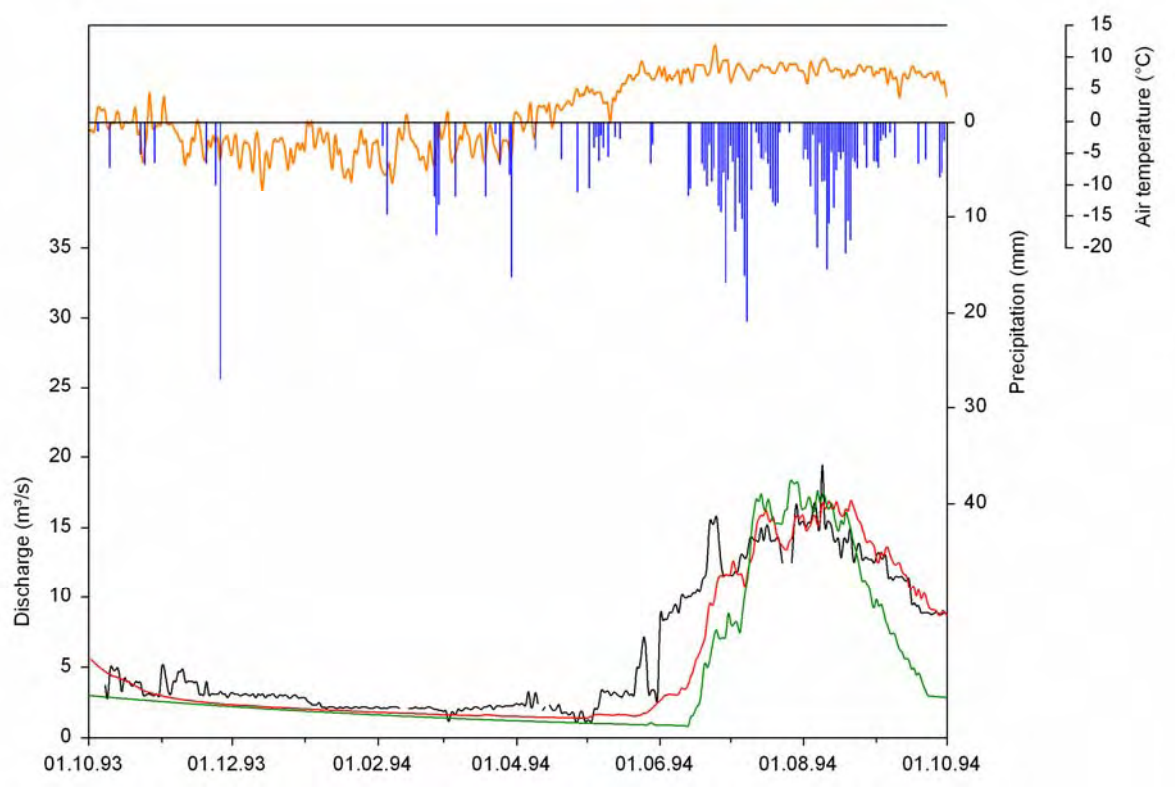

Figure 8.29: Comparison between measured (black) and simulated discharge with TAC^d (red) and HBV-ETH (green), 1993/94, Langtang Khola catchment

However, the HBV-ETH model underestimates the discharge both at the beginning of the monsoon season and during the post-monsoon season. These observations are typical for all simulated hydrological years. The great correspondence between the two models can be expressed by the large R^2-values as shown in Table 8.10.

Table 8.10: R^2-values of the comparison between the simulation results of TAC^d and HBV-ETH, Langtang Khola catchment

	R^2
1987/88	0.94
1988/89	0.86
1989/90	0.94
1990/91	0.93
1991/92	0.93
1992/93	0.91
1993/94	0.87
1994/95	0.89
1995/96	0.94
1996/97	0.96

It is difficult to compare the models due to their different spatial discretization. Therefore, Figure 8.30 shows the output from the snow and glacier routine and the input into the runoff generation routine of TAC^d as an average value of all HRUs and the storage levels related to the entire catchment for summer 1994. The output from the snow and glacier routine shows only minor differences between the two models. HBV-ETH gives higher values if precipitation contributes significantly to the composition of the output of the snow and glacier routine because there is no negative horizontal gradient for the calculation of basin precipitation. At the beginning and at the end of the monsoon season more water is retained in the soil routine in the HBV-ETH model than in the TAC^d model. The input into the runoff generation routine does not contribute to the filling of the upper storage of the HBV-ETH model until the middle of June 1994. The water is directed to the lower storage because the input into the upper storage is smaller than the fixed percolation rate (CPERC) of 1.5 mm/day. Therefore, the onset of discharge of the monsoon season simulated by the HBV-ETH model is delayed more than the simulated discharge of the TAC^d model. The upper storage of the HBV-ETH model empties continuously from the middle of August until the end of September 1994, whereas the upper storages of the TAC^d model remain at the same level. This causes the fast decline of discharge at the end of the monsoon season as simulated by the HBV-ETH model. The lower storage outflow of HBV-ETH maintains the winter discharge and the storage is filled during the monsoon season. A more detailed comparison of both models is not attempted here as it would be beyond the scope of this study. Nevertheless, it can be stated that the TAC^d model and the HBV-ETH model are applicable to the Langtang Khola catchment. Both models are able to simulate the melting of ice and snow appropriately. The advantage of the TAC^d model is the better redistribution of the water stored during the monsoon season. During calibration of the HBV-ETH model it became obvious that the model can either be calibrated to simulate the high flow season well or the low flow season in winter. It was not possible to get a good simulation of the entire hydrological year.

The more sophisticated and distributed runoff generation routine of TAC^d enables the storage of water for maintaining the rather high level of winter discharge and at the same time simulates well the discharge conditions of the monsoon season.

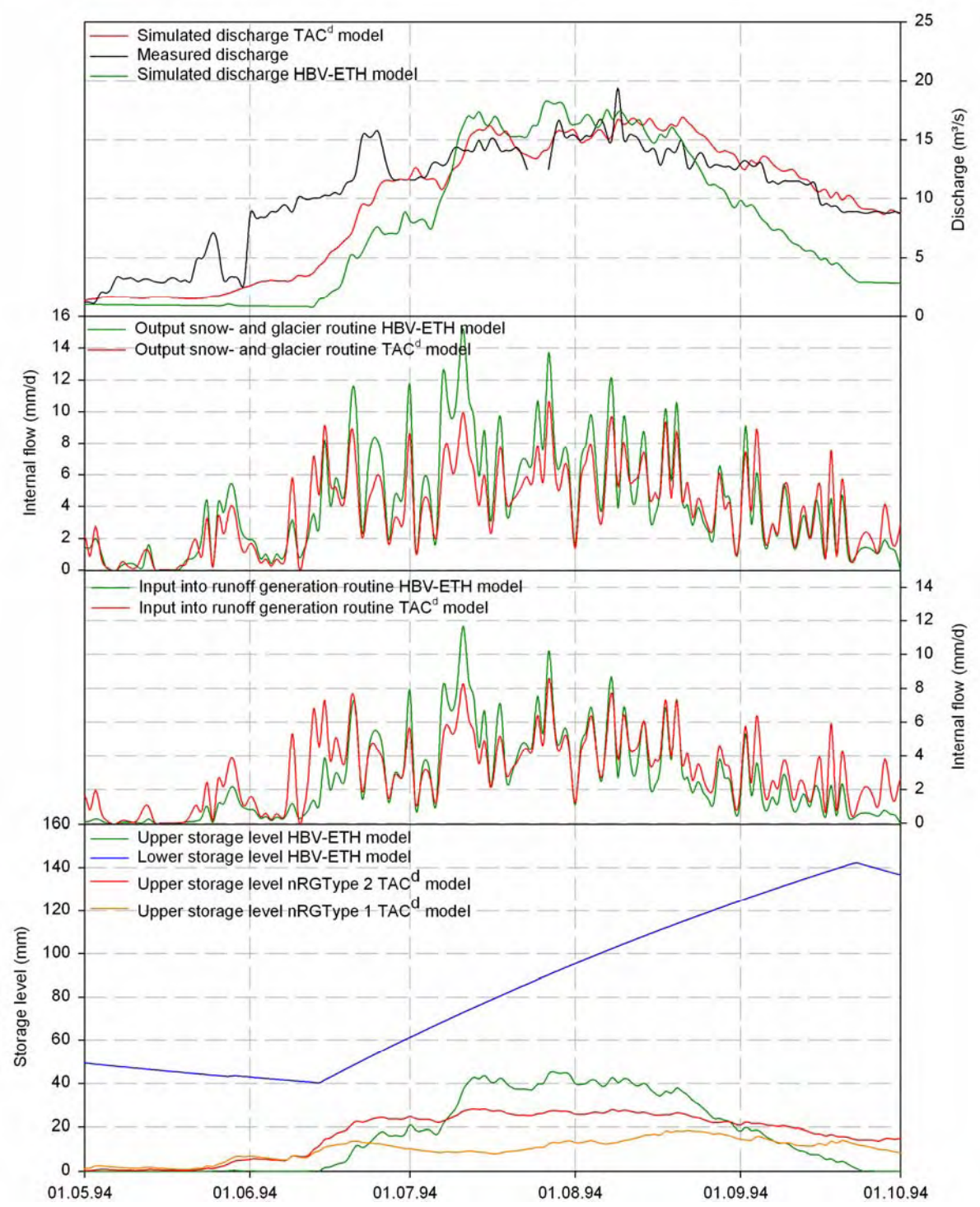

Figure 8.30: Comparison of the HBV-ETH model and the TAC^d model for summer 1994, Langtang Khola catchment

8.9 Conclusions

The model analysis and discussion was conducted using the data of the Langtang Khola catchment. The extrapolation methods for temperature and precipitation data are appropriate tools for bridging gaps in the time series or for redistributing cumulated precipitation sums. The regionalisation of air temperature and precipitation with fixed vertical and horizontal gradients is problematic because the seasonal variation of the gradients is not considered. Precipitation and air temperature measurements are provided at only one station in the catchments for the entire simulation period. Thus, it is not possible to use the advantages of a distributed model to apply sophisticated regionalisation methods for the climatological input data. The introduction of the horizontal gradient, however, enables a more realistic simulation of the basin precipitation. For the calculation of the potential evapotranspiration a simple sinusoidal approach was chosen, which is justified due to the minor importance of evapotranspiration with regard to the annual water balance of high alpine head watersheds.

The main advantage of the temperature-index method, the importance of which cannot be overestimated when working in alpine environments, is that data requirements may be limited to just average daily air temperatures. However, this is also potentially their biggest drawback, as factors other than air temperature control ablation rates. Ablation processes in cases where the air temperature is below the threshold temperature for melting (TT), e.g. sublimation, cannot be treated by the method. The introduction of the correction factor for the degree-day factor (RexpMap) enables the spatial and temporal distributed modelling of snow- and icemelt based on physiographic characteristics of the catchments. The approach seems to give realistic melt rates; for final evaluation, however, aerial photos of the snow cover distribution would still be required. The inclusion of debris-covered glacier surfaces supports the idea of distributed hydrological modelling and the parameter which controls melting over debris-covered glaciers turns out to be highly sensitive.

Mapped river networks of glacierized catchments generally end up at the glacier tongues and have to be extended to include subglacial drainage networks. This brought the expected improvement of the discharge simulation with TAC^d.

Inner annual distribution of water with spatial distributed storage concepts gives good simulation results as expressed by the objective evaluation criteria. However, the simulation of the onset of discharge at the beginning of the monsoon period is not satisfactory. Simple conceptual storage approaches to describe the hydrological situation of the Himalayan catchments can be considered as sufficient for the simulation of the runoff generation. The comparison with the HBV-ETH model in particular justifies the conceptualisation of the runoff generation routine of TAC^d. However, detailed experimental analyses of the discharge composition, especially of the low flow season, are essential for the evaluation of the conceptualisation of the runoff generation routine.

Spatial and temporal resolution of 200 x 200 m² and daily time steps causes a delay of the fast runoff components. The lowering of the time step from daily to hourly intervals is not possible because measurements are available only in daily resolution. A smaller spatial resolution would improve the simulation of fast runoff components. This is, however, problematic for the simulation of snow- and icemelt because detailed physiographic information gets lost with a smaller spatial resolution. Meltwater is an important component of the water balance and thus it is necessary to simulate these processes in as detailed a way as possible. Calibration of the snow and glacier routine was improved by using a multi-criteria calibration.

9 Final remarks and recommendations

Satisfactory simulation results of daily discharge could be achieved using the modified version of TAC^d and the HBV-ETH model in the highly glacierized Langtang Khola and Imja Khola catchments. The application of the models to the Modi Khola catchment is an example of the way in which hydrological models can be used in areas where the data base is poor. The models further reproduce some basic glaciological features such as the annual glacier mass balance. Calibrated rainfall-runoff models can give good estimates of discharge even if either spatial distribution of precipitation or melt processes are poorly simulated. Errors related to parameter uncertainties can be compensated for, especially when meltwater of glaciers is an additional input to the model beside precipitation. Additional glacier mass balance measurements enable a multi-criteria calibration which helps to improve the calibration of the snow and glacier routine and of parameters controlling regionalisation of climatic data. The simple conceptualisation of the routines of TAC^d and HBV-ETH require a rather modest amount of input data and the models can therefore be applied to Himalayan headwater catchments. A snow- and icemelt routine can be simple, due to the implicit information content of air temperature in the surface layer for the computation of the seasonal course of snowpack (Zappa, 2003). The robustness of the temperature-index method is the most important factor related to the quality of input data. Hydrological processes, especially melt processes, in alpine catchments are strongly varied, spatially and temporally. A distributed simulation of snow- and icemelt is therefore necessary and can be achieved by incorporating potential sunshine duration without any further input data other than information derived from digital elevation models. Within the scope of this work, a detailed evaluation of the snow and glacier routine was not possible and must be the subject of future investigation. The conceptualisation of the runoff generation routine is kept as simple as possible and it is designed to represent exclusively the most important runoff generation processes. Given the simplicity of the model structure and its effectiveness for discharge and glacier mass balance simulations, the models offer a useful tool for water resources management in remote high alpine regions. The models can further be used for quality checks of measured input data (precipitation and air temperature) as both models are highly sensitive to these data, and errors can be detected from simulation results.

The models do not account for seasonal variations of the subglacial drainage system. This evolution of the internal drainage system can be assumed to have a notable influence on discharge. Schaefli et al. (2005) suggest investigations of the time dependency of parameters of the snow and glacier routine, considering potential links between the parameters and climate variables. In that context, not only the fluctuations in hydraulic conditions of subglacial drainage systems must be considered, but also the fact that changing storage capacities of glaciers are crucial for a realistic discharge simulation, as revealed by the simulation results from the early simulation period. Detailed experimental investigations of runoff composition in both monsoon and winter seasons is necessary to verify the conceptualisation of the runoff generation routine of the distributed TAC^d model. If water is actually stored in the glacier tongues during the monsoon season, as the current conceptualisation implies, then the retreat of glaciers will have impacts on the hydrological cycle in two ways:

- Less meltwater can be produced during the monsoon season due to declining ice surfaces.
- Less water can be stored in the glacier tongues due to declining storage capacities and, as a result, winter discharge is remarkably reduced.

The authors consider research on the following topics, beside those already mentioned, to be most important for the further development of hydrological models in order to provide tools for a reliable water resources management of high Himalayan headwater catchments:

- Volumes of glacier tongues need to be investigated via aerial photography and geodetic measurements combined with geophysical measurements (e.g. ground radar or seismic) to determine the storage capacities.
- Even sporadic glacier mass balance measurements and snow surveys are very helpful for further calibration of model parameters.
- Detailed observations of avalanche activity during the monsoon and winter seasons would be helpful for estimating their impact on meltwater production at lower altitudes. Again aerial photography could be used to determine the spatial distribution of avalanche cones.
- Delineation of debris-covered glaciers from debris-covered moraines, e.g. by means of thermal images.
- Estimation of sublimation amounts at high altitudes via measurements of the terms of the energy balance at elevations where air temperature is below 0°C all year round.
- Estimation of ablation rates through wind erosion via parallel measurements of snow accumulation (e.g. by ultra-sonic devices) and wind speed at exposed ridges.

These investigations are necessary to gain confidence in model results so that the models can be used for studying the impacts of climate change on regional water resources. For sustainable water resources management, hydrological investigations need to be coupled with socio-economic studies to develop a comprehensive plan of action for managing the effects of global change in these climatically and hydrologically highly sensitive regions.

Appendix

Table A1: Missing data at the SGHU station in the Langtang Khola catchment

Hydrological year	Air temperature			Precipitation			Stage (water level)		
1987/88	Oct.:	14	days	Nov.:	30	days	Oct.:	2	days
	Nov.:	30	days				Nov.:	1	day
	Dec.:	7	days				Dec.:	2	days
	Jan.:	2	days				Mar.:	8	days
	Mar.:	2	days				May:	1	day
	June:	2	days				June:	1	day
	July:	2	days				July:	1	day
	Aug.:	1	day				Aug.:	1	day
							Sept.:	1	day
Sum		**60**	**days**		**30**	**days**		**18**	**days**
1988/89	Jan.:	1	day		0	days	Oct.:	7	days
	Mar.:	1	day				Nov.:	1	day
	Apr.:	2	days				Dec.:	2	days
							Jan.:	13	days
							Feb.:	8	days
							Mar.:	1	day
							Apr.:	17	day
							June:	13	day
							July:	6	days
							Aug.:	7	days
							Sept.:	5	days
Sum		**4**	**days**		**0**	**days**		**80**	**days**
1989/90		0	days	Dec.:	31	days	Oct.:	3	days
				July:	30	days	Nov.:	8	day
							Dec.:	5	days
							Jan.:	17	days
							July:	7	days
Sum		**0**	**days**		**61**	**days**		**40**	**days**
1990/91	Jan.:	2	day	Jan.:	31	days	Nov.:	1	day
				Feb.:	28	days	Dec.:	2	days
				Mar.:	30	days	Apr.:	5	days
				June:	3	days	May:	12	days
				Aug.:	3	days	June:	6	days
				Sept.:	27	days	July:	5	days
							Aug.:	4	days
							Sept.:	26	days
Sum		**2**	**day**		**122**	**days**		**61**	**days**
1991/92	Dec.:	21	days	Oct.:	2	days	Oct.:	3	days
				Nov.:	1	day	Nov.:	5	days
				July:	2	days	Dec.:	7	days
				Aug.:	1	day	Jan.:	10	days
							Feb.:	6	days
Sum		**21**	**days**		**6**	**days**		**31**	**days**
1992/93		0	days	Sept.:	1	day	Jan.:	3	days
							Feb.:	1	day
							Mar.:	2	days
							Apr.:	2	days
							May:	4	days
							June:	1	days
							July:	3	days
							Sept.:	7	days
Sum		**0**	**days**		**1**	**day**		**23**	**days**
1993/94		0	days	Feb.:	1	day	Oct.:	7	days
				July:	28	days	Feb.:	3	days
				Aug.:	1	day	Apr.:	2	days
							June:	1	day
							July:	3	days
Sum		**0**	**days**		**30**	**days**		**16**	**days**
1994/95		0	days	Oct.:	31	days	Feb.:	1	day
				Nov.:	30	days	Mar.:	1	day
				Dec.:	31	days	Apr.:	1	day
Sum		**0**	**days**		**92**	**days**		**3**	**days**

1995/96	Feb.:	1	day		0	days	Feb.:	2	days
							Apr.:	1	day
							June:	6	days
							July:	3	days
							Aug.:	6	days
							Sept.:	2	days
Sum		**1**	**day**		**0**	**days**		**20**	**days**
1996/97	Sept.:	3	days		0	days	Oct.:	4	days
							Nov.:	1	day
							Jan.:	2	days
							Feb.:	6	days
							Mar.:	3	days
							Apr.:	4	days
							May:	3	day
							June:	6	days
							July:	1	day
							Aug.:	2	days
							Sept.:	2	days
Sum		**3**	**days**		**0**	**days**		**34**	**days**
1997/98	Jan.:	1	day	Feb.:	1	day	Oct.:	5	days
	Aug.:	3	days				Nov.:	2	days
							Dec.:	21	days
							Jan.:	2	days
							Feb.:	1	day
							Mar.:	8	days
							Apr.:	2	days
							May:	13	days
							June:	8	days
							July:	2	days
							Aug.:	8	days
							Sept.:	4	days
Sum		**4**	**days**		**1**	**day**		**76**	**days**
1998/99	Dec.:	3	days		0	days	Jan.:	31	days
	May :	4	days				Feb.:	28	days
	July:	2	days				Mar.:	31	days
							Apr.:	30	days
							May:	31	days
							June:	30	days
							July:	31	days
							Aug.:	31	days
							Sept.:	30	days
							Oct.:	7	days
							Dec.:	1	day
Sum		**9**	**days**		**0**	**days**		**281**	**days**
1999/00	Oct.:	2	days	Feb.:	1	day	Jan.:	31	days
	Feb.:	1	day	July:	5	days	Feb.:	28	days
	July:	2	days				Mar.:	31	days
	Aug.:	1	day				Apr.:	30	days
							May:	31	days
							June:	30	days
							July:	31	days
							Aug.:	31	days
							Sept.:	30	days
							Oct.:	31	days
							Nov.:	30	days
							Dec.:	31	days
Sum		**6**	**days**		**6**	**days**		**365**	**days**

Table A2**:** Missing data at the SGHU station in the Modi Khola catchment

Hydrological year	Air temperature			Precipitation			Stage (water level)		
1991/92	Nov.:	2	days	Oct.:	24	days	Dec.:	12	days
				Nov.:	30	days	Jan.:	31	days
				Dec.:	31	days	Feb.:	29	days
				Mar.:	21	days	Mar.:	31	days
				Apr.:	19	days	Apr.:	30	days
				May.:	27	days	May.:	31	days
				June:	16	days	June:	7	days
							July:	14	days
							Aug.:	19	days
							Sept.:	3	days
Sum		**2**	**days**		**168**	**days**		**207**	**days**
1992/93	Jan.:	1	day	Mar.:	17	days	Oct.:	17	days
	Aug.:	2	days	Apr.:	11	days	Nov.:	9	days
				June:	9	days	Dec.:	16	days
				July:	16	days	Jan.:	31	days
				Aug.:	4	days	Feb.:	18	days
				Sept.:	4	days	Mar.:	19	days
							Apr.:	30	days
							May.:	31	days
							June:	30	days
							July:	19	days
							Sept.:	3	days
Sum		**3**	**days**		**61**	**days**		**223**	**days**
1993/94	Dec.:	2	days	Oct.:	1	day	Oct.:	31	days
	Jan.:	2	days	Nov.:	10	days	Nov.:	26	days
				Dec.:	31	days	Dec.:	6	days
				May.:	8	days	Jan.:	1	day
				June:	5	days	Feb.:	27	days
				July:	9	days	Mar.:	31	days
							Apr.:	29	days
							May.:	27	days
							June:	27	days
							July:	26	days
							Aug.:	24	days
							Sept.:	23	days
Sum		**4**	**days**		**64**	**days**		**278**	**days**

Table A3: Missing data at the SGHU station in the Imja Khola catchment

Hydrological year	Air temperature			Precipitation			Stage (water level)		
1987/88	Nov.:	19	days	Nov.:	30	days	Oct.:	13	days
	Jan.:	24	days	Jan.:	31	days	Jan.:	30	days
	Feb.:	15	days				Aug.:	21	days
	May.:	16	days				Sept.:	30	days
	June:	1	day						
	July:	3	days						
	Aug.:	10	days						
	Sept.:	1	day						
Sum		**89**	**days**		**61**	**days**		**94**	**days**
1988/89	Oct.:	1	day	Dec.:	31	days	Oct.:	4	days
	Feb.:	7	days	Jan.:	31	days	Jun.:	6	days
	Mar.:	12	days						
	Apr.:	5	days						
Sum		**25**	**days**		**62**	**days**		**10**	**days**
1989/90	Dec.:	3	days	Dec.:	31	days	Mar.:	1	day
	Mar.:	2	days						
	Apr.:	23	days						
	May.:	31	days						
	June:	30	days						
	July:	12	days						
Sum		**101**	**days**		**31**	**days**		**1**	**day**
1990/91	Oct.:	1	day	Aug.:	4	days		0	days
	Jan.:	12	days	Sept.:	30	days			
	Mar.:	2	days						
	May.:	10	days						
	Sept.:	3	days						
Sum		**28**	**days**		**34**	**days**		**0**	**days**

1991/92	Oct.:	8	days	Oct.:	16	days	Oct.:	12	days
	Nov.:	4	days	Nov.:	12	days	Nov.:	30	days
	Dec.:	2	days				Dec.:	31	days
	Jan.:	5	days						
	Feb.:	9	days						
	Mar.:	3	days						
	Apr.:	10	days						
	May.:	2	days						
	June:	5	days						
	July:	5	days						
	Aug.:	2	days						
	Sept.:	3	days						
Sum		**58**	**days**		**28**	**days**		**73**	**days**
1992/93	Oct.:	7	days	Jan.:	9	days	Jan.:	2	days
	Dec.:	10	days	Feb.:	18	days	Feb.:	28	days
	Aug.:	1	day	Mar.:	24	days	Mar.:	2	days
							Sept.:	30	days
Sum		**18**	**days**		**51**	**days**		**62**	**days**
1993/94	Dec.:	1	day		0	days	Oct.:	31	days
	May.:	1	day				Nov.:	30	days
	June:	2	days				Dec.:	31	days
							Jan.:	24	days
Sum		**4**	**days**		**0**	**days**		**116**	**days**
1994/95	June:	1	day		0	days		0	days
Sum		**1**	**day**		**0**	**days**		**0**	**days**
1995/96	Oct.:	12	days	Jan.:	31	days	Jan.:	31	days
	Dec.:	4	days	Feb.:	29	days	Feb.:	28	days
	Feb.:	1	day	Mar.:	31	days	Mar.:	31	days
	Apr.:	1	day	Apr.:	30	days	Apr.:	30	days
	June:	1	day	May.:	31	days	May.:	31	days
	Aug.:	1	day	June:	30	days	Aug.:	31	days
				July:	31	days			
				Aug.:	31	days			
				Sept.:	30	days			
Sum		**20**	**days**		**274**	**days**		**182**	**days**
1996/97	Oct.:	5	days	Oct.:	31	days	Oct.:	1	day
	Nov.:	10	days	Nov.:	30	days	Dec.:	1	day
	Dec.:	1	day	Dec.:	31	days	Jan.:	1	day
				Jan.:	31	days	Mar.:	31	days
				Feb.:	28	days	Apr.:	30	days
				Mar.:	31	days	May.:	31	days
				Apr.:	30	days	July:	1	day
				May.:	31	days	Aug.:	1	day
				June:	30	days			
				Aug.:	1	day			
				Sept.:	3	days			
Sum		**16**	**days**		**277**	**days**		**97**	**days**
1997/98	Apr.:	3	days	Oct.:	31	days	Oct.:	1	day
				Aug.:	31	days	Dec.:	31	days
				Sept.:	30	days	June:	8	days
							July:	31	days
							Aug.:	31	days
							Sept.:	30	days
Sum		**3**	**days**		**92**	**days**		**132**	**days**
1998/99	Nov.:	7	days	Oct.:	31	days	Oct.:	31	days
	Dec.:	31	days	Nov.:	30	days	Nov.:	30	days
	May.:	1	day	Dec.:	31	days	Dec.:	31	days
	June:	13	days	Jan.:	31	days			
	Aug.:	1	day	Feb.:	28	days			
				Mar.:	31	days			
				Apr.:	30	days			
				May.:	31	days			
				June:	30	days			
				July:	31	days			
				Aug.:	31	days			
				Sept.:	30	days			
Sum		**53**	**days**		**365**	**days**		**92**	**days**

Table A4: Optimized parameter set of TAC[d] for the investigated catchments. Red numbers are changed compared to the parameter set of the Langtang Khola catchment

Parameter	Description	Determination	Langtang Khola	Modi Khola	Imja Khola	Unit
Precipitation correction and regionalisation						
PCF	"Precipitation correction factor" for rain	Calibration	1.05	1.05	1.15	(-)
PGrad	Vertical precipitation gradient	Calibration (Externally set from values in the literature)	0.04	0.04	0.04	((%/100m)/100)
PHorizGrad	Horizontal precipitation gradient	Calibration (Externally set from values in the literature)	-0.03	0.0	0.0	((%/1000m)/100)
SFCF	"Snowfall correction factor"	Calibration	1.2	1.2	1.2	(-)
Temperature regionalisation						
TGrad	Vertical temperature gradient	Calibration (Externally set from values in the literature)	-0.5	-0.5	-0.5	(°C/100m)
Potential evaporation calculation and regionalisation						
ETmax	Maximum of potential evapotranspiration	Calibration (Externally set from values in the literature)	2.2	2.2	2.2	(mm/day)
ETGrad	Vertical evapotranspiration gradient	Calibration (Externally set from values in the literature)	-0.01	-0.01	-0.01	((%/100m)/100)
Snow and glacier routine						
TT	Threshold value of temperature for snowfall also general temperature correction	Calibration (Externally set from values in the literature)	-0.2	-0.2	-0.5	(°C)
Cfmax	Degree-day factor	Calibration	7.0	7.0	9.0	(mm/°C day)
CWH	Water holding capacity of snow	Literature (Bergström 1992)	0.1	0.1	0.1	(-)
CFR	Coefficient of refreezing	Literature (Bergström 1992)	0.05	0.05	0.05	(-)
Rexp	Correction factor for cells with maximum potential sunshine duration	Calibration	1.3	1.3	1.3	(-)
Rmult	Multiplicative factor to account for accelerated melt over ice as compared to snow	Calibration	1.4	1.4	1.4	(-)
Rmultd	Reduction factor of glaciermelt over debris-covered parts of the glacier	Calibration (Externally set from values in the literature)	0.3	0.3	0.6	(-)
Soil routine						
LP	Reduction parameter of field capacity	Literature (Menzel 1997)	0.6	0.6	0.6	(-)
Non-glacier area (nRGType 1)						
FC1	Maximum soil moisture storage (field capacity)	Calibration	20	20	20	(mm)
BETA1	Empirical parameter	Calibration	2.0	2.0	2.0	(-)
Glacier area (nRGType 2)						
FC2	Maximum soil moisture storage (field capacity)	Calibration	20	20	20	(mm)
BETA2	Empirical parameter	Calibration	1.5	1.5	1.5	(-)
Glacier area with inclination less 3° and debris cover (nRGType 3)						
FC3	Maximum soil moisture storage (field capacity)	Calibration	40	40	40	(mm)
BETA3	Empirical parameter	Calibration	1.5	1.5	1.5	(-)
Valley bottom with inclination less 8° (nRGType 4)						
FC4	Maximum soil moisture storage (field capacity)	Calibration	120	120	120	(mm)
BETA4	Empirical parameter	Calibration	2.5	2.5	2.5	(-)

Runoff generation routine						
Non-glacier area (nRGType 1)						
US_K1	Storage coefficient of upper storage	Calibration	0.13	0.13	0.13	(1/day)
LS_K1	Storage coefficient of lower storage	Calibration	0.005	0.005	0.005	(1/day)
US_P1	Percolation capacity	Calibration	1	1	1	(mm/day)
US_H1	Limit of upper storage	Calibration	100	100	100	(mm)
Glacier area (nRGType 2)						
US_K2	Storage coefficient of upper storage	Calibration	0.1	0.1	0.1	(1/day)
LS_K2	Storage coefficient of lower storage	Calibration	0.02	0.02	0.02	(1/day)
US_P2	Percolation capacity	Calibration	3	3	3	(mm/day)
US_H2	Limit of upper storage	Calibration	200	200	200	(mm)
Glacier area with inclination less 3° and debris cover (nRGType 3)						
GlacierLS_K	Storage coefficient of glacier storage	Calibration	0.01	0.01	0.01	(1/day)
GlacierLS_H	Limit of glacier storage	Calibration	3000	3000	3000	(mm)
Valley bottom with inclination less 8° (nRGType 4)						
ValleyLS_K	Storage coefficient of valley storage	Calibration	0.01	0.01	0.01	(1/day)
ValleyLS_H	Limit of valley storage	Calibration	1000	1000	1000	(mm)
Routing routine						
MaxBas	Empirical parameter	Set a priori	1	1	1	(-)

Table A5: Optimized parameter set of HBV-ETH model for the investigated catchments. Red numbers are changed compared to the parameter set of the Langtang Khola catchment

Parameter	Description of parameter	Langtang Khola	Modi Khola	Imja Khola	Unit
BETA	Empirical coefficient controlling the outflow from soil moisture	1.0	1.0	1.0	(-)
CMAX	Maximum of degree-day factor	6.0	6.0	7.0	(mm/°C day)
CMIN	Minimum of degree-day factor	2.0	2.0	4.0	(mm/°C day)
CPERC	Percolation capacity into lower zone	1.5	1.5	1.0	(mm/day)
CRFR	Coefficient of refreezing	0.05	0.05	0.05	(-)
CROUTE	Parameter of transformation function	1.0	1.0	1.0	(-)
CWH	Water holding capacity of snow	0.12	0.12	0.12	(-)
ETMAX	Maximum of potential evapotranspiration	2.2	2.2	2.0	(mm/day)
FC	Maximum soil moisture storage, field capacity	50	50	50	(mm)
K0	Storage coefficient of upper storage, fast component	0.2	0.2	0.2	(1/day)
K1	Storage coefficient of upper storage, medium component	0.08	0.08	0.08	(1/day)
K2	Storage coefficient of upper storage, slow component	0.005	0.005	0.005	(1/day)
LP	Limit of potential evapotranspiration	30	30	30	(mm)
LUZ	Limit of upper storage	80	80	80	(mm)
PGRAD	Vertical precipitation gradient	4.0	4.0	4.0	(%/100 m)
RCF	Precipitation correction factor for rain	0.7	1.2	1.3	(-)
REXP	Increasing of snow-, icemelt depending on orientation of the slope	1.2	1.2	1.3	(-)
RMULT	Multiplicative factor to account for accelerated melt over ice as compared to snow	1.3	1.3	1.6	(-)
SCF	Snowfall correction factor	1.24	1.24	1.5	(-)
T0	Threshold value of temperature for snowfall also general temperature correction	0.0	0.0	-0.3	(°C)
TGRAD	Vertical temperature gradient	-0.5	-0.5	-0.5	(°C/100 m)

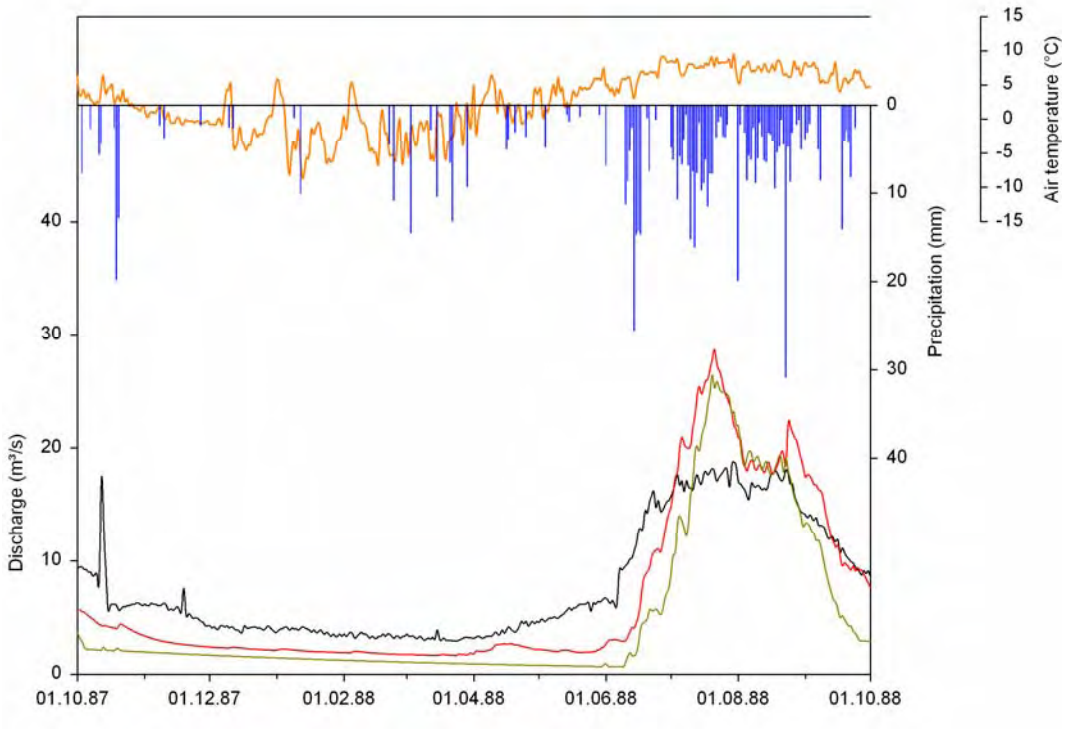

Figure A1-1: Comparison of measured (black) and simulated discharge (red: TAC[d]; green: HBV-ETH) with measured air temperature (orange) at the SGHU station and calculated basin precipitation (blue), Langtang Khola catchment, 1987-1988

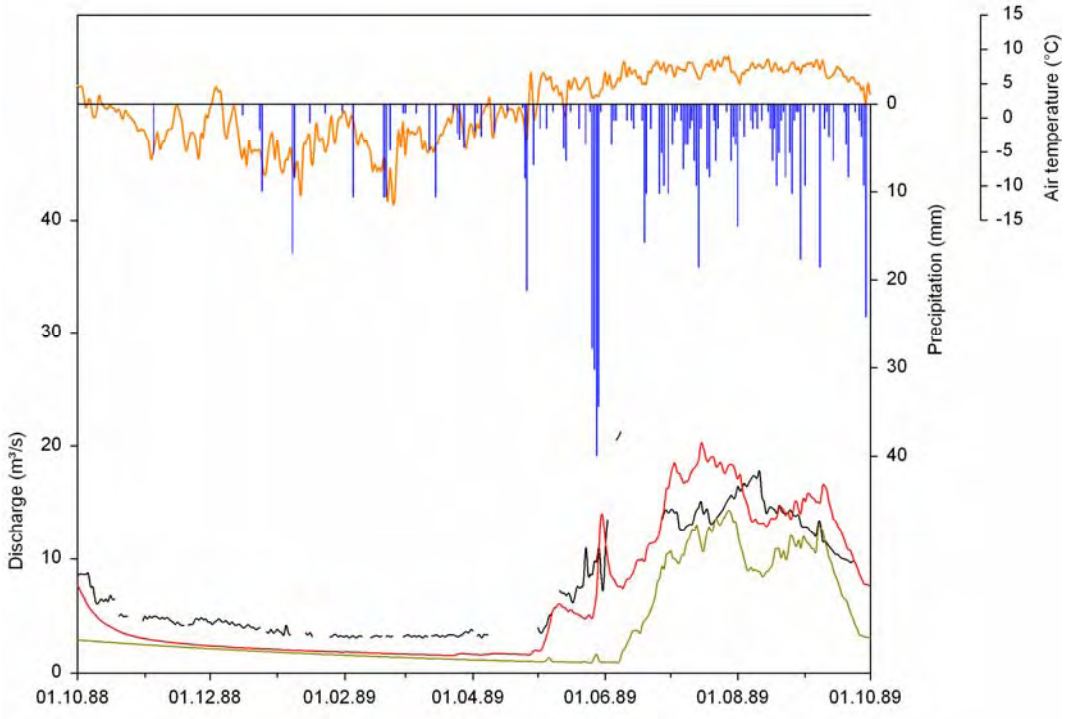

Figure A1-2: Comparison of measured (black) and simulated discharge (red: TAC[d]; green: HBV-ETH) with measured air temperature (orange) at the SGHU station and calculated basin precipitation (blue), Langtang Khola catchment, 1988-1989

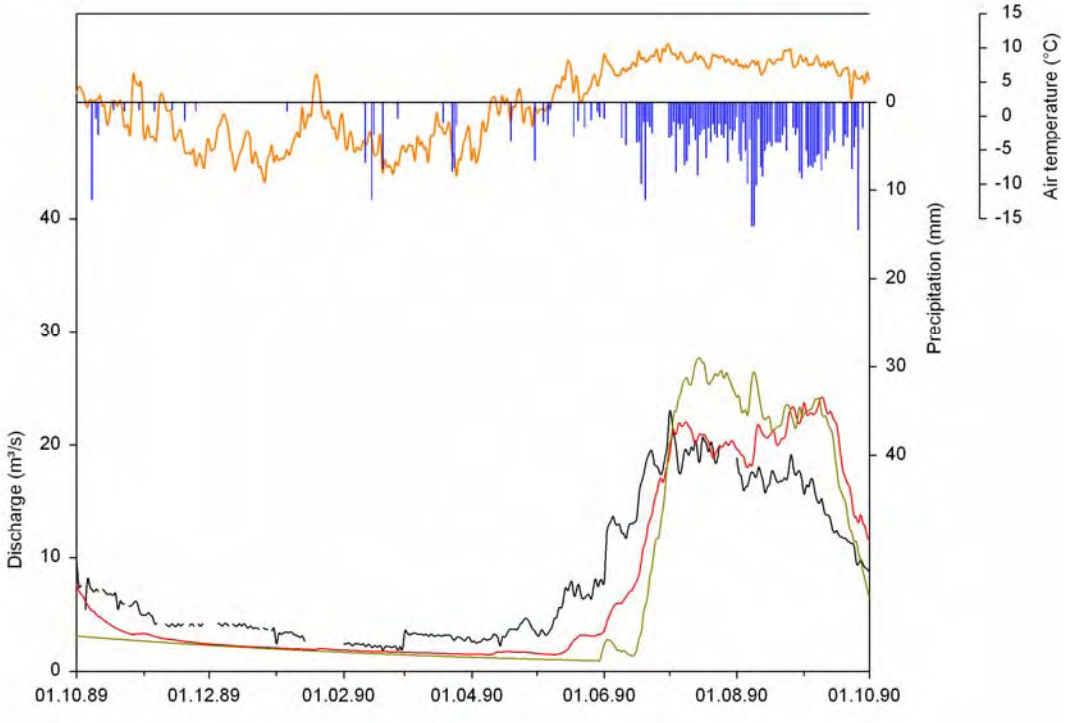

Figure A1-3: Comparison of measured (black) and simulated discharge (red: TAC[d]; green: HBV-ETH) with measured air temperature (orange) at the SGHU station and calculated basin precipitation (blue), Langtang Khola catchment, 1989-1990

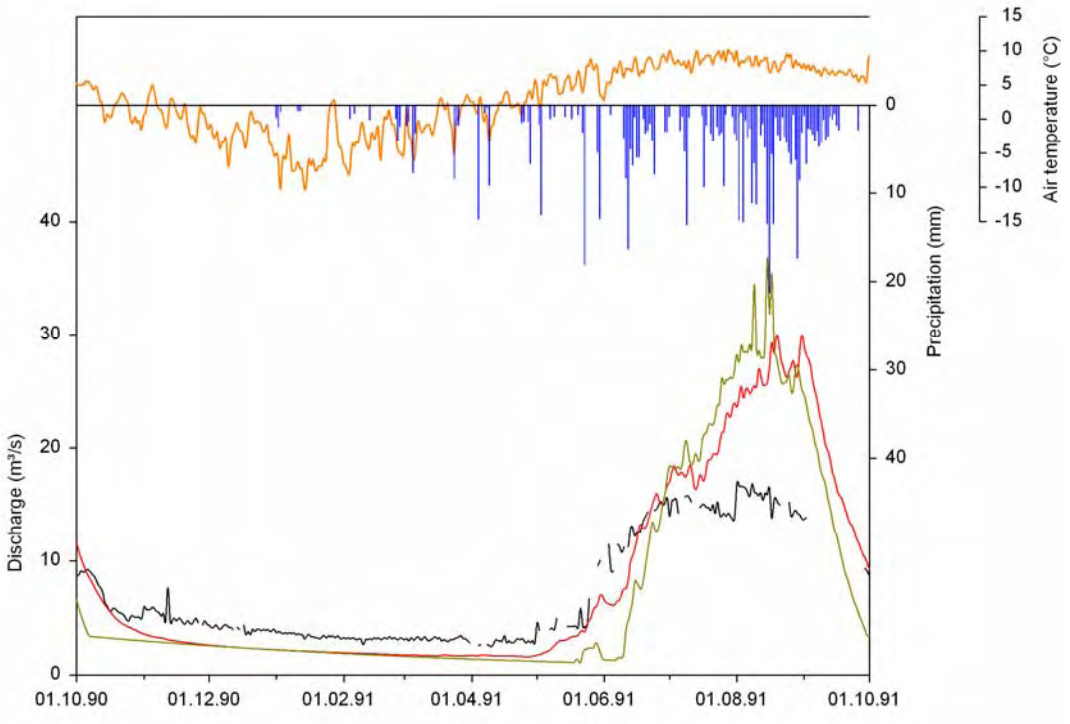

Figure A1-4: Comparison of measured (black) and simulated discharge (red: TAC[d]; green: HBV-ETH) with measured air temperature (orange) at the SGHU station and calculated basin precipitation (blue), Langtang Khola catchment, 1990-1991

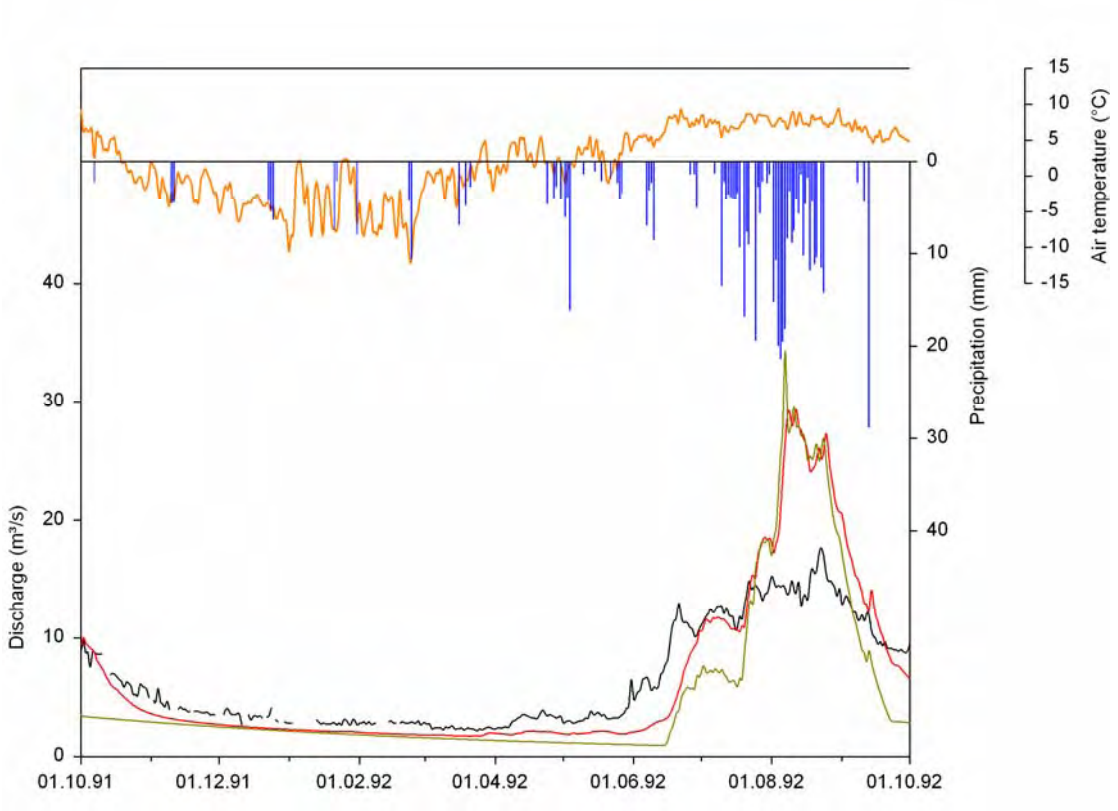

Figure A1-5: Comparison of measured (black) and simulated discharge (red: TAC[d]; green: HBV-ETH) with measured air temperature (orange) at the SGHU station and calculated basin precipitation (blue), Langtang Khola catchment, 1991-1992

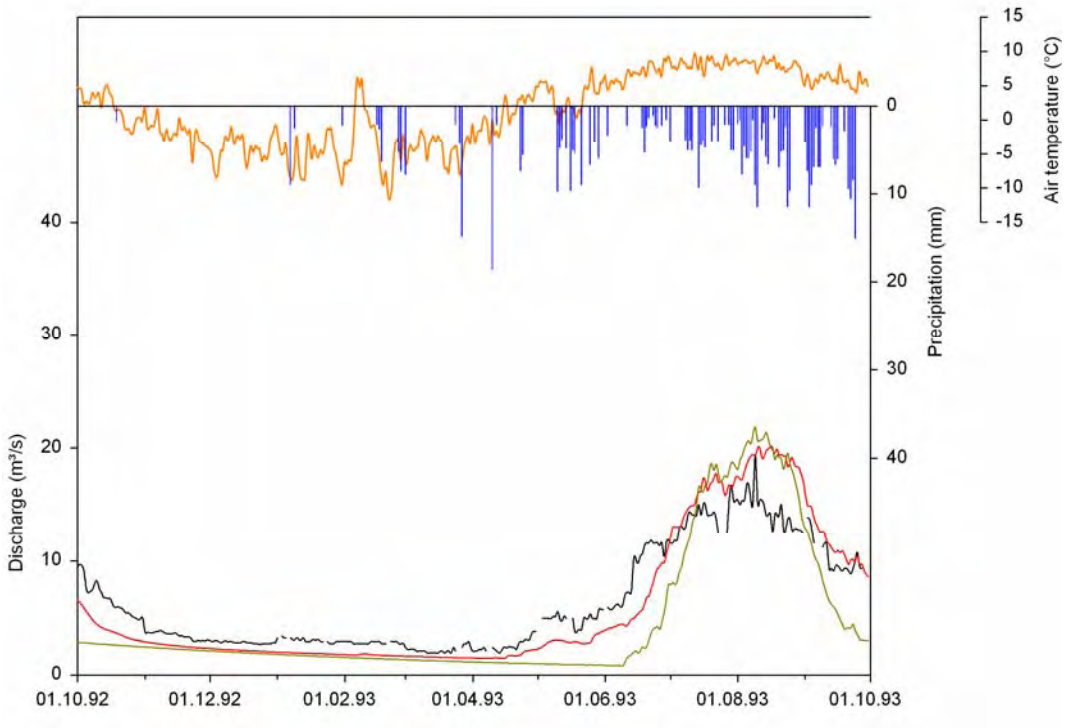

Figure A1-6: Comparison of measured (black) and simulated discharge (red: TAC[d]; green: HBV-ETH) with measured air temperature (orange) at the SGHU station and calculated basin precipitation (blue), Langtang Khola catchment, 1992-1993

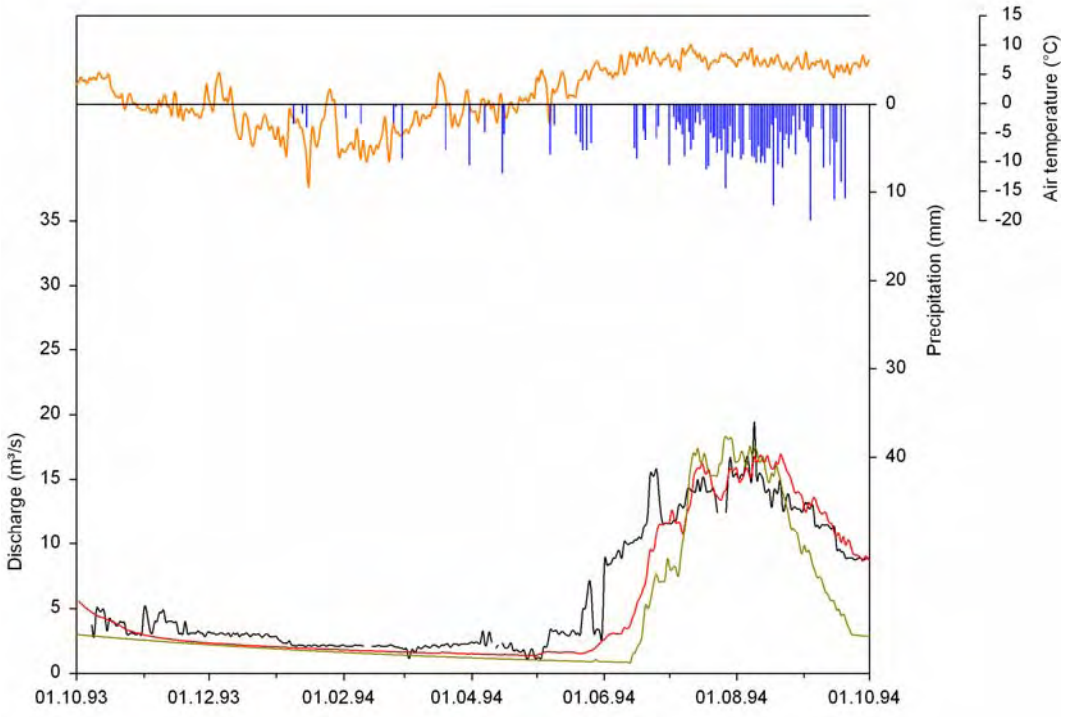

Figure A1-7: Comparison of measured (black) and simulated discharge (red: TAC[d]; green: HBV-ETH) with measured air temperature (orange) at the SGHU station and calculated basin precipitation (blue), Langtang Khola catchment, 1993-1994

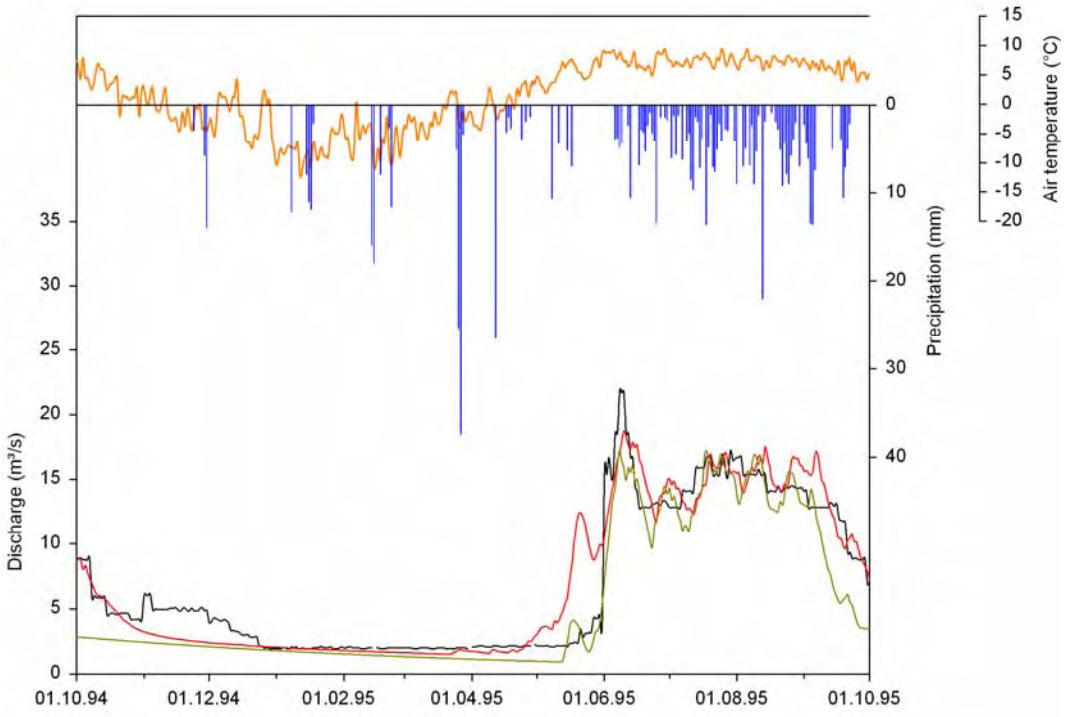

Figure A1-8: Comparison of measured (black) and simulated discharge (red: TAC[d]; green: HBV-ETH) with measured air temperature (orange) at the SGHU station and calculated basin precipitation (blue), Langtang Khola catchment, 1994-1995

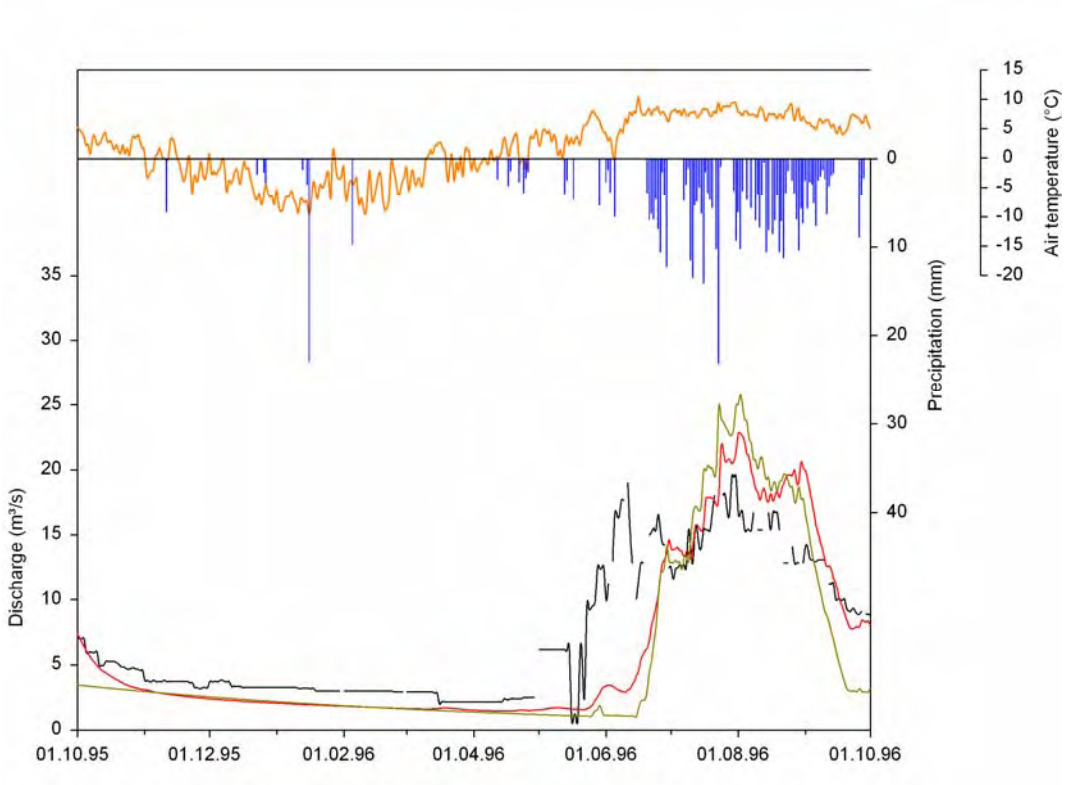

Figure A1-9: Comparison of measured (black) and simulated discharge (red: TAC[d]; green: HBV-ETH) with measured air temperature (orange) at the SGHU station and calculated basin precipitation (blue), Langtang Khola catchment, 1995-1996

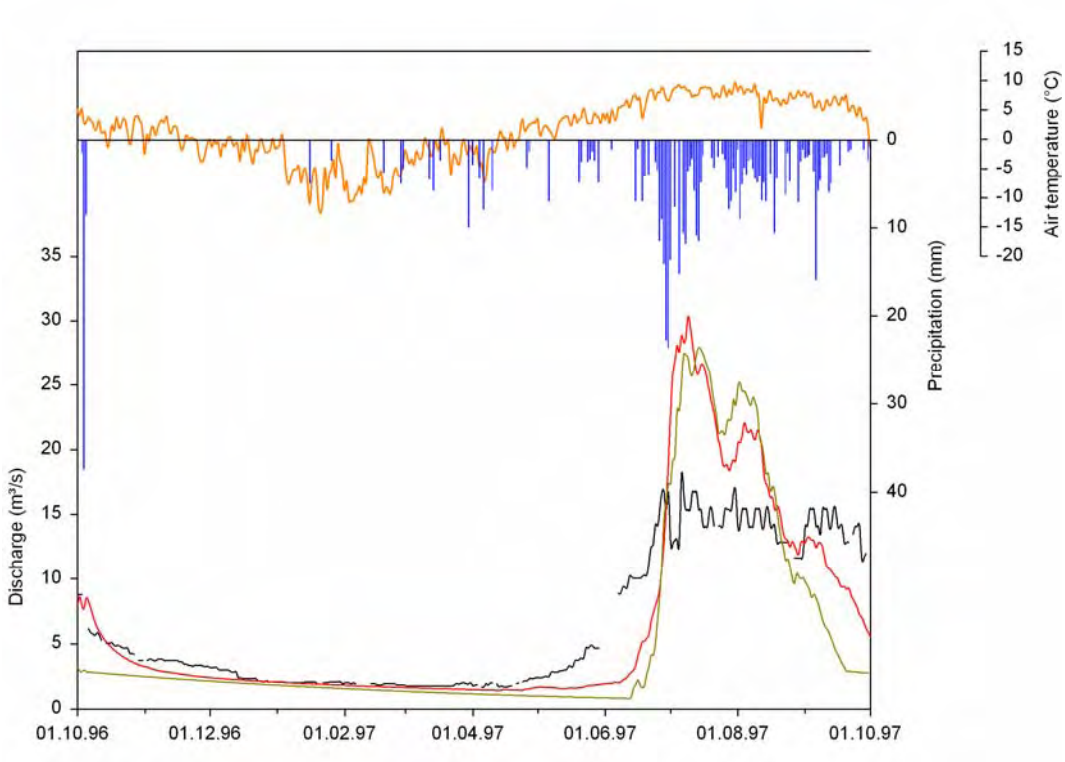

Figure A1-10: Comparison of measured (black) and simulated discharge (red: TAC[d]; green: HBV-ETH) with measured air temperature (orange) at the SGHU station and calculated basin precipitation (blue), Langtang Khola catchment, 1996-1997

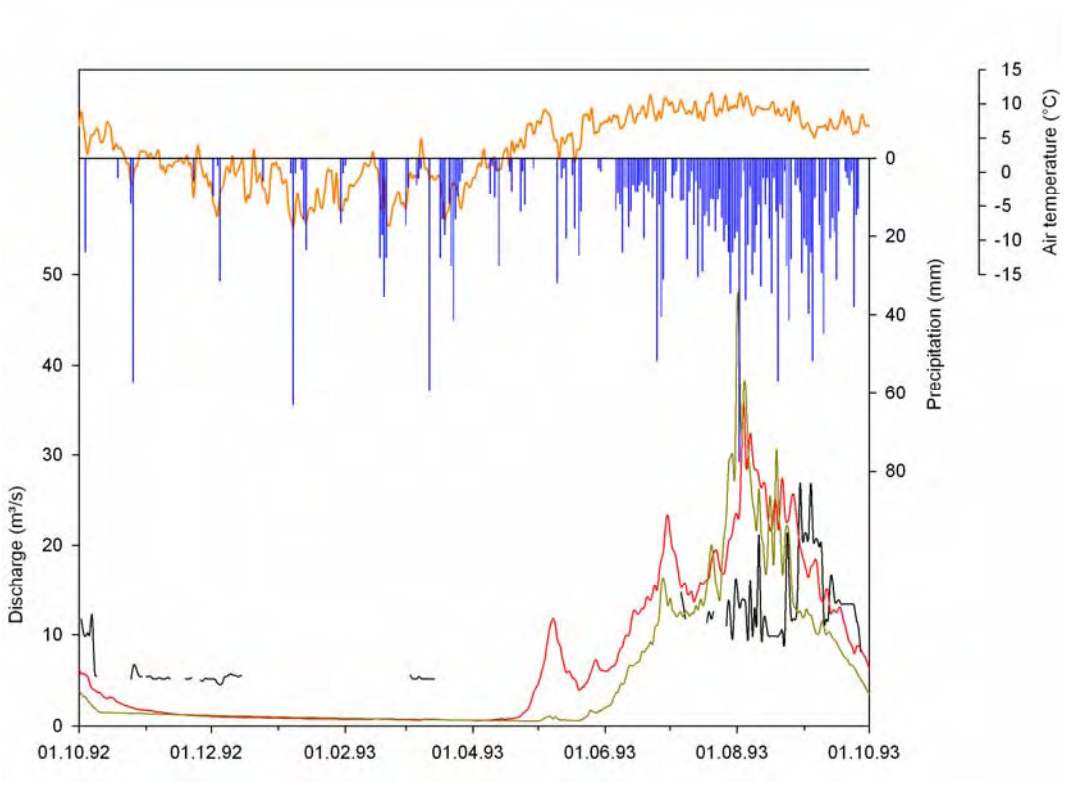

Figure A2-1: Comparison of measured (black) and simulated discharge (red: TAC[d]; green: HBV-ETH) with measured air temperature (orange) at the SGHU station and calculated basin precipitation (blue), Modi Khola catchment, 1992-1993

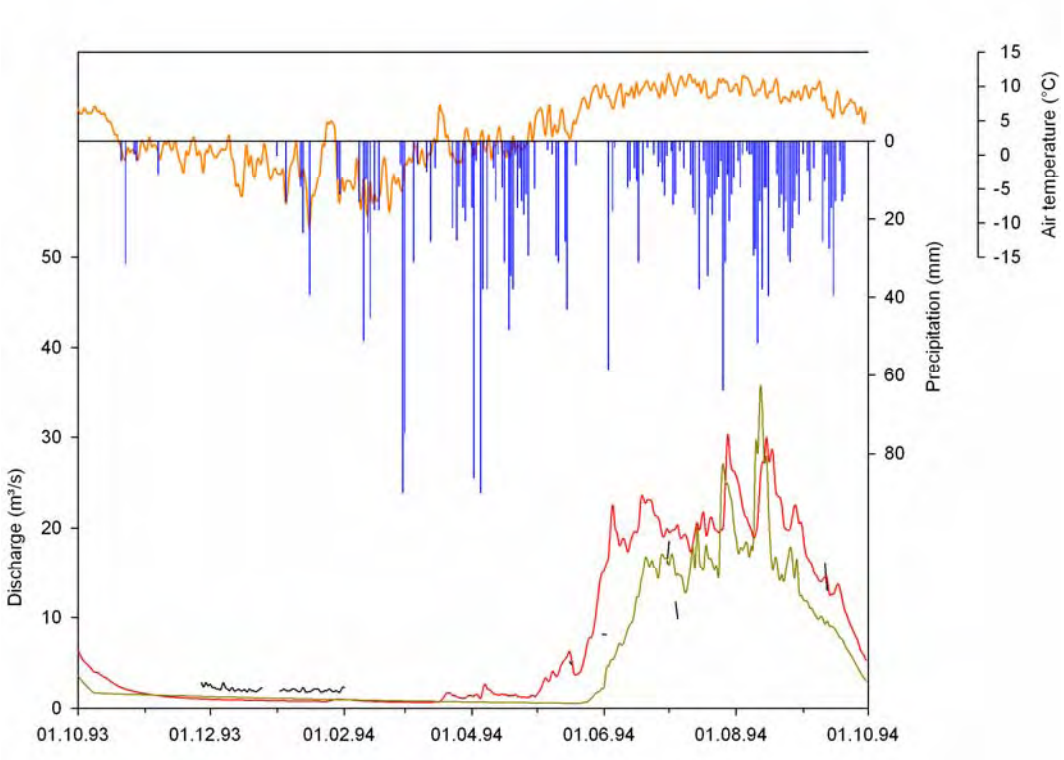

Figure A2-2: Comparison of measured (black) and simulated discharge (red: TAC[d]; green: HBV-ETH) with measured air temperature (orange) at the SGHU station and calculated basin precipitation (blue), Modi Khola catchment, 1993-1994

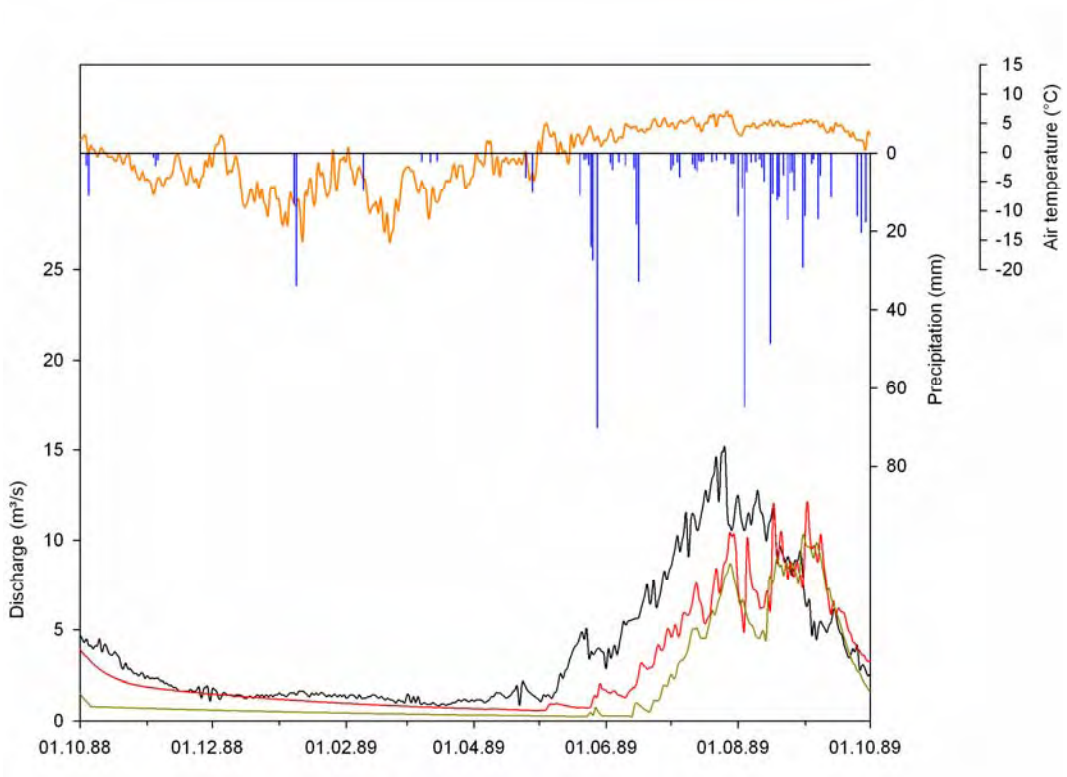

Figure A3-1: Comparison of measured (black) and simulated discharge (red: TAC[d]; green: HBV-ETH) with measured air temperature (orange) at the SGHU station and calculated basin precipitation (blue), Imja Khola catchment, 1988-1989

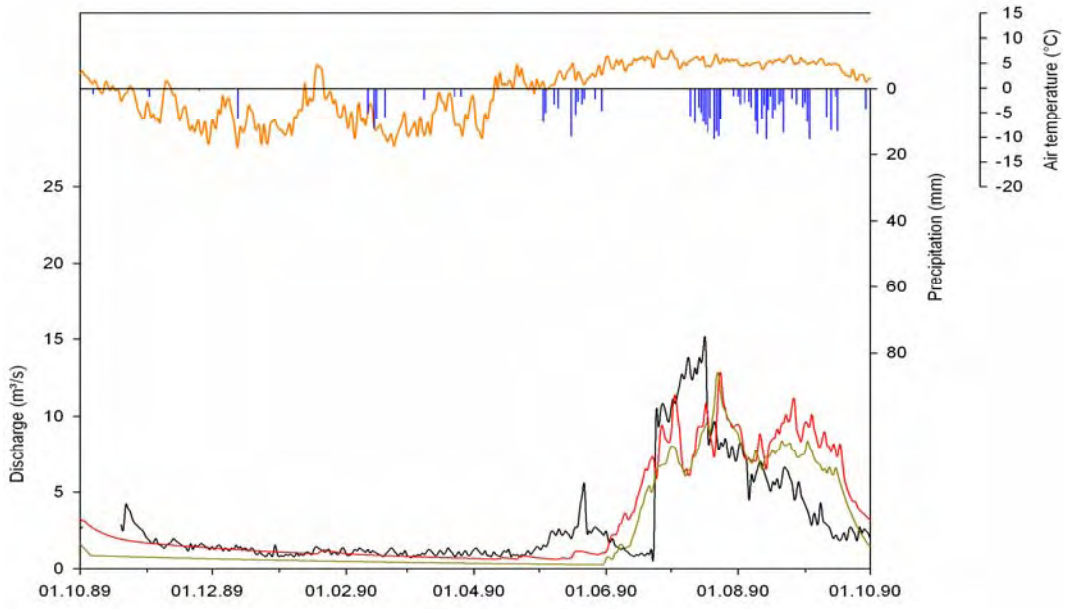

Figure A3-2: Comparison of measured (black) and simulated discharge (red: TAC[d]; green: HBV-ETH) with measured air temperature (orange) at the SGHU station and calculated basin precipitation (blue), Imja Khola catchment, 1989-1990

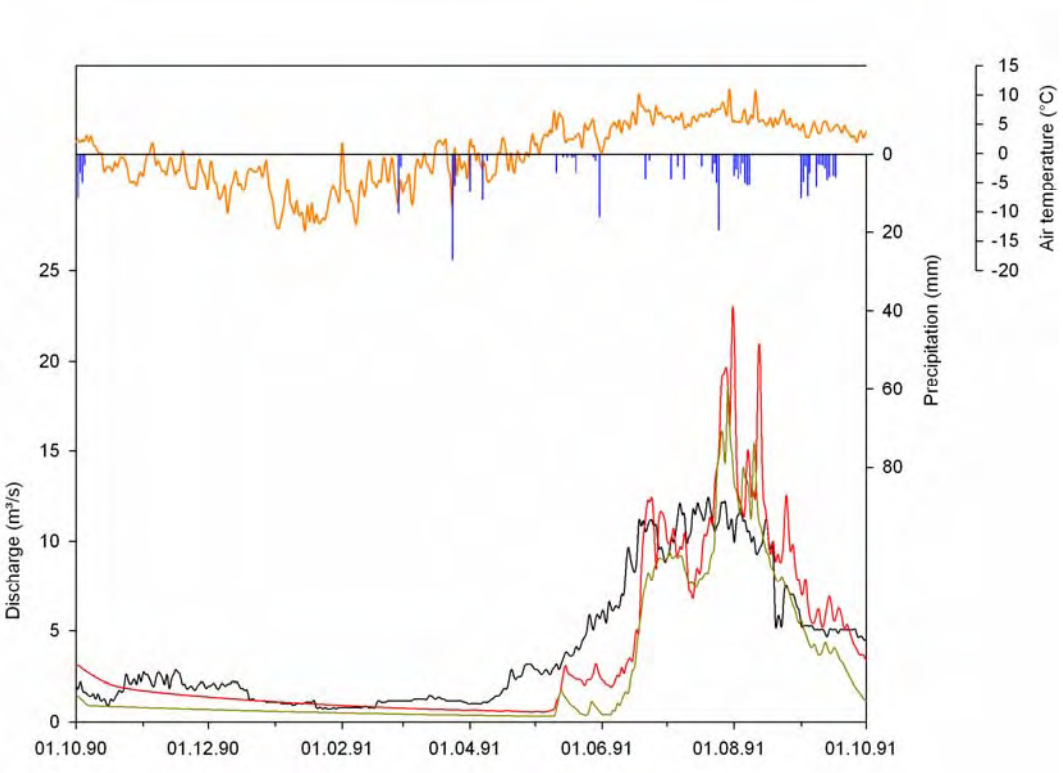

Figure A3-3: Comparison of measured (black) and simulated discharge (red: TAC[d]; green: HBV-ETH) with measured air temperature (orange) at the SGHU station and calculated basin precipitation (blue), Imja Khola catchment, 1990-1991

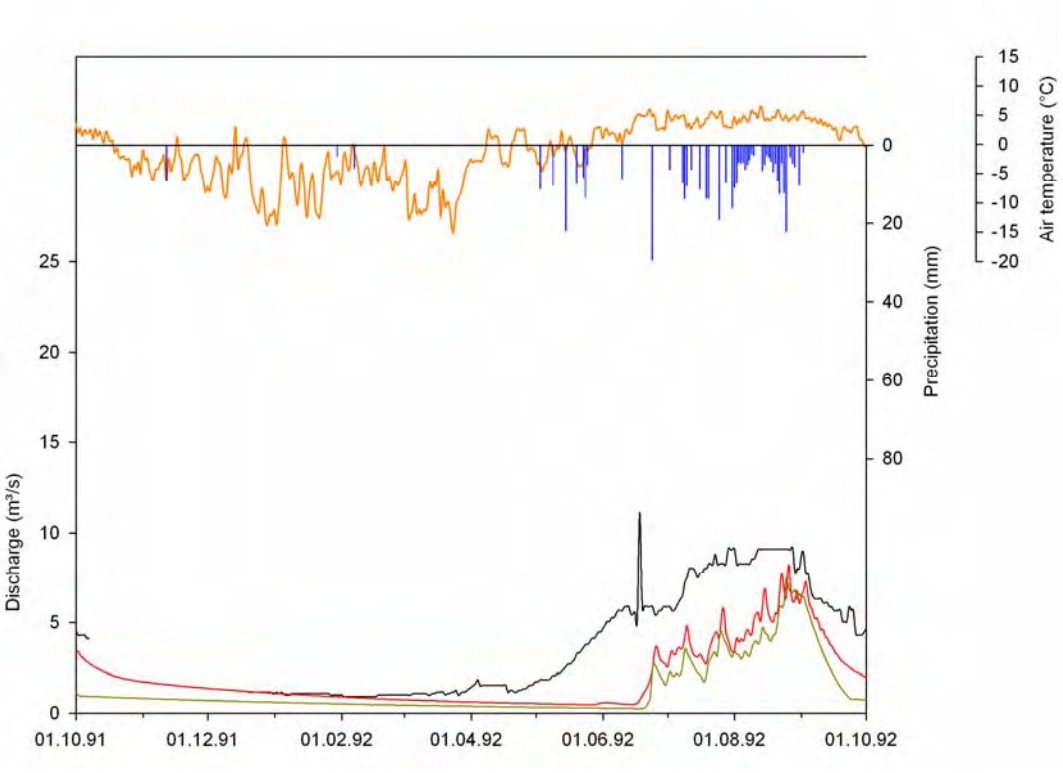

Figure A3-4: Comparison of measured (black) and simulated discharge (red: TAC[d]; green: HBV-ETH) with measured air temperature (orange) at the SGHU station and calculated basin precipitation (blue), Imja Khola catchment, 1991-1992

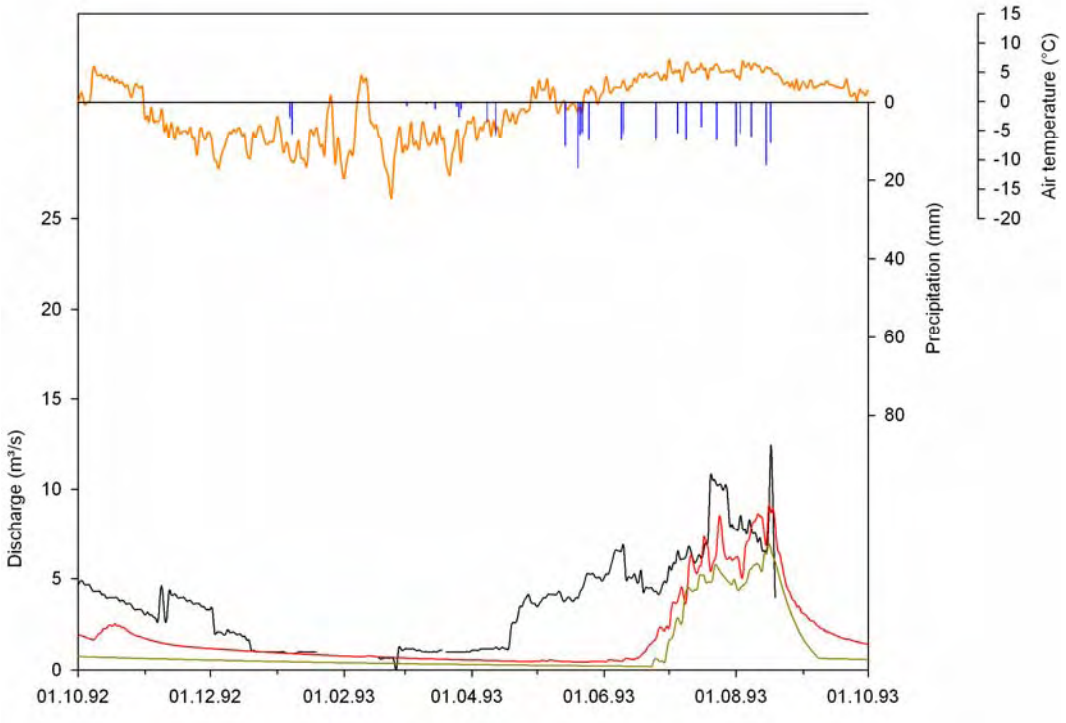

Figure A3-5: Comparison of measured (black) and simulated discharge (red: TAC[d]; green: HBV-ETH) with measured air temperature (orange) at the SGHU station and calculated basin precipitation (blue), Imja Khola catchment, 1992-1993

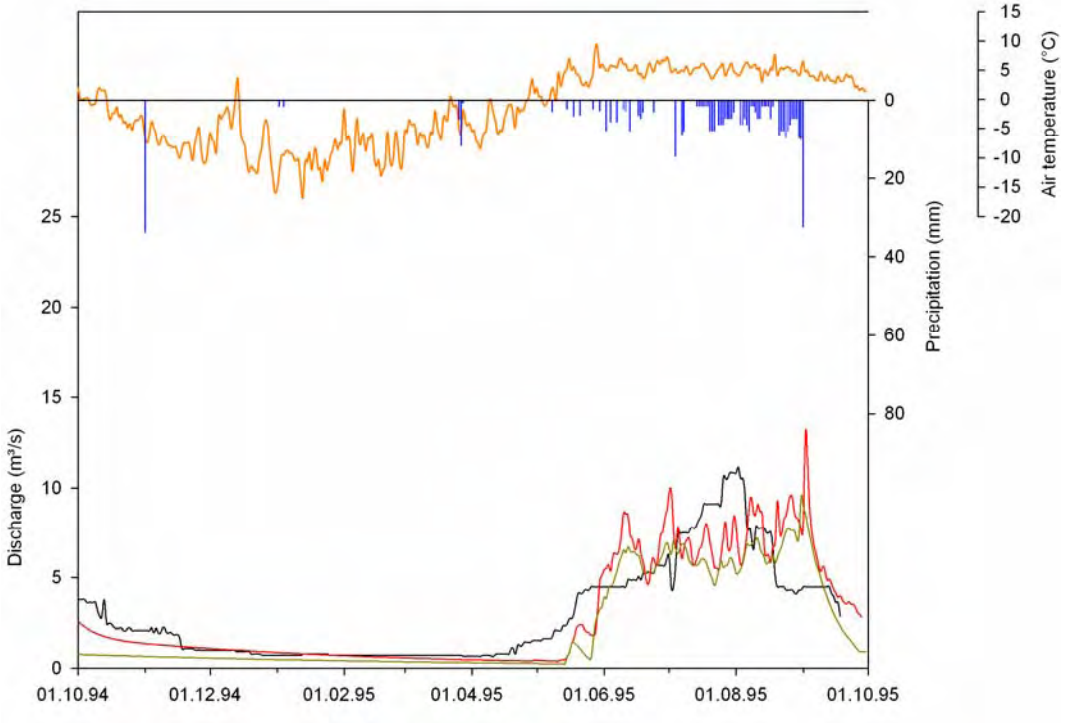

Figure A3-6: Comparison of measured (black) and simulated discharge (red: TAC[d]; green: HBV-ETH) with measured air temperature (orange) at the SGHU station and calculated basin precipitation (blue), Imja Khola catchment, 1994-1995

References

AMBACH, W. (1972): Floods caused by the melting of snow and ice. Piene: Loro previsione e difesa del suolo, Accademia Nazionale Dei Lincei, Quaderno N. 169. 121-136.

ASAHI, K. (1998): Recent glacier fluctuations and their factors of eastern part of Nepal Himalaya. Master thesis, Tokyo Meteropolitan University, 143pp. (In Japanese with English abstract).

BANDYOPADHYAY, J., D. KRAEMER, R. KATTELMANN and Z.W. KUNDZEWIEZ (1997): Highland waters – a resource of global significance. In Mountains of the World: A Global Priority, B. Messerli and J.D. Ives (Eds.), Parthenon, New York and London, 131-155.

BEEK, T. (2004): The further development of the process-based catchment model TAC^d and its application to the H.J. Andrews Experimental Forest, Oregon, USA. Diploma thesis at the Institute of Hydrology, Albert-Ludwigs-University Freiburg, Germany, (unpublished).

BERGSTRÖM, S. (1976): Development and application of a conceptual runoff model for Scandinavian catchments. PhD. Thesis SMHI Reports RH, No. 7, Norrköping.

BERGSTRÖM, S. (1992): The HBV-model - its structure and applications. SMHI Reports RH, No. 4, Norrköping.

BOLLASINA, M., L. BERTOLANI and G. TARTARI, (2002): Meteorological observations at high altitude in the Khumbu valley, Nepal Himalayas, 1994-1999. Bulletin of Glacier Research, 19, 1-11.

BRAUN, L.N. (1985): Simulation of snow melt-runoff in lowland and lower alpine regions of Switzerland. Züricher Geographische Schriften 21, Geographisches Institut ETH, Zurich.

BRAUN, L.N. and M. AELLEN (1990): Modelling discharge of glacierized basins assisted by direct measurements of glacier mass balance. IAHS Publication No.193, 99-106.

BRAUN, L.N. and C.B. RENNER (1992): Application of a conceptual runoff model in different physiographic regions of Switzerland. Hydrological Sciences Journal 37, 3, 217-231.

BRAUN, L.N., W. GRABS, W. and B. RANA (1993): Application of a conceptual precipitation runoff model in the Langtang Khola basin, Nepal Himalaya. IAHS Publication No. 218, 221-237.

BRAUN, L.N., Ch. HOTTELET, M. WEBER and W. GRABS (1998): Measurement and simulation of runoff from Nepalese head watersheds. IAHS Publication No. 248, 9-18.

BRAUN, L.N., M. SCHULZ and M. WEBER (2000): Consequences of climate change for runoff from Alpine regions. Annals of Glaciology 31, 19-25.

BRUBAKER, K., A. RANGO and W. KUSTAS (1996): Incorporating radiation inputs into the snowmelt runoff model. Hydrological Processes, 10, 1329-1343.

CAZORZI, F. and D.G. FONTANA (1996): Snowmelt modelling by combining air temperature and a distributed radiation index. Journal of Hydrology, 181, 169-187.

COLEBECK, S.C. (1972): A theory of water percolation in snow. Journal of Glaciology, 11 (63), 369-385.

ESCHER-VETTER, H. (1980): Der Strahlungshaushalt des Vernagtferners als Basis der Energiehaushaltsberechnung zur Bestimmung der Schmelzwasserproduktion eines Alpengletschers. Wissenschaftliche Mitteilungen, Meteorologisches Institut, München, 39.

ESCHER-VETTER, H. (2000): Modelling meltwater production with distributed energy balance method and runoff using a linear reservoir approach - Results from Vernagtferner, Oetztal Alps, for the ablation seasons 1992 to 1995. Zeitschrift für Gletscherkunde und Glazialgeologie, 36, 119-150.

FOX, A. (2003): A distributed, physically based snow melt and runoff model for alpine glaciers. PhD Thesis, St. Catherine' s College.

FUJITA, K., N. TAKEUCHI and K. SEKO (1998): Glaciological observations of Yala Glacier in the Langtang Valley, Nepal Himalayas, 1994 and 1996. Bulletin of Glacier Research, 16, 75-81.

FUJITA, K., F. NAKAZAWA and B. RANA (2001): Glaciological observations on Rikha Samba glacier in Hidden Valley, Nepal Himalayas, 1998 and 1999. Bulletin of Glacier Research, 18, 31-35.

GRABS, W. and A.P. POKHREL (1993): Establishment of a measuring service for snow and glacier hydrology in Nepal – conceptual and operational aspects. IAHS Publication No. 218, 3-16.

GRONOWSKI, T.V. (1992): Die natürliche Grundwasserneubildung in einem urban beeinflussten Einzugsgebiet im Voralpenraum. Züricher Geographische Schriften 50, Geographisches Institut ETH, Zurich.

HAGG, W. (2003): Auswirkungen von Gletscherschwund auf die Wasserspende hochalpiner Gebiete, Vergleich Alpen-Zentralasien. Münchener geographische Abhandlungen, Reihe A, Band A 53, Department für Geo- und Umweltwissenschaften der Universität München, Sektion Geographie.

HEUBERGER, H., L. MASCH, E. PREUSS and A. SCHROCKER (1984):Quaternary landslides and rock fusion in Central Nepal and in the Tyrolean Alps. Mountain Research and Development, 4, 345-362.

HOCK, R. (1998): Modelling of glaciermelt discharge. Züricher Geographische Schriften 70, Geographisches Institut ETH, Zurich.

HOCK, R. (1999): A distributed temperature-index ice- and snowmelt model including potential direct solar radiation. Journal of Glaciology 45 (149), 101-111.

HOCK, R. (2003): Temperature-index melt modelling in mountain areas. Journal of Hydrology 282 (1-4), 104-115.

HOOKE, R. (1989): Englacial and subglacial hydrology: a qualitative review. Arctic and Alpine Research 21 (3), 221-233.

HORMANN, K. (1994): Computer-based Climatological Maps for High Mountain Areas – New Methods and Their Application, with Examples from the Himalayas. ICIMOD, MEM Series No. 12.

HOTTELET, Ch., L.N. BRAUN, Ch. LEIBUNDGUT and A. RIEG (1993): Simulation of Snowpack and Discharge in an Alpine Karst Basin. IAHS Publication No. 218, 249-260.

HOTTELET et al. (1994): Application of the ETH snow model to three basins of different character in central Europe. Nordic Hydrology 25, 113-128.

ICIMOD and UNEP (2002): Inventory of glaciers, glacier lakes and glacier lake outburst floods monitoring and early warning systems in the Hindu Kush – Himalayan region. CD-ROM. ISBN 92 9115 359 1.

IIDA, H., O. WATANABA and M. TAKIKAWA (1984): First results from Himalayan glacier boring project in 1981-1982, Part II. Studies on internal structure and transformation process from snow and ice of Yala Glacier, Langtang Himal, Nepal. Glacial Studies in Langtang Valley, Data Center for Glacial Research, Japanese Society of Snow and Ice. Publication No. 2, 25-34.

JANSSON, P., R. HOCK and T. SCHNEIDER (2002): The concept of glacier storage: a review. Journal of Hydrology 282 (1-4), 116-129.

JOHST M., S. UHLENBROOK, N. TILCH, B. ZILLGENS and R. KIRNBAUER (2005): Process-oriented catchment modelling in an alpine catchment, Loehnersbach, Austria. Submitted to Journal of Nordic Hydrology, in review.

KADOTA, T., N. NAITO and H. CONWAY (2002): Some shrinking features of the uppermost ablation area of the Khumbu glacier, east Nepal, 1995-1999. Bulletin of Glacier Research 19, 37-40.

KAPPENBERGER, G., U. STEINEGGER, L.N. BRAUN and R. KOSTKA (1993): Recent changes in glacier tongues in the Langtang Khola basin, Nepal, determined by terrestrial photogrammetry. IAHS Publication No. 218, 95-101.

KATTELMANN, R. (1993): Role of snowmelt in generating streamflow during spring in east Nepal. IAHS Publication No. 218, 103-111.

KAYASTA, R.B., Y. TAKEUCHI, M. NAKAWO and Y. AGETA (2000): Practical prediction of ice melting beneath various thicknesses of debris cover on Khumbu Glacier, Nepal, using a positive degree-day factor. IAHS Publication No. 264, 71-81.

KOHLER, J. (1995): Determining the extent of pressurized flow beneath Storglaciären, Sweden, using results of tracer experiments and measurements of input and output discharge. Journal of Glaciology 41 (138), 217-231.

KOHSHIMA, S., K. SEKO, Y. YOSHIMURA (1993): Biotic acceleration of glaciermelting in Yala glacier, Langtang region, Nepal Himalaya. IAHS Publication No. 218, 309-316.

KONZ, M. (2003): HBV3-ETH9 User's manual. Internal report Bavarian Academy of Sciences, Commission of Glaciology, Munich.

KRAUS, H. (1966): Das Klima von Nepal. The series Khumbu Himal, Bd.1/4, 301-321.

LANG, H. (1968): Relation between glacier runoff and meteorological factors observed on and outside the glacier. IUGG Ge. Ass. 1967, Berne, IAHS Publication No. 79, 429-439.

LANG, H. (1981): Is evaporation an important component in high alpine hydrology? Nordic Hydrology 12 (4/5), 217-224.

MADER, H. (1992): Observations of the water-vein system in polycrystallinic ice. Journal of Glaciology 38, 333-347.

MALE, D.H. (1980): The seasonal snow cover. In: Colebeck, S.C.: Dynamics of snow and ice masses. Academic Press, New York.

MARTINEC, J. (1989): Hour-to-hour snowmelt rates and lysimeter outflow during an entire ablation period. IAHS Publication No. 183, 19-28.

MENZEL, L. (1997): Modellierung der Evapotranspiration im System Boden-Pflanze-Atmosphäre. Züricher Geographische Schriften 67, Geographisches Institut ETH, Zurich.

MENZIES, J. (2002): Modern & past glacial environments. Butterworth-Heinemann Ltd., Oxford.

MORIBAYASHI, S. (1974): On the characteristics of Nepal Himalayan glaciers and their recent variation, Seppyo 36, 11-21. (In Japanese with English abstract).

MOSER, H., H. ESCHER-VETTER, H. OERTER, O. REINWARTH and D. ZUNKE (1986): Abfluss in und von Gletschern. GSF-Bericht 41/86, Teil 1.

MOTOYAMA, H., T. OHTA and T. YAMADA (1987): Winter runoff in the glacialized drainage basin in Langtang Valley, Nepal Himalayas. Bulletin of Glacier Research 5, 29-33.

MOTOYAMA, H. and T. YAMADA (1989): Hydrological observations in the Langtang Valley, Nepal Himalayas during 1987 monsoon – postmonsoon season. Bulletin of Glacier Research 7, 195-201.

NAITO, N., T. KADOTA, K. FUJITA, A. SAKAI and M. NAKAWO (2002): Surface lowering over the ablation area of Lirung glacier, Nepal Himalayas. Bulletin of Glacier Research 19, 41-46.

NAKAWO, M. and G.J. YOUNG (1981): Field experiments to determine the effect of a debris layer on ablation of glacier ice. Annals of Glaciology 2, 85-91.

NAKAWO, M. and S. TAKAHASHI (1982): A simplified model for estimating glacier ablation under a debris layer. IAHS Publication No. 138, 137-145.

NAKAWO, M., K. FUJITA, Y. AGETA, K. SHANKAR, A.P. PHOKREL and T. YAO (1997): Basic studies for assessing the impacts of global warming on the Himalayan cryosphere, 1994-1996. Bulletin of Glacier Research 10, 1-10.

NASH, J.E. and J.V. SUTCLIFFE (1970): River flow forecasting through conceptual models, Part I – a discussion of principles. Journal of Hydrology 10, 282-290.

NESJE, A. and S.O. DAHL (2000): Glaciers and environmental change. Oxford University Press Inc., New York.

NYE, J.F. (1976): Water flow in glaciers; Jökulhlaups, tunnels and veins. Journal of Glaciology 17, 181-201.

OHMURA, A. (2001): Physical basis for the temperature-based melt-index method. Journal of Applied Meteorology 40, 753-761.

ONO, Y. (1986): Glacial fluctuations in the Langtang Valley, Nepal Himalaya. Göttinger Geographische Abhandlungen 81, 31-38.

ÖSTLING, M. and R. HOOKE (1986): Water storage in Storglaciären, Kebnekaise, Sweden. Geografiska Annaler 68A (4), 279-290.

OTT, B. (2002): Weiterentwicklung des Einzugsgebietsmodells TAC^{d} und Anwendung im Dreisameinzugsgebiet. Diploma thesis at the Institute of Hydrology, Albert-Ludwigs-University Freiburg, Germany (unpublished).

OTT B. and S. UHLENBROOK (2004): Quantifying the impact of land use changes at the event and seasonal time scale using a process-oriented catchment model. Hydrology and Earth System Science, 8(1), 62-78.

PATERSON, W.S.B. (1969): The physics of glaciers. 1st edition. Pergamon Press, Oxford.

PATERSON, W.S.B. (1994): The physics of glaciers. 4th edition. Pergamon Press, Oxford.

PCRaster (2004): Faculty of Geosciences, Utrecht University, The Netherlands. Internet: URL: http://www.pcraster.geog.uu.nl/.

POPOVNIN, V.V. and A.V. ROZOVA (2002): Influence of sub-debris thawing on ablation and runoff of the Djankuat glacier in the Caucasus. Nordic Hydrology 33 (1), 75-94.

RAMAGE, C.S. (1971): Monsoon meteorology. Academic Press.

RANA, B., M. NAKAWO, Y. FUKUSHIMA and Y. AGETA (1996): Runoff modelling of a river basin with a debris-covered glacier in Langtang Valley, Nepal Himalaya. Bulletin of Glacier Research 14, 1-6.

RANA, B., M. NAKAWO, Y. FUKUSHIMA and Y. AGETA (1997): Application of a conceptual precipitation-runoff model (HYCYMODEL) in a debris-covered glacierized basin in the Langtang Valles, Nepal Himalayas. Annals of Glaciology 25, 226-231.

RANGO, A. (1992): Worldwide testing of the snowmelt runoff model with application for predicting the effects of climate change. Nordic Hydrology 23, 155-172.

RENNER, C.B. and L.N. BRAUN (1990): Die Anwendung des Niederschlag-Anfluss Modells HBV3-ETH (V 3.0) auf verschiedene Einzugsgebiete in der Schweiz. Geographische Institut ETH Zürich. Berichte und Skripten Nr. 40.

RICHTER, D. (1995): Ergebnisse methodischer Untersuchungen zur Korrektur des systematischen Messfehlers des Hellmann-Niederschlagsmessers. Ber. d. Deutschen Wetterdienstes, 194.

ROSER, S. (2001): Flächendetaillierte Weiterentwicklung des prozessorientierten Einzugsgebietsmodells TAC und Visualisierung der Modellergebnisse in einem dynamischen GIS. Diploma thesis at the Institute of Hydrology, Albert-Ludwigs-University Freiburg, Germany (unpublished).

RÖTHLISBERGER, H. (1972): Water pressure in intra- and subglacial channels. Journal of Glaciology 11, 117-203.

RÖTHLISBERGER, H. and H. LANG (1987): Glacial Hydrology. In A.M. Gurnell and M.J. Clark (Ed.), Glacio-Fluvial Sediment Transfer – An Alpine Perspective, pp. 207-284. John Wiley and Sons, Chichester, New York, Toronto, Singapore.

SAKAI, A., K. FUJITA and J Kubota (2004): Evaporation and percolation effect on melting at debris-covered Lirung Glacier, Nepal Himalayas, 1996. Bulletin of Glacier Research, 21, 9-15.

SCHAEFLI, B., B. HINGRAY, M. NIGGLI and A. MUSY (2005): A conceptual glacio-hydrological model for high mountainous catchments. Hydrology and Earth System Sciences Discussions 2, 73-117.

SCHULER, T. (2002): Investigation of water drainage through an alpine glacier by tracer experiments and numerical modelling. Versuchsanstalt für Wasserbau, Hydrologie und Glaziologie der Eidgenössischen Technischen Hochschule Zürich. Mitteilung 177.

SCHULLA, J. (1997): Hydrologische Modellierung von Flussgebieten zur Abschätzung der Folge von Klimaänderungen. Züricher Geographische Schriften 69, Geographisches Institut ETH, Zurich.

SCHULZ, M. (1999): Bestimmung der Wasserhaushaltsgrößen ausgewählter hochalpiner Einzugsgebiete mittels Messung und Simulation. Diploma thesis at the Institute of Geography, Ludwig Maximilians Universität Munich, Germany (unpublished).

SEIBERT, J. (2000): Multi-criteria calibration of a conceptual runoff model using a genetic algorithm. Hydrology and Earth System Sciences 4 (2), 215-224.

SEIBERT, J. (2002): HBV light – User's manual. Uppsala University, Department of Earth Sciences, Hydrology.

SEKO, K. (1987): Seasonal variation of altitudinal dependence of precipitation in Langtang Valley, Nepal Himalayas. Bulletin of Glacier Research 5, 41-47.

SEVRUK, B. (1985): Systematischer Niederschlagsmessfehler in der Schweiz. In: Der Niederschlag der Schweiz. Beitr. z. Geol. d. Schweiz-Hydrol. 31. 65-86.

SHIRAIWA, T., K. UENO and T. YAMADA (1992): Distribution of mass input on glaciers in the Langtang Valley, Nepal Himalayas. Bulletin of Glacier Research 10, 21-30.

SHRESTHA, A. and M. SHRESTHA (2004): Recent trends and potential climate change impacts and glacier retreat/glacier lakes in Nepal and potential adaptation measures. Global forum on sustainable development: Development and climate change. OECD, Paris, 11-12 November 2004.

SHREVE, R.L. (1972): Movement of water in glaciers. Journal of Glaciology 11, 205-215.

SPREAFICO, M. and W. GRABS (1993): Determination of discharge with fluorescence tracers in Nepal Himalayas. IAHS Publication No. 218, 17-27.

STEINEGGER, U., L.N. BRAUN, G. KAPPENBERGER and G. TARTARI (1993): Assessment of annual snow accumulation over the past 10m years at high elevations in the Langtang region. IAHS Publication No. 218, 155-165.

TANGBORN, W. and B. RANA (2000): Mass balance and runoff of the partially debris-covered Langtang glacier, Nepal. IAHS Publication No. 264, 99-108.

TARAR, R.N. (1982): Water resources investigation in Pakistan with the help of Landsat imagery-snow surveys, 1975-1978. IAHS Publication No. 138, 177-190.

UENO, K. and T. YAMADA (1990): Diurnal variation of precipitation in Langtang Valley, Nepal Himalayas. Bulletin of Glacier Research 8, 93-101.

UENO, K., T. SHIRAIWA and T. YAMADA (1993): Precipitation environment in the Langtang Khola Valley, Nepal Himalayas. IAHS Publication No. 218, 207-219.

UHLENBROOK, S. (1999): Untersuchung und Modellierung der Abflussbildung in einem mesoskaligen Einzugsgebiet. Freiburger Schriften zur Hydrologie Schriften, Band 10, Institut für Hydrologie der Universität Freiburg i. Br.

UHLENBROOK, S. and Ch. LEIBUNDGUT (2002): Process-oriented catchment modelling and multiple-response validation. Hydrological Processes, 16, 423-440.

UHLENBROOK S., S. ROSER and N. TILCH (2004): Development of a distributed, but conceptual catchment model to represent hydrological processes adequately in the meso scale. Journal of Hydrology, 291, 278-296.

UHLENBROOK S. and A. SIEBER (2004): On the value of experimental data to reduce the prediction uncertainty of a process-oriented catchment model. Environmental Modelling and Software, 20, 19-32.

VALLON, M., J.R. PETIT and B. FABRE (1976): Study on ice core to bedrock in the accumulation zone of an alpine glacier. Journal of Glaciology 17 (75), 13-28.

VAN DAM, O. (2004): Modelling incoming potential radiation on a land surface with PCRaster. From website http://www.geog.uu.nl/fg/ovandam/potrad.htm (05.2005, since removed).

VAN DEURSEN, W.P.A. (1995): Geographical Information Systems and Dynamic Models: development and application of a prototype spatial modelling language. Ph.D. thesis, Faculty of Spatial Sciences, University of Utrecht, The Netherlands.

VERBUNT, M., J. GURTZ, K. JASPER, H. LANG, P. WARNERDAM and M. ZAPPA (2003): The hydrological role of snow and glaciers in alpine river basins and their distributed modelling. Journal of Hydrology 282, 36-55.

VIVIROLI, D. and R. WEINGARTNER (2004): The hydrological significance of mountains: from regional to global scale. Hydrology and Earth System Sciences, 8(6), 1016-1029.

WATANABE, T., T. SHIRAIWA and Y. ONO (1989): Distribution of periglacial landforms in the Langtang Valley, Nepal Himalaya. Bulletin of Glacier Research 7, 209-220.

WEBER, M. (1997): Aspekte zur Extrapolation von Tagesmittelwerten von Temperatur und täglichen Niederschlagssummen an hochgelegenen Gebirgsstationen aus Klimadaten des örtlichen Klimamessnetzes in Nepal. Internal report Bavarian Academy of Sciences, Commission of Glaciology, Munich.

WEBER, M. (2004): Mikrometeorologische Prozesse bei der Ablation eines Alpengletschers. PhD Thesis at the Institut of Meteorology and Geophysics University of Insbruck, Austria.

WISSMEIER, L. (2005): Implementation of distributed solute transport into the catchment model TAC^{d} and event based simulations using oxygen-18. Diploma thesis at the Institute of Hydrology, Albert-Ludwigs-University Freiburg, Germany, (unpublished).

YAMADA, T., T. SHIRAIWA, H. IIDA, T. KADOTA, T. WATANABE, B. RANA, Y. AGETA and H. FUSHIMI (1992): Fluctuations of the glaciers from 1970s to 1989 in the Khumbu, Shorong and Langtang regions, Nepal Himalayas. Bulletin of Glacier Research 10, 11-19.

YAMANE, T. (1964): Statistics – An Introductory Analysis. Harper & Row, New York.

ZAPPA, M., F. POS, U. STRASSER, P. WARMERDAM and J. GURTZ (2003): Seasonal water balance of an alpine catchment as evaluated by different methods for spatial distributed snowmelt modelling. Nordic Hydrology 34 (3), 179-202.

ZINGG, Th. (1951): Beziehung zwischen Temperatur und Schmelzwasser und ihre Bedeutung für Niederschlags- und Abflussfragen. IAHS Publication No. 32, 266-269.

Publications in the series IHP/HWRP-Berichte

The International Hydrological Programme (IHP) of UNESCO and the Hydrology and Water Resources Programme (HWRP) of WMO are administered in Germany by one national committee. Since March 2004 the national committee bears the name IHP/HWRP National Committee (previously IHP/OHP National Committee) and its secretariat IHP/HWRP Secretariat. The publication series now has the ISSN 1614-1180.

Heft 1	Problematik der Wasserbewirtschaftung der Insel Föhr *F. Steinmann und H. Ketelsen, 74 S., Koblenz 2004*
Heft 2	Studies in Mountain Hydrology *Edited by Andreas Herrmann and Ulrich Schröder, 104 S., Koblenz 2004*
Heft 3	Value of Water – Different Approaches in Transboundary Water Management *German IHP/HWRP National Committee, 128 S., Koblenz 2005*
Heft 4	Runoff from Nepalese Headwater Catchments – Measurements and Modelling *M. Konz, L.N. Braun, W. Grabs, A. Shrestha and S. Uhlenbrook, 166 S., Koblenz 2006*

Publications in the series IHP/OHP-Berichte

Publications Hefte 1 to 4 appeared in the series "Mitteilungen aus dem Tätigkeitsbereich der Arbeitsgruppen des Nationalkomitees der Bundesrepublik Deutschland für das Internationale Hydrologische Programm der UNESCO und das Operationelle Hydrologische Programm der WMO" (ISSN 0724-7621).

As from Heft 5 (1985) the series is continued under the heading "IHP/OHP-Berichte" (ISSN 0177-9915).

Hefte

Heft 1 Out of print	Untersuchungen über die urbane Hydrologie und Entwicklung mathematischer Modelle für die Hydrologie urbaner Gebiete in der Bundesrepublik Deutschland Sozio-ökonomische Aspekte der Hydrologie von Siedlungsgebieten Ein Beitrag für die Stadt Hannover *H. Massing, 90 S., Koblenz 1977*
Heft 2 Out of print	Metallanreicherungen in rezenten See-Sedimenten Geochemischer Background und zivilisatorische Einflüsse *U. Förstner, 66 S., Koblenz 1978*
Heft 3 Out of print	Haupttypen biotischer Veränderungen durch ausgewählte Schadstoffe Generelle Charakteristika von Seen und Stauseen *G. Friedrich, 39 S., Koblenz 1981*
Heft 4 Out of print	Hydrologische Untersuchungsgebiete in der Bundesrepublik Deutschland *IHP-Arbeitsgruppe, 323 S., Koblenz 1983*
Heft 5 Out of print	Empfehlung für die Auswertung der Meßergebnisse von kleinen hydrologischen Untersuchungsgebieten *IHP-Arbeitsgruppe, 92 S., Koblenz 1985*
Heft 6 Out of print	Wasser- und Materialbilanz der Ostsee *IHP-Arbeitsgruppe, 488 S., Koblenz 1985*
Heft 7 Out of print	Möglichkeiten der Niederschlagsvorhersage für hydrologische Zwecke – Statusbericht – *H. Fleer, W. Franke, K. Lecher, 73 S., Koblenz 1986*
Heft 8 Out of print	Die Belastung des Grundwassers im urbanen und ländlichen Raum unter besonderer Berücksichtigung kleiner Emissionen *V. Schenk, 84 S., Koblenz 1988*

Heft 9
Out of print
Meteorologische Systeme für hydrologische Anwendungen
IHP/OHP-Arbeitsgruppe, 176 S., Koblenz 1993

Heft 10
Out of print
Empfehlung zu Einrichtung und Betrieb kleiner hydrologischer Untersuchungsgebiete
IHP/OHP-Arbeitsgruppe, 156 S., Koblenz 1995

Heft 11
Out of print
IHD/IHP/OHP
Die Hydrologieprogramme von UNESCO und WMO in Deutschland
K. Hofius et al., 157 S., Koblenz 1998

Heft 12
Out of print
International Glossary of Hydrology, Second Edition 1992,
Version Englisch/Deutsch
Deutsches IHP/OHP-Nationalkomitee (Hrsg.), 243 S., Koblenz 1998

Heft 13
Out of print
Hydrologische Dynamik im Rheingebiet
Proceedings Internationale Rhein-Konferenz
Deutsches IHP/OHP-Nationalkomitee (Hrsg.), 233 S., Koblenz 1999

Heft 14
Hydrologische Untersuchungsgebiete in Deutschland
IHP/OHP-Arbeitsgruppe, 134 S., Koblenz 2003

Sonderhefte

Sonderheft 1
Out of print
Hydrological Principles for the Deep-Well Disposal of Liquid Wastes and Wastewaters
H. Aust, K. Kreysing und mit einem Beitrag von M. Wallner, 100 S., Koblenz 1985

Sonderheft 2
Out of print
Statistical Analysis in Hydrology
Material prepared for training courses
K. Hofius, H.-J. Liebscher, W. Löken, 155 S., Koblenz 1986

Sonderheft 3
Out of print
On Tides and Storm Surges. Theory, Practice, Instruments
Material prepared for workshops
compiled by W. Siefert, 312 S., Koblenz 1987

Sonderheft 4
Out of print
Storm Surges, River Flow and Combined Effects
State of the Art Report. International Workshop "STORM 91"
W. Siefert, T. S. Murty, 151 S., Koblenz 1991

Sonderheft 5
Out of print
Interaction of River Flow and Tide as well as Storm Surges
Suphat Vongvisessomjai, 114 S., Koblenz 1994

Sonderheft 6
Out of print
Early Warning Methodology for Surface and Groundwater Quality Monitoring
GEMS/Water Expert Consultation, 34 S., Koblenz 1994

Sonderheft 7
Out of print
Opportunities for Hydrological Data in Support of Climate Change Studies
NATO Advanced Research Workshop, 252 S., Koblenz 1994

Sonderheft 8
Out of print
IHP-IV Project H-2-2: Hydrology, water management and hazard reduction in low-lying coastal regions and deltaic areas in particular with regard to sea level changes
Joint contribution of the IHP/OHP National Committees of Germany and the Netherlands, 122 S., Koblenz 1996

Sonderheft 9
The River Rhine – Development and Management
100 S., Koblenz 1996

Sonderheft 10
River Flood Disasters
ICSU SC/IDNDR Workshop, 210 S., Koblenz 1997

Sonderheft 11
Floodplain Pollution Control Management (Vistula river, Poland)
compiled by A. Magnuszewski, Z. Mikulski, W.L.F. Brinkmann, 109 S., Koblenz 2000

Sonderheft 12
Hydrological Challenges in Transboundary Water Resources Management
Proceedings of the international conference 2001, 487 S., Koblenz 2001

Sonderheft 13
Low-lying coastal areas – Hydrology and integrated coastal zone management
Proceedings of the international symposium 2002, 424 S., Koblenz 2002

Sonderheft 14
Out of print
Hydrological networks for integrated and sustainable water resources management
Proceedings of the international workshop 2003, 140 S., Koblenz 2003